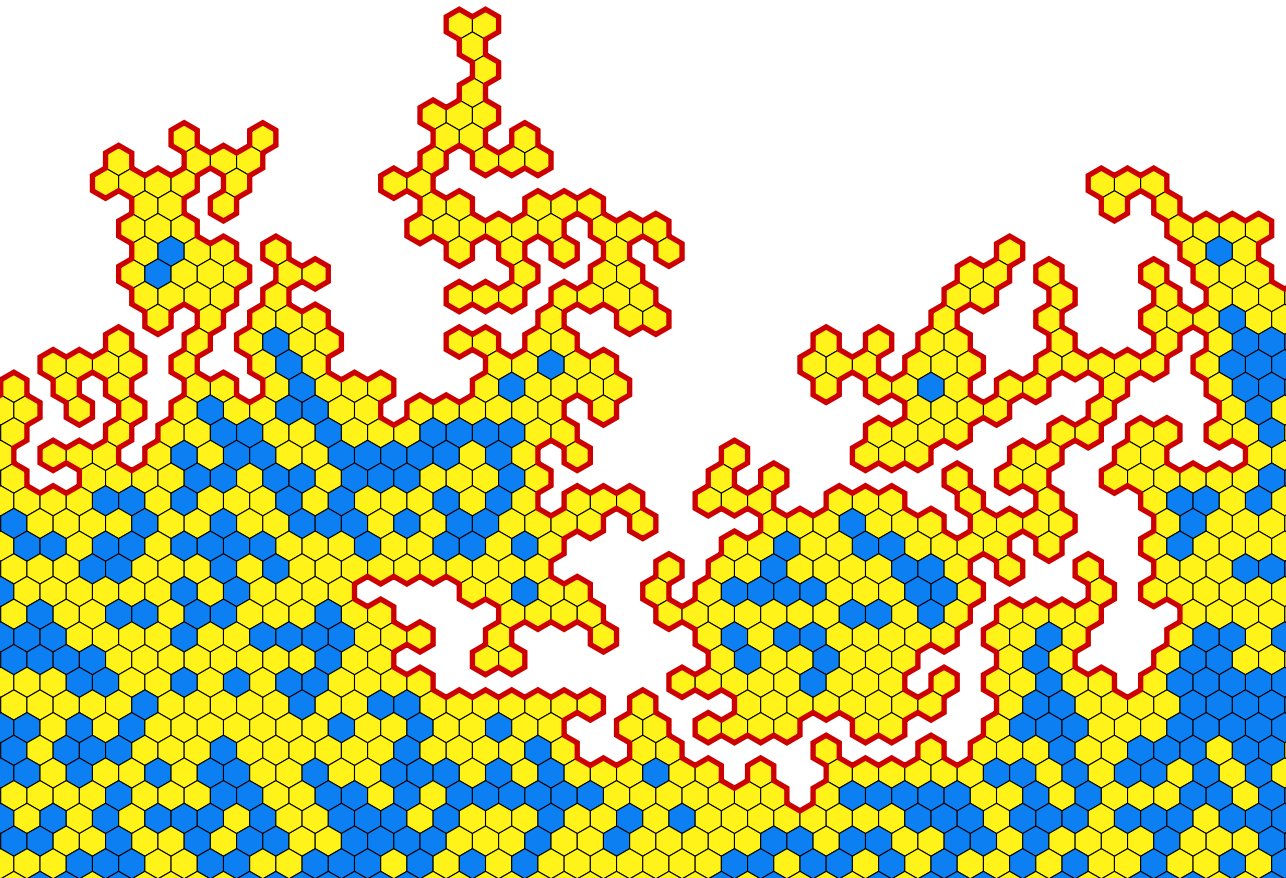


Conformally invariant paths in 2D statistical physics

With a guide to Schramm-Löwner Evolution

Wouter Kager



Conformally invariant paths in 2D statistical physics

With a guide to Schramm-Löwner Evolution

ACADEMISCH PROEFSCHRIFT

ter verkrijging van de graad van doctor aan de Universiteit van Amsterdam
op gezag van de Rector Magnificus prof. mr. P.F. van der Heijden ten
overstaan van een door het college voor promoties ingestelde commissie,
in het openbaar te verdedigen in de Aula der Universiteit

op dinsdag 21 maart 2006, te 14.00 uur

door Wouter Kager

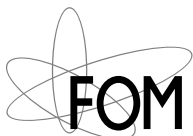
geboren te Amsterdam.

PROMOTIECOMMISSIE

Promotor: Prof. dr. B. Nienhuis

Overige leden: Prof. dr. J. van den Berg
Prof. dr. J. de Boer
Dr. J.-S. Caux
Prof. dr. R. W. van der Hofstad
Prof. dr. T. H. Koornwinder
Prof. dr. W. Werner

FACULTEIT DER NATUURWETENSCHAPPEN, WISKUNDE EN INFORMATICA



Dit werk maakt deel uit van het onderzoeksprogramma van de Stichting voor Fundamenteel Onderzoek der Materie (FOM), die financieel wordt gesteund door de Nederlandse Organisatie voor Wetenschappelijk Onderzoek (NWO).

This thesis is based on the following papers:

- Kager, W., Nienhuis, B. & Kadanoff, L.P. (2004). Exact solutions for Loewner evolutions. *J. Statist. Phys.* 115, pp. 805–822. [math-ph/0309006].
The original publication is available at www.springerlink.com.
- Kager, W. & Nienhuis, B. (2004). A guide to Stochastic Löwner Evolution and its applications. *J. Statist. Phys.* 115, pp. 1149–1229. [math-ph/0312056].
The original publication is available at www.springerlink.com.
- Kager, W. (preprint). Reflected Brownian motion in generic triangles and wedges. [math.PR/0410007].

Contents

Guidelines for the reader	vi
Index of terms and notation	viii
1 Random paths in statistical models	1
1.1 Phase transitions and conformal invariance	1
1.2 A random path in the Ising model	4
1.3 The percolation exploration process	8
1.4 Locality and reflected Brownian motion	11
2 Schramm-Löwner Evolution (SLE)	15
2.1 Löwner's method in the half-plane	15
2.2 Chordal SLE	18
2.3 Basic properties of the SLE trace	21
2.4 Radial and dipolar SLE	24
2.A Löwner's differential equation	27
2.B Solutions for chordal Löwner evolutions	31
2.C Solutions for dipolar Löwner evolutions	39
3 Connections between SLE and statistical models	42
3.1 The harmonic explorer	42
3.2 Loop-erased random walks and uniform spanning trees	44
3.3 Self-avoiding walks and the restriction property	46
3.4 Potts models and Fortuin-Kasteleyn clusters	48
3.5 $O(n)$ models	51
3.A Locality for SLE_6	53
3.B Restriction for $SLE_{8/3}$	55
4 SLE computations for critical systems	59
4.1 Two generalisations of Cardy's formula	59

4.2	SLE crossing exponents	63
4.3	Crossing exponents for critical percolation	66
4.4	Schramm's left-passage formula	70
4.5	Computations with dipolar SLE	74
5	Reflected Brownian motion (RBM)	79
5.1	Definition of reflected Brownian motion	79
5.2	Reflected random walk in a restricted geometry	83
5.3	Choice of lattice for a generic wedge	88
5.4	Reflected random walk in a generic wedge	91
5.A	Scaling limits of the reflected random walks	95
5.B	Intertwining relations and time-reversal	98
6	Hulls of local processes	104
6.1	Characterising hulls of local processes	104
6.2	Distribution functions for reflected Brownian motion	106
6.3	Simulations of self-avoiding trails	110
6.4	Distribution of the hull of a self-avoiding trail	114
6.A	Critical percolation and the last-visit distribution	119
 Appendix		
A	Conformal mapping theory	126
A.1	The Riemann mapping theorem	126
A.2	Extremal length and extremal distance	129
A.3	Conformal maps of the unit disk	132
A.4	Conformal maps of the upper half-plane	135
A.5	Hulls and capacity in the half-plane	137
A.6	The Schwarz-Christoffel formula	141
B	Stochastic processes and Itô calculus	145
B.1	Probability spaces and random variables	145
B.2	Conditional probability and expectation	148
B.3	Stochastic processes and stopping times	150
B.4	Martingales and optional sampling	152
B.5	Brownian motion	154
B.6	Stochastic integration and stochastic calculus	156
	Bibliography	161
	Samenvatting	167
	Dankwoord	173

Guidelines for the reader

This thesis is concerned with geometric aspects of conformally invariant random planar paths, in particular of paths obtained in the scaling limit of two-dimensional critical models. Over the past few years, SLE has established itself as a valuable new tool to study these random paths. SLE was introduced as Stochastic Löwner Evolution by Schramm [82], and developed in collaboration with Lawler and Werner leading to the computation of the intersection exponents of planar Brownian motion [55, 56, 57, 58]. Many more results have followed this pioneering work. In honour of Schramm's great contribution it is now customary to take the acronym SLE to stand for Schramm-Löwner Evolution.

Chapters 1–4 of this thesis provide a guide to Schramm-Löwner Evolution, aimed at an audience of physicists and mathematicians. In writing this text, I have benefited greatly from both elementary introductions to SLE [10, 25] and more technical reviews [53, 93] that are available in the literature. I have tried in this thesis to provide an introduction to SLE which at the same time clarifies some of the more technical aspects involved in computations and applications. Chapters 5 and 6 broaden the scope of this thesis by exploring connections with models of random paths that have the so-called locality property, specifically reflected Brownian motions and self-avoiding trails.

Advanced and technical topics that are not directly required for the main course of the text are treated in “advanced” sections at the end of a chapter. These advanced sections are numbered alphabetically (e.g. 2.A, 2.B) instead of numerically (e.g. 2.1, 2.2) to alert the reader. They may be skipped on the first reading. The advanced sections typically depend on background in conformal mapping theory or stochastic processes covered in the appendix. This dependence is indicated explicitly by marks in the margin, an example of which is given at the beginning of the following paragraph.

A.1 ◀ Marks as on the left of this line appear at the start of proofs, especially in the advanced sections, to signal the reader that results (and sometimes also notation) from the appendix are used. The mark at the start of this paragraph would for instance refer the reader to section A.1 of appendix A for background and used results. These marks also appear occasionally in the main text. Here they are also meant to point the reader to more background, but it should not be a problem to read on in these cases.

Let me now give an outline of the thesis. After a brief introduction into phase transitions and critical phenomena, chapter 1 presents two examples of random paths in critical models. Two special properties of the scaling limits of these random paths are identified. It is shown in chapter 2 that these two properties are sufficient to conclude that the scaling limits of the random paths must be described by SLE processes. Chapter 2 goes on to define Schramm-Löwner Evolutions and describe their basic properties.

Chapter 3 explains the connections between statistical models and SLE. Different models are considered that either have been proved or are believed to be described by SLE. We explain exactly which random path in the model is an SLE path in the scaling limit. Applications of SLE to critical models are studied in chapter 4. Several computations are shown, and their implications for our critical models are discussed.

Chapter 5 marks a change in focus away from SLE. It is concerned with Brownian motions in triangles, reflected on the boundary with fixed directions of reflection. These processes are closely related to SLE by the locality property. Chapter 6 looks more closely at the so-called *hulls* generated by local processes in general and reflected Brownian motion in particular. Computer simulations are discussed that were used to compare the hulls generated by reflected Brownian motions with the hulls generated by self-avoiding trails. The results are consistent with the hypothesis that the hull of a self-avoiding trail has the same distribution as the hull of a Brownian motion with perpendicular reflection on the boundary.

Wouter Kager
Januari 2006

Index of terms and notation

Below one finds a list of common terms and notation used throughout this thesis. For some of the items in the list, more information can be found in the section(s) following the ► sign.

Sets and special domains

\mathbb{N}	The natural numbers $\{0, 1, 2, \dots\}$.
\mathbb{Z}	The integers $\{\dots, -2, -1, 0, 1, 2, \dots\}$.
\mathbb{R}	The real numbers.
\mathbb{R}_+	The nonnegative real numbers $[0, \infty)$.
\mathbb{C}	The complex numbers, identified with \mathbb{R}^2 .
\mathbb{D}	$:= \{z \in \mathbb{C} : z < 1\}$.
\mathbb{H}	$:= \{z \in \mathbb{C} : \text{Im } z > 0\}$.
\mathbb{S}	$:= \{z \in \mathbb{C} : 0 < \text{Im } z < \pi/2\}$.
∂D	The boundary of D .
\bar{D}	The closure of D ; $\bar{D} = D \cup \partial D$.

Probability theory

\mathbf{P}	Probability (► B.1).
\mathbf{E}	Expectation (integration with respect to \mathbf{P}).
1_A	The indicator of the event A ; $1_A(\omega) = 1$ if $\omega \in A$ and $1_A(\omega) = 0$ if $\omega \notin A$ (► B.1).
a.s.	Almost surely, that is, with probability 1.
law of X	The measure $\mathbf{P}_X := \mathbf{P} \circ X^{-1}$ induced by X (► B.1, B.3).
martingale	A stochastic process whose expected value in the future is equal to the present value (► B.4).

Conformal maps and conformal invariants

hull in \mathbb{H}	A set $K \subset \bar{\mathbb{H}}$ such that $\mathbb{H} \setminus K$ is simply connected and $K = \overline{K \cap \mathbb{H}}$.
----------------------	--

g_K	The conformal transformation $g_K : \mathbb{H} \setminus K \rightarrow \mathbb{H}$ associated with the hull K , normalised such that $\lim_{z \rightarrow \infty} (g_K(z) - z) = 0$ (► A.5).
$\text{cap}_{\mathbb{H}}(K)$	The half-plane capacity of the hull K , that is, the unique number such that $g_K(z) - z = \text{cap}_{\mathbb{H}}(K)/z + O(z^{-2})$ for $z \rightarrow \infty$ (► A.5).
$d_D(A, B)$	The extremal distance in D between A and B (► A.2).
Λ	The modulus of the Teichmüller annulus (► A.2).

Löwner evolutions

$\xi, \xi(t)$	The driving function or driving process (► 2.1).
K_t	The family of growing hulls (► 2.1).
g_t	The Löwner maps $g_t := g_{K_t}$ of $\mathbb{H} \setminus K_t$ onto \mathbb{H} (► 2.1).
$\gamma, \gamma(t)$	The trace of the Löwner evolution (► 2.1).

Triangles

$T_{\alpha, \beta}$	The triangle in \mathbb{H} which has a vertex at 0 with interior angle $\alpha \in (0, \pi)$ and a vertex at 1 with interior angle $\beta \in (0, \pi)$.
$w_{\alpha, \beta}$	The vertex of $T_{\alpha, \beta}$ in \mathbb{H} , where $w_{\alpha, \beta} = \infty$ if $\alpha + \beta \geq \pi$.
$F_{\alpha, \beta}$	The unique conformal transformation of \mathbb{H} onto $T_{\alpha, \beta}$ such that $F_{\alpha, \beta}(0) = 0$, $F_{\alpha, \beta}(1) = 1$ and $F_{\alpha, \beta}(\infty) = w_{\alpha, \beta}$ (► A.6).
$G_{\alpha, \beta}$	The unique conformal transformation of \mathbb{H} onto $T_{\alpha, \beta}$ such that $G_{\alpha, \beta}(0) = 0$, $G_{\alpha, \beta}(1) = 1$ and $G_{\alpha, \beta}(-1) = w_{\alpha, \beta}$ (► A.6).
T_α	$:= T_{\alpha, \alpha}$.
w_α	$:= w_{\alpha, \alpha}$.
F_α	$:= F_{\alpha, \alpha}$.
G_α	$:= G_{\alpha, \alpha}$.

Miscellaneous

Δ	The Laplace operator.
$\lceil x \rceil$	The smallest natural number not smaller than x .
$\lfloor x \rfloor$	The largest natural number not larger than x .
$x \wedge y$	$:= \min(x, y)$.
$\cot x$	$:= \cos x / \sin x = 1 / \tan x$.
$\coth x$	$:= \cosh x / \sinh x = 1 / \tanh x$.
$\log x$	Natural (base e) logarithm of x .
$\log_{10} x$	Common (base 10) logarithm of x .
\bar{z}, \bar{g}	Complex conjugate of complex numbers and functions.
$a \cap b$	The clockwise arc from a to b along the boundary of a domain.
$a \cup b$	The counter-clockwise arc from a to b along the boundary of a domain.

1 Random paths in statistical models

Summary

Conformal invariance is one of the central concepts in our understanding of statistical models in two dimensions at a phase transition. A new approach to a description of their critical point was introduced recently by Schramm. This chapter considers two examples of critical models to which Schramm's method can be applied, thereby paving the way towards a detailed study of this approach in chapters 2, 3 and 4. Special attention is paid to the locality property and its consequences, which will play an important role in chapters 5 and 6.

1.1 Phase transitions and conformal invariance

Phase transitions are among the most striking phenomena in physics. A small change in an environmental parameter, such as the temperature or the external magnetic field, can induce macroscopic changes in the physical properties of a system. Typical examples are liquid-gas transitions and spontaneous magnetisation in ferromagnets. Many more examples are observed in nature in the most diverse systems, and for a long time physicists have been searching for explanations of these phenomena (for a nice introduction explaining the notions involved, see for example [72]).

To characterise phase transitions, one introduces an order parameter, a quantity which vanishes on one side of the phase transition and is non-zero on the other side. For magnets a suitable quantity is the magnetisation, while for liquid-gas transitions it can be defined by the density difference between the two phases. At the phase transition, the change in the order parameter can be either discontinuous or continuous. In the former case the transition is called first-order, in the latter case it is called continuous or second-order. Here we will be interested only in continuous phase transitions, and we focus on the behaviour near the so-called *critical point* where the transition occurs.

It is found experimentally that near continuous phase transitions many observable quantities have a power-law dependence on their parameters with certain (non-integer) powers, called critical exponents. Thus, the order parameter for example typically approaches zero like $(T_c - T)^\beta$ just below the transition temperature T_c , and observables such as the specific heat or the susceptibility typically diverge as $|T - T_c|^{-\alpha}$ near T_c . Moreover, the critical exponents appear to be universal in the sense that there are classes of different systems that show critical behaviour with the exact same values of the critical

exponents. This phenomenon is known as *universality* (some examples are given in the standard reference [65] on the theory of critical phenomena).

Universality allows one to draw parallels between different systems and different types of phase transitions. Theoretically, it leads to the conclusion that the behaviour near a critical point can be described by just a few relevant parameters, and that many microscopic details of the system become irrelevant near the critical point. It has been observed that the critical exponents are largely determined by just the dimension of the system, and the dimension and symmetries of the order parameter.

This observation justifies the use of simple model systems, in which many details of the interactions are neglected, to investigate critical behaviour. Examples of such models are the Ising model, the q -state Potts models and $O(n)$ models (definitions of these models will be given in sections 1.2, 3.4 and 3.5). The concept of universality is particularly useful in those cases where one of these simple models can be solved exactly, because such solutions determine the universal properties of a whole class of systems, including those far too difficult to solve exactly.

Generally, the behaviour of a system near a critical point is governed by its fluctuations. When one approaches the critical point from the disordered phase, these local fluctuations tend to be correlated over larger and larger distances as one gets closer to the transition point. The typical length-scale of these correlations, the correlation length, diverges as one approaches the critical point. Motivated by this observation, physicists introduced the idea of length-rescaling [45] as a tool for studying critical phenomena. This ultimately led to the formulation of the renormalisation group approach [96].

The core idea of this approach is that if one considers a given system at successively larger scales, then the correlation length will be successively reduced. Away from the critical point the correlation length is finite, and rescaling drives us further away from the transition. At the critical point, however, the correlation length is infinite, which implies that the system is invariant under rescaling.

The hypothesis of scale-invariance initiated the development of several techniques for the computation of critical exponents and other observables of critical behaviour, such as correlation functions. One of these techniques is the successful Coulomb Gas method [69, 70], which produces exact results provided certain qualitative assumptions are valid.

Another development came from a further refinement of the hypothesis of scale invariance. It was realised that systems whose interactions are only of a local nature must also be *locally* scale invariant. More precisely, the

system can be rescaled with a factor that depends on the position, and for a system with only local interactions one expects that the system is invariant under such transformations. This approach led people to believe that in the continuum limit, many model systems are not just scale-invariant, but are in fact conformally invariant (see [23] for a review).

Although the assumption of conformal invariance has significance also in higher dimensions (see e.g. [20, 28, 29, 81]), it is especially powerful in two dimensions. This is so because in two dimensions, *any* analytic function defines a conformal transformation and vice versa. Over the years, the assumption of conformal invariance has indeed been very successful in explaining critical behaviour of two-dimensional systems. The assumption is supported by the agreement of the results with those obtained from exactly solvable models [14].

However, the assumption of the existence of a continuum (scaling) limit of the discrete lattice models and the arguments for conformal invariance in the limit given by physicists are rather intuitive. Many questions remain, in particular of mathematical nature. For instance, what exactly should we take the scaling limit of? What do we mean precisely by conformal invariance for this limit? Can we identify the limit? If we know what the limit is, then what can we learn from it about the model? And so on.

Questions such as these have puzzled both mathematicians and physicists for a long time. Recently, new progress was made when Oded Schramm [82] introduced the one-parameter family of Stochastic Löwner Evolutions (SLE_κ), combining an old idea of Karl Löwner [63] from univalent-function theory with stochastic calculus. In Schramm's approach, we consider certain random paths defined in our two-dimensional critical models. One can prove that the scaling limits of these paths must be described by SLE_κ processes. Moreover, SLE allows us to compute properties of these random paths.

More specifically, Schramm proved in his original paper [82] that the scaling limit of the loop-erased random walk, if it exists and is conformally invariant, must be SLE_2 . He made similar conjectures relating critical percolation to SLE_6 and uniform spanning trees to SLE_8 . For loop-erased random walks and uniform spanning trees these conjectures were later proved in a fruitful collaboration of Schramm with Lawler and Werner [60].

Independently, and using different methods, Smirnov [87, 88] proved the existence and conformal invariance of the scaling limit of critical site percolation on the triangular lattice, thus establishing the connection with SLE_6 . It is believed that many other models in two dimensions, such as the self-avoiding walk, the q -state Potts models and the $O(n)$ models, also have conformally invariant scaling limits that are described by SLE_κ . Different models are then characterised by different values of κ .

This suggests that SLE_κ can be related to a conformal field theory (CFT) whose central charge is a function of κ . Various aspects of this relation have been studied in a series of papers by Bauer and Bernard [5, 6, 7, 8, 9], showing how results from SLE can be computed in the CFT language. The link between discrete systems and the corresponding CFT has been clarified further in the work of Friedrich and Werner [37, 38, 94], using the conformal restriction properties studied in [59]. The SLE-CFT connection is still an active area of research which is, however, outside the scope of this thesis.

The purpose of the first chapters of this thesis is to introduce Schramm's idea and explain the connection with models of statistical physics. To put us on track, in sections 1.2 and 1.3 of this introduction we shall describe for two specific models, namely the Ising model and the model of critical percolation, exactly which object is described in the scaling limit by SLE. This will pave the way for a detailed discussion of SLE in chapters 2, 3 and 4. It will also allow us to make a connection with reflected Brownian motion in section 1.4, which plays a central role in chapters 5 and 6.

1.2 A random path in the Ising model

As we explained in section 1.1, SLE has improved the mathematical understanding of scaling limits of critical models from statistical physics. In this section we shall look at one of the favourite models of statistical physics, the Ising model, and explain which aspect of this model is described by SLE. Two properties of the model are formulated which will allow us to make the connection with SLE in chapter 2.

To avoid some ambiguities arising on other lattices, we consider the Ising model on the triangular lattice $\mathcal{T} = \{j + k \exp(i\pi/3) : j, k \in \mathbb{Z}\}$. As our domain we take a rectangle D , which we approximate on the triangular lattice of mesh $\delta > 0$ by the set of vertices $D \cap \delta\mathcal{T}$. To each site j of this set we assign a spin variable s_j which takes values in $\{-1, +1\}$. The spin variables interact via a nearest-neighbour interaction, such that the energy of a configuration $\{s\}$ of all the spins is

$$H\{s\} = - \sum_{\langle j,k \rangle} s_j s_k, \quad (1.1)$$

where the sum is over all nearest-neighbour pairs of spins. Observe that neighbouring spins prefer to be in the same state, since this lowers the energy of the configuration.

This tendency to order is counteracted by the temperature. Higher temperatures flatten out energy differences via the Boltzmann weight $\exp(-\beta H\{s\})$ for

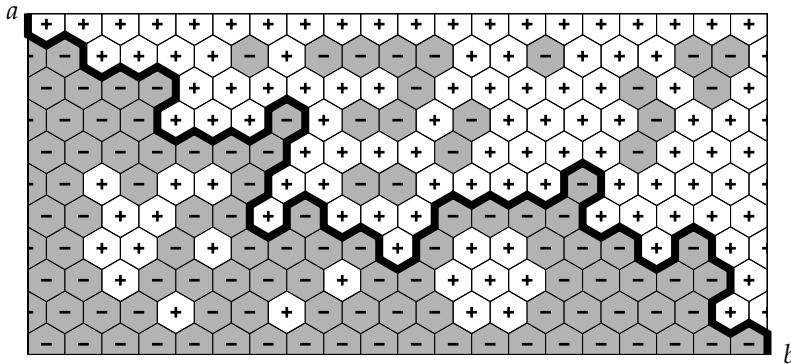


Figure 1.1. The exploration process of the Ising model in a rectangle.

each configuration, where β is the inverse temperature. The Boltzmann weight of a configuration is proportional to the probability that this configuration is realised, so that we may write

$$\mathbf{P}\{s\} = \frac{\exp(-\beta H\{s\})}{Z}, \quad (1.2)$$

where the normalisation constant $Z := \sum_{\{s\}} \exp(-\beta H\{s\})$ is called the *partition sum*. Balance between order and disorder is obtained at the critical temperature, where the system is on the brink of spontaneous magnetisation. We will assume henceforth that we are at this critical temperature.

In our discussion of the Ising model so far, we did not put any restrictions on the spins. To make the connection with SLE, however, we have to choose particular boundary conditions. A convenient choice is to pick two opposite corners a and b of the rectangle, and to make all the spins along the clockwise arc, denoted henceforth by $a \cap b$, of ∂D from a to b positive, and all the spins along the counter-clockwise arc $a \cup b$ negative. For a picture of a configuration satisfying these boundary conditions, see figure 1.1. In this figure, the centres of the hexagons are the sites of the original triangular lattice where the spin variables are located, and the hexagonal lattice is dual to this triangular lattice. We shall continue to work in this picture of the hexagonal lattice from now on.

B.3 ◀ With the boundary conditions chosen as described above, every allowed spin configuration of the Ising model contains a unique cluster of connected hexagons carrying positive spins attached to the arc $a \cap b$, and a unique cluster of connected hexagons carrying negative spins attached to the arc $a \cup b$. These two clusters meet at an interface, which is a random path on the hexagonal lattice separating the two clusters. See figure 1.1. We shall denote this path by γ . The distribution of the path γ is determined by the Boltzmann weights

of the spin configurations. We shall write $\mu_{D,a,b}^\delta$ for the law of γ (that is, the probability measure induced by γ on the space of paths in \overline{D}) on the lattice of mesh δ .

For a more precise definition of the measure $\mu_{D,a,b}^\delta$ we need to go into some topological issues. From now on, γ will represent a particular path and we shall denote by $\gamma(t)$ a parameterisation of γ in $[0, \infty)$, that is, $\gamma : [0, \infty) \rightarrow \overline{D}$, where $\overline{D} = D \cup \partial D$. For the path γ of the Ising model introduced above, we will further assume that the parameterised path is directed from a to b , that is, $\gamma(0) = a$ and $\gamma(\infty) := \lim_{t \rightarrow \infty} \gamma(t) = b$. The law $\mu_{D,a,b}^\delta$ of this path is a probability measure on the space of unparameterised continuous paths in \overline{D} . As a metric on such paths we can use the uniform metric $d(\cdot, \cdot)$ defined by

$$d(\gamma_1, \gamma_2) := \inf \sup_{t \in [0, \infty)} |\gamma_1(t) - \gamma_2(t)|, \quad (1.3)$$

where the infimum is over all choices of parameterisation of γ_1 and γ_2 . The same metric is used for instance in [22] and [60], where the connections of critical percolation and loop-erased random walks with SLE are established.

We conjecture that for the Ising model introduced above, as we let the mesh δ tend to zero, the measure $\mu_{D,a,b}^\delta$ converges weakly to a measure $\mu_{D,a,b}$ on the collection of continuous paths in \overline{D} . It is furthermore expected that this measure is supported on simple (non-self-intersecting) paths crossing D from a to b . As we shall see, SLE_κ is a stochastic process which can generate such paths. It is believed that for $\kappa = 3$ the SLE path has the same law as the scaling limit of the path γ for the Ising model.

To see what we mean by conformal invariance for this scaling limit, suppose that $f : D \rightarrow D'$ is a conformal transformation onto a simply connected domain D' whose boundary is a closed curve. This transformation maps continuous paths in \overline{D} onto continuous paths in \overline{D}' . Thus, from the measure $\mu_{D,a,b}$ on the collection of continuous paths in \overline{D} , f induces a measure on continuous paths in \overline{D}' . We conjecture that the measure induced by f coincides with the measure $\mu_{D',f(a),f(b)}$ obtained by taking the scaling limit of the Ising model in the domain D' . In other words, we conjecture that the measure $\mu_{D,a,b}$ of the Ising model has the following property:

Property I (Conformal invariance). *Let D and D' be simply connected domains with continuous boundaries and let $a, b \in \partial D$, $a \neq b$. Suppose that f is a conformal transformation of D onto D' . Then the measure induced from $\mu_{D,a,b}$ by f coincides with $\mu_{D',f(a),f(b)}$.*

The conjecture of conformal invariance alone is not enough to make the connection between the Ising model and SLE. Another property of the measure $\mu_{D,a,b}$ will be needed, which we shall describe next. We consider again the Ising

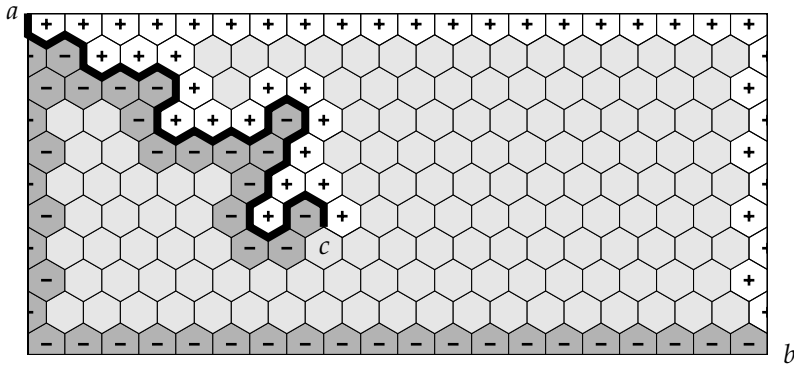


Figure 1.2. Conditioned on an initial subarc, the exploration path of the Ising model continues like the exploration process of the Ising model in the remaining domain.

model in the rectangle D on the triangular lattice of mesh δ with the appropriate boundary conditions, see figure 1.1. It will be useful for what comes to note that the path γ from a to b can be obtained dynamically (as a process *growing* from a to b), as follows.

We start the process in a with the values of the spins along the boundary fixed according to the boundary conditions and all other spins undecided. The path γ enters the rectangle via a side of a hexagon in between a positive and a negative spin. The path then meets a hexagon whose spin is undecided, and has to decide whether to turn left or right. The probabilities that the path turns left or right are equal to the probabilities that the spin takes the value -1 or $+1$, respectively. These probabilities are determined by the Boltzmann weights, summed over the remaining undecided spins. We choose the value of the spin, and hence the next step of γ , accordingly and take this spin value to be fixed forever onwards.

The path γ continues to explore the interface between positive and negative spins. Each time it meets a hexagon whose spin value is still undecided, the above procedure is repeated. Continuing in this fashion, the path eventually has to arrive at b , and the process ends. We shall call this process of exploring the interface between plus and minus spins dynamically the *exploration process* of the Ising model.

Suppose now that we denote by σ a subarc of the exploration process with one endpoint in a and the second endpoint c in the interior of D . See figure 1.2. From the discussion of the exploration process above it is clear that the law of $\gamma \setminus \sigma$ conditioned on σ is given precisely by the Ising model in the domain $D \setminus \sigma$ with positive boundary conditions along the arc $c \cap b$ and negative

boundary conditions along $c \cup b$. In other words, the law of $\gamma \setminus \sigma$ conditioned on σ is $\mu_{D \setminus \sigma, c, b}^\delta$. Assuming that this observation still holds after taking the scaling limit, this leads us to formulate the following property for the limit:

Property II (Stationarity). *Let D be a simply connected domain and let $a, b \in \partial D$, $a \neq b$. Suppose that γ is a random path in D from a to b with law $\mu_{D, a, b}$, and let σ be a subarc of γ with one endpoint in a . Denote the other endpoint of σ by c , and write D_σ for the connected component of $D \setminus \sigma$ whose boundary contains the point b . Then the law of $\gamma \setminus \sigma$ conditioned on σ is $\mu_{D_\sigma, c, b}$.*

We emphasise that the following feature of the model is essential for this stationarity property: the system in the domain D_σ should satisfy the same boundary conditions along the boundary arcs $c \cap b$ and $c \cup b$ that we started with in the domain D along the arcs $a \cap b$ and $a \cup b$. Note that then the distribution of $\gamma \setminus \sigma$ is determined only by the shape of σ . There are examples of models that are believed to have a conformally invariant scaling limit and allow one to define a random path from a to b , but fail to have the above feature. These models are not described by SLE (but one might be able to describe them with suitable generalisations of the SLE method).

In chapter 2 we shall see that properties I and II imply that the law of γ must coincide with that of an SLE process. The stationarity property II implies that the path γ can be described in terms of a Brownian motion with diffusion constant κ for some $\kappa > 0$. The value of κ that corresponds with the Ising model must be obtained by other means, for instance from the Hausdorff dimension of the path. For some models, other properties of the path γ can help to identify the value of κ . This is for instance the case for the exploration path of critical percolation, which we shall consider next.

1.3 The percolation exploration process

Consider again the triangular lattice $\mathcal{T} = \{j + k \exp(i\pi/3) : j, k \in \mathbb{Z}\}$. We define site percolation on the triangular lattice as follows. All vertices of the lattice are independently coloured blue with probability p or yellow with probability $1 - p$. An equivalent, and perhaps more convenient, viewpoint is to say that we colour all hexagons of the dual lattice blue or yellow with probabilities p and $1 - p$, respectively. It is well-known that for $p \leq 1/2$, there is almost surely no infinite cluster of connected blue hexagons, while for $p > 1/2$ there a.s. exists a unique infinite blue cluster. This makes $p = 1/2$ the critical point for site percolation on the triangular lattice. For the remainder of this section we assume that we are at this critical point.

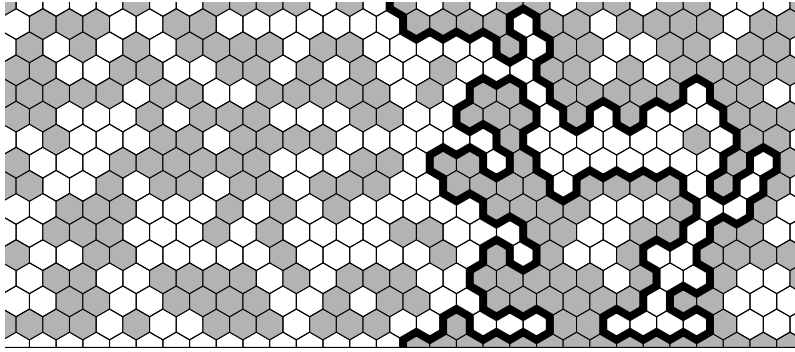


Figure 1.3. Initial segment of the percolation exploration path in the upper half-plane.

Let us for now restrict ourselves to the half-plane $\mathbb{H} := \{z \in \mathbb{C} : \text{Im } z > 0\}$. Suppose that as our boundary conditions we colour all hexagons intersecting the negative reals yellow, and all hexagons intersecting the positive reals blue. All other hexagons in the half-plane are independently coloured blue or yellow with equal probabilities. Then there exists a unique path over the edges of the hexagons, starting in the origin, which separates the cluster of blue hexagons attached to the positive reals from the cluster of yellow hexagons attached to the negative reals. This path is called the percolation exploration path from 0 to ∞ in the half-plane. See figure 1.3 for an illustration.

The exploration path can also be described as the unique path from the origin such that at each step there is a blue hexagon on the right, and a yellow hexagon on the left. This path can be generated dynamically, in a way very similar to the dynamic description of the exploration path in the Ising model of section 1.2. Initially, only the hexagons on the boundary are coloured blue or yellow according to the boundary conditions described above. Then after each step, the exploration process meets a hexagon. If this hexagon has not yet been coloured, we have to choose whether to make it blue or yellow, and the exploration process can turn left or right with equal probabilities. On the other hand, if the hexagon has already been coloured blue or yellow, then the exploration path is forced to turn left or right, respectively.

In the end we obtain a path in the upper half-plane from 0 to ∞ . We shall denote the law of this path by $\mu_{\mathbb{H},0,\infty}^\delta$. As for the Ising model, this law is a measure on the space of continuous paths in $\overline{\mathbb{H}}$ from 0 to ∞ . Taking the scaling limit as $\delta \rightarrow 0$, this measure converges to a measure $\mu_{\mathbb{H},0,\infty}$ on such paths. In contrast to the exploration process of the Ising model, the exploration process of critical percolation is not a simple path in the scaling limit, but a path which

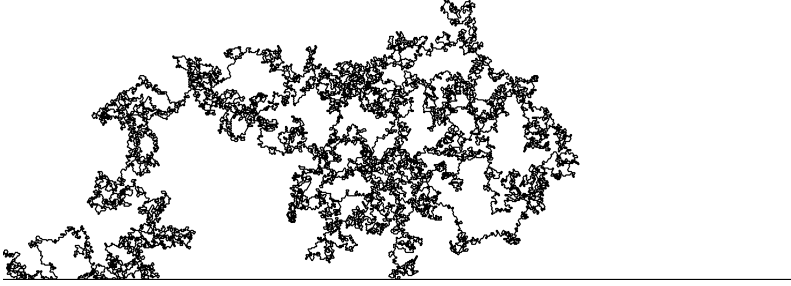


Figure 1.4. A piece of the percolation exploration path in the upper half-plane for a very fine mesh δ .

touches itself many times (see figure 1.4). Note, however, that the exploration process can never cross itself. This is apparent from the discrete description given above, since the exploration path is reflected away from its own past whenever it meets an already coloured hexagon.

In the discussion above we have restricted percolation to a half-plane, but we can of course consider other domains as well. For example, let D be a simply connected domain with continuous boundary, and let a and b be two points on the boundary. In an approximation of the domain by hexagons, colour all hexagons that intersect the arc $a \cup b$ of ∂D blue and all remaining hexagons intersecting ∂D yellow. Then there is a percolation exploration process in D from a to b , and we expect that the scaling limit of this process exists. The law of the exploration path will be a measure $\mu_{D,a,b}$ on continuous paths in \bar{D} from a to b .

It has been proved that the scaling limit of the percolation exploration process exists and is conformally invariant (see the discussion below), and hence property I of section 1.2 holds for the exploration path. Property II is also satisfied in the case of critical percolation for the same reasons why it holds for the Ising model. Thus we can expect that the exploration path of critical percolation is described by SLE_κ for some $\kappa > 0$. The value of κ in this case can be guessed from a special property of the exploration process, which we shall now describe.

Suppose that D is a simply connected subset of \mathbb{H} with continuous boundary containing the interval $[-1, 1]$. Pick a point $b \in \partial D \setminus (-1, 1)$ (it turns out that it will not matter which point we pick), and consider the critical percolation exploration process in D from 0 to b . Compare this process to the exploration process in \mathbb{H} from 0 to ∞ . Then we note that in the discrete approximation,

the two exploration processes behave exactly the same up to the time when they first touch a hexagon intersecting $\partial D \setminus (-1, 1)$, since all the hexagons in the interior of D are coloured blue or yellow independently. This leads us to define the following property of the exploration process in the scaling limit:

Theorem 1.1 (Locality property). *Let $\gamma(t)$ and $\gamma'(t)$ be the exploration processes of critical percolation in \mathbb{H} from 0 to ∞ and in D from 0 to b , respectively. Set $\tau := \inf\{t : \gamma(t) \in \partial D \setminus (-1, 1)\}$ and set $\tau' := \inf\{t : \gamma'(t) \in \partial D \setminus (-1, 1)\}$. Then, independently of the choice of b , $(\gamma(t) : t \leq \tau)$ and $(\gamma'(t) : t \leq \tau')$ have the same law modulo time-parameterisation.*

As we shall prove in section 3.A, SLE has the same locality property if and only if $\kappa = 6$. This means that the only candidate for the scaling limit of the exploration process of critical percolation is SLE_6 . A weaker result was proved by Smirnov [87, 88]. He showed that Cardy's formula for the crossing of a rectangle by a percolation cluster [24] holds for the scaling limit of critical site percolation on the triangular lattice, and thereby established conformal invariance in the limit. Together with the locality property this allows us to relate the so-called hull of SLE_6 to that of the percolation exploration process, as we shall explain in section 1.4.

Smirnov proposed that from Cardy's crossing formula and the locality property it should be possible to prove that the law of the percolation exploration process itself converges to the law of an SLE_6 process. With some adaptations to the approach proposed by Smirnov, the proof of this fact was recently completed by Camia and Newman [22].

1.4 Locality and reflected Brownian motion

In section 1.3 we claimed that the locality property together with Cardy's crossing formula allow us to make a connection between SLE_6 and the exploration process of critical percolation. The purpose of this section is to explain how this connection is made. Then we shall describe a model for reflected Brownian motion which also has the locality property of theorem 1.1 and satisfies Cardy's formula, and is therefore also related to SLE_6 .

We start by explaining Cardy's crossing formula for critical percolation. Carleson noted that this formula takes on a particularly nice form in an equilateral triangle, and we shall therefore choose this geometry here. Let T be the equilateral triangle in the upper half-plane with corners at 0, 1 and $a := \exp(i\pi/3)$. Let $x \in (0, 1)$ and consider critical percolation in T (as in section 1.3), with free boundary conditions. We are interested in the event that there is a

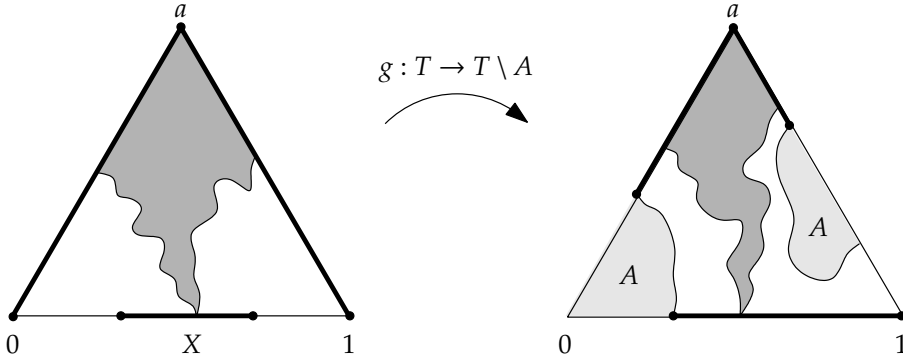


Figure 1.5. A hull K generated by the exploration process of critical percolation in an equilateral triangle. The law of K is determined by the probabilities that K avoids sets A such as shown on the right.

sequence of connected yellow hexagons that crosses T from the side $a \cap 1$ to the interval $(0, x)$. Carleson’s version of Cardy’s formula says that the probability of this event in the scaling limit is just x .

This result has a nice interpretation in terms of the exploration process. Indeed, consider the exploration process γ in T from a to a point $b \in [0, 1]$ (i.e. with blue boundary conditions along the arc $a \cup b$ and yellow boundary conditions along the arc $a \cap b$). It is easy to see that if there is a yellow crossing from $a \cap 1$ to $(0, x)$, then the exploration process must hit the interval $(0, x)$ before $(x, 1)$. On the other hand, if there is no such yellow crossing, then there must be a blue crossing from $0 \cap a$ to $(x, 1)$, and the exploration process must hit $(x, 1)$ before $(0, x)$.

Hence Carleson’s version of Cardy’s formula says that the probability that γ hits the interval $(0, x)$ before it hits the interval $(x, 1)$ is x . Observe that by the locality property, this probability does not depend on the choice of b . It follows that if we define $\tau := \inf\{t \geq 0 : \gamma(t) \in [0, 1]\}$, then $\gamma(\tau)$ has the uniform distribution on $[0, 1]$, independently of the choice of b .

We now define the *hull* K_t at time t as the compact set of points in \bar{T} that are either on $\gamma[0, t]$ or are disconnected from $\{0, 1\}$ by $\gamma[0, t]$. We are interested in the hull K_τ at the time when γ first hits $[0, 1]$. We claim that because of the locality property, the law of K_τ is completely determined by the distribution of the hitting point $\gamma(\tau)$. To understand this, we need to explain first what we mean exactly by the distribution of K_τ .

B.1 ◀ For this, let Ω denote the collection of all possible hulls K_τ at time τ . Define \mathcal{Q} as the collection of compact $A \subset \bar{T}$ with continuous boundary such

that $a \notin A$, $A = \overline{A \cap T}$ and $\overline{T} \setminus A$ is simply connected. Then it is not difficult to see that the distribution of K_τ is completely determined by the probabilities that $K_\tau \cap A = \emptyset$ for all $A \in \mathcal{Q}$ (see figure 1.5). Hence, we will endow Ω with the σ -field \mathcal{F} generated by the events $\{K \in \Omega : K \cap A = \emptyset\}$ for all $A \in \mathcal{Q}$. A probability measure \mathbf{P} on (Ω, \mathcal{F}) is then characterised by the values of $\mathbf{P}[K \cap A = \emptyset]$ for all $A \in \mathcal{Q}$ (see [59, lemma 3.2] for an equivalent statement in the half-plane). We say that such a measure \mathbf{P} determines the distribution of K_τ .

Theorem 1.2. *Suppose that γ and γ' are two random paths in T from a to $b \in (0, 1)$ that are conformally invariant and have the locality property. Let τ and τ' denote the first times when γ and γ' hit the interval $[0, 1]$, and write K and K' for the hulls of γ and γ' at times τ and τ' (as defined above). Assume that $\gamma(\tau)$ and $\gamma'(\tau')$ have the same distribution on $[0, 1]$. Then K and K' have the same law on the space (Ω, \mathcal{F}) .*

Proof. Let \mathbf{P} be the law of K , and $A \in \mathcal{Q}$. Suppose that $g : T \rightarrow T \setminus A$ is the conformal transformation which fixes a and maps the clockwise arc $0 \cap 1$ of ∂T onto the component of $\partial T \setminus A$ containing a , preserving orientation (see figure 1.5). Then $\mathbf{P}[K \cap A = \emptyset] = \mathbf{P}[\gamma(\tau) \in g^{-1}([0, 1] \setminus A)]$, by the locality property and conformal invariance. Likewise, $\mathbf{P}'[K' \cap A = \emptyset] = \mathbf{P}'[\gamma'(\tau') \in g^{-1}([0, 1] \setminus A)]$, where \mathbf{P}' denotes the law of K' . Since $\gamma(\tau)$ and $\gamma'(\tau')$ have the same distribution, the theorem follows. \blacksquare

Consider again a percolation exploration process in T from a to $b \in [0, 1]$, and consider also an SLE₆ path in T from a to b . Both processes have the locality property and arrive on the interval $[0, 1]$ with the uniform distribution (for SLE₆ we will prove these claims in sections 3.A and 4.1). It follows from theorem 1.2 that the two processes generate the same hull (more precisely, the hulls have the same law). Any other stochastic process in T which has the locality property and arrives on $[0, 1]$ with the uniform distribution will also generate the same hull. It was shown by Lawler, Schramm and Werner in [59] that one such process is a Brownian motion with a particular reflecting boundary condition. We now describe this process in more detail.

Let $B = (B(t) : t \geq 0)$ be a standard complex Brownian motion starting from a and set $v_1 := \exp(-i\pi/3)$ and $v_2 := \exp(-2i\pi/3)$. Then there exists a unique process Y in \overline{T} , stopped when it hits the interval $[0, 1]$, such that

$$Y(t) = B(t) + v_1 X_1(t) + v_2 X_2(t), \quad (1.4)$$

where X_1 and X_2 are continuous real-valued increasing processes adapted to B such that $X_1(0) = X_2(0) = 0$, X_1 increases only when Y is on the left side of the triangle T and X_2 increases only when Y is on the right side of T . The process Y is called the reflected Brownian motion in T with reflection vector fields v_1 and v_2 on the two sides. Observe that the directions of reflection on the two sides make an angle of 60° with the boundary of T .

It is not difficult to prove (as we will in section 5.1) that this reflected Brownian motion is conformally invariant and has the locality property. Moreover, if we set $\tau := \inf\{t \geq 0 : Y(t) \in [0, 1]\}$, then it can be shown that $Y(\tau)$ has the uniform distribution on $[0, 1]$ (see chapter 5, theorem 5.1). Therefore, by theorem 1.2, this reflected Brownian motion generates the same hull as SLE_6 and the exploration process of critical percolation.

Other reflected Brownian motions are obtained when we change the directions of the two vector fields v_1 and v_2 . By conformal invariance we can study these reflected Brownian motions on domains other than the equilateral triangle T . In particular, we will prove in chapter 5 that for any triangle with corners at $0, 1$ and $a \in \mathbb{H}$ there is a reflected Brownian motion which, started from a , will arrive on $[0, 1]$ with the uniform distribution. Note that by conformal invariance, theorem 1.2 then implies that every other local, conformally invariant process which, started from a , arrives on $[0, 1]$ with the uniform distribution will generate the same hull.

There are many other models that define random paths with the locality property. In chapter 6 we will study for instance a model for *self-avoiding trails* on the lattice, that is, paths that are not allowed to traverse the same edge of the lattice more than once. This model is closely related to percolation, yet the trails do not generate the same hull as a reflected Brownian motion with reflection angles of 60° . The results of computer simulations of the model are however consistent with the hypothesis that the hull has the same distribution as the hull generated by a reflected Brownian motion with perpendicular reflection on the boundary, as we shall see in chapter 6.

2 Schramm-Löwner Evolution (SLE)

Summary

In this chapter we study Löwner's method for describing paths slitting a domain from the boundary. We apply this method to the exploration processes of the Ising model and of critical percolation introduced in chapter 1. This leads to a stochastic description of these paths, which is called Schramm-Löwner Evolution (SLE). A precise definition of SLE is given, and its basic properties are discussed. Applications of SLE to critical models will be described in chapters 3 and 4.

2.1 Löwner's method in the half-plane

In this section we shall explain Löwner's method for describing a path crossing the upper half of the complex plane from a point on the real line to ∞ . In SLE, this method is used together with conformal invariance to obtain measures on paths crossing a given domain D between two given boundary points a and b , as discussed in sections 1.2 and 1.3. The presentation of Löwner's method in this section will be mostly descriptive. More details of Löwner's method including proofs are provided in section 2.A for the interested reader.

Consider a given continuous path γ that slits the upper half of the complex plane $\mathbb{H} := \{z \in \mathbb{C} : \text{Im } z > 0\}$ from the real line. We can represent this path as a continuous function $\gamma : [0, T) \rightarrow \overline{\mathbb{H}}$ such that $\gamma(0) \in \mathbb{R}$. We shall refer to the real parameter $t \in [0, T)$ along the path as time. In general, T can be finite or ∞ (as we shall see, there is a natural choice for the time parameterisation of γ , which determines the value of T). To describe the Löwner evolution for this path γ we have to introduce some notation that will be used throughout this thesis.

For all $t \in [0, T)$ we define the *hull* K_t at time t as the complement in $\overline{\mathbb{H}}$ of the unbounded connected component of $\overline{\mathbb{H}} \setminus \gamma[0, t]$. Alternatively, K_t is the union of $\gamma[0, t]$ and all bounded connected components of $\overline{\mathbb{H}} \setminus \gamma[0, t]$ (the "loop-holes" created by the path γ). Finally, K_t is also the set of points in $\overline{\mathbb{H}}$ that are disconnected from ∞ by $\gamma[0, t]$. In a sense, the hull K_t represents the part of space explored by the path up to time t . We will assume that γ is such that for all $0 \leq s < t < T$, K_s is a proper subset of K_t . This means that γ is a path which has to reflect off into open space immediately after it touches itself or when it hits the real line. The path is not allowed to enter the parts of space it has already explored. See figure 2.1 for an example of such a path and the definition of the hull.

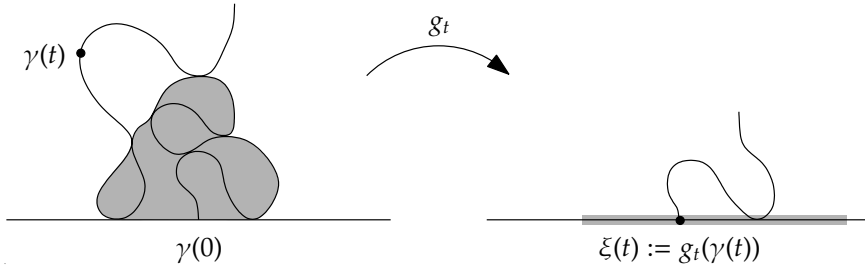


Figure 2.1. A path γ , the hull K_t it generates up to time t (the union of the shaded area and $\gamma[0, t]$), and the Löwner map at time t . The shaded segment of the real line on the right represents the image of the boundary of the hull under the map g_t .

A.5 ◀ At every time $t \in [0, T)$ there exists a unique conformal transformation $g_t : \mathbb{H} \setminus K_t \rightarrow \mathbb{H}$ (see figure 2.1) which satisfies the normalisation

$$\lim_{z \rightarrow \infty} (g_t(z) - z) = 0. \quad (2.1)$$

This transformation has an expansion of the form $g_t(z) = z + \sum_{n=1}^{\infty} a_n(K_t)z^{-n}$ for $z \rightarrow \infty$. The expansion coefficients are all real, and depend only on K_t . The first coefficient $a_1(K_t)$ is called the *half-plane capacity* of the hull K_t , and will henceforth be denoted by $\text{cap}_{\mathbb{H}}(K_t)$. For all paths as described above, it is possible to choose a parameterisation such that $\text{cap}_{\mathbb{H}}(K_t) = 2t$, and we shall always assume that we work with this parameterisation.

Löwner's differential equation describes how the conformal maps g_t (that in turn describe the path γ) evolve in time. With the time-parameterisation chosen such that $\text{cap}_{\mathbb{H}}(K_t) = 2t$, the Löwner equation reads

$$\frac{\partial g_t(z)}{\partial t} = \frac{2}{g_t(z) - \xi(t)}; \quad g_0(z) = z, \quad (2.2)$$

where ξ is a continuous real-valued function defined by $\xi(t) := g_t(\gamma(t))$. That is, $\xi(t)$ is the point on the real line to which the tip of the slit $\gamma[0, t]$ is mapped. It is to be noted that the two-dimensional path γ is now fully described by the one-dimensional function ξ through Löwner's equation. It is this fact which makes Löwner's method so useful.

For each fixed point $z \in \overline{\mathbb{H}} \setminus \{0\}$, the Löwner equation describes the flow of $g_t(z)$ starting from the point $g_0(z) = z$. The flow is directed towards the real line, as can be seen by taking the imaginary part of Löwner's equation (2.2). Let us define by $T(z)$ the first time when z is in the hull generated by γ , that is

$$T(z) := \inf \{t \in [0, T) : z \in K_t\}, \quad (2.3)$$

setting $T(z) := T$ if $z \notin \cup_{t \in [0, T]} K_t$. Then one may prove for $T(z) < T$ that at time $T(z)$, $g_t(z)$ hits the real line in the point $\xi(t)$ and the solution of Löwner's equation for the starting point z is no longer defined after the time $T(z)$.

At this stage of the discussion it is useful to give a brief summary of Löwner's method. We have seen that a given path γ generates a family of growing hulls $(K_t : t \in [0, T])$, which stands in one-to-one relation with a family $(g_t : t \in [0, T])$ of conformal transformations. Löwner's differential equation in turn brings this family of transformations into a one-to-one correspondence with a real-valued, continuous driving function ξ . This function completely describes the original path γ .

The above procedure may be reversed: starting from a continuous, real-valued function $\xi : [0, T] \rightarrow \mathbb{R}$, the solution of Löwner's equation can be shown (see section 2.A, theorem 2.7) to be a family $(g_t : t \in [0, T])$ of conformal transformations of the form $g_t : \mathbb{H} \setminus K_t \rightarrow \mathbb{H}$, where $(K_t : t \in [0, T])$ is a family of growing hulls and $\text{cap}_{\mathbb{H}}(K_t) = 2t$. However, it is not in general true that there exists a path γ such that the hulls (K_t) are the hulls corresponding to γ . We shall now briefly discuss this.

In the reversed Löwner procedure, i.e. starting from a given driving function ξ , for each fixed $z \in \overline{\mathbb{H}} \setminus \{0\}$ we define $T(z)$ to be the first time when $g_t(z)$ hits $\xi(t)$. That is,

$$T(z) := \inf \left\{ t \in [0, T] : \lim_{s \uparrow t} (g_s(z) - \xi(s)) = 0 \right\}, \quad (2.4)$$

setting $T(z) := T$ if $g_t(z)$ never hits $\xi(t)$. If we then define

$$H_t := \{z \in \mathbb{H} : T(z) > t\}, \quad K_t := \{z \in \overline{\mathbb{H}} : T(z) \leq t\}, \quad (2.5)$$

then $H_t = \mathbb{H} \setminus K_t$ is the domain of the conformal transformation g_t and K_t is the corresponding hull.

Now, if ξ is a smooth enough function so that

$$\gamma(t) := \lim_{y \downarrow 0} g_t^{-1}(\xi(t) + iy) \quad (2.6)$$

exists for all $t \in [0, T]$ and is continuous, then K_t is indeed the hull generated by γ up to time t [78, theorem 4.1]. In that case, we call γ the *trace* of the Löwner evolution. However, it is not true for all continuous ξ that the limit in equation (2.6) exists and is continuous. The necessary conditions for the trace to exist are at present unknown. A sufficient condition was obtained by Marshall, Rohde and Lind [62, 66], who have shown that functions ξ that are Hölder continuous with exponent $1/2$ and norm smaller than 4 generate simple continuous curves γ slitting the half-plane. In section 2.B we will derive exact

solutions of Löwner's equation for various driving functions, illustrating the transition that occurs at Hölder norm 4.

For our study of Löwner evolutions in the half-plane it will be useful to understand how the solution changes under transformations of the driving function. We shall end this section with a discussion of two such transformations for which the change in the solution can be described explicitly. The changes in the solution under these transformations are essential for the conformal invariance and stationarity of SLE, as we shall see in section 2.2.

For the first transformation, suppose that $(g_t : t \in [0, T])$ is the family of conformal maps for the driving function $(\xi(t) : t \in [0, T])$, and let $(K_t : t \in [0, T])$ be the corresponding hulls. Then we may define a new family of conformal maps and driving function by

$$\tilde{g}_t(z) := \frac{1}{\alpha} g_{\alpha^2 t}(\alpha z) \quad \text{and} \quad \tilde{\xi}(t) := \frac{1}{\alpha} \xi(\alpha^2 t), \quad (2.7)$$

where $\alpha > 0$. It is easily verified that these conformal maps and driving function again satisfy Löwner's equation (2.2). Observe that the maps \tilde{g}_t are the conformal transformations that take the complements of the hulls $\tilde{K}_t = K_{\alpha^2 t}/\alpha$ onto the half-plane with the correct time-parameterisation, $\text{cap}_{\mathbb{H}}(\tilde{K}_t) = 2t$. We conclude that to change the scale of the hulls generated by the Löwner equation, one must rescale the driving function as in equation (2.7).

Likewise, to shift the hulls generated by the Löwner equation to the left or right, it suffices to shift the driving function by the same amount. More precisely, the conformal maps and driving function defined by

$$\tilde{g}_t(z) := g_t(z - \alpha) + \alpha \quad \text{and} \quad \tilde{\xi}(t) := \xi(t) + \alpha, \quad (2.8)$$

where $\alpha \in \mathbb{R}$, also satisfy the Löwner equation (2.2). Here the maps \tilde{g}_t are the conformal transformations of the complements of the hulls $\tilde{K}_t = K_t + \alpha$ onto the half-plane with the correct time-parameterisation.

2.2 Chordal SLE

Let us now recall our discussion of the scaling limits of the Ising model and of percolation in sections 1.2 and 1.3. There we considered random paths crossing a given domain D from a to b , and we argued that the measure on such paths in the scaling limit should have the conformal invariance and stationarity properties I and II. Using conformal invariance, we can study for both models the case where the exploration process is a path in the upper half-plane from 0

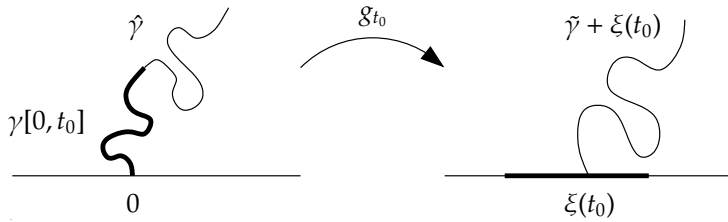


Figure 2.2. Stationarity for SLE says that the path γ has the same law as the union of an initial subarc $\gamma[0, t_0]$ (the thick arc in the figure) and the image under the map $g_{t_0}^{-1}$ of an independent SLE path starting from $\xi(t_0)$.

to ∞ . As we discussed in section 2.1, such paths can be described by Löwner’s equation with an appropriate driving function.

In the case of the Ising model and percolation, the exploration path is a random path, and so Löwner’s method allows us to describe this path by a stochastic process ξ . This will be a continuous, real-valued stochastic process whose law is determined by the law $\mu_{\mathbb{H},0,\infty}$ of the exploration path in the scaling limit. Schramm’s key observation in [82] was that the conformal invariance and stationarity properties of the measure $\mu_{\mathbb{H},0,\infty}$ imply that ξ must be a Brownian motion. This in turn implies that standard methods of stochastic calculus can be used to compute properties of the exploration process. Since this is such a vital observation, let us give a precise statement and proof.

Theorem 2.1. *Let γ be a path with law $\mu_{\mathbb{H},0,\infty}$ satisfying the properties I and II from section 1.2. Let ξ be the driving process for γ using Löwner’s method. Then there is a $\kappa > 0$ such that ξ has the law of Brownian motion with diffusion constant κ .*

Proof. Let γ and $\tilde{\gamma}$ be two independent paths with the law $\mu_{\mathbb{H},0,\infty}$. Denote by g_t, \tilde{g}_t the corresponding conformal transformations and by $\xi, \tilde{\xi}$ the Löwner driving processes of these paths. Fix $t_0 > 0$. By properties I and II the paths γ and $\hat{\gamma} := \gamma[0, t_0] \cup g_{t_0}^{-1}(\tilde{\gamma} + \xi(t_0))$ have the same law. See figure 2.2.

We claim that for $t > t_0$ the Löwner map \hat{g}_t for the path $\hat{\gamma}$ is given by

$$\hat{g}_t(z) = \tilde{g}_{t-t_0}(g_{t_0}(z) - \xi(t_0)) + \xi(t_0). \tag{2.9}$$

To see this, observe that \hat{g}_t is a transformation from the complement of the hull generated by $\hat{\gamma}$ up to time t onto the half-plane. Moreover, $\hat{g}_t(z) = z + 2t/z + O(z^{-2})$ for $z \rightarrow \infty$, which specifies the transformation uniquely. Differentiating (2.9) with respect to t , using the Löwner equation (2.2) for $\tilde{g}_t(z)$, gives

$$\frac{\partial \hat{g}_t(z)}{\partial t} = \frac{2}{\hat{g}_t(z) - [\xi(t_0) + \tilde{\xi}(t - t_0)]}. \tag{2.10}$$

Thus, the Löwner driving process for the path $\hat{\gamma}$ is $\hat{\xi}(t) = \xi(t_0) + \tilde{\xi}(t - t_0)$ for $t > t_0$, and by continuity this also holds for $t = t_0$.

Now for any fixed sequence $0 \leq t_0 < t_1 < \dots < t_n < \infty$ consider the increments $\{\xi(t_i) - \xi(t_{i-1}) : i = 1, \dots, n\}$. Since ξ and $\tilde{\xi}$ are independent and $\tilde{\xi}$ has the same law as ξ , from the above we can conclude that these increments are independent and their distributions depend on t_i, t_{i-1} only through the difference $t_i - t_{i-1}$. Hence ξ is a continuous process with independent, stationary increments. It is standard that then the increments $\xi(t_i) - \xi(t_{i-1})$ of the process ξ are Gaussian, by an elementary proof analogous to that of the central limit theorem, see for instance [44, section 1.4]. By symmetry ξ has no drift and hence is Brownian motion for some diffusion constant $\kappa > 0$. ■

Theorem 2.1 leads us to define SLE_κ as the solution of Löwner's differential equation driven by a Brownian motion with diffusion constant κ . In section 2.1 we explained that the solution of this equation for a given continuous real-valued driving function ξ generates families (g_t) and (K_t) of conformal maps and corresponding hulls, and, if ξ is smooth enough, a continuous path γ . When ξ is a Brownian motion it is not at all clear a priori whether the solution does indeed generate a path γ .

However, it was shown for $\kappa \neq 8$ by Rohde and Schramm [78] that with probability 1, the trace of the Löwner evolution exists and is a continuous path such that $\lim_{t \rightarrow \infty} |\gamma(t)| = \infty$. For $\kappa = 8$ this result holds as well, because SLE_8 is known to describe the scaling limit of the path winding around a uniform spanning tree [60]. So for all $\kappa > 0$, Löwner's equation defines in a deterministic way for almost every realisation of the driving process ξ a path γ in the upper half-plane from 0 to ∞ . The law of this path is the law induced from the law of ξ by Löwner's method. We are led to the following definition:

Definition 2.2 (Chordal SLE). *Let $\kappa > 0$, and let $B(t)$ denote standard Brownian motion starting from 0. The solution $(g_t : t \geq 0)$ of the Löwner equation*

$$\frac{\partial g_t(z)}{\partial t} = \frac{2}{g_t(z) - \xi(t)}; \quad g_0(z) = z, \quad z \in \mathbb{H}, \quad (2.11)$$

with driving process $\xi(t) = \sqrt{\kappa}B(t)$ is called chordal SLE_κ . The trace γ of chordal SLE_κ is defined by

$$\gamma(t) := \lim_{z \rightarrow 0} g_t^{-1}(z + \xi(t)), \quad (2.12)$$

where the limit is taken from within the upper half-plane (almost surely, this limit exists for all $t \geq 0$ and γ is a continuous path from 0 to ∞).

Lemma 2.3 (Stationarity). *Chordal SLE_κ is stationary in the following sense. Let T be any stopping time for the process. Set $\tilde{\gamma}(t) := g_T(\gamma(T + t)) - \xi(T)$. Then $\tilde{\gamma}$ has the law of an SLE_κ trace in \mathbb{H} from 0 to ∞ , and $\tilde{\gamma}$ is independent from $\{\gamma(t) : t \leq T\}$.*

- B.5 ◀ **Proof.** The Löwner maps for the path $\tilde{\gamma}$ are $\tilde{g}_t(z) := g_{T+t} \circ g_T^{-1}(z + \xi(T)) - \xi(T)$. Taking the derivative with respect to t shows that $(\tilde{g}_t : t \geq 0)$ is driven by the process $\tilde{\xi}$ defined by $\tilde{\xi}(t) := \xi(T+t) - \xi(T)$, which has the same law as ξ and is independent from $\{\xi(t) : t \leq T\}$. ■

The acronym SLE was introduced by Oded Schramm and stands originally for Stochastic Löwner Evolution, but gradually the name Schramm-Löwner Evolution has become more and more common. The process introduced above is called *chordal* SLE because the trace γ of this process is growing from the origin to infinity, that is, it connects two points on the boundary of the domain (this may be more apparent once we have defined chordal SLE in an arbitrary domain below). Other versions of SLE are possible, for instance growing from a boundary point to a point in the interior of the domain. These other versions are introduced in section 2.4.

- B.5 ◀ To conclude this section, we define chordal SLE_κ in an arbitrary domain D and show that it is conformally invariant. We will need the scaling property of Löwner's differential equation, expressed in equation (2.7). This property says that if one transforms the driving function ξ according to $\xi(t) \mapsto \alpha\xi(t/\alpha^2)$ where $\alpha > 0$, then the hulls generated by this driving function are rescaled by a factor α . But when $\xi(t) = \sqrt{\kappa}B(t)$, the rescaled driving process has the same law as the original driving process (lemma B.9). This shows that SLE_κ in \mathbb{H} from 0 to ∞ is scale invariant.

Now let D be a simply connected domain with distinct points a and b on the boundary, and let $f : \mathbb{H} \rightarrow D$ be a conformal map such that $f(0) = a$ and $f(\infty) = b$. Then we define chordal SLE_κ in D from a to b as the image of chordal SLE_κ in \mathbb{H} from 0 to ∞ under the map f . Even though the transformation f is not uniquely determined, this definition makes sense because the transformation f is unique up to composition with a rescaling of the upper half-plane. Conformal invariance of SLE_κ is now a trivial consequence of the definition of SLE_κ in an arbitrary domain.

2.3 Basic properties of the SLE trace

The behaviour of the trace of SLE_κ depends on the value of the parameter κ . One purpose of this section is to point out that we can discern three different phases in the behaviour of this trace, with phase transitions at the values $\kappa = 4$ and $\kappa = 8$. The three different phases were characterised in the same paper of Rohde and Schramm [78] that proves the existence of the SLE trace. A simplified sketch of what the three phases look like is given in figure 2.3.

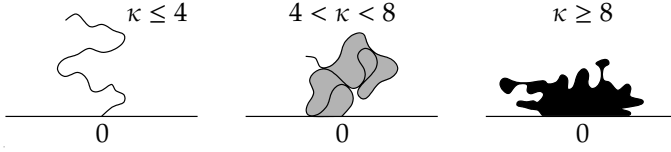


Figure 2.3. Simplified impression of SLE in the three different phases. The trace of the SLE process is shown in black. The union of the black path and the grey areas represents the hull.

For $\kappa \in [0, 4]$ the SLE_κ trace γ is almost surely a simple path, i.e. $\gamma(s) \neq \gamma(t)$ for all $0 \leq t < s$. Moreover, the trace a.s. does not hit the real line but stays in the upper half-plane after time 0. Clearly then, the hulls K_t of the process coincide with $\gamma[0, t]$. It is instructive to consider the proof of these facts, as an illustration of how we can do computations with SLE.

Recall from section 2.1 that a point z is in the hull K_t if and only if $g_s(z)$ has hit $\xi(s)$ before time t . We will prove below that for any given $x \in (0, \infty)$, $g_s(x)$ does not hit $\xi(s)$ in finite time (with probability 1) if $\kappa \leq 4$. This implies that γ does not intersect the interval $[x, \infty)$, for if γ touches the real line in $y > 0$, then all the points to the left of y must be in the hull at that time. Since γ does not intersect $[x, \infty)$ for any $x > 0$, using symmetry this shows that γ never intersects $\mathbb{R} \setminus \{0\}$. By stationarity (lemma 2.3) it follows that γ can not hit its own past after any fixed (rational) time $t > 0$, which implies that γ is a simple path. So it suffices to prove the following:

Theorem 2.4. *Let $\kappa \leq 4$ and $z \in \overline{\mathbb{H}} \setminus \{0\}$. Then with probability 1, $g_t(z) - \xi(t)$ does not hit 0 in finite time.*

Proof. Let us assume first that $z = x + iy \in \mathbb{H}$ and define $X(t) := g_t(z) - \xi(t)$. Note that the differential equation for X reads

$$dX(t) = \frac{2}{X(t)} dt - d\xi(t). \quad (2.13)$$

It is easy to see from this equation that X does not become infinite in finite time. Observe furthermore that the drift term pushes X away from 0, so that $|X|$ can only hit 0 if the diffusion term is strong enough. It therefore suffices to consider only the case $\kappa = 4$.

We will write $f_{a,b}(x + iy)$ for the probability that $|X|$ hits b before a , where $a < |x + iy| < b$. We emphasise that $f_{a,b}$ is a function of both x and y . Our goal is to show that $\lim_{a \rightarrow 0} f_{a,b}(x + iy) = 1$. To find an expression for $f_{a,b}$, suppose that we let the Löwner flow run for an infinitesimal time dt . Then by stationarity (lemma 2.3), the probability that $|X|$ hits b before a is equal

to $f_{a,b}(X(dt))$ averaged over all possible realisations of ξ up to time dt . In other words, $\mathbf{E}[f_{a,b}(X(dt))] = f_{a,b}(x + iy)$. Taking the real and imaginary parts of equation (2.13) and using $\mathbf{E}[\xi(dt)] = 0$, $\mathbf{E}[\xi(dt)^2] = \kappa dt$ we can expand $\mathbf{E}[f_{a,b}(X(dt))]$ to order dt . This shows that $f_{a,b}$ satisfies

$$\left(\frac{2x}{x^2 + y^2}\right) \frac{\partial f_{a,b}(x + iy)}{\partial x} - \left(\frac{2y}{x^2 + y^2}\right) \frac{\partial f_{a,b}(x + iy)}{\partial y} + \frac{\kappa}{2} \frac{\partial^2 f_{a,b}(x + iy)}{\partial x^2} = 0. \quad (2.14)$$

Here we have assumed that $f_{a,b}$ is sufficiently differentiable. Below we shall explain how we can justify this assumption to make the proof rigorous.

For now, let us assume that $f_{a,b}$ does satisfy the given differential equation. It is not difficult to verify that for $\kappa = 4$ the solution is

$$f_{a,b}(x + iy) = \frac{\log|x + iy| - \log a}{\log b - \log a}. \quad (2.15)$$

In the limit $a \rightarrow 0$ we obtain $f_{0,b}(x + iy) = 1$, which shows that with probability 1, $|X|$ hits b before it hits 0. Since b is arbitrary and $|X|$ cannot become infinite in finite time, it follows that a.s. z does not become part of the hull in finite time.

B.4 ◀ To make this rigorous, let us simply *define* $f_{a,b}(x + iy)$ by equation (2.15),
B.6 and let $T := \inf\{t \geq 0 : |X(t)| \in \{a, b\}\}$. Then an application of Itô's formula will show that $f_{a,b} \circ X$ considered up to time T is a bounded martingale. Moreover, it is easy to see that $f_{a,b}(X(T))$ is the indicator of the event that X hits b before a . Now because $f_{a,b} \circ X$ is a bounded martingale up to time T , we may conclude from the optional sampling theorem B.7 that $\mathbf{E}[f_{a,b}(X(T))] = f_{a,b}(x + iy)$, which shows that $f_{a,b}(x + iy)$ is indeed the probability that X hits b before a . This completes the proof in the case $z \in \mathbb{H}$.

The case $z = x \in \mathbb{R} \setminus \{0\}$ can be handled similarly. This time we define $X(t)$ as $g_t(x) - \xi(t)$ and let $f_{a,b}(x)$ denote the probability that $|X|$ will hit b before a . Following the same reasoning as above one can derive the following differential equation for $f_{a,b}$:

$$\frac{2}{x} \frac{\partial f_{a,b}(x)}{\partial x} + \frac{\kappa}{2} \frac{\partial^2 f_{a,b}(x)}{\partial x^2} = 0. \quad (2.16)$$

For $\kappa = 4$ the solution is $f_{a,b}(x) = \log(|x|/a) / \log(b/a)$. In the limit $a \rightarrow 0$ we obtain $f_{0,b}(x) = 1$. The proof is then completed as in the case $z \in \mathbb{H}$. ■

When κ is larger than 4 the trace is no longer simple. In fact, for all $\kappa > 4$ every point $z \in \overline{\mathbb{H}} \setminus \{0\}$ a.s. becomes part of the hull in finite time. For a given point x on the real line this can be seen easily from the proof of theorem 2.4. Indeed, for $\kappa \neq 4$ one may verify that the probability $f_{a,b}(x)$ that $|g_t(x) - \xi(t)|$ hits b before a (where $a < x < b$) becomes

$$f_{a,b}(x) = \frac{|x|^{1-4/\kappa} - a^{1-4/\kappa}}{b^{1-4/\kappa} - a^{1-4/\kappa}}. \quad (2.17)$$

When $\kappa > 4$, taking the limit $a \rightarrow 0$ reveals that for every $\varepsilon > 0$ there is a $b > 0$ such that $|g_t(x) - \xi(t)|$ reaches 0 before b with probability at least $1 - \varepsilon$. From this it follows that almost surely the point x becomes part of the hull after a finite time.

This result can be generalised to points $z \in \mathbb{H}$ [78, lemma 6.5]. It follows that for $\kappa > 4$ every point is either on the trace, or is disconnected from infinity by the trace. But as long as $\kappa < 8$, it can be shown that the former happens with probability zero [78, theorem 6.4]. Hence, for $\kappa \in (4, 8)$ we have a phase where the trace is not dense but does eventually disconnect all points from infinity. In other words, the trace now intersects both itself and the real line, and the hulls K_t consist of the union of the trace $\gamma[0, t]$ and all bounded components of $\overline{\mathbb{H}} \setminus \gamma[0, t]$ (figure 2.3 gives only a crude sketch for the trace in this phase; a more realistic picture for $\kappa = 6$ is provided by figure 1.4 on page 10).

Finally, when $\kappa \geq 8$ the trace becomes dense in \mathbb{H} . In fact, we are then in a phase where $\gamma[0, \infty) = \overline{\mathbb{H}}$ with probability 1 and the hulls K_t coincide with the trace $\gamma[0, t]$ again [78, corollary 7.4]. Since the trace is space-filling in this phase, the Hausdorff dimension of the set $\gamma[0, \infty)$ is 2.

For $\kappa \in (0, 8)$ the Hausdorff dimension of $\gamma[0, \infty)$ is a non-trivial number. Rohde and Schramm [78] showed that its value is bounded from above by $1 + \kappa/8$, and the proof that for $\kappa \neq 4$ the Hausdorff dimension is in fact $1 + \kappa/8$ was completed by Beffara [17, 18]. In the physics literature the Hausdorff dimensions of the paths that are believed to converge to SLE were predicted by Duplantier and Saleur [35, 80]. These predictions can be used to guess the values of κ that correspond to various statistical models.

In the case $\kappa > 4$ the hull of SLE_κ is not a simple path, and it is natural to consider also the Hausdorff dimension of the boundary of K_t for some fixed value of $t > 0$. Its value is conjectured to be $1 + 2/\kappa$, because (based on a duality relation derived by Duplantier [35]) it is believed that the boundary of the hull for $\kappa > 4$ looks locally like an $\text{SLE}_{16/\kappa}$ trace. This duality for SLE was studied in more detail by Dubédat in [32]. The dimension of the hull boundary is known rigorously only for $\kappa = 6$ (where it is $4/3$) and for $\kappa = 8$ (where it is $5/4$). For $\kappa = 6$ this follows from the study of the “conformal restriction measures” in [59], for $\kappa = 8$ this is a consequence of the strong relation between loop-erased random walks and uniform spanning trees [60] (see section 3.2).

2.4 Radial and dipolar SLE

Chordal SLE is a stochastic process which generates a path crossing a given domain between two fixed boundary points. In this section we will introduce

two other versions of SLE, namely radial and dipolar SLE, with different growth conditions on the trace. In radial SLE the trace grows from a given point on the boundary to a given point in the interior of the domain. Dipolar SLE is similar to chordal SLE in the sense that the trace starts and ends on the boundary, except that in dipolar SLE the endpoint is random.

We first consider radial SLE, which is most conveniently defined on the unit disk $\mathbb{D} := \{z \in \mathbb{C} : |z| < 1\}$. In this domain the driving process for the Löwner evolution is a Brownian motion on the unit circle, that is, we take $\xi(t) := \exp(i\sqrt{\kappa}B(t))$. As before, we can take $B(0) = 0$ which will make the trace start from 1, but in some applications it makes sense to take $B(0)$ random with the uniform distribution on $[0, 2\pi)$. Radial SLE_κ is defined as the solution of the Löwner equation

$$\frac{\partial g_t(z)}{\partial t} = g_t(z) \frac{\xi(t) + g_t(z)}{\xi(t) - g_t(z)}; \quad g_0(z) = z; \quad z \in \mathbb{D}. \quad (2.18)$$

As in chordal SLE, for each fixed $z \in \mathbb{D}$ the solution of this equation exists up to the time $T(z)$ which is the first time t such that $\lim_{s \uparrow t} (g_s(z) - \xi(s)) = 0$. If we set

$$H_t := \{z \in \mathbb{D} : T(z) > t\}, \quad K_t := \{z \in \overline{\mathbb{D}} : T(z) \leq t\}, \quad (2.19)$$

then g_t is a conformal map of $\mathbb{D} \setminus K_t = H_t$ onto \mathbb{D} . The normalisation of the maps g_t for radial SLE is given by the conditions $g_t(0) = 0$ and $g'_t(0) > 0$. In fact it is easy to see from the radial Löwner equation that $g'_t(0) = \exp(t)$, which specifies the time-parameterisation.

The trace of radial SLE_κ is defined by $\gamma(t) := \lim_{z \rightarrow 0} g_t^{-1}(z + \xi(t))$, where the limit is to be taken from within the unit disk. The trace grows from the starting point $\xi(0)$ on the boundary to the origin. Given an arbitrary simply connected domain D with fixed points a on the boundary and b in the interior, we define radial SLE_κ in D from a to b as the image of radial SLE_κ in the unit disk (starting from 1) under the unique conformal transformation of \mathbb{D} onto D which maps 1 to a and 0 to b .

Dipolar SLE is a version of SLE introduced by Bauer and Bernard in [11], which fixes two given points on the boundary of a domain. A convenient domain for dipolar SLE is the horizontal strip $\mathbb{S} := \{z \in \mathbb{C} : 0 < \text{Im } z < \pi/2\}$ of height $\pi/2$. The dipolar Löwner equation in the strip which fixes the boundary points at $-\infty$ and $+\infty$ reads

$$\frac{\partial g_t(z)}{\partial t} = \frac{2}{\tanh(g_t(z) - \xi(t))}; \quad g_0(z) = z; \quad z \in \mathbb{S}. \quad (2.20)$$

Dipolar SLE_κ is defined as the solution of this equation, driven by the Brownian motion $\xi(t) := \sqrt{\kappa}B(t)$. The hulls and trace of the process are defined as in chordal and radial SLE.

Exact (deterministic) solutions for the dipolar Löwner equation are given in section 2.C for the driving functions $\xi(t) = 2\alpha t$, $\alpha \geq 0$. As we shall see, for $\alpha < 1$ the trace is a path which intersects the top boundary. However, for $\alpha > 1$ the trace never reaches the top boundary, but instead escapes to ∞ while staying within distance $\pi/(\alpha + 1)$ of the real line. In the case of the Brownian driving process of dipolar SLE_κ , the trace is a path which does not escape to infinity but will land at a random point on the top boundary of the strip. The distribution of this point will be computed in section 4.5. Note that this behaviour of the trace implies that for $\kappa > 4$ the hull of dipolar SLE will not fill the entire domain when $t \rightarrow \infty$, as is the case in chordal SLE.

When it comes to applications to critical models, dipolar SLE is an interesting alternative to chordal SLE. For the Ising model in the strip \mathbb{S} , for instance, it is believed that dipolar SLE_3 describes the scaling limit with positive boundary conditions on the positive reals, negative boundary conditions on the negative reals, and free boundary conditions on the top boundary of the strip. The dipolar SLE_3 path is then the scaling limit of the exploration path between the plus and minus clusters starting from the origin. Note that this path should indeed land at a random point on the top boundary of the strip. For other values of κ the connection of dipolar SLE with critical models can be understood from a CFT interpretation of dipolar SLE, as is explained in [12].

All versions of SLE can be generalised to so-called $\text{SLE}(\kappa, \rho)$ processes, which were introduced for chordal SLE in [32, 59]. A chordal $\text{SLE}(\kappa, \rho)$ process is a version of chordal SLE (defined by equation (2.11)) where the driving process receives an extra drift term. The basic idea is to introduce a “force point” $x \in \mathbb{R}$ and to let $\xi(t)$ be either attracted to or repelled from the point $g_t(x)$ during the evolution. To this end, we define the driving process ξ through the pair of differential equations

$$\begin{cases} d\xi(t) = \sqrt{\kappa} dB(t) + \frac{\rho dt}{\xi(t) - X(t)}; & \xi(0) = 0; \\ dX(t) = \frac{2dt}{X(t) - \xi(t)}; & X(0) = x. \end{cases} \quad (2.21)$$

Here, $X(t)$ can be interpreted as $g_t(x)$. One can show that this definition makes sense for all $\kappa > 0$ and $\rho > -2$. This basic definition of $\text{SLE}(\kappa, \rho)$ can be extended to include more than one force point that may sit in the interior of the domain, see [85].

It turns out that the three different versions of SLE (chordal, radial and dipolar) are very closely related in terms of $\text{SLE}(\kappa, \rho)$ processes. For instance, suppose that ψ is a conformal transformation of \mathbb{H} onto \mathbb{D} such that $\psi(0) = 1$. Let T denote the time at which the point $\psi^{-1}(0)$ becomes part of the hull of chordal SLE_κ . Then up to the time T , the image of chordal SLE_κ under ψ is (modulo a time-change) a radial $\text{SLE}(\kappa, \kappa - 6)$ process with a force point at $\psi(\infty)$. Similar relations hold between chordal and dipolar SLE, and between

radial and dipolar SLE. This unifying framework between the different versions of SLE was introduced by Schramm and Wilson in [85].

For us, the most important conclusion from this unifying framework is that the three different versions of SLE define laws on random paths that are equivalent in a sense described first in [55] and explained in greater depth in [92]. Loosely speaking, the traces generated by different versions of SLE_κ “look the same”. In particular, the traces have the same Hausdorff dimension. Also, in each version of SLE we can discern the same three phases with phase transitions at $\kappa = 4$ and $\kappa = 8$. This assures us that the different versions of SLE at the same value of κ all relate to the same critical model (but with different boundary conditions).

2.A Löwner's differential equation

In this section we derive Löwner's differential equation in the upper half-plane, and then we will prove that this differential equation generates a family of growing hulls when it is driven by a continuous real-valued function ξ . Here we will use properties of half-plane capacity from section A.5 of appendix A. A slightly more general theorem is proved in [55, theorem 2.6], using similar ideas. To derive Löwner's equation, suppose that we are given a path $\gamma : [0, T) \rightarrow \overline{\mathbb{H}}$ satisfying the conditions discussed in section 2.1. Let $(K_t : t \in [0, T))$ and $(g_t : t \in [0, T))$ be the corresponding families of hulls and conformal maps, and set $\xi(t) := g_t(\gamma(t))$. Then the following holds:

Theorem 2.5. *Both $\text{cap}_{\mathbb{H}}(K_t)$ and $\xi(t)$ are continuous in t .*

A.2 ◀ **Proof.** The proof uses properties of extremal length discussed in appendix A, **A.5** section A.2. We shall only show left-continuity of $\text{cap}_{\mathbb{H}}(K_t)$ and $\xi(t)$, but right-continuity can be shown in the same way. Without loss of generality we may assume that $\gamma(0) = 0$. Fix $a \in [0, T)$, let $R := \sup\{|z| : z \in K_a\}$ be the radius of K_a and set $Q := \{z \in \mathbb{H} : |z| > 2R\}$. Let $t \in [0, a]$ be fixed. Then for each $r > 0$, we shall denote by C_r the circle of radius r centred at $\gamma(t)$.

Now choose an $\varepsilon > 0$, and set $S := C_\varepsilon \cap H_t$, where $H_t := \mathbb{H} \setminus K_t$. Then by continuity of γ , there exists a $\delta > 0$ such that S disconnects $K_t \setminus K_{t-\delta}$ from Q in the domain $H_{t-\delta}$. See figure 2.4. Observe that the set $K_t \setminus K_{t-\delta}$ may be just a piece of γ , but that it can also be much larger when γ has a self-intersection or an intersection with the real line in the interval $[t - \delta, t]$, as in figure 2.4. Since every rectifiable arc in $H_{t-\delta}$ that connects $K_t \setminus K_{t-\delta}$ to Q contains a subarc connecting C_ε to C_R in \mathbb{C} , the extremal distance \mathcal{L} between $K_t \setminus K_{t-\delta}$ and Q in $H_{t-\delta}$ is at least $\log(R/\varepsilon)/2\pi$. Note that by conformal invariance, \mathcal{L} is also the extremal distance between $K_{t,\delta} := g_{t-\delta}(K_t \setminus K_{t-\delta})$ and $g_{t-\delta}(Q)$ in \mathbb{H} .

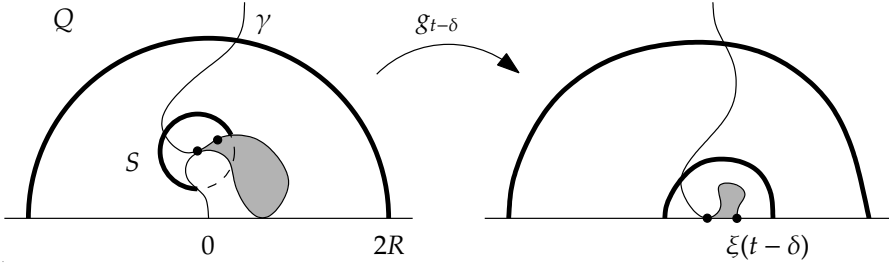


Figure 2.4. A path γ with two points representing $\gamma(t)$ and $\gamma(t-\delta)$, and the L\"owner map $g_{t-\delta}$. The shaded areas are the set $K_t \setminus K_{t-\delta}$ and its image.

By corollary A.19, the distance from $\xi(t-\delta)$ to $g_{t-\delta}(Q)$ is at most $3R$. Now let $r := \sup\{|z - \xi(t-\delta)| : z \in K_{t,\delta}\}$. Then Teichm\"uller's theorem A.7 implies that $\mathcal{L} \leq 2\Lambda(3R/r) \leq \log(64R/r)/\pi$, where Λ is the modulus of the Teichm\"uller annulus. If we combine this with the inequality $\mathcal{L} \geq \log(R/\varepsilon)/2\pi$ from the previous paragraph, it follows that the set $K_{t,\delta}$ is contained in a half-disk centred at $\xi(t-\delta)$ whose radius is $O(\varepsilon^{1/2})$. Hence, by the summation rule of capacity, $\text{cap}_{\mathbb{H}}(K_t) - \text{cap}_{\mathbb{H}}(K_{t-\delta}) = \text{cap}_{\mathbb{H}}(K_{t,\delta}) = O(\varepsilon)$ (equation (A.20) and theorem A.18), proving left-continuity of $\text{cap}_{\mathbb{H}}(K_t)$.

To prove left-continuity of $\xi(t)$, let δ and ε be as above, and denote by $g_{t,\delta}$ the normalised map $g_{K_{t,\delta}}$ associated with the hull $K_{t,\delta}$. Corollary A.19 shows that $|g_{t,\delta}(z + \xi(t-\delta)) - (z + \xi(t-\delta))| = O(\varepsilon^{1/2})$ for all $z \in \mathbb{H} \setminus K_{t,\delta}$. In other words, $g_{t,\delta}$ converges uniformly to the identity as $\delta \rightarrow 0$, which proves left-continuity of $\xi(t)$ (remember that $\xi(t)$ is defined as $g_t(\gamma(t))$ and refer to figure 2.4). In the same way one can prove right-continuity of $\text{cap}_{\mathbb{H}}(K_t)$ and $\xi(t)$. \blacksquare

Theorem 2.6. *Assume that the time parameterisation of γ is chosen such that $\text{cap}_{\mathbb{H}}(K_t) = 2t$ for $t \in [0, T)$ (note that this is possible by theorem 2.5). Consider a fixed point $z \in \mathbb{H}$, and define the time $T(z) := \inf\{t \in [0, T) : z \in K_t\}$, setting $T(z) := T$ if $z \notin \cup_{t \in [0, T)} K_t$. Then for $0 < t < T(z)$, $g_t(z)$ satisfies the L\"owner differential equation*

$$\frac{\partial g_t(z)}{\partial t} = \frac{2}{g_t(z) - \xi(t)}; \quad g_0(z) = z. \quad (2.22)$$

A.5 \blacktriangleleft **Proof.** Our proof is based on the proof of theorem 2.5 and the Poisson integral formula (theorem A.20), which implies that the map $g_{t,\delta}$ satisfies

$$g_{t,\delta}(z) - z = \frac{1}{\pi} \int_{-\infty}^{\infty} \frac{\text{Im } g_{t,\delta}^{-1}(x)}{g_{t,\delta}(z) - x} dx; \quad z \in \mathbb{H} \setminus K_{t,\delta}, \quad (2.23)$$

while the capacity $\text{cap}_{\mathbb{H}}(K_{t,\delta})$ is given by the integral

$$\text{cap}_{\mathbb{H}}(K_{t,\delta}) = \frac{1}{\pi} \int_{-\infty}^{\infty} \text{Im } g_{t,\delta}^{-1}(x) dx. \quad (2.24)$$

First consider the left-derivative of $g_t(z)$. Using the same notations as in the proof of theorem 2.5 we can write $g_t = g_{t,\delta} \circ g_{t-\delta}$. We know that $g_{t,\delta}$ converges to the identity as $\delta \rightarrow 0$, and that the set $\{x \in \mathbb{R} : \text{Im } g_{t,\delta}^{-1}(x) > 0\}$ shrinks to the point $\xi(t)$. Moreover, using the summation rule (A.20) of capacity, equation (2.24) gives $\int \text{Im } g_{t,\delta}^{-1}(x) dx = 2\pi\delta$. Hence from equation (2.23) we obtain

$$\lim_{\delta \rightarrow 0} \frac{g_t(z) - g_{t-\delta}(z)}{\delta} = \lim_{\delta \rightarrow 0} \frac{1}{\pi\delta} \int_{-\infty}^{\infty} \frac{\text{Im } g_{t,\delta}^{-1}(x)}{g_t(z) - x} dx = \frac{2}{g_t(z) - \xi(t)}. \quad (2.25)$$

In the same way one obtains the right-derivative. ■

These two theorems show how one can encode a path γ by a real-valued function ξ using Löwner's differential equation. Next we are going to show that oppositely, a real-valued function ξ can be used to drive Löwner's differential equation to obtain a family of growing hulls. This family of hulls, however, does not necessarily correspond to the hulls generated by a continuous path γ , as we already discussed in section 2.1.

Theorem 2.7. *Let $\xi : [0, T) \rightarrow \mathbb{R}$ be continuous, and for every $t \in [0, T)$ let $g_t(z)$ be the solution of the Löwner equation (2.22). Introduce for each fixed $z \in \mathbb{H} \setminus \{0\}$ the time*

$$T(z) := \inf \left\{ t \in [0, T) : \lim_{s \uparrow t} (g_s(z) - \xi(s)) = 0 \right\}, \quad (2.26)$$

setting $T(z) := T$ if $g_t(z)$ never hits $\xi(t)$. If we define

$$H_t := \{z \in \mathbb{H} : T(z) > t\}, \quad K_t := \{z \in \overline{\mathbb{H}} : T(z) \leq t\}, \quad (2.27)$$

then $g_t(z)$ is a conformal map of the domain $H_t = \mathbb{H} \setminus K_t$ onto \mathbb{H} which satisfies

$$g_t(z) = z + \frac{2t}{z} + O(z^{-2}), \quad z \rightarrow \infty. \quad (2.28)$$

Proof. It is easy to see from Löwner's equation (2.22) that g_t is analytic on H_t . We will prove (i) that the map g_t is conformal on the domain H_t , (ii) that this map is of the form (2.28), and (iii) that $g_t(H_t) = \mathbb{H}$.

To prove (i), we have to verify that g_t has nonzero derivative on H_t and is injective. So consider equation (2.22) for times $t < T(z)$. Then the differential equation behaves nicely, and we can differentiate with respect to z to obtain

$$\frac{\partial \log g'_t(z)}{\partial t} = -\frac{2}{(g_t(z) - \xi(t))^2}. \quad (2.29)$$

This gives $|\partial_t \log g'_t(z)| \leq 2/[\text{Im } g_t(z)]^2$. But from considering the imaginary part of (2.22) it is clear that $t \mapsto \text{Im } g_t(z)$ is strictly decreasing. Hence, if we fix $t_0 < T(z)$, then the change in $\log g'_t(z)$ is uniformly bounded for all times $t < t_0$. It follows that $\log g'_{t_0}(z)$ is well-defined and bounded and hence, that $g'_t(z)$ is well-defined and nonzero for all $t < T(z)$.

Next, choose two different points $z, w \in \mathbb{H}$ and let $t < \min\{T(z), T(w)\}$. Then

$$\frac{\partial \log[g_t(z) - g_t(w)]}{\partial t} = -\frac{2}{(g_t(z) - \xi(t))(g_t(w) - \xi(t))}. \quad (2.30)$$

It follows that $g_t(z) \neq g_t(w)$ for all $t < \min\{T(z), T(w)\}$, using a similar argument as in the previous paragraph. We conclude that $g_t(z)$ is conformal on the domain H_t .

For the proof of (ii), we note that (i) implies that the map $g_t(z)$ can be expanded for $z \rightarrow \infty$. We can determine the form of the expansion by integrating the Löwner differential equation from 0 to t . This yields

$$g_t(z) - z = \int_0^t \frac{2ds}{g_s(z) - \xi(s)}. \quad (2.31)$$

Consider this equation in the limit $z \rightarrow \infty$. Then it is easy to see that the expansion of $g_t(z)$ has no terms of quadratic or higher power in z , and no constant term. The form (2.28) follows immediately.

Finally, we prove (iii), i.e. we will show that $g_t(H_t) = \mathbb{H}$. To see this, let w be any fixed point in \mathbb{H} , and let t_0 be a fixed time. Define $h_t(w)$ for $0 \leq t \leq t_0$ as the solution of the problem

$$\frac{\partial h_t(w)}{\partial t} = -\frac{2}{h_t(w) - \xi(t_0 - t)}; \quad h_0(w) = w. \quad (2.32)$$

The imaginary part of this equation shows that $\partial_t \text{Im } h_t(w) > 0$ and hence, that $\text{Im } h_t(w)$ is increasing in time. Since $|\partial_t h_t(w)| \leq 2/\text{Im } h_t(w)$, it follows that $h_t(w)$ is well-defined for all $0 \leq t \leq t_0$.

Now set $z := h_{t_0}(w)$ and $\tilde{g}_t(z) := h_{t_0-t}(w)$. Then it follows from the differential equation for $h_t(w)$ that $\tilde{g}_t(z)$ satisfies equation (2.22). In other words, $h_t(w)$ describes the inverse of the Löwner flow (2.22) starting from $z = h_{t_0}(w) \in H_{t_0}$. We conclude that for all $w \in \mathbb{H}$ there exists a $z \in H_{t_0}$ such that $g_{t_0}(z) = w$. This completes the proof. \blacksquare

We conclude this section with an interesting observation which follows from the last two paragraphs of the previous proof. Namely, suppose that for $0 \leq t \leq t_0$ we set $\xi(-t) := \xi(t_0 - t)$, and we run the Löwner evolution (2.22) in

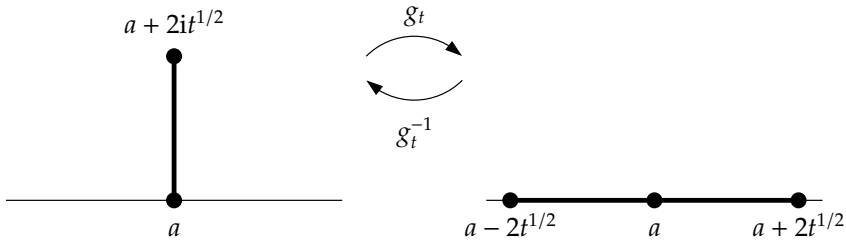


Figure 2.5. The trace for chordal Löwner evolution with a constant driving function $\xi(t) = a$ is a vertical line segment.

the negative time direction up to time $-t_0$. Then by what we said above, for each fixed $w \in \mathbb{H}$, $g_t(g_{-t_0}(w))$ is the Löwner flow from $g_{-t_0}(w)$ to w in the time interval $[0, t_0]$. In particular, $g_{t_0}(g_{-t_0}(w)) = w$, which shows that g_{-t_0} is exactly the inverse of the conformal transformation g_{t_0} .

Thus, the inverse mappings g_t^{-1} of the Löwner transformations g_t may be obtained by running the Löwner evolution backwards in time. In the case of SLE, this implies that if we take ξ to be two-sided Brownian motion (i.e. Brownian motion both in the forward time direction and in the backward time direction starting from 0) multiplied by \sqrt{k} , then the solution of Löwner’s equation at time $-t$ has exactly the law of the inverse of the solution at time t . This observation plays a central role in Rohde and Schramm’s paper [78].

2.B Solutions for chordal Löwner evolutions

In this section we shall find exact solutions for chordal Löwner evolutions for various driving functions. These exact solutions provide illustrative examples of the connection between driving functions for the Löwner equation and the paths encoded by these driving functions. Each driving function for which we have an exact solution is considered in a separate subsection.

2.B.1 Constant driving function

Here we look at the driving function $\xi(t) = a$, where $a \in \mathbb{R}$. In this case the solution of the chordal Löwner equation is easily seen to be

$$g_t(z) = a + [(z - a)^2 + 4t]^{1/2}. \tag{2.33}$$

The inverse map has the same form as the direct one, namely

$$g_t^{-1}(w) = a + [(w - a)^2 - 4t]^{1/2}, \tag{2.34}$$

from which we obtain for the trace of the Löwner evolution

$$\gamma(t) := g_t^{-1}(a) = a + 2it^{1/2}. \quad (2.35)$$

We conclude that for a constant driving function, the trace of the chordal Löwner evolution is a vertical line segment growing towards infinity. The map g_t maps the complement of the segment $\gamma[0, t]$ in the half-plane onto the half-plane. Observe that under this transformation, the left side of $\gamma[0, t]$ is mapped to the left of a , and the right side is mapped to the right of a . See figure 2.5 for an illustration.

2.B.2 Linear driving function

Next we consider the case of the linear driving function $\xi(t) = t$. Note that other linear driving functions are covered by the scaling and translation relations of equations (2.7) and (2.8). For $\xi(t) = t$, if we define $F(z) := z + 2 \log(2 - z)$, then a simple computation shows that $F(g_t(z) - t)$ satisfies

$$\frac{\partial F(g_t(z) - t)}{\partial t} = -1. \quad (2.36)$$

Integrating this equation with the initial condition $g_0(z) = z$ gives

$$F(g_t(z) - t) = F(z) - t. \quad (2.37)$$

For the trace of this Löwner evolution we must have $g_t(\gamma(t)) = t$, so that the trace is given by the solution of the equation

$$F(\gamma(t)) = F(0) + t = 2 \log 2 + t. \quad (2.38)$$

More insight can be gained by finding an explicit parametric expression for the trajectory $\gamma(t)$ in the following way. First we substitute the polar representation $2 - \gamma(t) = r(t) \exp(-i\varphi(t))$ into equation (2.38). Then we split the result in its real and imaginary parts to obtain

$$\begin{cases} 2 \log r(t) - r(t) \cos \varphi(t) = 2 \log 2 + t - 2; \\ r(t) = 2\varphi(t) / \sin \varphi(t). \end{cases} \quad (2.39)$$

Substituting the second of these equations into the first gives

$$\log \frac{\varphi(t)}{\sin \varphi(t)} - \frac{\varphi(t) \cos \varphi(t)}{\sin \varphi(t)} = \frac{1}{2}t - 1. \quad (2.40)$$

We want to show from this equation that $\varphi(t)$ increases monotonously with time from $\varphi(0) = 0$ to $\varphi(\infty) = \pi$.

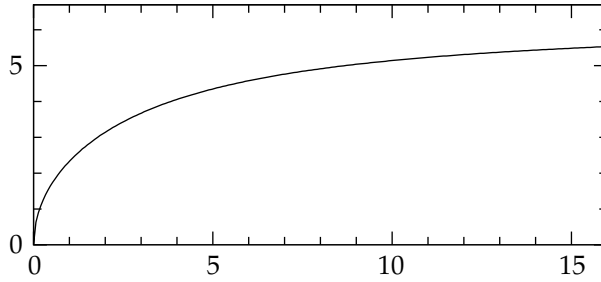


Figure 2.6. The trace for the driving function $\xi(t) = t$ displayed up to the time $t = 20$.

To do so, we differentiate with respect to $\varphi = \varphi(t)$. This gives

$$\frac{1}{2} \frac{dt}{d\varphi} = \frac{\sin^2 \varphi - 2\varphi \cos \varphi \sin \varphi + \varphi^2}{\varphi \sin^2 \varphi}. \tag{2.41}$$

For $0 < \varphi < \pi$, the denominator of this expression is positive, and it only remains to show that the numerator is positive as well. This is easily shown by taking the derivative of the numerator with respect to φ , which is positive for $0 < \varphi < \pi$. Since the numerator is 0 for $\varphi = 0$, we find that φ is indeed monotonously increasing with t from 0 to π .

We then conclude from equation (2.39) that in terms of the parameter $\varphi(t)$, the trace of the Löwner evolution can be written as

$$\gamma(t) = 2 - 2\varphi(t) \cot \varphi(t) + 2i\varphi(t). \tag{2.42}$$

Thus, the trace is a path which moves outward to infinity but stays within fixed distance of the real axis. Figure 2.6 shows what this trace looks like.

2.B.3 Increasing square-root driving function

Here we consider the driving function $\xi(t) = 2(\kappa t)^{1/2}$, where $\kappa \geq 0$. The scaling equation (2.7) for chordal Löwner evolutions already shows that in this case the trace must be a straight half-line emanating from the origin. Below we will determine the angle at which this trace is set to the real axis in terms of the parameter κ , and the speed at which the trace grows towards infinity. We settle these issues by solving the Löwner equation.

To find the solution of Löwner’s equation, we define $G_t(z) := g_t(z)/t^{1/2}$. Then $G = G_t(z)$ satisfies

$$t \frac{\partial G}{\partial t} = -\frac{G}{2} + \frac{2}{G - 2\kappa^{1/2}} = \frac{(G - y_+)(G - y_-)}{2(2\kappa^{1/2} - G)}, \tag{2.43}$$

where $y_{\pm} = y_{\pm}(\kappa) = \kappa^{1/2} \pm (\kappa + 4)^{1/2}$. It follows that

$$t \frac{\partial G}{\partial t} \left[\frac{y_-}{G - y_+} - \frac{y_+}{G - y_-} \right] = \frac{1}{2}(y_+ - y_-). \quad (2.44)$$

Therefore, if we set

$$H(G) := \frac{2y_+ \log(G - y_-) - 2y_- \log(G - y_+)}{y_+ - y_-}, \quad (2.45)$$

then $t\partial H(G)/\partial t = -1$ which integrates to

$$-H(G) = \log t + c(z). \quad (2.46)$$

To determine the constant $c(z)$, observe that when t approaches 0,

$$H(G) + \log t = \frac{2y_+ \log(g_t(z) - y_- t^{1/2}) - 2y_- \log(g_t(z) - y_+ t^{1/2})}{y_+ - y_-} \rightarrow 2 \log z. \quad (2.47)$$

Therefore, our solution (2.46) becomes

$$H(g_t(z)/t^{1/2}) = 2 \log(z/t^{1/2}). \quad (2.48)$$

Substituting the condition $g_t(\gamma(t)) = \xi(t)$ we obtain for the trace of the Löwner evolution the expression

$$\gamma(t) = Bt^{1/2} \quad \text{where} \quad B = \exp\left[\frac{1}{2}H(2\kappa^{1/2})\right]. \quad (2.49)$$

More explicitly the coefficient is

$$B = 2 \left(\frac{(\kappa + 4)^{1/2} + \kappa^{1/2}}{(\kappa + 4)^{1/2} - \kappa^{1/2}} \right) \frac{1}{2} \left(\frac{\kappa}{\kappa + 4} \right)^{1/2} \exp \left[\frac{1}{2} \pi i \left(1 - \left(\frac{\kappa}{\kappa + 4} \right)^{1/2} \right) \right], \quad (2.50)$$

so that the trace is set at an angle ϑ to the real axis which is

$$\vartheta = \frac{1}{2} \pi \left(1 - \left(\frac{\kappa}{\kappa + 4} \right)^{1/2} \right). \quad (2.51)$$

For $\kappa = 0$ the line is (as we know) perpendicular to the real axis while as $\kappa \rightarrow \infty$ the angle of intersection becomes smaller and smaller.

2.B.4 Decreasing square-root driving function

We now come to the most interesting case for which we can obtain an exact solution, namely the Löwner evolution for a driving function which has a square-root singularity after a finite time. To be precise, we take as our driving

function $\xi(t) = 2[\kappa(1-t)]^{1/2}$ where $\kappa \geq 0$ and $t \leq 1$. To find the solution for this case, we define $G_t(z) := g_t(z)/(1-t)^{1/2}$. Then $G = G_t(z)$ satisfies

$$(1-t)\frac{\partial G}{\partial t} = \frac{G}{2} + \frac{2}{G-2\kappa^{1/2}} = -\frac{(G-y_+)(G-y_-)}{2(2\kappa^{1/2}-G)}, \quad (2.52)$$

where $y_{\pm} = y_{\pm}(\kappa) = \kappa^{1/2} \pm (\kappa-4)^{1/2}$. Observe that the coefficients y_{\pm} are real and positive for $\kappa \geq 4$, but complex for $\kappa < 4$. Therefore, we expect a qualitative change in the solution at $\kappa = 4$.

We further observe that equation (2.52) closely resembles equation (2.43). From this we see that in the present case the solution becomes

$$H(g_t(z)/(1-t)^{1/2}) = -\log(1-t) + H(z), \quad (2.53)$$

where H is given by the same equation as before, but with different y_{\pm} :

$$H(G) := \frac{2y_+ \log(G-y_-) - 2y_- \log(G-y_+)}{y_+ - y_-}. \quad (2.54)$$

The trace of the Löwner evolution is then given by the equation

$$H(2\kappa^{1/2}) = -\log(1-t) + H(\gamma(t)). \quad (2.55)$$

Note that this equation tells us that $H(\gamma(t))$ must approach $-\infty$ when t approaches 1. Below we shall consider the behaviour of the trace in more detail for the three separate cases $\kappa < 4$, $\kappa > 4$ and $\kappa = 4$.

Logarithmic spirals for $\kappa < 4$

When $\kappa < 4$, the real and imaginary parts of $H(z)$ are

$$\begin{aligned} \operatorname{Re} H(z) &= \left(\frac{\kappa}{4-\kappa}\right)^{1/2} \operatorname{Arg}(z-y_-) + \log|z-y_-| \\ &\quad - \left(\frac{\kappa}{4-\kappa}\right)^{1/2} \operatorname{Arg}(z-y_+) + \log|z-y_+|, \end{aligned} \quad (2.56)$$

$$\begin{aligned} \operatorname{Im} H(z) &= \operatorname{Arg}(z-y_-) - \left(\frac{\kappa}{4-\kappa}\right)^{1/2} \log|z-y_-| \\ &\quad + \operatorname{Arg}(z-y_+) + \left(\frac{\kappa}{4-\kappa}\right)^{1/2} \log|z-y_+|, \end{aligned} \quad (2.57)$$

from which it follows that $H(2\kappa^{1/2})$ is a positive real constant. Since the real part of $H(\gamma(t))$ must go to $-\infty$ when t approaches 1 we conclude that $\gamma(1) = y_+$, since the other possible candidate for the limit, y_- , is in the wrong half-plane.

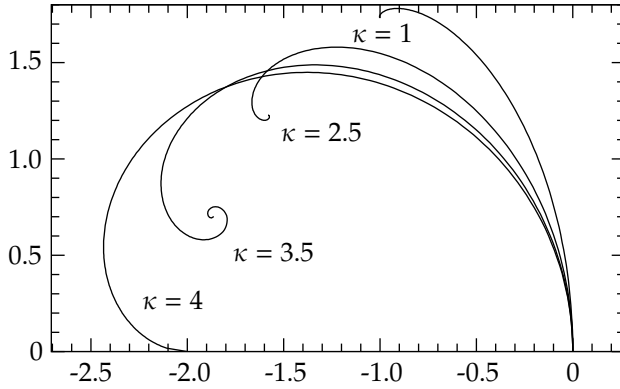


Figure 2.7. The trace for the square-root driving function given by $\xi(t) = 2[\kappa(1-t)]^{1/2} - 2\kappa^{1/2}$ is spiralling in for $\kappa < 4$. For $\kappa = 4$ the trace starts to intersect the real line. Note that the traces have been shifted to the left compared to the solution in the text.

It then follows from the observation that $\text{Im}H(\gamma(t))$ must vanish, that the trace must have wrapped around y_+ an infinite number of times. Hence, the trace is spiralling in towards the point y_+ . This is shown in figure 2.7.

To find a more explicit expression for the asymptotics, notice that when $\gamma(t)$ is close to y_+ we can make the approximations

$$\log |\gamma(t) - y_-| \approx \log 2(4 - \kappa)^{1/2}, \quad (2.58)$$

$$\text{Arg} |\gamma(t) - y_-| \approx \pi/2. \quad (2.59)$$

Splitting equation (2.55) in its real and imaginary parts, and substituting the above approximate values then gives a system of two equations that we can solve for the unknowns $\log |\gamma(t) - y_+|$ and $\text{Arg}(\gamma(t) - y_+)$. This gives the result

$$\log |\gamma(t) - y_+| \approx [A(\kappa) + (4 - \kappa) \log(1 - t)]/4, \quad (2.60)$$

$$\text{Arg}(\gamma(t) - y_+) \approx [B(\kappa) - \kappa^{1/2}(4 - \kappa)^{1/2} \log(1 - t)]/4, \quad (2.61)$$

where the constants are

$$A(\kappa) = \log 16 + (\kappa - 2) \log(4 - \kappa) + (2 \text{Arg}(y_+) - \pi) \kappa^{1/2} (4 - \kappa)^{1/2}, \quad (2.62)$$

$$B(\kappa) = \kappa^{1/2} (4 - \kappa)^{1/2} \log(4 - \kappa) + (\pi - 2 \text{Arg}(y_+)) \kappa - 2\pi. \quad (2.63)$$

Thus, the distance between $\gamma(t)$ and y_+ decreases like a power law with t , whereas the winding number of $\gamma(t)$ around y_+ grows only logarithmically.

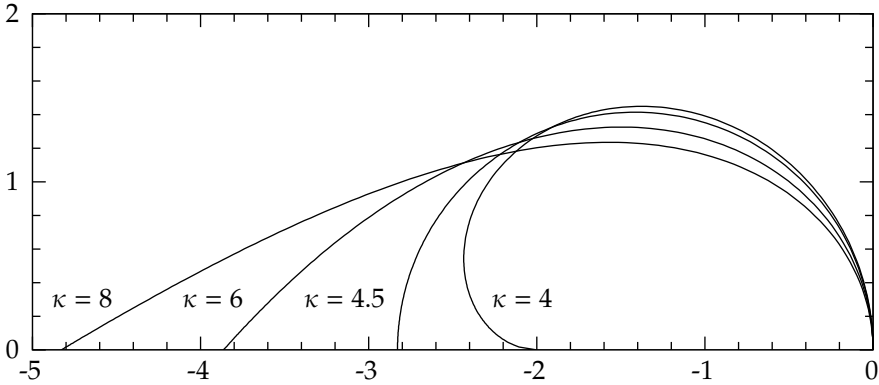


Figure 2.8. For $\kappa \geq 4$, the trace for a square-root driving function $\xi(t) = 2[\kappa(1-t)]^{1/2} - 2\kappa^{1/2}$ intersects the real line at an angle which varies with κ . Note that again the traces have been shifted to the left compared to the solution in the text.

Intersection with the real axis for $\kappa > 4$

For $\kappa > 4$ the real and imaginary parts of $H(z)$ are

$$\operatorname{Re} H(z) = \left(1 + \left(\frac{\kappa}{\kappa - 4}\right)^{1/2}\right) \log|z - y_-| + \left(1 - \left(\frac{\kappa}{\kappa - 4}\right)^{1/2}\right) \log|z - y_+|, \quad (2.64)$$

$$\operatorname{Im} H(z) = \left(1 + \left(\frac{\kappa}{\kappa - 4}\right)^{1/2}\right) \operatorname{Arg}(z - y_-) + \left(1 - \left(\frac{\kappa}{\kappa - 4}\right)^{1/2}\right) \operatorname{Arg}(z - y_+), \quad (2.65)$$

and $H(2\kappa^{1/2})$ is again a positive real number. This time, as t approaches 1, $\gamma(t)$ must approach the point y_- on the real line. See figure 2.8. In fact, we can calculate the angle at which the trace intersects the real line from the observation that $\operatorname{Im} H(\gamma(t))$ must vanish.

Indeed, if we denote by $\varphi = \varphi(\kappa)$ the angle at which $\gamma(t)$ hits the real line, then we have that as $t \rightarrow 1$, $\operatorname{Arg}(\gamma(t) - y_+) \rightarrow \pi$ whereas $\operatorname{Arg}(\gamma(t) - y_-) \rightarrow \varphi$. The condition $\operatorname{Im} H(\gamma(t)) = 0$ then gives

$$\varphi = \pi \frac{\kappa^{1/2} - (\kappa - 4)^{1/2}}{\kappa^{1/2} + (\kappa - 4)^{1/2}}. \quad (2.66)$$

As we can see, we have a glancing incidence for $\kappa = 4$ and $\kappa \rightarrow \infty$, while for $\kappa = 9/2$ the incidence is perpendicular. The case $\kappa = 9/2$ is somewhat special, since for this value of κ we may show explicitly that $\gamma[0, 1]$ is a half-circle, as we shall discuss next.

First observe that for $\kappa = 9/2$, $y_- = \sqrt{2}$ and $y_+ = 2\sqrt{2}$. Substituting these

values into expression (2.54) for H , we see that equation (2.55) becomes

$$\log \frac{(\gamma(t) - \sqrt{2})^2}{\gamma(t) - 2\sqrt{2}} = \log(4\sqrt{2}(1-t)^{1/2}). \quad (2.67)$$

This in turn gives us a quadratic equation for $\gamma(t)$:

$$\gamma(t)^2 - 2\sqrt{2}(1+2(1-t)^{1/2})\gamma(t) + 2 + 16(1-t)^{1/2} = 0. \quad (2.68)$$

To solve this equation, we substitute $\gamma(t) = x(t) + iy(t)$ and split the result in its real and imaginary parts. From the imaginary part we readily obtain

$$x(t) = 2\sqrt{2}(1-t)^{1/2} + \sqrt{2}. \quad (2.69)$$

Using this expression for $x(t)$ in the real part, it follows that $y(t)$ satisfies the equation

$$y(t)^2 + (x(t) - 2\sqrt{2})^2 = 2. \quad (2.70)$$

We conclude that between times 0 and 1, γ traces out a half-circle of radius $\sqrt{2}$ with its centre at the point $2\sqrt{2}$.

The critical curve for $\kappa = 4$

Another special case for which we can obtain an explicit expression for the trace γ is the case $\kappa = 4$. In this case, equation (2.52) may be rewritten as

$$(1-t) \frac{\partial G}{\partial t} \left[\frac{2}{G-2} - \frac{4}{(G-2)^2} \right] = 1. \quad (2.71)$$

Integration is straightforward and gives

$$2 \log(G_t(z) - 2) + \frac{4}{G_t(z) - 2} = -\log(1-t) + 2 \log(z-2) + \frac{4}{z-2}, \quad (2.72)$$

where we have determined the integration constant from the initial condition $G_0(z) = z$. The trace is determined by the condition that $G_t(\gamma(t)) = 4$.

Substituting $\gamma(t) - 2 = r(t) \exp(i\varphi(t))$ and splitting the equation in real and imaginary parts leads to the expression

$$\gamma(t) = 2 + \frac{\sin 2\varphi(t)}{\varphi(t)} + 2i \frac{\sin^2 \varphi(t)}{\varphi(t)} \quad (2.73)$$

for the critical curve in terms of the parameter $\varphi(t)$. Here, φ is a function which increases with time from $\varphi(0) = 0$ to $\varphi(1) = \pi$ (this follows from the same reasoning as for the linear driving function considered in section 2.B.2).

2.C Solutions for dipolar Löwner evolutions

In section 2.B we studied exact solutions of the chordal Löwner equation for various driving functions. For the radial and dipolar Löwner equations examples of exact solutions seem harder to obtain. For the radial equation, an exact solution for which the Löwner equation does not generate a simple slit was given by Kufarev [51]. In this section we shall derive exact solutions for the dipolar Löwner equation in the strip $\mathbb{S} = \{z \in \mathbb{C} : 0 < \text{Im } z < \pi/2\}$ for linear driving functions $\xi(t) = 2\alpha t$, $\alpha \geq 0$. We shall see that there is a qualitative change in the solution at $\alpha = 1$.

Let us assume first that $\alpha \neq 1$, and consider the dipolar Löwner equation

$$\frac{\partial g_t(z)}{\partial t} = \frac{2}{\tanh(g_t(z) - \xi(t))}; \quad g_0(z) = z. \quad (2.74)$$

Setting $f_t(z) := g_t(z) - \xi(t)$, it is easily verified that $f_t(z)$ satisfies

$$\frac{\tanh f_t(z)}{1 - \alpha \tanh f_t(z)} \frac{\partial f_t(z)}{\partial t} = \frac{\sinh f_t(z)}{\cosh f_t(z) - \alpha \sinh f_t(z)} \frac{\partial f_t(z)}{\partial t} = 2. \quad (2.75)$$

A straightforward computation then shows that

$$\frac{\partial}{\partial t} \left(\log[\cosh f_t(z) - \alpha \sinh f_t(z)] + \alpha f_t(z) \right) = 2(1 - \alpha^2), \quad (2.76)$$

and hence using $f_0(z) = z$ we obtain the solution

$$\log \left(\frac{\cosh f_t(z) - \alpha \sinh f_t(z)}{\cosh z - \alpha \sinh z} \right) + \alpha(f_t(z) - z) = 2(1 - \alpha^2)t. \quad (2.77)$$

To find the trace γ we substitute $\gamma(t)$ for z in the previous expression, use the fact that $f_t(\gamma(t)) = 0$, and exponentiate on both sides to obtain

$$\frac{1}{2}(1 - \alpha)e^{(\alpha+1)\gamma(t)} + \frac{1}{2}(1 + \alpha)e^{(\alpha-1)\gamma(t)} = e^{2(\alpha^2-1)t}. \quad (2.78)$$

To see that this expression implies a qualitative change in the behaviour of $\gamma(t)$ at $\alpha = 1$, let us consider the limit $t \rightarrow \infty$. For $\alpha < 1$, the right-hand side of (2.78) tends to zero, from which it is then easily seen that

$$\lim_{t \rightarrow \infty} \gamma(t) = \frac{1}{2} \log \left(\frac{1 + \alpha}{1 - \alpha} \right) + i \frac{\pi}{2}; \quad \alpha < 1. \quad (2.79)$$

Hence, the trace intersects the top boundary of the strip. On the other hand, when $\alpha > 1$ the right-hand side of (2.78) tends to ∞ as $t \rightarrow \infty$. It then follows that in the left-hand side of (2.78), $\text{Re } \gamma(t)$ must tend to ∞ as well, while $\text{Im } \gamma(t) \rightarrow \pi/(1 + \alpha)$ because $\exp((\alpha + 1)\gamma(t))$ dominates $\exp((\alpha - 1)\gamma(t))$. This

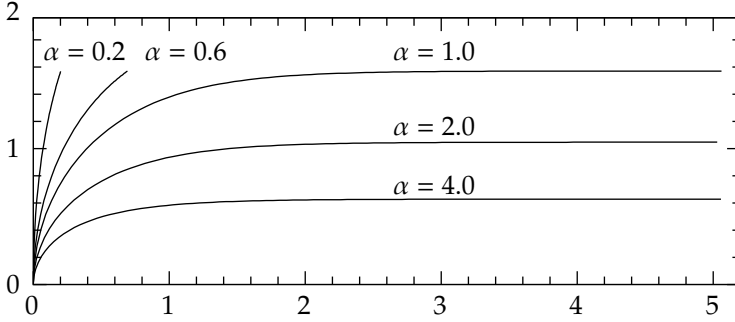


Figure 2.9. Traces for the dipolar Löwner equation with driving function $\xi(t) = 2\alpha t$ for different values of α .

shows that for $\alpha > 1$ the trace does not intersect the top boundary of the strip, but approaches the line $\text{Im} z = \pi/(1 + \alpha)$ asymptotically.

We can in fact find an explicit expression for the trace γ for all $\alpha \neq 1$ by substituting $\gamma(t) = x(t) + iy(t)$ into equation (2.78). Taking the imaginary part of the equation then shows that

$$x(t) = \frac{1}{2} \log \left(\frac{\alpha + 1}{\alpha - 1} \frac{\sin[(\alpha - 1)y(t)]}{\sin[(\alpha + 1)y(t)]} \right). \quad (2.80)$$

Substituting this result into the equation for the real part allows us to express $y = y(t)$ in terms of t as

$$2e^{2(\alpha^2-1)t} = (1 - \alpha) \left(\frac{\alpha + 1}{\alpha - 1} \frac{\sin[(\alpha - 1)y]}{\sin[(\alpha + 1)y]} \right)^{\frac{1}{2}(\alpha+1)} \cos[(\alpha + 1)y] \\ + (1 + \alpha) \left(\frac{\alpha + 1}{\alpha - 1} \frac{\sin[(\alpha - 1)y]}{\sin[(\alpha + 1)y]} \right)^{\frac{1}{2}(\alpha-1)} \cos[(\alpha - 1)y]. \quad (2.81)$$

It remains to prove that $y(t)$ increases monotonously with t from the value $y(0) = 0$ to $y(\infty) = \min(\pi/(\alpha + 1), \pi/2)$.

To prove this, write $h(y) = h_\alpha(y(t))$ for the complicated right-hand side of (2.81). We want to investigate whether the function h is increasing or decreasing with y . It turns out to be convenient to consider the derivative of $\log(h(y)/2)$ with respect to y . This derivative equals

$$\frac{\alpha^2 \sin^2 y + (1 - \alpha^2) \sin^4 y + \sin^2(\alpha y) \cos^2 y - 2\alpha \sin(\alpha y) \sin y \cos(\alpha y) \cos y}{\cos y \sin y \sin[(\alpha - 1)y] \sin[(\alpha + 1)y]}. \quad (2.82)$$

Observe that for $\alpha > 1$ and $0 < y < \pi/(\alpha + 1)$ the denominator is positive, whereas it is negative for $\alpha < 1$ and $0 < y < \pi/2$. Next we look at the sign of

the numerator. The derivative of the numerator with respect to y is

$$-4 \sin y \cos y \left[\cos^2 y - \cos(\alpha y)^2 \right] (1 - \alpha^2). \quad (2.83)$$

This derivative is positive both for $\alpha > 1$, $0 < y < \pi/(\alpha + 1)$ and for $\alpha < 1$, $0 < y < \pi/2$. Since the numerator is zero for $y = 0$, we conclude that the function $h(y)$ in the range $0 < y < \min(\pi/(\alpha + 1), \pi/2)$ is monotonously increasing with y for $\alpha > 1$ and decreasing for $\alpha < 1$. Considering equation (2.81) it follows that $y(t)$ is monotonously increasing with t for all $\alpha \neq 1$.

Thus we have found an explicit expression for the trace of the dipolar Löwner equation with driving function $\xi(t) = 2\alpha t$ for $\alpha \neq 1$. Figure 2.9 shows these traces for several values of α . We conclude this section with the derivation of the solution of the dipolar equation for $\xi(t) = 2t$, i.e. the case $\alpha = 1$. In this case one may verify that $f_t(z)$ satisfies the differential equation

$$\frac{\partial}{\partial t} \left(\frac{1}{2} e^{2f_t(z)} - f_t(z) \right) = 4 \quad (2.84)$$

which has the solution

$$\frac{1}{2} e^{2f_t(z)} - \frac{1}{2} e^{2z} - f_t(z) + z = 4t. \quad (2.85)$$

Substituting $z = \gamma(t)$ yields the following equation for the trace:

$$\gamma'(t) - \frac{1}{2} e^{2\gamma(t)} = 4t - \frac{1}{2}. \quad (2.86)$$

Writing $\gamma(t) = x(t) + iy(t)$ in the previous equation and splitting the equation in real and imaginary parts, we find that

$$x(t) = \frac{1}{2} \log \frac{2y(t)}{\sin 2y(t)}, \quad (2.87)$$

where $y(t)$ satisfies

$$\log \frac{2y(t)}{\sin 2y(t)} - \frac{2y(t) \cos 2y(t)}{\sin 2y(t)} = 8t - 1. \quad (2.88)$$

It follows from the last equation that $y(t)$ is monotonously increasing with t from $y(0) = 0$ to $y(\infty) = \pi/2$ by the same reasoning which we used for the chordal Löwner equation with linear driving function in section 2.B.2. Hence, the trace γ approaches the top boundary of the strip asymptotically.

3 Connections between SLE and statistical models

Summary

We argued in chapter 2 that any random path that has the properties I and II from section 1.2 must be described by SLE_κ for some value of κ . It is believed, for instance, that the exploration path of the Ising model corresponds to $\kappa = 3$ and it is known that the exploration process of critical percolation corresponds to $\kappa = 6$. In this chapter an overview is given of random paths in other models of statistical physics that are, or are believed to be, described by SLE.

3.1 The harmonic explorer

The harmonic explorer is a random path similar to the exploration process of critical percolation. Its definition is motivated by a special property of SLE_4 , which we shall describe below. The path of the harmonic explorer was defined by Schramm and Sheffield [84] to have the same property already at the discrete level, so that the scaling limit must be SLE_4 .

B.4 ◀ To motivate the definition of the model, let us consider the transformations
B.6 ($g_t : t \geq 0$) of chordal SLE_κ in the half-plane, as defined in section 2.2. Write $X = X(t, z) := g_t(z) - \xi(t)$. Then one can use Itô's formula to show that $\log X$ satisfies the differential equation

$$d \log X(t, z) = \left(2 - \frac{\kappa}{2}\right) \frac{dt}{X(t, z)^2} - \frac{d\xi(t)}{X(t, z)}. \quad (3.1)$$

Observe that for $\kappa = 4$ the drift term vanishes. This implies that for $\kappa = 4$, $E[\text{Arg } X/\pi]$ is conserved. In particular, if we condition on the SLE process up to time t , then the expected value of $\text{Arg } X/\pi$ at a later time is $\text{Arg } X(t, z)/\pi$. In other words, $\text{Arg } X/\pi$ is a martingale which is bounded in the interval $[0, 1]$.

It is easy to see that $\text{Arg } X(t, z)/\pi$ is the harmonic function in $\mathbb{H} \setminus \gamma[0, t]$ which tends to 1 when z tends to the arc $-\infty \cup \gamma(t)$ and tends to 0 when z tends to $\gamma(t) \cup \infty$ (we use the fact that γ is a simple path for $\kappa = 4$). In other words, $\text{Arg } X(t, z)/\pi$ is the probability that a two-dimensional Brownian motion started from z leaves the domain $\mathbb{H} \setminus \gamma[0, t]$ through the part of the boundary to the left of $\gamma(t)$ (theorem B.14). In particular, $\lim_{t \rightarrow \infty} \text{Arg } X(t, z)/\pi$ is the probability that z lies to the left of the path γ . The fact that $\text{Arg } X(t, z)/\pi$ is a martingale then implies that at time t , $\text{Arg } X(t, z)/\pi$ is the probability that conditioned on $\gamma[0, t]$, z will lie to the left of the path γ .

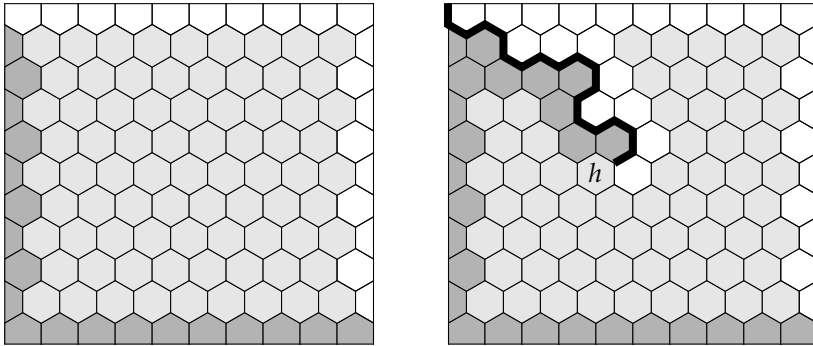


Figure 3.1. Left: the initial configuration for the harmonic explorer, with blue hexagons (dark faces), yellow hexagons (white faces) and uncoloured hexagons (light faces). Right: a part of the harmonic explorer process. The colour of the marked hexagon is determined as described in the text.

We will define the harmonic explorer as a lattice path such that the probability that the next lattice point is passed on the right is determined by the discrete harmonic function which is 1 on the “left side” of the boundary and 0 on the “right side” of the boundary. To be specific, consider an approximation of a bounded domain with hexagons, as in figure 3.1. Like we did for critical percolation in section 1.3, we partition the set of hexagons on the boundary of our domain into two components, and colour the one component yellow and the other blue. The hexagons in the interior are initially uncoloured.

The harmonic explorer is a path over the edges of the hexagons that starts out on the boundary with a blue hexagon on its right and a yellow hexagon on its left. Like the exploration path of critical percolation (see section 1.3), the path turns left whenever it meets a blue hexagon, and it turns right whenever it meets a yellow hexagon. The only difference with the exploration process of critical percolation is in the way the colour of an as yet uncoloured hexagon is determined. In critical percolation this colour is chosen by flipping a fair coin, for the harmonic explorer the coin is biased as explained below.

Suppose that the harmonic explorer meets an uncoloured hexagon h (see figure 3.1). Let f be the function defined on the faces of the hexagons that takes the value 1 on the yellow hexagons, the value 0 on the blue hexagons, and is discrete harmonic on the uncoloured hexagons. Then the probability that the hexagon h is coloured yellow is given by the value of f on h . Note that this implies that given the path so far, the value of f on h gives the probability that the next hexagon will lie to the left of the path. Observe how this property corresponds in the scaling limit to the property of SLE_4 discussed above.

To find the scaling limit, one can consider the harmonic explorer in the upper half-plane from 0 to ∞ on the lattice of mesh $\delta > 0$. The discrete path can be described by a Löwner evolution (see sections 2.1 and 2.2). The law of the driving process for the discrete model can be shown to converge to that of SLE_4 as $\delta \rightarrow 0$. This is sufficient to identify the scaling limit of the harmonic explorer with the trace of chordal SLE_4 . We refer to [84] for the details.

3.2 Loop-erased random walks and uniform spanning trees

In this section we consider loop-erased random walks (LERWs) and uniform spanning trees (USTs). We shall define both models first, and we will point out the close relation between the two. Then we will discuss the connection with SLE in the scaling limit, proved by Lawler, Schramm and Werner in [60]. The proofs of convergence of the LERW to SLE_2 and of the Peano curve winding around a UST to SLE_8 are not restricted to a particular choice of lattice. For simplicity, however, here we will restrict our description to finite subgraphs of the square grid $\delta\mathbb{Z}^2$ with mesh $\delta > 0$.

Suppose that G is a finite connected subgraph of $\delta\mathbb{Z}^2$. Let a be a vertex of G and let V be a collection of vertices of G not containing a . Then the LERW from a to V in G is defined by taking a simple random walk in G from a to V and erasing all its loops in chronological order. More precisely, if $(\omega(0), \dots, \omega(T_V))$ are the vertices visited by a simple random walk starting from a and stopped at the first time T_V when it visits a vertex in V , then its loop-erasure $(\beta(0), \dots, \beta(T))$ is defined as follows. We start by setting $\beta(0) = \omega(0)$. Then for $n \in \mathbb{N}$ we define inductively: if $\beta(n) \in V$ then $T = n$ and we are done, and otherwise we set $\beta(n+1) = \omega(1 + \max\{m \leq T_V : \omega(m) = \beta(n)\})$. The path $(\beta(0), \dots, \beta(T))$ is then a sample of the LERW in G from a to V .

Next we define uniform spanning trees in G . A *spanning tree* T in G is a subgraph of G such that every two vertices of G are connected via a unique simple path in T . A *uniform spanning tree* (UST) in G is a spanning tree chosen with the uniform distribution from all spanning trees in G . It is well-known that the distribution of the unique simple path connecting two distinct vertices a and b of G in the UST is the same as that of the LERW from a to $\{b\}$ in G .

In fact, the connection between LERWs and USTs is even stronger. For suppose that we fix an ordering (v_0, \dots, v_n) of the vertices in G . Let $T_0 = \{v_0\}$ and inductively define T_{m+1} as the union of T_m and a LERW from v_{m+1} to T_m , $T_{m+1} = T_m$ if $v_{m+1} \in T_m$. Then T_n is a UST in G , regardless of the chosen ordering of the vertices of G . This algorithm for generating USTs from LERWs is known as Wilson's algorithm [95]. See also [60, 82] and references therein for more background.

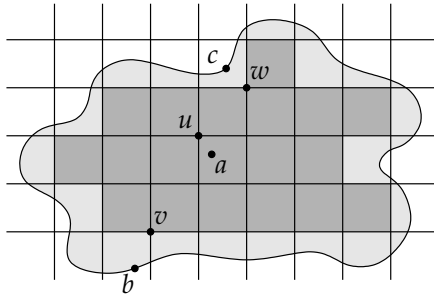


Figure 3.2. The discrete approximation (dark shaded region) of a domain.

Having introduced LERWs and USTs, we will now describe how one takes the scaling limits of these models and makes the connection with SLE. We shall work with a fixed, bounded, simply connected domain D with continuous boundary. Fix the mesh $\delta > 0$, and let G be the subgraph of $\delta\mathbb{Z}^2$ consisting of all vertices and edges that are contained in \overline{D} . Then the set of all points in \mathbb{C} that are disconnected from ∞ by G is a discrete approximation D' of the domain D , see figure 3.2.

Suppose that a is a fixed interior point of D and let u be the vertex of G which is closest to a . Consider the LERW on $\delta\mathbb{Z}^2$ from u to the set of vertices that are not in G . In the scaling limit, this is a random path from a to the boundary of D . We are interested in the time-reversal of this path. Schramm proved in his original paper that if we assume the existence and conformal invariance of the scaling limit of this path, then it must have the law of a radial SLE_2 process from ∂D to a . The starting point of the SLE_2 process on the boundary is chosen according to the image of the uniform law on the boundary of the unit disk \mathbb{D} under the conformal transformation $f : \mathbb{D} \rightarrow D$ such that $0 \rightarrow a$ and $f'(0) > 0$.

To identify the scaling limit of the LERW with an SLE trace, Schramm showed in [82] that the time-reversal of the LERW path has the stationarity property II in the scaling limit. Observe that for the LERW it is not immediately obvious that stationarity holds even at the discrete level, in contrast to the Ising model, percolation, and other models discussed in this section. The value of κ was obtained by Schramm from estimates on the winding number of radial SLE_κ and the LERW around the origin. The proof that the scaling limit of the LERW is SLE_2 was completed by Lawler, Schramm and Werner in [60], by showing that the driving process for the discrete LERW path converges in the scaling limit to that of SLE_2 .

The fact that the LERW converges to an SLE_2 process proves that the LERW is conformally invariant in the scaling limit. Because of the close connection

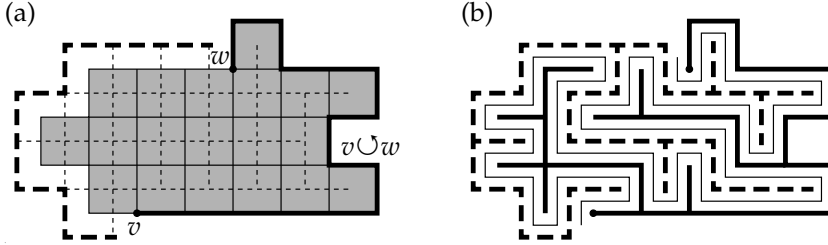


Figure 3.3. Part (a) shows again the discrete approximation of figure 3.2, with the graph G in solid lines and the dual graph G^+ in dashed lines. The thick lines connect vertices that are identified. In part (b) we see a spanning tree on G and its dual on G^+ (thick lines), and the Peano curve winding between them (thin line).

between LERWs and USTs, this leads to the conclusion that the UST also has a conformally invariant scaling limit. In fact, we can define a random Peano path associated to the UST that converges in the scaling limit to the trace of SLE_8 . This path is defined as we shall now explain.

Consider again the domains D , D' and graph G (see figure 3.2). This time, let b and c be distinct points of ∂D , and let v and w be distinct vertices of G on $\partial D'$ closest to b and c , respectively. We identify all vertices on the counter-clockwise arc $v \cup w$ of $\partial D'$. Now let G' be the graph consisting of all edges (and corresponding vertices) of the lattice dual to $\delta\mathbb{Z}^2$, that intersect edges of G but not $v \cup w$. Then we define the dual graph G^+ of G as the union of G' and those edges (and corresponding vertices) outside D' needed to connect the vertices of G' that are outside D' via the shortest possible path outside D' , see figure 3.3(a). On this dual graph, we identify all vertices not in D' .

Suppose that T is a UST in G . Then there is a dual tree T^+ in G^+ , consisting of all those edges that do not intersect edges of the tree T , see figure 3.3(b). Observe that T^+ is a UST in G^+ . The Peano path is defined as the path winding between T and T^+ on the square lattice with vertices at the points $\frac{\delta}{2}\mathbb{Z}^2 + (\frac{\delta}{4}, \frac{\delta}{4})$. Note that this curve is space-filling in the sense that it visits all vertices of the lattice that are disconnected from ∞ by $G \cup G^+$. In the scaling limit the Peano path defined as above converges to the trace of a chordal SLE_8 process from b to c in D [60].

3.3 Self-avoiding walks and the restriction property

A self-avoiding walk (SAW) of length n on the square lattice $\delta\mathbb{Z}^2$ with mesh $\delta > 0$ is a walk $\omega = (\omega(0), \omega(1), \dots, \omega(n))$ on the vertices of the lattice such that

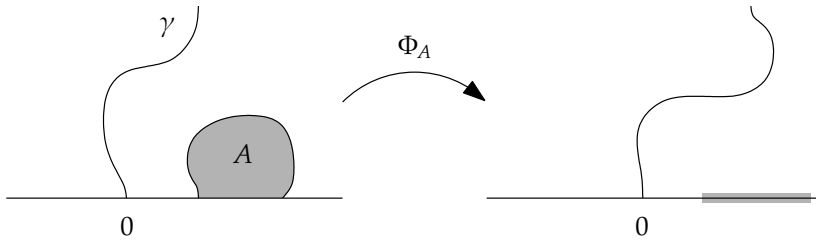


Figure 3.4. We say that a path γ has the restriction property if, conditioned on $\gamma[0, \infty) \cap A = \emptyset$, $\Phi_A \circ \gamma$ has the same law as γ .

$|\omega(j) - \omega(j - 1)| = \delta$ for $j = 1, 2, \dots, n$ and no vertex is visited more than once. The law of SAWs of length n is the uniform law on all such self-avoiding paths. In this section we shall be interested in SAWs that start in the origin and stay in the upper half-plane afterwards. The idea is to define a stochastic process, called the *half-plane infinite SAW*, which in the scaling limit $\delta \rightarrow 0$ is believed to converge to the trace of chordal $\text{SLE}_{8/3}$.

Following [61] we write Λ_n^+ for the set of all SAWs ω of length n that start in the origin and stay above the real line afterwards. For a given ω in Λ_n^+ , let $Q_k^+(\omega)$ be the fraction of walks ω' in Λ_{n+k}^+ whose initial subarc is ω , i.e. such that $\omega'(j) = \omega(j)$ for $0 \leq j \leq n$. Define $Q^+(\omega)$ as the limit of $Q_k^+(\omega)$ as $k \rightarrow \infty$. Then $Q^+(\omega)$ is roughly the fraction of very long SAWs in the upper half-plane whose beginning is ω . It was shown by Lawler, Schramm and Werner in [61] that the limit $Q^+(\omega)$ exists.

Now we can define the half-plane infinite self-avoiding walk as the discrete-time stochastic process X such that for all $\omega = (0, \omega(1), \dots, \omega(n)) \in \Lambda_n^+$,

$$\mathbf{P}[X_0 = 0, X_1 = \omega(1), \dots, X_n = \omega(n)] = Q^+(\omega). \tag{3.2}$$

We believe that the scaling limit of this process as the mesh δ tends to 0 exists and is conformally invariant. Moreover, since the law of SAWs of length n is the uniform law on all self-avoiding paths of length n , the scaling limit should have the following property:

Conjecture 3.1 (Restriction property). *Let $A \subset \overline{\mathbb{H}}$ be a hull which is bounded away from 0, and let $\Phi_A : \mathbb{H} \setminus A \rightarrow \mathbb{H}$ be the conformal transformation such that $\Phi_A(0) = 0$ and $\Phi_A(z)/z \rightarrow 1$ as $z \rightarrow \infty$. Let γ be the scaling limit of the SAW in \mathbb{H} from 0 to ∞ . Then $\Phi_A \circ \gamma$ conditioned on $\gamma[0, \infty) \cap A = \emptyset$ has the same law as γ .*

It can be shown that SLE has the same restriction property if and only if $\kappa = 8/3$ (see section 3.B). Therefore, the scaling limit of the SAW has to be $\text{SLE}_{8/3}$, as was pointed out by Lawler, Schramm and Werner in [61]. In the same

paper, predictions for the critical exponents (e.g. $\nu = 4/3$, $\gamma = 43/32$) of SAWs are obtained from the connection with $\text{SLE}_{8/3}$. At this moment it is unknown how the existence, let alone conformal invariance, of the scaling limit of the SAW could be proved. However, there is strong numerical evidence [47, 48] supporting the SLE predictions on SAWs.

3.4 Potts models and Fortuin-Kasteleyn clusters

The models discussed so far in this thesis could all be connected with SLE at specific values of κ . Schramm's approach however suggests a further connection with continuous families of models, of which we will discuss the two most obvious examples in this section and in section 3.5. This section deals with the q -state Potts models. Below we will show a standard treatment [16] which relates the partition sum of the Potts model to an ensemble of multiple paths on the lattice. In the scaling limit these paths will be the candidates for the traces of SLEs.

The q -state Potts model can be seen as a generalisation of the Ising model where the spin variables can be in q different states instead of just the two possible states in the Ising case. We define the model on a finite subset of the square lattice \mathbb{Z}^2 . Each site j carries a spin variable s_j which takes values in $\{1, 2, \dots, q\}$. These spin variables have only nearest-neighbour interactions, such that the energy of a pair of neighbouring spins is -1 if both variables are in the same state and 0 otherwise. Thus the energy of a configuration $\{s\}$ of all the spins is given by the Hamiltonian

$$H\{s\} = - \sum_{\langle j,k \rangle} \delta_{s_j, s_k}, \quad (3.3)$$

where the sum is over all nearest-neighbour pairs of spins.

As in the Ising model, the probability of each configuration $\{s\}$ is proportional to the Boltzmann-weight $\exp(-\beta H\{s\})$, with β the inverse temperature. The normalisation is provided by the canonical partition sum over all possible configurations

$$Z = \sum_{\{s\}} \exp(-\beta H\{s\}) = \sum_{\{s\}} \exp \left(\beta \sum_{\langle j,k \rangle} \delta_{s_j, s_k} \right). \quad (3.4)$$

The model is known to be disordered at high temperatures and ordered at low temperatures. Here, one of the signatures of the ordered phase is that the probability that two distant s -variables are in the same state does not decay

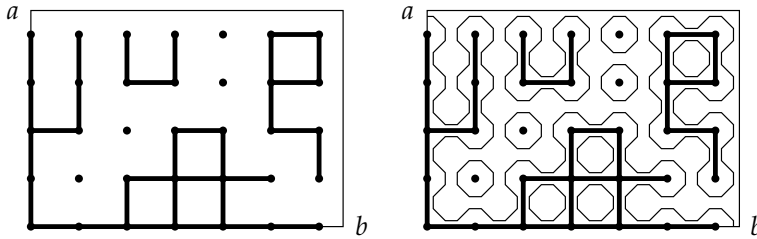


Figure 3.5. The Potts model in a rectangular domain. On the left we illustrate the graph decomposition, on the right we have drawn in the corresponding configuration of paths.

to zero with increasing distance. We will be interested in the behaviour at the transition point.

In order to make the connection with SLE, we will express the partition sum as a sum over configurations of paths on the lattice. With appropriate boundary conditions, one of these paths should converge to an SLE trace in the scaling limit. The transformation of the partition sum involves making a high-temperature expansion, in which we express the partition sum in powers of a parameter which is small when β is small.

The first step is to write the summand in our expression for the partition sum as a product:

$$Z = \sum_{\{s\}} \prod_{\langle j,k \rangle} [1 + (e^\beta - 1)\delta_{s_j, s_k}]. \tag{3.5}$$

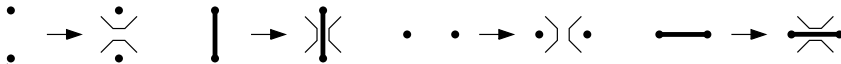
The product can be expanded by making a choice between the two summands 1 and $(e^\beta - 1)\delta_{s_j, s_k}$ for every edge of the lattice, multiplying the chosen terms, and then summing over all possible ways of choosing between the summands. Each of these choices can be represented graphically by leaving an edge of the lattice vacant when the term 1 is chosen and placing a bond on this edge when the term $(e^\beta - 1)\delta_{s_j, s_k}$ is chosen, see figure 3.5. The sum over all possible choices may then be interpreted as a sum over all possible graphs on the lattice.

Next we consider the outer summation over the spin configurations. Observe that if two neighbouring sites are connected by bonds, then their respective s -variables must take the same value. Otherwise, the two s -variables are independent. As a result, the summation over $\{s\}$ yields a factor q for each connected component of the graph. Hence

$$Z = \sum_{\text{graphs}} (e^\beta - 1)^{\#b} q^{\#c}, \tag{3.6}$$

where $\#c$ is the number of connected components of the graph and $\#b$ the number of bonds. The model defined by this partition sum is known by the names of *Fortuin-Kasteleyn cluster model* or *random cluster model* [36]. Note that while q has been introduced as the (integer) number of states, in this expansion it can take any value. The Ising model ($q = 2$), bond percolation ($q = 1$) and uniform spanning trees ($q \rightarrow 0$) are included as special cases.

As our final step, we rewrite the graph expansion as an expansion in terms of paths on a new lattice. This new lattice, the *medial lattice*, has a vertex in the middle of every edge of the original lattice. The graphs on the original lattice are rewritten into polygon decompositions on the medial lattice, as follows. To every vertex of the medial lattice we assign a configuration of two non-intersecting path segments, such that these path segments intersect the corresponding edge of the original lattice if and only if this edge is vacant:



As a result of these transformations the medial lattice will carry a collection of non-intersecting paths as illustrated in figure 3.5.

Note that after these transformations every component of the original graph is surrounded by one of the closed paths on the medial lattice, and that the closed circuits of the graph are also inscribed by these paths. By Euler's relation the number of components $\#c$ of the graph can be expressed in the number of bonds $\#b$, the total number of sites N and the number of polygons $\#p$: $\#c = (N - \#b + \#p)/2$. Thus we may write the partition sum as

$$Z = \sum_{\text{graphs}} \left(\frac{e^\beta - 1}{\sqrt{q}} \right)^{\#b} q^{(N + \#p)/2}. \quad (3.7)$$

At the critical point β_c the relation $\exp(\beta_c) = 1 + \sqrt{q}$ holds, so that the partition sum simplifies: each graph is simply weighted by \sqrt{q} raised to the number of polygons (the overall factor of $q^{N/2}$ can be ignored).

We will now consider this model at the critical point on a rectangular domain. The lattice approximation of this domain is chosen such that the lower-left corner of the rectangle coincides with a site of the lattice, while the upper-right corner coincides with a site of the dual lattice. The sides of the rectangle are parallel to the edges of the lattice, as in figure 3.5. We will denote the upper-left corner by a and the lower right-corner by b . Our aim is to define a random path from a to b by choosing appropriate boundary conditions.

We propose the following boundary conditions. Along the arc $a \cup b$ all edges of the lattice must carry bonds, and all edges intersecting the arc $a \cap b$ are forbidden to carry bonds. For the spin variables this means that all the

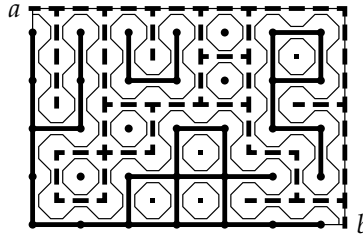


Figure 3.6. Graph decomposition of the Potts model with dual graph (dashed lines) and path configuration (thin lines).

spins on the left and lower sides are in the same state, while all other spins are unconstrained. These boundary conditions may be formulated in an alternative way when we associate to each graph G on the original lattice the dual graph G^\dagger of the dual lattice consisting of those bonds that do not intersect bonds of G (see figure 3.6). Then we see that along the arc $a \cup b$ all edges of the original lattice must carry bonds, and along the arc $a \cap b$ all edges of the dual lattice must carry bonds.

With these boundary conditions every graph in (3.7) contains one path γ from a to b , and all the other paths are closed polygons, see figure 3.6. The scaling limit of γ is obtained by covering the rectangle with a square grid of finer and finer mesh. The scaling limit is believed to coincide with an SLE_κ trace from a to b for some value of κ [78]. The value of κ may be guessed from the Hausdorff dimension of the path γ . Predictions of the Hausdorff dimensions for the q -state Potts models appear in [35, 80]. These can be compared to the Hausdorff dimensions of the SLE traces computed by Beffara [17, 18] to find the relation between κ and q :

$$q = 2 + 2 \cos(8\pi/\kappa), \quad 4 \leq \kappa \leq 8. \quad (3.8)$$

Only in a few cases this relation between SLE_κ and the Potts partition sum has been made rigorous. For instance, in the limit $q \rightarrow 0$ the graph expansion reduces to the uniform spanning tree, which has SLE_8 as its scaling limit.

3.5 $O(n)$ models

We now turn to the $O(n)$ model, which is another well-known model where a high-temperature expansion results in a sum over configurations of paths. In this model the dynamic variables s_j are n -component vectors of a fixed length. A configuration $\{s\}$ of the model is characterised by the directions of

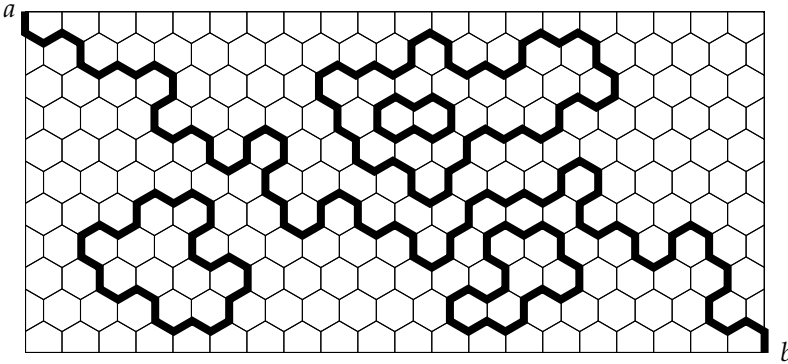


Figure 3.7. One of the graphs that contribute to the correlation function between the spins at a and b in the $O(n)$ model.

these vectors. The Hamiltonian of the model is invariant under rotations in the n -dimensional space. The simplest high-temperature expansion is obtained when the Boltzmann weight of a configuration $\{s\}$ is chosen as

$$\exp(-\beta H\{s\}) = \prod_{\langle j,k \rangle} (1 + x s_j \cdot s_k), \quad (3.9)$$

where the product is over nearest neighbours on a hexagonal lattice.

The partition sum is defined as the integral of this expression over the directions of the spin vectors. As for the Potts model one can expand the product under the integral and do the bookkeeping of the terms by means of graphs. To do so, for each factor in (3.9) the choice of the term $x s_j \cdot s_k$ is indicated by a bond, and the choice of the term 1 is indicated by the absence of a bond. Then the graphs that survive the integration over the spin variables have only even vertices, i.e. on the hexagonal lattice only vertices with zero or two bonds.

It follows that all graphs that contribute to the partition sum consist of a collection of closed paths on the lattice. In a well-chosen normalisation of the measure and the length of the spin vectors, the partition sum is the following sum over even graphs

$$Z = \sum_{\text{graphs}} x^L n^M, \quad (3.10)$$

where M is the number of closed loops, and L their combined length. Note that this expression for the partition sum is well-defined also when the number of spin components n is not integer. It is known [15, 68] that the critical point is at $x_c = [2 + (2 - n)^{1/2}]^{-1/2}$ for $0 \leq n \leq 2$. When x is larger than this critical value the model also shows critical behaviour.

Consider now this model on a bounded domain, and take a correlation function between two spins on the boundary. The diagrams that contribute to this function contain one path between the two specified boundary points and any number of closed polygons in the interior (see figure 3.7). We conjecture that at the critical value of x the measure on the paths between the two boundary spins in the scaling limit approaches that of SLE _{κ} with $n = -2 \cos(4\pi/\kappa)$ and $8/3 \leq \kappa \leq 4$ (e.g. using Coulomb Gas arguments, see [25, section 3.6]). For larger values of x the scaling limit would again be SLE _{κ} with the same relation between κ and n , but now with $4 \leq \kappa \leq 8$.

3.A Locality for SLE₆

In this chapter we have considered several models of statistical physics that are or are believed to be related to SLE in the scaling limit. We explained in chapter 2 that for the connection with SLE it is sufficient to show that there is a random path in the model whose law is conformally invariant and stationary, i.e. that satisfies properties I and II in section 1.2. The value of κ that corresponds to the model has to be determined by separate means, for instance from a property that the model shares with SLE _{κ} for only one specific value of κ .

In this section we will show that SLE _{κ} has the same locality property as the exploration process of critical percolation (theorem 1.1 in section 1.3) if and only if $\kappa = 6$. In section 3.B we will show that SLE _{κ} has the same restriction property as self-avoiding walks (conjecture 3.1 in section 3.3) if and only if $\kappa = 8/3$. Thus, the only candidate for the scaling limit of critical percolation is SLE₆ and the only candidate for the scaling limit of the self-avoiding walk is SLE_{8/3}. To prove these properties of SLE for $\kappa = 6$ and $\kappa = 8/3$ we will follow [59]. A different, more difficult proof of locality for SLE₆ appears in [55].

Both locality and restriction have to do with the behaviour of SLE under conformal transformations. The restriction property will be discussed in section 3.B. As for the locality property, let A be a hull in the upper half-plane which is bounded away from 0. Write Φ_A for the conformal transformation of $\mathbb{H} \setminus A$ onto \mathbb{H} such that $\Phi_A(0) = 0$ and $\Phi_A(z)/z \rightarrow 1$ as $z \rightarrow \infty$, that is, $\Phi_A(z) = g_A(z) - g_A(0)$ where $g_A : \mathbb{H} \setminus A \rightarrow \mathbb{H}$ such that $\lim_{z \rightarrow \infty} (g_A(z) - z) = 0$. For chordal SLE _{κ} in the half-plane, let $T := \inf\{t \geq 0 : K_t \cap A \neq \emptyset\}$ and $T' := \inf\{t \geq 0 : K_t \cap \Phi_A(\partial A \cap \mathbb{H}) \neq \emptyset\}$, where by convention the infimum of the empty set is ∞ . Then SLE _{κ} has the locality property if $(K_t : t \leq T')$ has the same law as $(\Phi_A(K_t) : t \leq T)$ modulo a time-change. We will prove the following:

Theorem 3.2. *Consider chordal SLE _{κ} in \mathbb{H} from 0 to ∞ . Then $(K_t : t \leq T')$ has the same law as $(\Phi_A(K_t) : t \leq T)$ modulo a time-change if and only if $\kappa = 6$.*

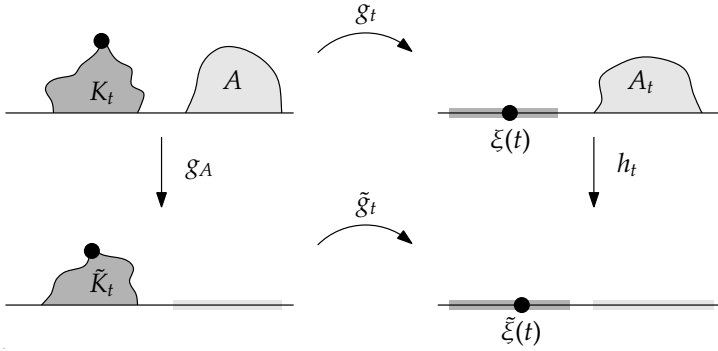


Figure 3.8. Relations between conformal transformations that remove the hulls $K_t, A, \tilde{K}_t := g_A(K_t)$ and $A_t := g_t(A)$.

A.5 ◀ **Proof.** We have to study the image of SLE_κ under Φ_A . For $t < T$ we will write
 B.5 $A_t := g_t(A), \tilde{K}_t := g_A(K_t)$ and $\tilde{g}_t := g_{\tilde{K}_t}$. The half-plane capacity of \tilde{K}_t will be
 B.6 denoted by $a(t)$. Then from the proof of Löwner’s theorem (section 2.A) it follows that \tilde{g}_t satisfies

$$\frac{\partial \tilde{g}_t(z)}{\partial t} = \frac{\partial a(t)}{\partial t} \frac{1}{\tilde{g}_t(z) - \tilde{\xi}(t)}; \quad \tilde{g}_0(z) = z, \tag{3.11}$$

where

$$\tilde{\xi}(t) := h_t(\xi(t)), \quad h_t := \tilde{g}_t \circ g_A \circ g_t^{-1} = g_{A_t}. \tag{3.12}$$

Here, $\xi(t) = \sqrt{\kappa}B(t)$ is the driving process for g_t . For the convenience of the reader, the relations between the various conformal maps are depicted in figure 3.8.

We will prove that $\tilde{\xi}$ is Brownian motion multiplied by $\sqrt{\kappa}$ modulo a time-change if and only if $\kappa = 6$. From this it follows that the hulls \tilde{K}_t grow just like the hulls K_t , except at a different clock rate. To show this, we note that Itô’s formula (here we have to use [75, exercise IV(3.12)]) for $t < T$ tells us that

$$d\tilde{\xi}(t) = dh_t(\xi(t)) = \left(\frac{\kappa}{2} h_t''(\xi(t)) + \frac{\partial h_t(\xi(t))}{\partial t} \right) dt + h_t'(\xi(t)) d\xi(t). \tag{3.13}$$

Note that if we could demonstrate that the drift term in this equation vanishes, then it would follow that $\tilde{\xi}$ is indeed Brownian motion multiplied by $\sqrt{\kappa}$ if we change time according to $ds = h_t'(\xi(t))^2 dt$ (theorem B.11). To this end we now compute the time-derivative of h_t at $\xi(t)$.

To compute this derivative we need an expression for the time-derivative of $a(t)$. Observe that $\text{cap}_{\mathbb{H}}[g_t(K_{t+\Delta t} \setminus K_t)] = 2\Delta t$. Then from the scaling rule of half-plane capacity, for positive Δt tending to 0 we find that $\text{cap}_{\mathbb{H}}[h_t \circ g_t(K_{t+\Delta t} \setminus K_t)]$

tends to $2\Delta t h'_t(\xi(t))^2$. Hence,

$$\frac{\partial a(t)}{\partial t} = 2h'_t(\xi(t))^2. \quad (3.14)$$

Now we can compute the time-derivative of $h_t(z)$ for $z \in \mathbb{H} \setminus A_t$. We have to use Löwner's equation for g_t^{-1} , the inverse of g_t , which is easily obtained from $\partial_t g_t(g_t^{-1}(z)) = 0$:

$$\frac{\partial g_t^{-1}(z)}{\partial t} = -\frac{2(g_t^{-1})'(z)}{z - \xi(t)}. \quad (3.15)$$

From $h_t = \tilde{g}_t \circ g_A \circ g_t^{-1}$, using the chain rule, we find

$$\frac{\partial h_t(z)}{\partial t} = \frac{2h'_t(\xi(t))^2}{h_t(z) - \xi(t)} - \frac{2h'_t(z)}{z - \xi(t)}. \quad (3.16)$$

Note that this equation is also valid on the real line in a neighbourhood of $\xi(t)$.

Taking the limit $z \rightarrow \xi(t)$, Taylor-expanding $h'_t(z)$ and $h_t(z)$ to first and second order respectively, we obtain

$$\frac{\partial h_t(\xi(t))}{\partial t} = \lim_{z \rightarrow \xi(t)} \left(\frac{2h'_t(\xi(t))^2}{h_t(z) - \xi(t)} - \frac{2h'_t(z)}{z - \xi(t)} \right) = -3h''_t(\xi(t)). \quad (3.17)$$

Plugging this result into equation (3.13), we see that the drift term vanishes if and only if $\kappa = 6$. It follows that for $\kappa = 6$, $\tilde{\xi}$ is Brownian motion multiplied by $\sqrt{\kappa}$ modulo the time-change such that $ds = h'_t(\xi(t))^2 dt$. ■

3.B Restriction for SLE_{8/3}

To show that SLE _{κ} has the restriction property if and only if $\kappa = 8/3$, we have to follow up the computations of section 3.A. We start by proving the following result:

Theorem 3.3 (Restriction property of SLE_{8/3}). *Let γ be the trace of chordal SLE_{8/3} in \mathbb{H} from 0 to ∞ and let A be a hull which is bounded away from 0. Then*

$$\mathbb{P}[\gamma[0, \infty) \cap A = \emptyset] = \Phi'_A(0)^{5/8}, \quad (3.18)$$

where $\Phi_A : \mathbb{H} \setminus A \rightarrow \mathbb{H}$ is the unique conformal transformation such that $\Phi_A(0) = 0$ and $\Phi_A(z)/z \rightarrow 1$ as $z \rightarrow \infty$.

B.4 ◀ **Proof.** Differentiating (3.16) with respect to z gives
B.6

$$\frac{\partial h'_t(z)}{\partial t} = -\frac{2h'_t(\xi(t))^2 h'_t(z)}{(h_t(z) - \xi(t))^2} + \frac{2h'_t(z)}{(z - \xi(t))^2} - \frac{2h''_t(z)}{z - \xi(t)}. \quad (3.19)$$

As before, we take the limit $z \rightarrow \xi(t)$ to obtain

$$\frac{\partial h'_t(\xi(t))}{\partial t} = \frac{h''_t(\xi(t))^2}{2h'_t(\xi(t))} - \frac{4}{3}h'''_t(\xi(t)). \quad (3.20)$$

Using Itô's formula (see [75, exercise IV(3.12)]) we can now derive the stochastic differential equation for $h'_t(\xi(t))$. We find

$$dh'_t(\xi(t)) = \left(\frac{h''_t(\xi(t))^2}{2h'_t(\xi(t))} + \left(\frac{\kappa}{2} - \frac{4}{3} \right) h'''_t(\xi(t)) \right) dt + h'_t(\xi(t)) d\xi(t). \quad (3.21)$$

Note that the drift term doesn't quite vanish for $\kappa = 8/3$. However, if we consider $Y(t) = h'_t(\xi(t))^\alpha$ for $\alpha > 0$, then Itô's formula gives

$$\frac{dY(t)}{\alpha Y(t)} = \left((1 + (\alpha - 1)\kappa) \frac{h''_t(\xi(t))^2}{2h'_t(\xi(t))^2} + \left(\frac{\kappa}{2} - \frac{4}{3} \right) \frac{h'''_t(\xi(t))}{h'_t(\xi(t))} \right) dt + \frac{h''_t(\xi(t))}{h'_t(\xi(t))} d\xi(t). \quad (3.22)$$

This time, the drift term *does* vanish if and only if $\kappa = 8/3$ and $\alpha = 5/8$. Since $0 \leq h'_t(\xi(t)) \leq 1$ for $t < T$, this shows that the process Y considered up to time T is a bounded martingale if and only if $\kappa = 8/3$ and $\alpha = 5/8$.

Next we consider $Y(T) := \lim_{t \rightarrow T} Y(t)$. At this point we note that we may assume that $\partial A \cap \mathbb{H}$ is smooth, see [59, proposition 3.3]. Lemma 3.4 below shows that for smooth hulls the limit $Y(T)$ is the indicator of the event that γ avoids A . Hence, for $\kappa = 8/3$ and $\alpha = 5/8$, since Y is a martingale up to time T , the optional sampling theorem B.7 implies that $Y(0) = \mathbf{E}[Y(T)] = \mathbf{P}[\gamma[0, \infty) \cap A = \emptyset]$. The theorem follows. \blacksquare

Lemma 3.4. *Suppose that γ is a simple path generated by a deterministic Löwner evolution with driving function ξ such that $\lim_{t \rightarrow \infty} |\gamma(t)| = \infty$. Let A be a hull bounded away from 0 such that $\partial A \cap \mathbb{H}$ is a smooth curve, and let T be the first time when γ hits A (setting $T = \infty$ if γ avoids A). Then $\lim_{t \rightarrow T} h'_t(\xi(t)) = 1_{\{\gamma[0, \infty) \cap A = \emptyset\}}$.*

Before we prove the lemma, let us first show that theorem 3.3 implies that the law of the $\text{SLE}_{8/3}$ trace has the same restriction property as the self-avoiding walk (conjecture 3.1 in section 3.3). To see this, let A and B be two hulls that are bounded away from 0. Then (see figure 3.9)

$$\begin{aligned} \mathbf{P}[(\Phi_A \circ \gamma)[0, \infty) \cap B = \emptyset \mid \gamma[0, \infty) \cap A = \emptyset] &= \mathbf{P}[\gamma[0, \infty) \cap \Phi_A^{-1}(B) = \emptyset \mid \gamma[0, \infty) \cap A = \emptyset] \\ &= \frac{\mathbf{P}[\gamma[0, \infty) \cap (\Phi_A^{-1}(B) \cup A) = \emptyset]}{\mathbf{P}[\gamma[0, \infty) \cap A = \emptyset]} = \frac{(\Phi_B \circ \Phi_A)'(0)^{5/8}}{\Phi_A'(0)^{5/8}} \quad (3.23) \\ &= \Phi_B'(0)^{5/8} = \mathbf{P}[\gamma[0, \infty) \cap B = \emptyset]. \end{aligned}$$

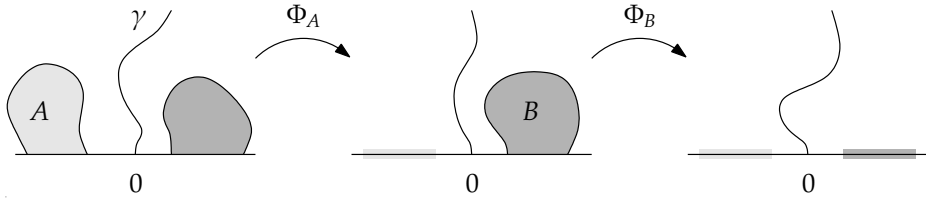


Figure 3.9. The law of $\Phi_A \circ \gamma$ conditioned on $\gamma[0, \infty) \cap A = \emptyset$ is determined by the probabilities that $\Phi_A \circ \gamma$ avoids hulls B .

Since the distribution of $\gamma[0, \infty)$ is determined by the probabilities to avoid hulls B (just as in section 1.4), this shows that the trace of $SLE_{8/3}$ has the same restriction property as the self-avoiding walk.

Conversely, it can be shown that any random path that has the restriction property of the self-avoiding walk must satisfy

$$\mathbf{P}[\gamma[0, \infty) \cap A = \emptyset] = \Phi'_A(0)^\alpha \tag{3.24}$$

for some exponent $\alpha > 0$, see [59]. Hence, if SLE_κ has the restriction property, then

$$\mathbf{P}[\gamma[0, \infty) \cap A = \emptyset \mid \gamma[0, t]] = 1_{\{\gamma[0, t] \cap A = \emptyset\}} h'_t(\xi(t))^\alpha \tag{3.25}$$

for some $\alpha > 0$. Therefore, if we set $X(t) := h'_t(\xi(t))^\alpha$, then the process X must be a martingale for $t < T$. We have seen in the proof of theorem 3.3 that this can only be true for $\kappa = 8/3$ and $\alpha = 5/8$. Hence SLE_κ has the restriction property only for $\kappa = 8/3$ and exponent $\alpha = 5/8$.

We conclude this section with a proof of lemma 3.4, which depends quite heavily on background covered in appendix A. Our proof follows the proof appearing in [59, lemma 6.2] for the case that γ avoids A . We use a deterministic strategy different from the proof in [59, lemma 6.3] (which is more probabilistic) for the case that γ intersects A .

A.2 ◀ **Proof of lemma 3.4.** Let A_t , g_t and h_t be defined as before. By symmetry we
A.3 may assume that $A \cap (-\infty, 0] = \emptyset$. We first consider the case that γ does not
A.4 intersect A , and hence $T = \infty$. In that case, the extremal distance in $\mathbb{H} \setminus \gamma[0, t]$
A.5 between A and the union of $(-\infty, 0]$ and the left-hand side of $\gamma[0, t]$ tends to ∞ as $t \rightarrow \infty$, since every arc connecting the two sets has to cross a semi-annulus of larger and larger modulus. By conformal invariance it follows that $d_{\mathbb{H}}((-\infty, \xi(t)), A_t)$ tends to ∞ as $t \rightarrow \infty$ (where $d_{\mathbb{H}}$ denotes extremal distance with respect to \mathbb{H}).

Now pick a point $x \in A \cap \mathbb{R}$ and write $x(t) := g_t(x)$. Let D_t be the smallest half-disk centred at $x(t)$ that contains A_t and let $r(t)$ be its radius.

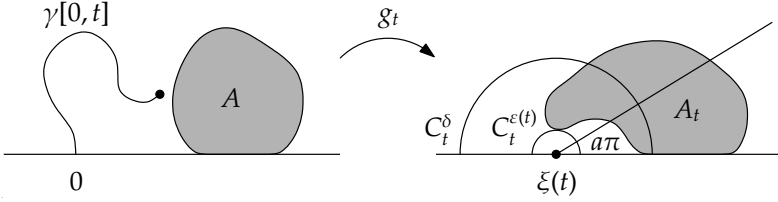


Figure 3.10. The L\"owner map g_t for a path γ that is about to hit a hull A .

Then Teichm\"uller's theorem implies that $d_{\mathbb{H}}((-\infty, \xi(t)], A_t) \leq 2\Lambda(|x(t) - \xi(t)|/r(t))$, and we conclude that $|x(t) - \xi(t)|/r(t) \rightarrow \infty$ as $t \rightarrow \infty$ (see the discussion in section A.2 of appendix A). Observe that $g_{D_t}(z) = z + r(t)^2/(z - x(t))$, so that $g'_{D_t}(\xi(t)) \rightarrow 1$ as $t \rightarrow \infty$. But $h'_t(\xi(t)) \geq g'_{D_t}(\xi(t))$, because g_{D_t} is the composition of h_t with the map $g_{h_t(D_t \setminus A_t)}$, and any normalised map g_K associated with a hull K satisfies $0 \leq g'_K(x) \leq 1$ for $x \in \mathbb{R} \setminus K$. Hence $\lim_{t \rightarrow \infty} h'_t(\xi(t)) = 1$, as desired.

Next we consider the case that γ intersects A , and hence $T < \infty$. We set $R := \sup\{|z| : z \in A \cup \gamma[0, T]\}$ and $Q := \{z \in \mathbb{H} : |z| > 5R\}$. Note that by corollary A.19 the distances from $g_t(Q)$ and $h_t(g_t(Q))$ to the origin are in the range $[4R, 6R]$ for all $t \leq T$. For $t < T$, we denote by $\varepsilon(t)$ the distance from $\xi(t)$ to A_t , and we write C_t^r for the circle of radius r centred at $\xi(t)$. Observe that by smoothness of ∂A there exist a number $\delta > 0$ and $0 < a < 1$ such that every arc in $\mathbb{H} \setminus A_T$ from $\xi(T)$ to $g_T(Q)$ contains a subarc from $\xi(T)$ to C_T^δ in the sector $\{z \in \mathbb{H} : \text{Arg}(z - \xi(T)) > a\pi\}$. Since the maps g_t converge uniformly to g_T as $t \rightarrow T$ (see section 2.A), it follows that there exists $0 < a < 1$ such that for all $t < T$ close enough to T , every arc in $\mathbb{H} \setminus A_t$ that connects $C_t^{\varepsilon(t)}$ to $g_t(Q)$ contains a subarc connecting $C_t^{\varepsilon(t)}$ to C_t^δ in the sector $\{z \in \mathbb{H} : \text{Arg}(z - \xi(t)) > a\pi\}$. See figure 3.10.

It follows that $d_{\mathbb{H} \setminus A_t}(C_t^{\varepsilon(t)}, g_t(Q)) \geq d_{\mathbb{H} \setminus A_t}(C_t^{\varepsilon(t)}, C_t^\delta) \geq \log(\delta/\varepsilon(t))/(1-a)\pi$. On the other hand, let $r(t) := \sup\{|z - h_t(\xi(t))| : z \in h_t(C_t^{\varepsilon(t)}) \cap \mathbb{H}\}$. Then Teichm\"uller's theorem A.7 implies that $d_{\mathbb{H} \setminus A_t}(C_t^{\varepsilon(t)}, g_t(Q)) \leq 2\Lambda(6R/r(t))$. Hence by lemma A.8 there is a universal constant C such that $r(t) \leq CR\delta^{-1/(1-a)}\varepsilon(t)^{1/(1-a)}$. To complete the argument, we now observe that the map h_t can be extended to an analytic function on the domain $\{z \in \mathbb{C} : |z - \xi(t)| < \varepsilon(t)\}$ by the Schwarz reflection principle A.16. If we now set

$$f_t(z) := \frac{h_t(\varepsilon(t)z + \xi(t)) - h_t(\xi(t))}{\varepsilon(t)h'_t(\xi(t))}, \quad (3.26)$$

then $f_t(z)$ is a conformal map of the unit disk such that $f_t(0) = 0$ and $f'_t(0) = 1$. Our bound on $r(t)$ gives $\sup\{|f_t(z)| : z \in \mathbb{D}\} \leq CR\delta^{-1/(1-a)}\varepsilon(t)^{a/(1-a)}|h'_t(\xi(t))|^{-1}$. But Koebe's one-quarter theorem A.14 says that $\sup\{|f_t(z)| : z \in \mathbb{D}\} \geq 1/4$. Since $0 < a < 1$ it follows that $h'_t(\xi(t)) \rightarrow 0$ as $t \rightarrow T$, as desired. \blacksquare

4 SLE computations for critical systems

Summary

In this chapter we present SLE computations and discuss applications to critical systems. Non-rigorous derivations of formulas are complemented by proofs involving stochastic calculus (appendix B), which the reader may skip on the first reading. Two generalisations of Cardy's formula are derived. Crossing exponents for SLE_6 are used to derive critical exponents for critical percolation. Finally, we obtain a formula for the probability that a chordal SLE trace passes a given point on the left, and formulas for the probabilities that a given point is in the hull or to the left of the hull for dipolar SLE.

4.1 Two generalisations of Cardy's formula

We start this chapter with the computation of Cardy's crossing formula for the scaling limit of critical percolation (using SLE_6). In fact, we will generalise this formula to models corresponding to SLE_κ with a different value of $\kappa > 4$ (see sections 3.4 and 3.5 for the connection between these SLEs and critical models). We consider the fixed rectangular domain $R_L := (0, L) \times (0, \pi)$ and a chordal SLE_κ process in R_L from $i\pi$ to L , where $\kappa > 4$. The trace γ of this process will hit the arc $0 \cup L + i\pi$ at a (finite) random time τ . We are interested in the probability of the event E that $\gamma(\tau) \notin [0, L]$, see figure 4.1.

In the case of SLE_6 , this event has the following interpretation. We may regard the trace γ as the scaling limit of the critical percolation exploration process in R_L with blue boundary conditions along the arc $i\pi \cup L$ and yellow boundary conditions along $i\pi \cap L$ (section 1.3). Thus, the event E is equivalent to the event that there is a blue left-to-right crossing contained in the interior of the rectangle. On the discrete level this corresponds to the event that there is a sequence of connected blue hexagons containing a hexagon intersecting the left side of the rectangle and a hexagon intersecting the right side, but no hexagons intersecting the bottom side.

A.6 ◀ To compute the probability of the event E , we use a simplification of the proof of a more general theorem appearing in [55], which is quoted as theorem 4.7 in section 4.2 below. Let f be the conformal transformation of R_L onto the upper half-plane such that $f(i\pi) = 0$, $f(0) = 1$, and $f(L) = \infty$. Then the image $-R < 0$ of $L + i\pi$ by f is uniquely determined. By conformal invariance of chordal SLE_κ , it follows that the probability of the event E is equal to the probability that for chordal SLE_κ in \mathbb{H} from 0 to ∞ , the point $-R$ becomes part of the hull before the point 1.

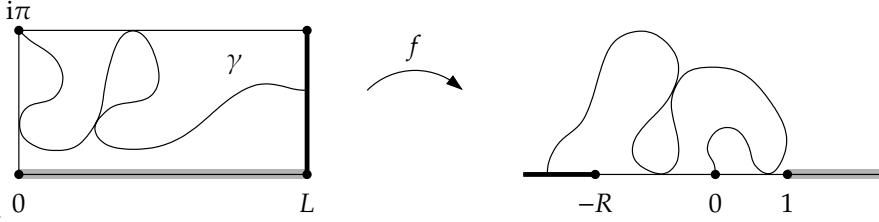


Figure 4.1. An SLE path crossing a rectangle and its conformal image in the half-plane.

By scale invariance, the probability of this event depends only on the ratio $R/(R+1)$. Introducing the variable $x = x(R) = R/(R+1)$ to denote this ratio, we will write $h(x)$ for the probability that 1 is in the hull before $-R$, so that $\mathbf{P}[E] = 1 - h(x)$. Suppose that we now let the chordal SLE_κ trace grow for an infinitesimally small time dt , and then apply the Löwner map g_{dt} to remove the hull K_{dt} . Then it is clear from stationarity of SLE (lemma 2.3) that if we define Z (as the natural analogue of x at a later time) by

$$Z(t) = \frac{\xi(t) - g_t(-R)}{g_t(1) - g_t(-R)}, \quad (4.1)$$

then $\mathbf{E}[h(Z(dt))] = h(x)$, where the average is over all realisations of $Z(dt)$. Here, as usual, $\xi(t) = \sqrt{\kappa}B(t)$ is the driving process of chordal SLE_κ in the half-plane.

Assuming that h is sufficiently differentiable, we may Taylor-expand the equation $\mathbf{E}[h(Z(dt))] = h(x)$ to first order in dt . Here we use Löwner's differential equation (2.11) together with $\mathbf{E}[\xi(dt)] = 0$, $\mathbf{E}[\xi(dt)^2] = \kappa dt$. Noting that $1 - x = (R+1)^{-1}$, we conclude that h must satisfy the differential equation

$$\frac{\kappa}{4}h''(x) + h'(x)\left(\frac{1}{x} - \frac{1}{1-x}\right) = 0. \quad (4.2)$$

The boundary conditions are $h(0) = 0$ and $h(1) = 1$, so that the unique solution becomes

$$h(x) = \frac{\int_0^x t^{-4/\kappa}(1-t)^{-4/\kappa} dt}{\int_0^1 t^{-4/\kappa}(1-t)^{-4/\kappa} dt}. \quad (4.3)$$

We conclude that $\mathbf{P}[E] = 1 - h(x) = h(1-x)$. This result may also be written in terms of a hypergeometric function [71], yielding the formula (4.4) in theorem 4.1 below. For $\kappa = 6$, this is Cardy's formula [24]. Note, however, that we have assumed that h is sufficiently differentiable. Strictly speaking we therefore still have to prove the result. This is done using a standard procedure, as follows:

Theorem 4.1 (First generalisation of Cardy's formula). *Consider chordal SLE_κ in the rectangle $R_L = (0, L) \times (0, \pi)$ from $i\pi$ to L , where $\kappa > 4$. Let E be the event that the trace of this process hits $L \cup L + i\pi$ before $[0, L]$. Then*

$$\mathbf{P}[E] = \frac{\Gamma\left(2 - \frac{8}{\kappa}\right)}{\Gamma\left(2 - \frac{4}{\kappa}\right)\Gamma\left(1 - \frac{4}{\kappa}\right)} (1-x)^{1-\frac{4}{\kappa}} {}_2F_1\left(\frac{4}{\kappa}, 1 - \frac{4}{\kappa}; 2 - \frac{4}{\kappa}; 1-x\right), \quad (4.4)$$

where $x = R/(R+1)$, $-R$ being the image of $L + i\pi$ under the conformal transformation $f : R_L \rightarrow \mathbb{H}$ such that $f(i\pi) = 0$, $f(0) = 1$ and $f(L) = \infty$.

B.4 ◀ **Proof.** Define the real-valued process Z by equation (4.1) and the function **B.6** $h : [0, 1] \rightarrow [0, 1]$ by equation (4.3). Let T be the first time when the trace of chordal SLE_κ in \mathbb{H} from 0 to ∞ hits $(-\infty, -R] \cup [1, \infty)$. Then it is clear from the definition of Z that $0 < Z(t) < 1$ for $t < T$ and $Z(T)$ is the indicator of the event that 1 is in the hull before $-R$. From the definition of h it follows that $h(Z(T))$ is also the indicator of this event.

Let us now introduce the notations $U(t) = \xi(t) - g_t(-R)$, $V(t) = \xi(t) - g_t(1)$ and $W(t) = U(t) - V(t)$. Then $Z(t) = U(t)/W(t)$, and it is easily verified that

$$dU(t) = \frac{2 dt}{U(t)} + d\xi(t), \quad dW(t) = \frac{2 dt}{U(t)} - \frac{2 dt}{V(t)} = \frac{1}{1-Z(t)} \frac{2 dt}{U(t)}. \quad (4.5)$$

From a simple application of Itô's formula it follows that Z satisfies the stochastic differential equation

$$dZ(t) = \frac{2 dt}{W(t)^2} \left(\frac{1}{Z(t)} - \frac{1}{1-Z(t)} \right) + \frac{d\xi(t)}{W(t)}. \quad (4.6)$$

Another application of Itô's formula then reveals that $h \circ Z$ considered up to time T is a martingale since h satisfies the differential equation (4.2). The optional sampling theorem **B.7** implies that $\mathbf{E}[h(Z(T))] = h(Z(0)) = h(x)$. Hence $h(x)$ is the probability that 1 is in the hull before $-R$. Applying the conformal transformation f^{-1} (see figure 4.1), this proves the theorem. ■

A.6 ◀ This first generalisation of Cardy's formula has a particularly nice interpretation in a well-chosen triangle for $4 < \kappa < 8$. To see this, fix $4 < \kappa < 8$ and let $T = T_{(1-4/\kappa)\pi}$ be the triangle in the upper half of the complex plane which has corners at 0 and 1 , both with interior angles $(1 - 4/\kappa)\pi$. Consider the function

$$F(z) = F_{(1-4/\kappa)\pi}(z) = \frac{\int_0^z t^{-4/\kappa} (1-t)^{-4/\kappa} dt}{\int_0^1 t^{-4/\kappa} (1-t)^{-4/\kappa} dt}. \quad (4.7)$$

This function is the unique conformal transformation of \mathbb{H} onto T which fixes 0 and 1 and sends ∞ to the third corner $w = w_{(1-4/\kappa)\pi}$ of T . Observe that

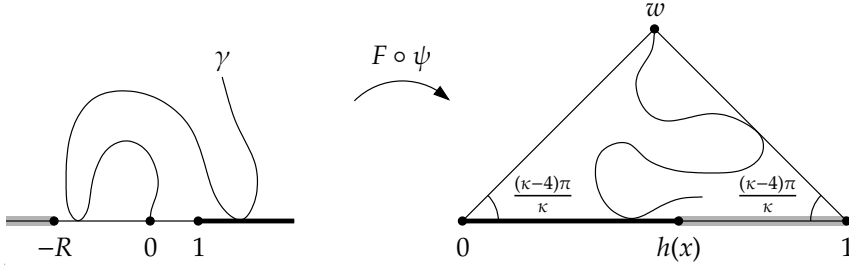


Figure 4.2. An SLE_κ path crossing a triangle, defined as the image of chordal SLE_κ in the half-plane.

$h(x) = F(x)$, which hints at the fact that the triangle T is special for chordal SLE_κ (this was observed by Dubédat in [30]).

Now let ψ be the conformal self-map of \mathbb{H} such that $\psi(-R) = 1$, $\psi(0) = \infty$ and $\psi(1) = 0$, that is,

$$\psi(z) = \frac{R}{R+1} \frac{z-1}{z} = x \frac{z-1}{z}; \quad z \in \mathbb{H}. \tag{4.8}$$

Then $F \circ \psi$ is a conformal map of \mathbb{H} onto T which takes $-R, 0$ and 1 onto the three corners of the triangle. Note in particular that the image under $F \circ \psi$ of chordal SLE_κ in the half-plane from 0 to ∞ is chordal SLE_κ in T from w to $h(x)$, see figure 4.2.

Recall that $h(x)$ is the probability that chordal SLE_κ in the half-plane visits $[1, \infty)$ before $(-\infty, -R]$. Applying the map $F \circ \psi$, this implies that the probability that chordal SLE_κ in T from w to $h(x)$ first hits the interval $[0, 1]$ to the left of $h(x)$ is precisely $h(x)$. For $\kappa = 6$, this result together with the locality property proves the following fact (see also the discussion in section 1.4):

Theorem 4.2 (Carleson’s version of Cardy’s formula). *Consider chordal SLE_6 in the triangle $T_{\pi/3}$ from $w_{\pi/3}$ to any point $b \in [0, 1]$. Let τ be the first time when the trace γ visits $[0, 1]$. Then $\gamma(\tau)$ has the uniform distribution on $[0, 1]$.*

A second generalisation of Cardy’s formula for $4 < \kappa < 8$ can be obtained as follows. Consider again chordal SLE_κ from 0 to ∞ , but this time let $R > 1$. Then either the point 1 becomes part of the hull before R , or both points are absorbed by the hull at the same time. The probability $f(R)$ that 1 and R are absorbed at the same time can be computed in a way analogous to the computation of $h(x)$ above [78, lemma 6.6]. With $F = F_{(1-4/\kappa)\pi}$ as before and $\varphi(z) = (1-z)^{-1}$ one finds

$$f(R) = \frac{\int_R^\infty t^{-4/\kappa} (t-1)^{8/\kappa-2} dt}{\int_1^\infty t^{-4/\kappa} (t-1)^{8/\kappa-2} dt} = \frac{(F \circ \varphi)(R)}{(F \circ \varphi)(1)}. \tag{4.9}$$

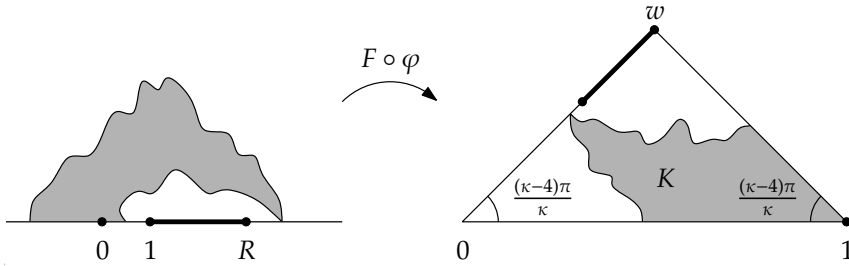


Figure 4.3. The partition induced by chordal SLE_κ from 1 to 0 in a well-chosen triangle, stopped when it hits the arc $w \cup 0$.

Here the second equality follows from the substitution $t = 1 - u^{-1}$. This proves the following generalisation of Cardy’s formula (see also figure 4.3):

Theorem 4.3 (Second generalisation of Cardy’s formula). *Consider chordal SLE_κ for fixed $4 < \kappa < 8$ in the triangle $T = T_{(1-4/\kappa)\pi}$ from 1 to 0. Let τ be the first time when the trace γ hits the boundary arc $0 \cap w = w_{(1-4/\kappa)\pi}$. Then $\gamma(\tau)$ has the uniform distribution on this boundary arc.*

Note that the chordal SLE process of theorem 4.3 considered up to time τ partitions T into three components: the hull $K = \overline{\cup_{t < \tau} K_t}$ generated up to time τ and the two connected components of the complement to the left and right of this hull in T . See figure 4.3. By studying the process $(g_t(z) - \xi(t))/(g_t(1) - \xi(t))$ for chordal SLE in \mathbb{H} one can compute the probabilities that a point $z \in T$ is in one of these components, as was shown by Dubédat in [30]. We will prove an analogous result for dipolar SLE in section 4.5 using similar arguments. For the chordal case we cite the following results from Dubédat [30]:

Theorem 4.4. *For $4 < \kappa < 8$, consider chordal SLE_κ as in theorem 4.3. Then for a given point $z \in T$, the probability that $z \in K$ is given by the distance from z to the line through 0 and w divided by the distance from 1 to this line. Likewise, the probability that z is to the left (right) of K is given by the distance from z to the line through 1 and w (0 and 1) divided by the distance from 0 (w) to this line.*

Corollary 4.5. *The hull K and both components of the complement of K in T each have an expected area equal to $1/3$ of the area of the triangle T .*

4.2 SLE crossing exponents

Reconsider chordal SLE_κ in the rectangle $R_L = (0, L) \times (0, \pi)$ from $i\pi$ to L , as in section 4.1. Theorem 4.1 gives the probability of the event E that the trace

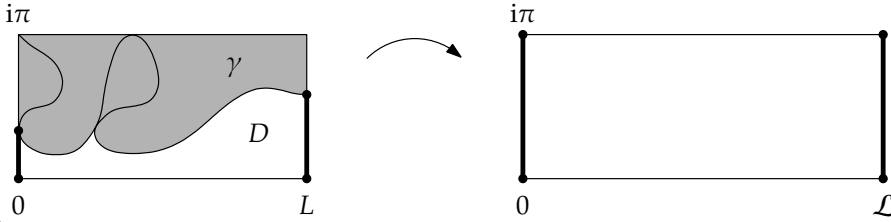


Figure 4.4. Definition of the extremal distance \mathcal{L}/π between the two thick arcs below a crossing of a rectangle.

of this SLE crosses the rectangle left-to-right without touching the bottom. Probabilities such as these are expected to decay for $L \rightarrow \infty$ with certain critical exponents, and this case is no exception. The following corollary of theorem 4.1 shows that the associated exponent in the half-plane is $1 - 4/\kappa$:

Corollary 4.6. *The probability of the event E satisfies*

$$\mathbf{P}[E] \asymp \exp \left[- \left(1 - \frac{4}{\kappa} \right) L \right] \quad \text{as } L \rightarrow \infty, \quad (4.10)$$

where \asymp indicates that each side is bounded by a constant times the other side.

A.6 ◀ **Proof.** For $0 < x < 1$, the hypergeometric function in theorem 4.1 is bounded between two constants, see for instance [71]. Recall that $x = R/(R+1)$, so that $1-x = (R+1)^{-1}$. By lemma A.22, $\exp(L)/16 \leq R+1 \leq \exp(L)/16+1 \leq 17 \exp(L)/16$. The result follows. ■

A.2 ◀ This result can be generalised in the following way. As before, let τ denote the first time when γ hits the arc $0 \cup L + i\pi$. On the event E , let D be the connected component of $R_L \setminus \gamma[0, \tau]$ whose boundary contains the interval $[0, L]$. Then there is a unique number \mathcal{L} such that there is a conformal transformation of D onto the rectangle $R_{\mathcal{L}} = (0, \mathcal{L}) \times (0, \pi)$ which maps $(0 \cap i\pi) \cap \partial D$ onto $0 \cap i\pi$ and $L \cup \gamma(\tau)$ onto $\mathcal{L} \cup \mathcal{L} + i\pi$. See figure 4.4. The number \mathcal{L} is π times the extremal distance between $0 \cap i\pi$ and $L \cup L + i\pi$ in D .

We may now consider the expected value of $1_E \exp(-\lambda \mathcal{L})$ for any $\lambda \geq 0$ (here, 1_E is the indicator of the event E , i.e. the function which is 1 on the event E and 0 otherwise). This value decays to zero for $L \rightarrow \infty$ with a certain power of $\exp(-L)$, giving rise to a new critical exponent $u(\kappa, \lambda)$. This exponent is called the *one-sided crossing exponent*, since it measures the extremal distance on one side of an SLE_{κ} path crossing the rectangle. Clearly, for $\lambda = 0$ the exponent has to reduce to the value $1 - 4/\kappa$ by theorem 4.1. The one-sided crossing exponent was computed in [55]. Here we content ourselves with just stating the result:

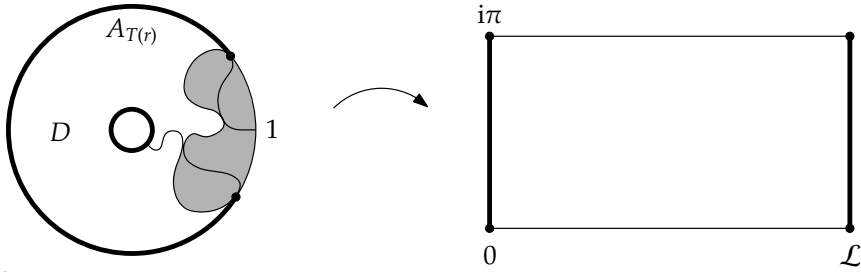


Figure 4.5. An SLE path crossing an annulus, and the definition of the extremal distance \mathcal{L}/π between the two thick arcs in the remaining domain.

Theorem 4.7 (One-sided crossing exponent). For any $\lambda \geq 0$ and $\kappa > 4$,

$$\mathbf{E}[1_E \exp(-\lambda \mathcal{L})] \asymp \exp[-u(\kappa, \lambda)L] \quad \text{as } L \rightarrow \infty, \tag{4.11}$$

where the one-sided crossing exponent $u(\kappa, \lambda)$ is given by

$$u(\kappa, \lambda) = \lambda + \frac{\kappa - 4 + \sqrt{(\kappa - 4)^2 + 16\kappa\lambda}}{2\kappa}. \tag{4.12}$$

An analogue of the one-sided crossing exponent for radial SLE was derived in [56] using a very similar approach. This exponent, called the *annulus crossing exponent*, is defined as follows. Consider radial SLE_κ in the unit disk for any $\kappa > 0$, starting from 1. For any $t > 0$ set $A_t := \partial\mathbb{D} \setminus K_t$, where K_t is the hull of the SLE at time t . Then the set A_t is either an arc of the unit circle or $A_t = \emptyset$ (the latter occurs if γ has closed a loop around the origin).

Now, for any $r > 0$ let $T(r)$ denote the first time when the SLE trace intersects $B_r = \{z : |z| \leq r\}$ and let E_r be the event that $A_{T(r)}$ is nonempty. Observe that on the event E_r the domain $D = \mathbb{D} \setminus (B_r \cup K_{T(r)})$ is conformally equivalent to a rectangle. More precisely, there is a unique number \mathcal{L} such that there is a conformal transformation of D onto the rectangle $R_\mathcal{L} = (0, \mathcal{L}) \times (0, \pi)$ which maps $|z| = r$ onto $0 \cap i\pi$ and $A_{T(r)}$ onto $L \cup L + i\pi$. Similarly to the case of the one-sided crossing exponent, \mathcal{L} is π times the extremal distance between $|z| = r$ and $|z| = 1$ in D . See figure 4.5 for a picture. The following theorem was proved by Lawler, Schramm and Werner in [56]:

Theorem 4.8 (Annulus crossing exponent). For any $\lambda > 0$ and $\kappa > 0$,

$$\mathbf{E}[1_E \exp(-\lambda \mathcal{L})] \asymp r^{v(\kappa, \lambda)} \quad \text{as } r \rightarrow 0, \tag{4.13}$$

where the annulus crossing exponent $v(\kappa, \lambda)$ is given by

$$v(\kappa, \lambda) = \frac{8\lambda + \kappa - 4 + \sqrt{(\kappa - 4)^2 + 16\kappa\lambda}}{16}. \tag{4.14}$$

4.3 Crossing exponents for critical percolation

The connection between SLE_6 and critical site percolation on the triangular lattice can be used to verify rigorously the values of certain percolation exponents, as is explained by Smirnov and Werner in [89]. In this section we shall consider how for example the multi-arm exponents for percolation can be calculated. This makes use of the SLE crossing exponents appearing in section 4.2. Predictions for the values of these exponents have been given before in several places in the physics literature, see for instance [34] and references therein.

4.3.1 Half-plane exponents

Consider critical site percolation on the triangular lattice with fixed mesh, as defined in section 1.3. Let $A^+(r, R)$ be a discrete approximation by hexagons of the semi-annulus $\{z : r < |z| < R, \text{Im } z > 0\}$, and denote by $f_k^+(r, R)$ the probability that there exist k disjoint crossings of arbitrary colours from the inner circle to the outer circle in $A^+(r, R)$. By a crossing we mean a sequence of distinct connected hexagons, all in the same colour, whose first and last hexagons are adjacent to a hexagon intersecting the inner and outer circle, respectively. Obviously, r has to be large enough if the definition of $f_k^+(r, R)$ is to make sense, i.e. $r > \text{const}(k)$.

It is well-known that the probability $f_k^+(r, R)$ does not depend on the choice of colours of the different crossings. The reason for this is that one can always flip the colours of crossings without changing probabilities. To see this, start by considering the clockwise-most crossing. If desired, its colour can be flipped by flipping the colours of all hexagons. Then one proceeds by each time considering the clockwise-most crossing to the left of the previous one. If desired, its colour can be flipped by flipping the colours of all hexagons to the left of this previous crossing. In the end one obtains a configuration with all crossings in the desired colours, without changing probabilities. Therefore, we may take $f_k^+(r, R)$ to be the probability of k crossings of alternating colours.

We are now ready to make the connection with SLE. Suppose that we colour all hexagons on the boundary of the semi-annulus blue if they intersect the arc $-r \cup R$, and yellow if they intersect $-r \cap R$. Then the probability $f_k^+(r, R)$ is exactly the probability that the exploration process from $-r$ to R makes k crossings before it hits the interval $[r, R]$. By the connection with SLE_6 , this translates in the scaling limit into the probability that a chordal SLE_6 process from $-r$ to R in the semi-annulus makes k crossings before it hits the interval $[r, R]$, see figure 4.6.

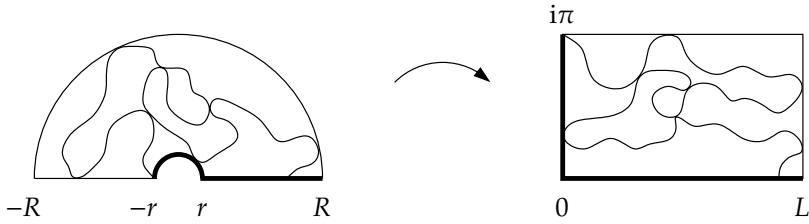


Figure 4.6. An SLE₆ path which crosses a semi-annulus three times, and the conformal image in a rectangle. The part of the boundary drawn thick is considered to carry blue boundary conditions.

It is more convenient now to map the problem to a rectangle using the logarithmic map. Suppose that $g_k^+(L)$ denotes the probability that an SLE₆ trace from $i\pi$ to L in the rectangle $R_L := (0, L) \times (0, \pi)$ makes k horizontal crossings before it hits the bottom. Then, by conformal invariance, we want to determine $g_k^+(L)$ for $L = \log(R/r)$. For $k = 1$, corollary 4.6 immediately gives $g_1^+(L) \asymp \exp(-L/3)$. Exponents for larger values of k can be determined with the help of theorem 4.7, as we shall now discuss.

Let T be the time at which the SLE₆ trace has crossed the rectangle for the first time and let E be the event that up to time T the trace has not hit the bottom. Then the process still has to make $k - 1$ crossings in the domain remaining below this first crossing. Hence, if \mathcal{L} denotes π times the extremal distance between the left and right sides of R_L in this remaining domain (as explained in section 4.2), we have

$$g_k^+(L) = \mathbb{E}[1_E g_{k-1}^+(\mathcal{L})]. \tag{4.15}$$

It is now clear from $g_1^+(L) \asymp \exp(-L/3)$ and theorem 4.7 that $g_k^+(L) \asymp \exp(-a_k^+ L)$ for all $k \geq 1$ and some a_k^+ , and that the numbers a_k^+ can be determined recursively.

In terms of the one-sided crossing exponent $u(\kappa, \lambda)$, the recursion formula for the a_k^+ reads $a_k^+ = u(6, a_{k-1}^+)$. It follows that

$$a_k^+ = \frac{k(k+1)}{6}. \tag{4.16}$$

Returning to the case of discrete percolation in the semi-annulus, this result implies that

$$f_k^+(r, R) \asymp R^{-k(k+1)/6} \quad \text{when } R \rightarrow \infty. \tag{4.17}$$

To make this transition to discrete percolation completely rigorous some more work is required. We refer to [89] and [22, appendix A] for more details. To

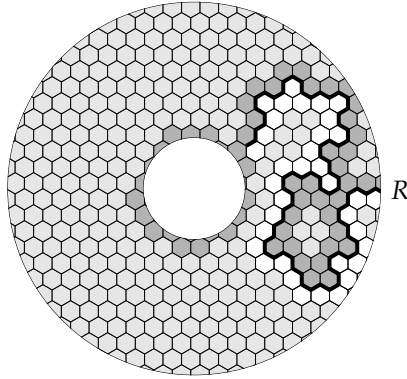


Figure 4.7. Part of the percolation exploration process in an annulus.

complete the discussion, we finally note that for odd k , $f_k^+(r, R)$ is also the probability that there exist $j = (k + 1)/2$ disjoint blue clusters crossing the semi-annulus.

4.3.2 Plane exponents

We now turn to the planar case. Suppose that $A(r, R)$ is an approximation of the full annulus $\{z : r < |z| < R\}$ by hexagons, where r is again assumed to be large enough. We are interested in the probability that there are k crossing of the annulus in critical percolation. As in section 4.3.1, this probability can be determined by considering a suitably defined exploration process in the annulus. This exploration process is defined as we shall now discuss.

We start by colouring all hexagons intersecting the inner circle $|z| = r$ blue. The exploration process starts at R with a blue hexagon on its right and a yellow hexagon on its left. Each time the exploration process hits a hexagon on the outer circle $|z| = R$ that was not visited before, we look at the argument of the tip of the exploration path at that time (where the argument is determined continuously, so that it makes no jumps after completing a circle). If the argument is positive, the hexagon on the boundary is coloured blue, and otherwise it is coloured yellow. See figure 4.7 for an illustration.

At the time T when the exploration process described above first hits the inner circle, it defines unambiguously a clockwise-most blue crossing of the annulus and a counter-clockwise-most yellow crossing such that the point R lies between them. Moreover, it is clear that after time T the exploration process continues like a chordal process in the domain remaining between these two

crossings, where we may now assume that all hexagons intersecting the outer circle are coloured yellow.

Observe that the remaining domain for the exploration process after time T is conformally equivalent to a semi-annulus. Consider the probability that the exploration process crosses this remaining domain $k - 2$ times before it disconnects the inner circle from the outer circle. By our discussion in section 4.3.1, this probability is equal to the probability that there are $k - 2$ crossings of arbitrary colours of this domain.

Now let us denote by $f_k(r, R)$ the probability that the exploration process defined above crosses the annulus a total number of $k - 1$ times. Then for even k , $f_k(r, R)$ is precisely the probability that there exist k crossings of the annulus which are not all of the same colour. To see this, observe that we have the freedom of choosing alternating colours for the crossings. The point R is then always located in between a clockwise-most blue and a counter-clockwise-most yellow crossing, which proves the point.

For odd k , the situation is different and $f_k(r, R)$ is not exactly equal to the probability that there exist k crossings of the annulus which are not all of the same colour. However, it can be shown that the two probabilities differ only by a multiplicative constant, as is explained in [89]. Therefore, for odd k the exponent with which $f_k(r, R)$ decays to zero is still the critical exponent for the event that there exist k crossings of the annulus which are not all of the same colour.

We now make the connection with SLE_6 . In the continuum limit, the discrete exploration process converges to the following SLE_6 process. First, we do radial SLE_6 in the annulus from R to 0 up to the first time T that the process hits the inner circle. Afterwards, the process continues like a chordal SLE_6 process in the remaining domain. We further define E to be the event that up to time T the process has not disconnected the inner circle from the outer circle. On this event we let \mathcal{L} denote π times the extremal distance between the two circles in the remaining domain, as explained in section 4.2.

Denote by $g_k(r, R)$ the probability that this SLE_6 process crosses the annulus $k - 1$ times before it disconnects the inner circle from the outer circle. Then

$$g_k(r, R) = \mathbf{E}[1_E g_{k-2}^+(\mathcal{L})] \asymp \mathbf{E}[1_E e^{-a_{k-2}^+ \mathcal{L}}], \quad (4.18)$$

where $g_k^+(L)$ is the probability of k crossings of the rectangle $(0, L) \times (0, \pi)$, as before, and a_k^+ is the corresponding exponent. Theorem 4.8 now tells us that $g_k(r, R) \asymp (R/r)^{-a_k}$, where

$$a_k = v(6, a_{k-2}^+) = \frac{k^2 - 1}{12}. \quad (4.19)$$

Returning to discrete percolation, it follows from this result that the probability of k crossings of the annulus $A(r, R)$ which are not all of the same colour behaves like

$$f_k(r, R) \asymp R^{-(k^2-1)/12} \quad \text{when } R \rightarrow \infty. \quad (4.20)$$

Again, all of this can be made rigorous [22, 89]. Observe also that we can again interpret the result in terms of crossings of clusters. In this case we have that for k even, $f_k(r, R)$ is comparable to the probability that there exist $j = k/2$ disjoint blue clusters crossing the annulus.

So far we have only considered the dichromatic exponents associated with the probability of k percolation crossings of an annulus that are *not* all of the same colour. The corresponding monochromatic exponents for k crossings that *are* of the same colour are known to have different values. They are not so easily accessible through SLE as the dichromatic exponents. However, SLE computations in [54] have confirmed that the one-arm exponent ($k = 1$) has the value $5/48$, and in the same article a description of the backbone exponent ($k = 2$) as the leading eigenvalue of a differential operator was given.

4.4 Schramm's left-passage formula

In section 4.3 we reviewed how the values of the multi-arm exponents for critical percolation have been confirmed rigorously using SLE. We will now turn our attention to an SLE computation yielding a new result for critical models, that has not been predicted before in the physics literature. This computation leads to a formula for the probability that a chordal SLE_κ path in the upper half-plane passes to the left of a given point $z \in \mathbb{H}$. It was derived by Schramm in [83].

We consider chordal SLE_κ in \mathbb{H} from 0 to ∞ for some fixed value of $\kappa \in (0, 8)$. Let $z = x + iy \in \mathbb{H}$ be fixed. Note that for $\kappa \leq 4$ (since γ is a simple path) it is clear what we mean by the statement that γ passes to the left of z . For $4 < \kappa < 8$, however, z becomes part of the hull after a finite time. In that case, we say that γ passes to the left of z if z is disconnected from ∞ by a piece of γ with passes around z in the clockwise direction. See figure 4.8 for examples.

Observe that by scale invariance the probability that the trace γ of SLE_κ passes to the left of z can depend only on the ratio $u = x/y$. We will write $h(u)$ for this probability. Now let us define $X(t) := \text{Re } g_t(z) - \xi(t)$, $Y(t) := \text{Im } g_t(z)$ and $U(t) := X(t)/Y(t)$, where ξ is the driving process of chordal SLE_κ and g_t are the Löwner maps. Suppose that we let the trace grow for an infinitesimal time dt . Then, by stationarity (lemma 2.3), we must have $\mathbf{E}[h(U(dt))] = h(u)$.

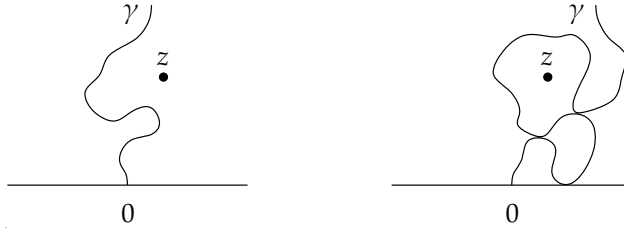


Figure 4.8. SLE_κ trace passing to the left of z for $\kappa \leq 4$ and $4 < \kappa < 8$, respectively.

Assuming that h is sufficiently differentiable, we can Taylor-expand this expression to order dt using the real and imaginary parts of Löwner's differential equation (2.11). It follows that the function h must satisfy

$$\frac{\kappa}{2}h''(u) + \frac{4u}{1+u^2}h'(u) = 0, \tag{4.21}$$

with the boundary conditions $h(\infty) = 1$ and $h(-\infty) = 0$. This has the unique solution

$$h(u) = \frac{\int_{-\infty}^u (1+t^2)^{-4/\kappa} dt}{\int_{-\infty}^{\infty} (1+t^2)^{-4/\kappa} dt}. \tag{4.22}$$

Thus we have derived a formula for the probability that γ passes to the left of z , under the assumption that h is sufficiently differentiable. This formula can also be written in terms of a hypergeometric function [71], yielding equation (4.23) below. We now make this result rigorous.

Theorem 4.9 (Schramm's left-passage formula). *Let $\kappa \in (0, 8)$ and $z = x+iy \in \mathbb{H}$, and denote by E the event that the trace γ of chordal SLE_κ in \mathbb{H} from 0 to ∞ passes to the left of z . Then*

$$\mathbf{P}[E] = \frac{1}{2} + \frac{\Gamma\left(\frac{4}{\kappa}\right)}{\sqrt{\pi}\Gamma\left(\frac{8-\kappa}{2\kappa}\right)} {}_2F_1\left(\frac{1}{2}, \frac{4}{\kappa}; \frac{3}{2}; -\frac{x^2}{y^2}\right) \frac{x}{y}. \tag{4.23}$$

B.4 ◀ **Proof.** Define $X(t)$, $Y(t)$ and $U(t)$ as above, and define the function $h : \mathbb{R} \rightarrow [0, 1]$ by equation (4.22). Let $T(z)$ be the first time when z is in the hull of chordal SLE_κ (note that for $\kappa \leq 4$, $T(z) = \infty$ a.s.). Observe that $U(t)$ is finite for $t < T(z)$. We will show in the following paragraph that if γ passes z on the left, then $U(t)$ tends to $+\infty$ when $t \rightarrow T(z)$, whereas if γ passes z on the right, then $U(t)$ tends to $-\infty$ when $t \rightarrow T(z)$. Hence, $h \circ U(T(z))$ is the indicator of the event E .

To see this, assume first that γ passes to the left of z . In that case it is clear that the harmonic measure at z of the union of $[0, \infty)$ and the right-hand side

of $\gamma[0, t]$ in the domain $\mathbb{H} \setminus \gamma[0, t]$ tends to 1 as $t \rightarrow T(z)$ (e.g. by theorem B.14). By conformal invariance of harmonic measure, it follows that the harmonic measure of $[\xi(t), \infty)$ at $g_t(z)$ in \mathbb{H} tends to 1 as $t \rightarrow T(z)$. This implies that $U(t) \rightarrow +\infty$ on the event E (corollary B.15). On the other hand, if γ passes to the right of z , then the harmonic measure tends to 0 as $t \rightarrow T(z)$ which implies that $U(t) \rightarrow -\infty$.

Now observe that by taking the real and imaginary parts of Löwner's differential equation we obtain

$$dX(t) = \frac{2X(t) dt}{X(t)^2 + Y(t)^2} - d\xi(t), \quad dY(t) = -\frac{2Y(t) dt}{X(t)^2 + Y(t)^2}. \quad (4.24)$$

Applying Itô's formula it follows that U satisfies the stochastic differential equation

$$dU(t) = \frac{4U(t)}{1 + U(t)^2} \frac{dt}{Y(t)^2} - \frac{d\xi(t)}{Y(t)}. \quad (4.25)$$

Another application of Itô's formula then reveals that for $t < T(z)$ the process $h \circ U$ is a martingale, since h satisfies the differential equation (4.21). Note that in fact, $h \circ U$ is bounded for $t \leq T(z)$. Hence the optional sampling theorem B.7 implies that $\mathbf{E}[h \circ U(T(z))] = h(U(0)) = h(x/y)$, proving that $h(x/y)$ is the probability of the event E . ■

Using the fact that the SLE_6 trace is the scaling limit of the percolation exploration process, theorem 4.9 has a nice interpretation for the scaling limit of critical percolation in the unit disk. Again following Schramm [83], consider critical site percolation on the intersection of a triangular lattice with mesh $\delta > 0$ and the unit disk \mathbb{D} . Fix $\vartheta \in (0, 2\pi)$ and let A_ϑ be the arc of the unit circle between the angles 0 and ϑ , that is, $A_\vartheta := \{\exp(is) : 0 \leq s \leq \vartheta\}$. We are interested in the probability of the event E_ϑ that there is a cluster of blue hexagons connected to A_ϑ such that the union of this cluster with the arc A_ϑ surrounds the origin.

Theorem 4.10. *In the scaling limit, the probability of the event E_ϑ satisfies*

$$\lim_{\delta \rightarrow 0} \mathbf{P}[E_\vartheta] = \frac{1}{2} - \frac{\Gamma\left(\frac{2}{3}\right)}{\sqrt{\pi} \Gamma\left(\frac{1}{6}\right)} {}_2F_1\left(\frac{1}{2}, \frac{2}{3}; \frac{3}{2}; -\cot^2 \frac{\vartheta}{2}\right) \cot \frac{\vartheta}{2}. \quad (4.26)$$

Proof. Consider the chordal exploration process in the unit disk from 1 to the point $\exp(i\vartheta)$. Let γ^{ep} denote the trace of this process. Then E_ϑ is equal to the event that the origin is in a connected component of $\mathbb{D} \setminus \gamma^{\text{ep}}$ which lies on the right-hand side of the exploration process. See figure 4.9 for an illustration.

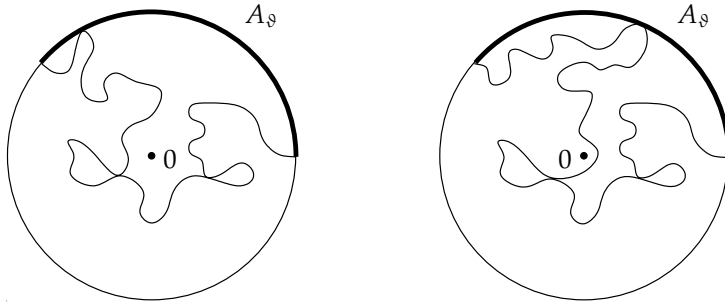


Figure 4.9. A percolation exploration process in the unit disk passing to the left or the right of the origin, respectively. In the former case, there is a blue cluster connected to the arc A_ϑ which surrounds the origin, in the latter case there is no such cluster.

Suppose that we now map the unit disk onto the upper half-plane in such a way that 1 maps to 0 and $\exp(i\vartheta)$ maps to ∞ . It is easy to see that an inverse map with the desired properties is

$$\varphi(z) = e^{i\vartheta} \frac{z + \cot \frac{\vartheta}{2} - i}{z + \cot \frac{\vartheta}{2} + i}; \quad z \in \mathbb{H}, \tag{4.27}$$

since this is just the composition of the standard map $(z - i)/(z + i)$ of \mathbb{H} onto \mathbb{D} with a translation and a rotation. Observe that the point z_0 which maps to the origin is $z_0 = i - \cot(\vartheta/2)$. In the scaling limit $\delta \rightarrow 0$ the event E_ϑ has the same probability as the event that the SLE_6 trace in the half-plane passes to the left of the point z_0 . The probability of this event is given by theorem 4.9. The result follows. ■

For values of $\kappa \in (4, 8)$ other than $\kappa = 6$ the same reasoning gives us a conjecture for the scaling limit of the Fortuin-Kasteleyn cluster models (section 3.4). We consider the cluster model for the value of q corresponding to κ . The boundary conditions are such that there is a Fortuin-Kasteleyn cluster along the arc A_ϑ and a dual cluster along $\partial D \setminus A_\vartheta$, as discussed in section 3.4. Then we conjecture the following:

Conjecture 4.11. *The probability that the origin is surrounded by the Fortuin-Kasteleyn cluster which is connected to the arc A_ϑ tends in the scaling limit to*

$$\frac{1}{2} - \frac{\Gamma\left(\frac{4}{\kappa}\right)}{\sqrt{\pi} \Gamma\left(\frac{8-\kappa}{2\kappa}\right)} {}_2F_1\left(\frac{1}{2}, \frac{4}{\kappa}; \frac{3}{2}; -\cot^2 \frac{\vartheta}{2}\right) \cot \frac{\vartheta}{2}. \tag{4.28}$$

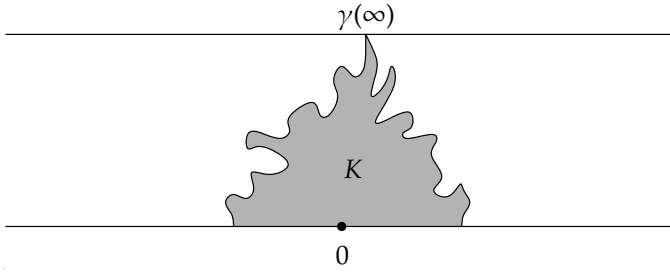


Figure 4.10. The hull K generated by dipolar SLE in a strip for $\kappa > 4$.

4.5 Computations with dipolar SLE

Dipolar SLE allows us to do computations for critical systems with boundary conditions that differ from those of chordal SLE. In this section we give an overview of results appearing in [11, 12]. We consider dipolar SLE in the strip $\mathcal{S} := \{z \in \mathbb{C} : 0 < \text{Im} z < \pi/2\}$, as defined in section 2.4. Then for $\kappa = 3$, for instance, the trace of dipolar SLE_κ is believed to be the scaling limit of the exploration path of the Ising model with positive boundary conditions along the positive reals, negative boundary conditions along the negative reals and free boundary conditions along the top boundary of the strip (see [12] for simulations supporting this conjecture).

In the case of critical percolation ($\kappa = 6$) we have similar boundary conditions: blue on the negative reals, yellow on the positive reals, and free on the top boundary of the strip. For values of κ between 4 and 8, it is natural to conjecture that dipolar SLE_κ describes the limit of a Fortuin-Kasteleyn cluster model with a cluster along the positive reals, a dual cluster along the negative reals and free boundary conditions along the top boundary of the strip. We refer to [12] for a discussion in terms of the connection between dipolar SLE and conformal field theory.

As we indicated in section 2.4, the trace γ of dipolar SLE_κ will land at a random point $\gamma(\infty)$ on the top boundary of the strip (see figure 4.10). Our first aim is to compute the distribution of this point. To do so, for $z = x + i\pi/2$ with $x \in \mathbb{R}$ we set $X(t) := g_t(z) - \xi(t) - i\pi/2$, where g_t are the Löwner maps and $\xi(t) = \sqrt{\kappa}B(t)$ is the driving process for dipolar SLE_κ . Note that $g_t(z)$ stays on the top boundary of the strip, so that X is a real-valued process. The dipolar Löwner equation (2.20) readily shows that X satisfies

$$dX(t) = 2 \tanh X(t) dt - d\xi(t), \quad X(0) = x. \quad (4.29)$$

Let $h(x)$ be the probability that z lies to the left of $\gamma(\infty)$. Suppose that we let the trace grow for an infinitesimal time dt . Then from the stationarity of SLE we

conclude that $\mathbf{E}[h(X(dt))] = h(x)$. Assuming that h is sufficiently differentiable, Taylor-expansion in dt then gives the following differential equation for h :

$$2h'(x) \tanh x + \frac{\kappa}{2} h''(x) = 0. \quad (4.30)$$

The boundary conditions are clearly $h(-\infty) = 1$ and $h(\infty) = 0$. As in previous sections of this chapter, the unique solution will give the probability that x is to the left of $\gamma(\infty)$. We find for any $\kappa > 0$

$$\mathbf{P}[x + i\pi/2 \text{ is to the left of } \gamma(\infty)] = \frac{\int_x^\infty (\cosh t)^{-4/\kappa} dt}{\int_{-\infty}^\infty (\cosh t)^{-4/\kappa} dt}. \quad (4.31)$$

This is of course also the probability that $\gamma(\infty)$ lies to the right of $z = x + i\pi/2$, and hence describes the distribution of $\gamma(\infty)$.

In a similar way one can compute the probability that a point x on the real line never ends up in the hull of the dipolar SLE. Clearly this makes sense only for $\kappa > 4$, since the trace does not intersect the real line for $\kappa \leq 4$. Here we will not spell out the computation in detail, but instead we simply state the result that for $x \in \mathbb{R}$,

$$\mathbf{P}[x \text{ is not in the hull}] = \frac{\int_0^{|x|} (\sinh t)^{-4/\kappa} dt}{\int_0^\infty (\sinh t)^{-4/\kappa} dt}. \quad (4.32)$$

This also describes the probability that the hull does not spread beyond the point x on the real line.

It turns out that for $\kappa > 4$ both formulas (4.31) and (4.32) above can be generalised to points in the interior of the domain. To see this, let $z \in \mathbb{S}$ and write $h(z)$ for the probability of either the event that z is to the left of the hull, or the event that z is in the hull. We will distinguish between the two events later by imposing appropriate boundary conditions. Consider the dipolar Löwner evolution of $g_t(z)$ for an infinitesimal time. Using stationarity and Taylor-expanding $\mathbf{E}[h(g_{dt}(z) - \xi(dt))] = h(z)$ we find that h must obey

$$2h'(z) \coth z + \frac{\kappa}{2} h''(z) = 0. \quad (4.33)$$

Bauer, Bernard and Houdayer observed in [12] that this equation has harmonic solutions with appropriate boundary conditions for the probabilities we are interested in. It was not noticed in [12] that these solutions have a simple interpretation in terms of a conformal transformation from the strip to a well-chosen triangle. Here we shall write the solutions of (4.33) in terms of this transformation, from which it is immediate that solutions satisfying the appropriate boundary conditions exist.

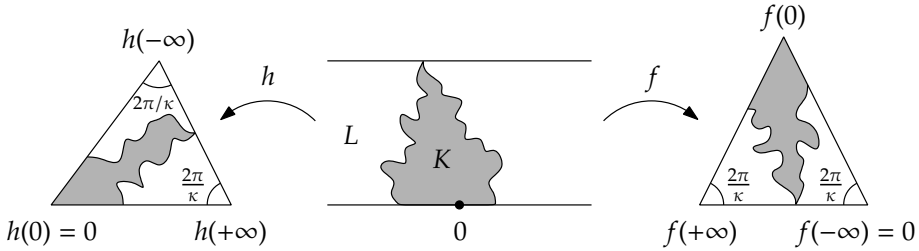


Figure 4.11. Conformal transformations of dipolar SLE in a strip to triangles.

A.6 ◀ We start by observing that a solution of the differential equation (4.33) is given by

$$h(z) = h_\kappa(z) = \int_0^z (\sinh t)^{-4/\kappa} dt, \quad z \in \mathbb{S}. \quad (4.34)$$

Next we make the substitution $u = \tanh t$. Note that \tanh is the conformal transformation of \mathbb{S} onto the upper half-plane \mathbb{H} such that $\tanh(0) = 0$ and $\tanh(\pm\infty) = \pm 1$. Observing that $\sinh^2 t = u^2/(1-u^2)$ and $\cosh^2 t = 1/(1-u^2)$ we obtain

$$h(z) = \int_0^{\tanh z} u^{-4/\kappa} (1-u)^{2/\kappa-1} (1+u)^{2/\kappa-1} du, \quad z \in \mathbb{S}. \quad (4.35)$$

This is precisely the conformal transformation of \mathbb{S} onto a triangle with corners at $h(0) = 0$, $h(+\infty) > 0$ and $h(-\infty) \in \mathbb{H}$. The interior angles at the corners are $(1-4/\kappa)\pi$, $2\pi/\kappa$ and $2\pi/\kappa$, respectively. Figure 4.11 illustrates the mapping.

We now show how this mapping onto a triangle helps us to find the probabilities that a point $z \in \mathbb{S}$ is either in the hull or to the left of the hull of dipolar SLE_κ . Let us write \overline{K} for the hull generated by the dipolar SLE in the limit $t \rightarrow \infty$, that is, $\overline{K} := \bigcup_{t \geq 0} \overline{K}_t$. We denote by L the (unbounded) component of the complement of \overline{K} in \mathbb{S} that lies to the left of \overline{K} . Then our first claim is that

$$\mathbf{P}[z \in L] = \frac{\text{Im } h(z)}{\text{Im } h(-\infty)}. \quad (4.36)$$

To see this, we only need to verify that this function satisfies the appropriate boundary conditions: it must be 0 on the positive reals, tend to 0 for $z \rightarrow +\infty$, and tend to 1 for $z \rightarrow -\infty$. But it is clear from the mapping onto a triangle that the formula (4.36) indeed satisfies these conditions.

Next we consider the probability of the event $\{z \in K\}$. In this case, the solution should tend to 0 both for $z \rightarrow +\infty$ and for $z \rightarrow -\infty$ and should be 1 at $z = 0$. To find such a solution, we define the map f by

$$f(z) := e^{i(1+2/\kappa)\pi} (h(z) - h(-\infty)). \quad (4.37)$$

Then f is a conformal transformation of \mathbb{S} onto the triangle with corners at $f(-\infty) = 0$, $f(0) \in \mathbb{H}$ and $f(+\infty) < 0$ with interior angles $2\pi/\kappa$ at $f(\pm\infty)$, see figure 4.11. In terms of f it is easily seen that we must have

$$\mathbf{P}[z \in K] = \frac{\operatorname{Im} f(z)}{\operatorname{Im} f(0)} \tag{4.38}$$

because this function satisfies the appropriate boundary conditions.

We conclude that $\mathbf{P}[z \in L]$ and $\mathbf{P}[z \in K]$ have a particularly nice form for dipolar SLE in a well-chosen triangle. To make this precise, we first introduce some notation. By T_α we denote the triangle in the upper half-plane with vertices at 0 and 1 with interior angles α . The third vertex is denoted by $w_\alpha \in \mathbb{H}$. We consider dipolar SLE_κ in $T = T_{2\pi/\kappa}$ started from $w = w_{2\pi/\kappa}$ and with 0 and 1 fixed under the evolution. This process partitions T into three components: the hull and the two components of the complement of the hull in T . According to equations (4.36) and (4.38) we should then have for dipolar SLE the following analogue of theorem 4.4 in section 4.1 for chordal SLE:

Theorem 4.12. *For $\kappa > 4$, consider dipolar SLE_κ in the triangle $T = T_{2\pi/\kappa}$ started from $w = w_{2\pi/\kappa}$ and with 0 and 1 fixed under the Löwner evolution. Then for a given point $z \in T$, the probability that z is in the hull is given by the distance from z to the line through 0 and 1 divided by the distance from w to this line. Likewise, the probability that z is to the left (right) of the hull is given by the distance from z to the line through 1 and w (0 and w) divided by the distance from 0 (1) to this line.*

A.2 ◀ **Proof.** By conformal invariance it is sufficient to establish (4.36) and (4.38) for
 B.4 dipolar SLE_κ in the strip \mathbb{S} . Set $Z(t) := g_t(z) - \xi(t)$, where g_t are the Löwner maps
 B.6 and ξ is the driving process, and let $T = T(z) := \inf\{t \geq 0 : \lim_{s \uparrow t} Z(s) = 0\}$. Define f and h by equations (4.37) and (4.35). Applying Itô’s formula, it is easily seen that $h \circ Z$ (and hence also $f \circ Z$) is a bounded martingale for $t < T$. Therefore, by the optional sampling theorem B.7, $\mathbf{E}[h(Z(T))] = h(z)$ and $\mathbf{E}[f(Z(T))] = f(z)$.

Note that by definition of T , $\lim_{t \rightarrow T} Z(t) = 0$ if z is in the hull. We now show that $\lim_{t \rightarrow T} Z(t) = -\infty$ if z is to the left of the hull. To see this, on the event $\{z \in L\}$ let γ_z be a rectifiable arc extending from z to $-\infty$ in $\mathbb{S} \setminus K$. Then the extremal distance in $\mathbb{S} \setminus K_t$ from γ_z to the union of $[0, \infty)$ and the side of the hull K_t to the right of $\gamma(t)$ tends to ∞ as $t \rightarrow \infty$, because every arc connecting the two sets must cross an annulus centred at $\gamma(\infty)$ of larger and larger modulus, see figure 4.12.

Now we apply the map $f_t : w \mapsto \exp(2g_t(w) - 2\xi(t))$. Noting that $\exp(2w)$ maps the strip onto the upper half-plane, we see that f_t transforms the arc γ_z into an arc in \mathbb{H} connecting $\hat{z}(t) := \exp(2Z(t))$ to 0. From the previous paragraph we conclude that $d_{\mathbb{H}}(f_t(\gamma_z), [1, \infty)) \rightarrow \infty$ as $t \rightarrow \infty$, where $d_{\mathbb{H}}$ denotes extremal distance with respect to \mathbb{H} . But by symmetry, $d_{\mathbb{H}}(f_t(\gamma_z), [1, \infty))$ is twice the

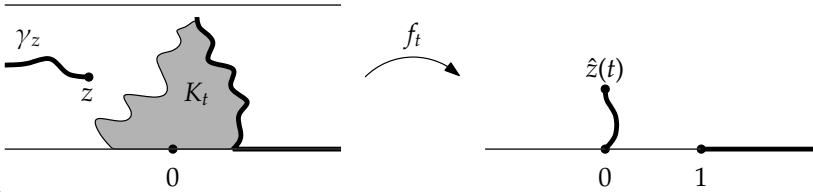


Figure 4.12. The extremal distance between the two thick arcs on the left tends to ∞ as $t \rightarrow \infty$, which implies that $|\hat{z}(t)| \rightarrow 0$.

extremal distance in \mathbb{C} between $[1, \infty)$ and the union of $f_t(\gamma_z)$ with its reflection in the real axis. Teichmüller's theorem A.7 then implies that $d_{\mathbb{H}}(f_t(\gamma_z), [1, \infty)) \leq 2\Lambda(|\hat{z}(t)|^{-1})$. It follows that $|\hat{z}(t)| \rightarrow 0$ or in other words, $Z(t) \rightarrow -\infty$ if z is to the left of the hull. By symmetry, we then also have $Z(t) \rightarrow +\infty$ if z is to the right of the hull.

This shows that $\lim_{t \rightarrow T} \text{Im } h(Z(t)) / \text{Im } h(-\infty)$ is the indicator of the event $\{z \in L\}$ and $\lim_{t \rightarrow T} \text{Im } f(Z(t)) / \text{Im } f(0)$ is the indicator of the event $\{z \in K\}$. Thus the theorem follows from the optional sampling theorem B.7. Note also that the argument above can be used to show that $Z(t) \rightarrow -\infty$ when z is on the boundary of \mathcal{S} and to the left of the hull. This can be used to give a rigorous derivation of the formulas (4.31) and (4.32). ■

As a corollary of this result we can compute the expected areas of the hull of dipolar SLE_κ in the corresponding triangle, and of the two components of the complement of this hull. To do so, we simply integrate the probabilities to be in one of these components over the triangular domain. This leads to the following analogue of corollary 4.5 in section 4.1:

Corollary 4.13. *The hull and both components of the complement of the hull in T each have an expected area equal to $1/3$ of the area of the triangle T .*

5 Reflected Brownian motion (RBM)

Summary

This chapter marks a shift in focus away from SLE. Here we study a family of random walks whose scaling limits are processes satisfying conformal invariance and the locality property. The scaling limits are identified as reflected Brownian motions (RBMs). We show that in any given triangle there is a unique RBM which, started from a corner, will arrive at a point on the opposite side of the triangle which is uniformly distributed. This completely specifies the law of the hull generated by the RBM, as we explained in section 1.4.

5.1 Definition of reflected Brownian motion

So far in this thesis we have encountered only one conformally invariant random process satisfying the locality property: SLE_6 , which is the scaling limit of the exploration process of critical percolation. We have proved in section 4.1 that this process has the property that in an equilateral triangle, the point where it first hits a given side of the triangle will be uniformly distributed if the process is started from the opposite corner. In this chapter we will prove that there exists another local, conformally invariant process with the same property. In fact, we will prove that in every triangle there is a local, conformally invariant process which, started from a given corner, will arrive on the opposite side with the uniform distribution.

In the spirit of previous chapters, this process will be constructed as the scaling limit of a discrete random walk. The scaling limit can be identified as a Brownian motion with a particular oblique reflection condition on the boundary. It will be useful to first define these reflected Brownian motions as continuous processes, and to show that they are conformally invariant and satisfy locality. For this we will follow the discussion in chapter 5 of Werner's review paper [93].

For convenience we will work in the upper half-plane. Suppose that we are given two angles $\vartheta_L, \vartheta_R \in (0, \pi)$, which denote the angles of reflection with respect to the real intervals $(-\infty, 0)$ and $(0, \infty)$ respectively. Define the reflection vector fields v_L on the negative reals by $v_L := \exp(i\pi - i\beta)$ and v_R on the positive reals by $v_R := \exp(i\alpha)$. Let B denote standard complex Brownian motion. Then there exists a unique process Z in $\overline{\mathbb{H}}$ such that

$$Z(t) = B(t) + v_L Y_L(t) + v_R Y_R(t), \tag{5.1}$$

where Y_L and Y_R are two real-valued increasing continuous processes adapted to B such that $Y_L(0) = Y_R(0) = 0$ and Y_L (respectively Y_R) increases only when Z is on the negative (respectively positive) reals. The process Z is called the reflected Brownian motion (RBM) in \mathbb{H} with reflection vector field $v(x) = v_L 1_{\{x < 0\}} + v_R 1_{\{x \geq 0\}}$ on the boundary. Such reflected Brownian motions were characterised and studied by Varadhan and Williams in [90] (compare in particular their equation (2.4) with the definition given above).

B.6 ◀ Now suppose that g is a conformal transformation of \mathbb{H} onto a domain D with smooth boundary. Consider the sum

$$g(Z(t)) - g(Z(0)) = \sum_{j=1}^N [g(Z(jt/N)) - g(Z((j-1)t/N))]. \quad (5.2)$$

To compute the sum we expand each term using Taylor's theorem. Letting $N \rightarrow \infty$ and using the fact that the real and imaginary parts of g are harmonic, just as in the proof of Itô's formula (see for instance [40, sections 4.2 and 4.3] or [46, section 3.3]) one obtains

$$g(Z(t)) - g(Z(0)) = \int_0^t g'(Z(s)) dB(s) + v_L \int_0^t g'(Z(s)) dY_L(s) + v_R \int_0^t g'(Z(s)) dY_R(s). \quad (5.3)$$

The first integral in (5.3) is the usual expression for the conformal image of Brownian motion. If we make the usual time-change $du = |g'(Z(t))|^2 dt$ (see Revuz and Yor [75, theorem V(2.5)]), then we may conclude from equation (5.3) that in the new time parameter u the process $g \circ Z$ is a reflected Brownian motion in D with reflection vector fields $v_L g'(g^{-1}(\cdot))$ and $v_R g'(g^{-1}(\cdot))$ on $g(-\infty, 0)$ and $g(0, \infty)$. Note in particular that because g is an angle-preserving transformation, the process $g \circ Z$ is also reflected at the angles ϑ_L and ϑ_R with respect to the boundary of D . This shows that the RBM with these angles of reflection is conformally invariant.

We may use the same reasoning to explain what we mean by the locality property for the RBM. For this we assume that the domain D is a simply connected subset of \mathbb{H} with continuous boundary containing the interval $[-1, 1]$. As above, g is a conformal map of \mathbb{H} onto D . We assume that g fixes the origin and the points ± 1 . Set $\tau := \inf\{t \geq 0 : Z(t) \in \mathbb{R} \setminus (-1, 1)\}$. Then from the calculation above we conclude that up to the stopping time τ , $g \circ Z$ is just a time-changed RBM in D with reflection angles ϑ_L and ϑ_R on $g(-\infty, 0)$ and $g(0, \infty)$, respectively. Now let $\sigma := \inf\{t \geq 0 : Z(t) \in \partial D \setminus (-1, 1)\}$. Then by the discussion above, modulo a time-change the laws of $(g(Z(t)) : t \leq \tau)$

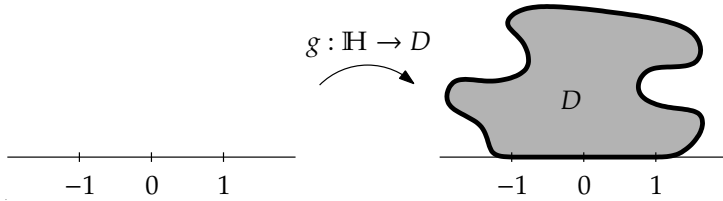


Figure 5.1. The locality property says that an RBM in \mathbb{H} started from 0 and stopped when it leaves D through $\partial D \setminus (-1, 1)$ behaves just like an RBM in D started from 0 with the same reflection vector field on the real line.

and $(Z(t) : t \leq \sigma)$ are the same. In other words, the RBM satisfies the locality property. See figure 5.1 for an illustration.

We will now introduce some notation that will be used throughout this chapter. Given two angles $\alpha, \beta \in (0, \pi)$ such that $\alpha + \beta < \pi$, we define the wedge $W_{\alpha, \beta}$ as the set $\{z \in \mathbb{C} : \alpha - \pi < \arg z < -\beta\}$, see figure 5.2. We also define $T_{\alpha, \beta}$ as the triangle in the upper half of the complex plane such that one side coincides with the interval $(0, 1)$ and the interior angles at the corners 0 and 1 are equal to α and β , respectively. The third corner (which is in the upper half-plane) will be denoted by $w_{\alpha, \beta}$. When $\alpha + \beta \geq \pi$, the domain $T_{\alpha, \beta}$ is similarly defined as the (unbounded) polygon having one side equal to the interval $(0, 1)$ and interior angles α and β at the corners 0 and 1. We then identify the point at ∞ with the “third corner” $w_{\alpha, \beta}$.

Suppose now that ϑ_L and ϑ_R denote two angles of reflection on the left and right sides of the wedge $W = W_{\alpha, \beta}$, respectively, measured from the boundary with small angles denoting reflection away from the origin ($0 < \vartheta_L, \vartheta_R < \pi$). We shall use the abbreviation $\text{RBM}_{\vartheta_L, \vartheta_R}$ to denote the corresponding reflected Brownian motion in the wedge W . This process can be defined as the conformal image of the reflected Brownian motion introduced above. For readers familiar with Varadhan and Williams’ paper we note that here we have used a different convention for the reflection angles, namely, the angles ϑ_1 and ϑ_2 in their paper correspond in our notation to the angles $\vartheta_L - \pi/2$ and $\vartheta_R - \pi/2$.

The goal of this chapter is to show that in every wedge $W_{\alpha, \beta}$ there is a unique $\text{RBM}_{\vartheta_L, \vartheta_R}$ with the following property: started from the origin, the first hitting point of the RBM of any horizontal line segment across the wedge is uniformly distributed. This special behaviour is obtained by taking the reflection angles equal to the angles of the wedge, that is, $\vartheta_L = \alpha$ and $\vartheta_R = \beta$ (observe that ϑ_L does not depend on β and ϑ_R does not depend on α). See figure 5.2. Restricting the wedge to a triangle we can reformulate this result as follows:

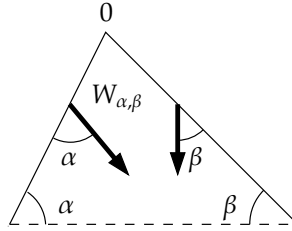


Figure 5.2. The thick arrows in this figure represent the directions of reflection of the reflected Brownian motion described in the text. The reflection angles are such that the Brownian motion will hit the dashed line with the uniform distribution.

Theorem 5.1. *Let $\alpha, \beta \in (0, \pi)$, $\alpha + \beta < \pi$, and let $(Z(t) : t \geq 0)$ be an $\text{RBM}_{\alpha, \beta}$ in the triangle $T_{\alpha, \beta}$ started from $w_{\alpha, \beta}$ and stopped when it hits $[0, 1]$. Let τ be the hitting time $\tau := \inf\{t \geq 0 : Z(t) \in [0, 1]\}$ and $X := Z(\tau)$. Then X is uniform in $[0, 1]$.*

To prove this theorem we will cover the wedge $W_{\alpha, \beta}$ with a well-chosen lattice, and then define a random walk on this lattice. By construction, this random walk will have the desired property that it arrives on each horizontal row of vertices on the lattice with the uniform distribution. Taking the scaling limit will then yield the desired result, as will be shown in section 5.A.

This approach uses the fact that an RBM in the wedge $W = W_{\alpha, \beta}$ may be defined alternatively as the scaling limit of a random walk $(X_n : n \geq 0)$ in the wedge. Below we will briefly discuss sufficient conditions for this random walk to converge to reflected Brownian motion (as defined above). We assume that the walk makes only steps of bounded length. In order that the walk converges to Brownian motion in the interior of W , it suffices that each step $X_n - X_{n-1}$ of the random walk has uncorrelated real and imaginary parts with the same variance σ^2 whenever X_{n-1} is in the interior of W . It remains to specify how the walk should behave when X_{n-1} is within fixed distance from the left side of W , or within fixed (possibly different) distance from the right side of W .

Suppose that the random walk satisfies the following conditions. Whenever X_{n-1} is within fixed distance from the left boundary, the expected value of the next step of the random walk $\mathbf{E}[X_n - X_{n-1}]$ has the constant value v_L . Likewise, $\mathbf{E}[X_n - X_{n-1}] = v_R$ whenever X_{n-1} is within fixed distance from the right boundary. In a bounded region around 0 we may not be able to meet both conditions at the same time, but the exact definition of the walk in this region will not matter for the scaling limit as long as the time it spends here is sufficiently short. We claim that under the conditions above plus a mild condition on the time spent by the walk near the boundary of W , the scaling limit of the random walk is a reflected Brownian motion in W with reflection

vector field given by v_L and v_R on the two sides. For more details we refer to the proof in section 5.A of the fact that the random walks that will be introduced in sections 5.2–5.4 converge to reflected Brownian motion in the scaling limit.

Sections 5.2–5.4 will be devoted to the random walk construction. We will show that for any given wedge there is a random walk whose horizontal coordinate has the uniform distribution on a horizontal crosscut of the wedge at all times. This idea was first introduced in [59] for the case of an equilateral triangle ($\alpha = \beta = \pi/3$) and generalised by Dubédat in [31] to the case of isosceles triangles ($\alpha = \beta$). In these cases, one can define the random walk on a rectangular lattice and take the scaling limit. Here we are concerned with the generalisation to asymmetric triangles for which it seems natural to use an asymmetric triangular lattice instead, as we do in this chapter.

For the class of triangles considered in section 5.2, where $\alpha, \beta \in (0, \pi/2]$ such that $\pi/2 \leq \alpha + \beta < \pi$, the choice of a triangular lattice does indeed provide the simplest and most natural extension of the methods used in [31]. This approach is however considerably more complicated for other triangles, as we shall see in sections 5.3–5.4. We would therefore like to remark that the arguments used in sections 5.3–5.4 could also be applied to rectangular lattices. The random-walk construction on a rectangular lattice is simpler than on the triangular lattice we use here. This provides an alternative way of proving the main results of this chapter. However, only triangles for which the ratio $\tan \alpha / \tan \beta$ is rational can be covered nicely using a rectangular lattice. An extra limiting argument would then be needed to extend the proofs to other triangles.

5.2 Reflected random walk in a restricted geometry

Throughout this section we assume that the angles α and β are fixed and restricted to the range $(0, \pi/2]$ such that $\pi/2 \leq \alpha + \beta < \pi$. We shall construct a random walk in the wedge $W = W_{\alpha, \beta}$ whose horizontal coordinate is uniformly distributed all the time. In section 5.A it is shown that the scaling limit of the random walk is an $\text{RBM}_{\alpha, \beta}$, from which theorem 5.1 follows for these restricted values of α and β . The generalisation to a generic triangle will be treated in sections 5.3 and 5.4.

Our first concern is to introduce the family of triangular lattices on which we will define our random walks. Let φ and ψ be two angles in the range $(0, \pi/2]$ such that $\pi/2 \leq \varphi + \psi < \pi$ (as we shall see later on, the range for φ and ψ is chosen such that the transition probabilities for our random walk are positive). We define $\Gamma_{\varphi, \psi} := \{j \sin(\varphi + \psi) - k \exp(i\varphi) \sin \psi : j, k \in \mathbb{Z}\}$, the set of vertices building the triangular lattice depicted in figure 5.3. Throughout this

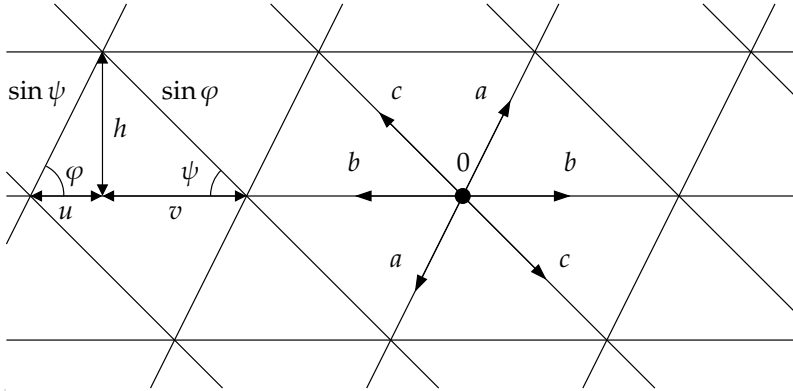


Figure 5.3. Picture of the lattice, showing the dimensions on the left, and the transition probabilities for a step of the random walk (from the origin in this picture) on the right.

chapter we shall make use of the variables $u := \cos \varphi \sin \psi$, $v := \sin \varphi \cos \psi$ and $h := \sin \varphi \sin \psi$ to denote the lattice dimensions. When we use these variables, the values of φ and ψ will always be clear from the context.

Observe that the wedge $W = W_{\alpha, \beta}$ is covered nicely with vertices of the lattice $\Gamma_{\varphi, \psi}$ when we set $\varphi := \alpha$ and $\psi := \beta$. For the duration of this section we take these values of φ and ψ to be fixed. In sections 5.3 and 5.4, where we generalise to arbitrary wedges, the relation between φ, ψ and α, β will not be so simple. This is why we already reserve the symbols φ, ψ to denote the angles of the lattice, while the symbols α, β are reserved for the angles of wedges and triangles.

We shall denote by $G = G_{\alpha, \beta}$ the set of vertices obtained by taking the intersection of $\Gamma = \Gamma_{\varphi, \psi}$ with \overline{W} . We shall call the vertices of G having six nearest neighbours along the lattice directions *interior vertices*. The origin will be called the *apex* of G , and the remaining vertices will be referred to as the *boundary vertices*. The set of boundary vertices may be further subdivided into *left boundary vertices* and *right boundary vertices*, with the obvious interpretation.

Our goal is to define a random walk on G which converges to Brownian motion in the interior of the wedge, and has the property that it arrives on every horizontal row of vertices of G with the uniform distribution. We will write $(X_n : n \geq 0)$ for the positions of the random walk. If we want to emphasise that the walk starts from a given vertex x of G , we will write $(X_n^x : n \geq 0)$ for the positions of the random walk started from $X_0^x = x$. The steps of the random walk will be denoted by $S_n = X_n - X_{n-1}$, so that $X_n = X_0 + S_1 + \cdots + S_n$. Each

step S_n is a complex-valued random variable whose real and imaginary parts will be denoted by U_n and V_n , respectively.

As a first step in defining the random walk, we choose the steps of the walk from the interior vertices such that the scaling limit will be Brownian motion in the interior. To be precise, when X_{n-1} is an interior vertex, X_n is chosen among the nearest-neighbours of X_{n-1} according to the probabilities a , b and c as depicted in figure 5.3. The step S_n of the walk thus takes on the possible values

$$S_n = \begin{cases} \pm(u + ih) & \text{with probability } a; \\ \pm(u + v) & \text{with probability } b; \\ \pm(v - ih) & \text{with probability } c. \end{cases} \quad (5.4)$$

Here, the probabilities a , b and c have to be chosen such that $\mathbf{E}[U_n V_n] = 0$ and $\mathbf{E}[U_n^2] = \mathbf{E}[V_n^2]$, i.e. the covariance matrix of U_n and V_n must be a multiple of the identity. This is sufficient to let the walk converge to Brownian motion in the interior of the wedge.

It is easily verified that to achieve this, the correct choice for the transition probabilities is

$$a = \lambda \cot \psi (\cot \varphi + \cot \psi), \quad (5.5)$$

$$b = \lambda (1 - \cot \varphi \cot \psi), \quad (5.6)$$

$$c = \lambda \cot \varphi (\cot \varphi + \cot \psi), \quad (5.7)$$

where $\lambda = \frac{1}{2} [\cot \varphi (\cot \varphi + \cot \psi) + \sin^{-2} \psi]^{-1}$ is the normalisation constant. Here, the angles φ and ψ must satisfy $\pi/2 \leq \varphi + \psi < \pi$ to make all three probabilities nonnegative. It is for this reason that we have put the restriction $\pi/2 \leq \alpha + \beta < \pi$ on the angles α and β for the duration of this section.

Our next concern is to define the transition probabilities for the random walk X from the boundary vertices and the apex. As we discussed in section 5.1, we want the expected value of a step of the random walk from every left boundary vertex to be the same, and likewise for the right boundary vertices. Then the scaling limit of the random walk will be a reflected Brownian motion (as is proved in section 5.A). Here, the direction of reflection on the boundary of the wedge is given by the expected value of a step of the random walk from a boundary vertex. Thus by playing with the transition probabilities from the boundary vertices we may define random walks which have different RBMs as their scaling limits.

There is, however, only one choice of transition probabilities for which the random walk has the following special property: started from the origin, the random walk first arrives on any row of the lattice with the uniform

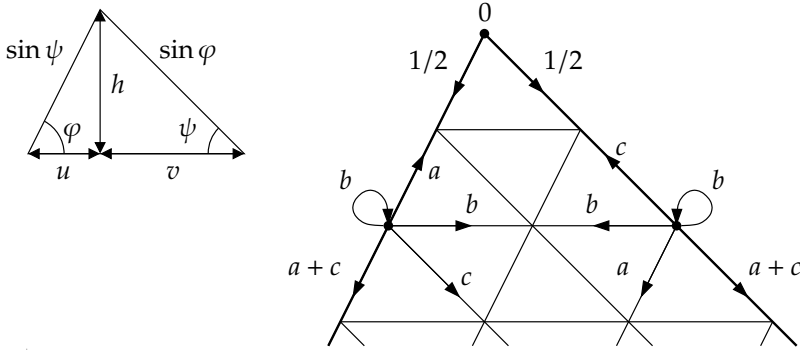


Figure 5.4. Definition of the reflected random walk in a wedge.

distribution on the vertices of that row. We will refer to this special case as the *uniform (random) walk*. To derive its transition probabilities one proceeds as follows. In a picture where we represent the steps of the walk by arrows, we have to make sure that every vertex in a given row has incoming arrows with total probability b from vertices in the same row, and incoming arrows with total probability $a + c$ both from vertices in the row above and from vertices in the row below. This completely determines the transition probabilities from the boundary vertices, see figure 5.4 for a picture of the solution.

Expressed in formula, if x is a left boundary vertex, then we have the following transition probabilities for the uniform walk:

$$\begin{cases} p[x, x] = p[x, x + (u + v)] = b, \\ p[x, x + u + ih] = a, \\ p[x, x - u - ih] = a + c, \\ p[x, x + v - ih] = c, \end{cases} \quad (5.8)$$

and the transition probabilities from the right boundary vertices are defined symmetrically, as is shown in figure 5.4. At the apex we simply choose the transition probabilities to both vertices directly below the apex equal to $1/2$.

It will now be convenient to decompose the position X_n at each step of the uniform walk as $(u + v)J_n - (u + ih)K_n$. Then K_n is a nonnegative integer denoting a row of vertices on the lattice, and J_n is a nonnegative integer denoting the position on the K_n th row. Observe that there are a total of $N(k) = k + 1$ vertices on the k th row, so that J_n ranges from 0 to $N(K_n) - 1$. Henceforth in this chapter we shall always adopt this convention of numbering rows on the lattice in top-down order, and vertices on each row from left to right.

By construction, the uniform random walk X^0 started from the origin has the property that at every time $n \geq 0$, the position of the walker is uniformly

distributed on the rows of the lattice. More precisely, for the uniform walk X^0 the following lemma holds:

Lemma 5.2. *For all $n \in \mathbb{N}$, if k_0, k_1, \dots, k_n is a sequence of natural numbers such that $k_0 = 0$ and $|k_m - k_{m-1}| \leq 1$ for all $m = 1, 2, \dots, n$, then for each $j = 0, 1, \dots, N(k_n) - 1$,*

$$\mathbf{P}[J_n = j \mid K_0 = k_0, \dots, K_n = k_n] = \mathbf{P}[J_n = j \mid K_n = k_n] = \frac{1}{N(k_n)}.$$

In particular, if $k \in \mathbb{N}$ and $T := \min\{n \geq 0 : K_n = k\}$ is the first time at which the walk visits row k , then for each $j = 0, 1, \dots, N(k) - 1$, $\mathbf{P}[J_T = j] = 1/N(k)$.

Proof. The first claim of the lemma is proved by induction. For $n = 0, 1$ the claim is trivial. For $n > 1$,

$$\mathbf{P}[J_n = j \mid K_n = k_n] = \frac{\sum_{k_{n-1}} \mathbf{P}[J_n = j, K_n = k_n \mid K_{n-1} = k_{n-1}] \mathbf{P}[K_{n-1} = k_{n-1}]}{\sum_{k_{n-1}} \mathbf{P}[K_n = k_n \mid K_{n-1} = k_{n-1}] \mathbf{P}[K_{n-1} = k_{n-1}]} \quad (5.9)$$

Using the induction hypothesis, the conditional probabilities in the numerator and denominator of this expression are easily computed from the transition probabilities of the walk. We first assume $k_n > 1$. Then for $k_{n-1} = k_n$ these conditional probabilities are $2b/N(k_n)$ and $2b$, respectively. For $k_{n-1} = k_n \pm 1$ they are $(a+c)/N(k_{n-1})$ and $(a+c)N(k_n)/N(k_{n-1})$, and for all other k_{n-1} they vanish. When $k_n \leq 1$ the contributions from the apex take a different form, but the computation is equally straightforward. Now observe that the quotient in equation (5.9) has the same value if we replace the event $\{K_{n-1} = k_{n-1}\}$ by $\{K_0 = k_0, \dots, K_{n-1} = k_{n-1}\}$. The first claim of the lemma follows. The second claim of the lemma is then a straightforward consequence. ■

We now compute $\mathbf{E}_z[S_1]$, the expected value of the first step of the uniform random walk from the boundary vertex z . As we discussed in section 5.1, this expected value gives us the direction of reflection from the boundary in the scaling limit. More precisely, the angles of reflection with respect to the left and right sides of the wedge in the scaling limit will be given by

$$\vartheta_L + \alpha = \text{Arg}(-\mathbf{E}_z[S_1]) \quad \text{and} \quad \vartheta_R + \beta = -\text{Arg}(\mathbf{E}_y[S_1]), \quad (5.10)$$

where z is any left boundary vertex and y any right boundary vertex.

By symmetry it is enough to compute only ϑ_R . From the transition probabilities one may verify that

$$\cot(\vartheta_R + \beta) = -\frac{\mathbf{E}_z[\text{Re } S_1]}{\mathbf{E}_z[\text{Im } S_1]} = \frac{(a-b)\cot\psi - (a+b)\cot\varphi}{2a}. \quad (5.11)$$

Substituting equations (5.5)–(5.7) then yields

$$\cot(\vartheta_R + \beta) = \frac{\cot^2\psi - 1}{2\cot\psi} = \cot(2\psi) = \cot(2\beta). \quad (5.12)$$

Thus, the angle of reflection with respect to the right side is simply $\vartheta_R = \beta$. Similarly, the angle of reflection on the left side is given by $\vartheta_L = \alpha$.

We conclude that the scaling limit of the uniform random walk will be a reflected Brownian motion with fixed reflection angles on the two sides of the wedge. The angles of reflection are α and β with respect to the left and right sides, respectively. A proof of this is given in section 5.A. It follows from lemma 5.2 that the $\text{RBM}_{\alpha,\beta}$ has the special property that in the wedge $W_{\alpha,\beta}$, the RBM first arrives on any horizontal cross-section of the wedge with the uniform distribution. By a simple translation it follows that in the triangle $T_{\alpha,\beta}$, the $\text{RBM}_{\alpha,\beta}$ started from the top $w_{\alpha,\beta}$ will land on $[0, 1]$ with the uniform distribution. This establishes theorem 5.1 for angles $\alpha, \beta \in (0, \pi/2]$ that satisfy $\pi/2 \leq \alpha + \beta < \pi$ (see section 5.A).

Observe in particular that this result covers the case $\alpha = \beta = \pi/3$. Thus we have shown that in an equilateral triangle there is indeed a reflected Brownian motion which arrives on the base of the triangle with the uniform distribution. This particular RBM has reflection angles of 60° with respect to the sides of the triangle. As we claimed in section 1.4, it follows that this RBM generates the same hull as an SLE_6 process and as the exploration process of critical percolation in the scaling limit.

5.3 Choice of lattice for a generic wedge

In section 5.2 we constructed a random walk in the wedge $W_{\alpha,\beta}$ for angles $\alpha, \beta \in (0, \pi/2]$ such that $\pi/2 \leq \alpha + \beta < \pi$, whose scaling limit is an $\text{RBM}_{\alpha,\beta}$ in the wedge. We now want to generalise this construction to a generic triangle. That is, we now choose the angles α and β arbitrarily in the range $(0, \pi)$ such that $\alpha + \beta < \pi$. These values of α and β are assumed fixed for the duration of this section and section 5.4. In this section we will discuss how we choose a lattice covering the wedge $W = W_{\alpha,\beta}$ in a nice way. The definition of the random walk on this wedge will be given in section 5.4.

For the choice of lattice we will make use of the triangular lattices $\Gamma_{\varphi,\psi}$ introduced in section 5.2. Consider such a lattice $\Gamma_{\varphi,\psi}$ and choose two vertices x_L and x_R on the first row of the lattice such that x_R is to the right of x_L . Then the two half-lines $\{tx_L : t \geq 0\}$ and $\{tx_R : t \geq 0\}$ define the left and right sides of a wedge that is covered nicely by vertices of $\Gamma_{\varphi,\psi}$. We will show below that for any given wedge W there is a choice of the lattice angles φ, ψ and the two points x_L and x_R such that the wedge thus defined coincides with W .

We start by introducing some notation. Given the lattice $\Gamma_{\varphi,\psi}$ and the two vertices x_L and x_R , we may introduce two integers n_L and n_R that count the

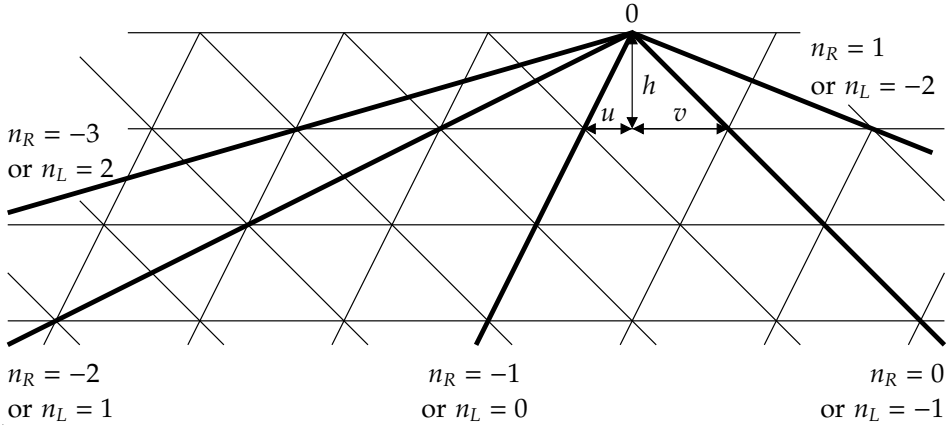


Figure 5.5. Different wedges can be covered by the same triangular lattice, by changing the directions of the two sides as shown. Each thick line can represent either the right side of a wedge (the direction of which can be expressed in the corresponding number n_R , see the text), or the left side of a wedge (with corresponding number n_L).

positions of x_L and x_R on the first row of the lattice. More precisely, the integers n_L and n_R are defined such that $x_L = -u - n_L(u + v) - ih$ and $x_R = v + n_R(u + v) - ih$ (see figure 5.5 for an illustration). Conversely, given two integers n_L and n_R and the lattice $\Gamma_{\varphi, \psi}$, the vertices x_L and x_R are fixed by these equations. Observe that n_L and n_R must satisfy $n_L + n_R \geq 0$ to make sure that x_R lies to the right of x_L . Figure 5.5 shows the wedges one obtains for different choices of n_L and n_R on a given lattice.

The main claim of this section is that for any choice of the angles α and β there is a choice of integers n_L, n_R and of the lattice angles φ, ψ such that the wedge one obtains as described above coincides with the wedge $W_{\alpha, \beta}$. This result is a direct consequence of lemma 5.3 stated below. The proof of the lemma, which will give explicit formulas for n_L, n_R and φ, ψ in terms of the angles α and β , is postponed to the end of this section.

Lemma 5.3. *Let $\alpha, \beta \in (0, \pi)$ such that $\alpha + \beta < \pi$. Then there is a choice of (possibly negative) integers n_L and n_R with $n_L + n_R \geq 0$, and angles $\varphi, \psi \in (0, \pi/2]$ with $\pi/2 \leq \varphi + \psi < \pi$, such that*

$$\cot \alpha = n_L(\cot \varphi + \cot \psi) + \cot \varphi; \tag{5.13}$$

$$\cot \beta = n_R(\cot \varphi + \cot \psi) + \cot \psi. \tag{5.14}$$

We remind the reader that in section 5.2 we considered a random walk on a wedge with angles $\alpha, \beta \in (0, \pi/2]$ such that $\pi/2 \leq \alpha + \beta < \pi$. The situation

described there corresponds to the special choice of $n_L = n_R = 0$, $\varphi = \alpha$ and $\psi = \beta$ in lemma 5.3. Thus the random walk construction of section 5.2 is a special case of the more general construction we are undertaking here. We would also like to remark that the choice of n_L, n_R and φ, ψ in lemma 5.3 is not unique in general. For instance, we will see in the proof of lemma 5.3 that it is always possible to choose the angles φ, ψ in the range $[\pi/4, \pi/2]$. Thus, there are angles α, β such that the choices made in the proof of the lemma and in the construction of section 5.2 are different.

From now on, we will assume that the values of n_L, n_R and φ, ψ are fixed as in lemma 5.3, so that the lattice $\Gamma = \Gamma_{\varphi, \psi}$ is fixed. As we explained above, the lattice provides a nice covering of the wedge $W = W_{\alpha, \beta}$. Following the conventions introduced in section 5.2, we shall denote by $G = G_{\alpha, \beta}$ the set of vertices obtained by taking the intersection of Γ with \overline{W} . We again subdivide the set G into the *apex*, *interior vertices* and *left and right boundary vertices*. We now conclude this section with the proof of lemma 5.3.

Proof of lemma 5.3. Assume first that both α and β are smaller than $\pi/2$. Then we can take

$$n_L = \lceil \cot \alpha \rceil - 1, \quad n_R = \lceil \cot \beta \rceil - 1, \quad (5.15)$$

and solve equations (5.13) and (5.14) for φ and ψ to obtain

$$\cot \varphi = \frac{n_R + 1}{n_L + n_R + 1} \cot \alpha - \frac{n_L}{n_L + n_R + 1} \cot \beta; \quad (5.16)$$

$$\cot \psi = \frac{n_L + 1}{n_L + n_R + 1} \cot \beta - \frac{n_R}{n_L + n_R + 1} \cot \alpha. \quad (5.17)$$

Observe that since $n_L < \cot \alpha \leq n_L + 1$ and $n_R < \cot \beta \leq n_R + 1$, the angles φ and ψ are in the range $(\pi/4, \pi/2)$.

It remains to consider the case when either α or β is at least $\pi/2$, and by symmetry it suffices to assume $\alpha \geq \pi/2$. Then we can for instance set $k = \lceil \cot \alpha + \cot \beta \rceil$ and let l be the smallest positive integer such that we have $l/(k+l) > -\cot \alpha / \cot \beta$. We then set

$$n_L := -l, \quad n_R := k + l - 1, \quad (5.18)$$

and the angles φ and ψ are given by the equations (5.16) and (5.17) as before. From the fact that $k \geq \cot \alpha + \cot \beta$ and the inequalities

$$\frac{l}{k+l} > -\frac{\cot \alpha}{\cot \beta} \geq \frac{l-1}{k+l-1}, \quad (5.19)$$

it follows that $\varphi \in [\pi/4, \pi/2)$ and $\psi \in (\pi/4, \pi/2]$. This completes the proof. \blacksquare

5.4 Reflected random walk in a generic wedge

We now consider the random walk construction on the set $G = G_{\alpha,\beta}$ covering the wedge $W = W_{\alpha,\beta}$ for fixed angles $\alpha, \beta \in (0, \pi)$ such that $\alpha + \beta < \pi$. As in section 5.2, we will focus on the special case of the uniform walk, i.e. the random walk on the lattice that stays uniform on the rows all the time. Earlier we explained how one defines this random walk in the case $n_L = n_R = 0$. In this section we will describe what one has to do to generalise to other wedges, i.e. to the case where n_L or n_R or both are nonzero.

It is clear that we should define the transition probabilities from the interior vertices in the same way as before. This will guarantee that the random walk will converge to Brownian motion in the interior of the wedge. The nontrivial task is to define the transition probabilities from the boundary vertices and at the top of the wedge. Here we face two complications, both arising from the fact that for a general wedge each row of the lattice G may contain more than one left boundary vertex and more than one right boundary vertex. Let us now identify these complications and show how to deal with them.

Remember that the boundary vertices are defined as those vertices having less than six nearest-neighbours in G . Now consult figure 5.5. Then we see that for a given value of n_L , the number of left boundary vertices on each row of the lattice is fixed and equals $N_L = |n_L| + 1_{\{n_L \geq 0\}}$. Likewise, for a given n_R the number of right boundary vertices on each row is $N_R = |n_R| + 1_{\{n_R \geq 0\}}$. Note, however, that if either n_L or n_R is negative, then on the first few rows of the lattice the number of boundary vertices is less than $N_L + N_R$. This implies that on the first few rows of G we have to define the transition probabilities separately. We shall deal with this complication first.

Consider once again figure 5.5 and recall the definition of the integers n_L and n_R in section 5.3, illustrated in the figure. Then one notes that each row of the lattice contains exactly $n_L + n_R + 1$ vertices more than the row above. In other words, the total number of vertices on row k of the lattice is $N(k) = (n_L + n_R + 1)k + 1$. From this one can compute that if either n_L or n_R is negative, then the first row of the lattice that contains at least $N_L + N_R$ boundary vertices is row k_0 , where

$$k_0 = \left\lceil \frac{|n_L - n_R|}{n_L + n_R + 1} \right\rceil. \quad (5.20)$$

For example, for $n_L = 2$ and $n_R = -1$ the numbers of left and right boundary vertices are $N_L = 3$ and $N_R = 1$, respectively. However, the first two rows of G contain only $N(0) = 1$ and $N(1) = 3$ vertices in total, so that the first row of the lattice that contains at least $N_L + N_R$ vertices is row 2. The definition of k_0 is extended in a natural way to the case that n_L and n_R are both nonnegative by setting $k_0 = 1$ in that case.

On the first k_0 rows of the lattice we now define the transition probabilities as follows. At the apex (that is, if $X_n = 0$) the walk may move to either of the vertices on row 1 of G with probability $1/N(1)$. In case $k_0 > 1$ the transition probabilities on the remaining $k_0 - 1$ rows below the apex are chosen as follows. For every $k = 1, \dots, k_0 - 1$ we set the transition probability from each vertex in row k to each vertex in rows $k \pm 1$ equal to $(a + c)/N(k)$. Furthermore, for every vertex in row k that has both a left and a right neighbour we set the transition probabilities to these two neighbours to b . Finally, if X_n is a vertex on row k on the boundary of W , then the walk may step to the neighbouring vertex on row k with probability b or stay where it is with probability b .

This takes care of all the nonzero transition probabilities near the top of the wedge. It remains to define the transition probabilities from the boundary vertices. We recall that we want these transition probabilities to satisfy the following three conditions:

1. The summed transition probability to a given vertex from vertices in the row above is $a + c$, and likewise from vertices in the row below.
2. The summed transition probability to a given vertex from vertices in the same row is $2b$.
3. The expected value of the first step of the walk from every left boundary vertex is the same, and likewise for the right boundary vertices.

Observe that condition 1 introduces an up-down symmetry which is not inherent in the geometry of the problem, but will be of importance later.

We will now show that for any n_L, n_R it is possible to choose the transition probabilities from the boundary vertices such that they satisfy conditions 1–3. We shall give below explicit expressions for the transition probabilities from the left boundary vertices for arbitrary $n_L > 0$. This is in fact sufficient to allow us to derive the transition probabilities for all possible wedges (i.e. for all combinations of n_L and n_R), as we shall explain first.

Observe that by left-right symmetry we can derive the transition probabilities from the right boundary vertices for any given n_R , if we know the corresponding transition probabilities from the left boundary vertices for $n_L = n_R$. Because the case $n_L = 0$ was already covered in section 5.2, it only remains to show that one can obtain the transition probabilities from the left boundary vertices for negative n_L from those for positive n_L .

To show this, observe from figure 5.5 that the left side of a wedge W with given $n_L < 0$ coincides with the right side of a (different) wedge W' with $n_R = -n_L - 1$. We propose that at the j th vertex counted from the left on row k of W one can take the probability of a step S equal to the probability of the step $-S$ at the j th vertex counted from the right on row k of W' . Here we exploit the up-down symmetry inherent in condition 1 above. It follows

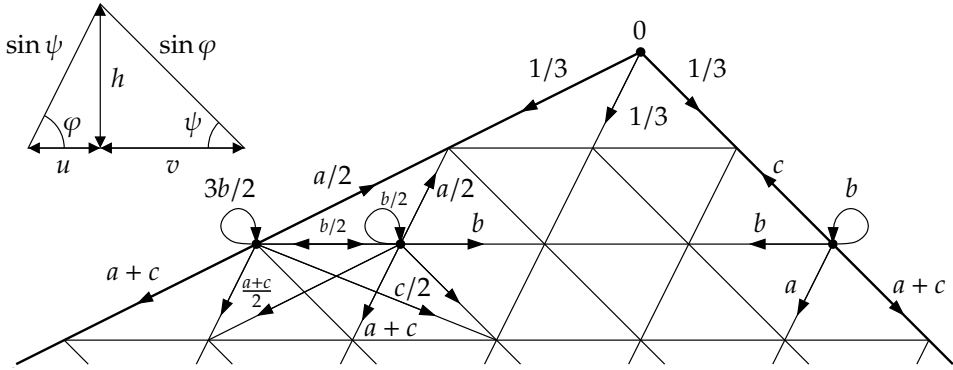


Figure 5.6. Transition probabilities for the reflected random walk in a wedge with $n_L = 1$ and $n_R = 0$. The inset shows the lattice dimensions.

that it is indeed sufficient to provide the transition probabilities from the left boundary vertices for positive n_L only.

So let $n_L > 0$ be fixed. To specify the transition probabilities we will need some notation. We write $p_0[j, l]$ for the transition probability from the j th vertex on a row k to the l th vertex on the same row. By $p_{\pm}[j, l]$ we denote the transition probability from the j th vertex on a row k to the l th vertex on the row $k \pm 1$ (vertices on a row k are numbered $0, 1, \dots, N(k) - 1$ from left to right). These transition probabilities are to be used for all rows $k \geq k_0$ of the lattice. Finally, we write $q_j[S]$ for the probability of a step S from the j th vertex on a row k . Remember from the previous discussion that there are $N_L = n_L + 1$ left boundary vertices on the rows of G , so that we have to give the transition probabilities for $j = 0, 1, \dots, n_L$.

First we specify the transition probabilities from a given row to the row above. For all $j = 0, 1, \dots, n_L$,

$$p_{-}[j, 0] = q_j[u + (u + v)(n_L - j) + ih] = \frac{1}{n_L + 1}a. \tag{5.21}$$

Secondly we specify the transition probabilities to the same row. For $j = 0, 1, \dots, n_L$ these are given by

$$p_0[j, j + 1] = q_j[u + v] = \frac{j + 1}{n_L + 1}b, \tag{5.22}$$

$$p_0[j, j - 1] = q_j[-(u + v)] = \frac{j}{n_L + 1}b, \tag{5.23}$$

$$p_0[j, j] = q_j[0] = \frac{2(n_L - j) + 1}{n_L + 1}b. \tag{5.24}$$

Thirdly we consider the transition probabilities to the row below. For each of the boundary vertices $j = 0, 1, \dots, n_L$ we have

$$p_+[j, 2n_L + 1] = q_j[-u + (u + v)(n_L + 1 - j) - ih] = \frac{1}{n_L + 1}c. \quad (5.25)$$

However, for $j = 0$ we have

$$p_+[0, n_L] = q_0[-u - ih] = \frac{n_L}{n_L + 1}(a + c), \quad (5.26)$$

$$p_+[0, 0] = q_0[-u - (u + v)n_L - ih] = a + c, \quad (5.27)$$

whereas for $j = 1, 2, \dots, n_L - 1$,

$$p_+[j, j] = q_j[-u - (u + v)n_L - ih] = \frac{n_L}{n_L + 1}(a + c), \quad (5.28)$$

$$p_+[j, n_L + j] = q_j[-u - ih] = \frac{n_L}{n_L + 1}(a + c), \quad (5.29)$$

$$p_+[j, 2j] = q_j[-u - (u + v)(n_L - j) - ih] = \frac{1}{n_L + 1}(a + c), \quad (5.30)$$

and finally, for $j = n_L$ we have

$$p_+[n_L, 2n_L] = q_{n_L}[-u - ih] = a + c, \quad (5.31)$$

$$p_+[n_L, 2(n_L - n) - 1] = q_{n_L}[-u - (u + v)(2n + 1) - ih] = \frac{1}{n_L + 1}(a + c), \quad (5.32)$$

where in the last equation n is an integer taking values in $\{0, 1, \dots, n_L - 1\}$. The above list specifies all the nonzero transition probabilities from the left boundary vertices. Figure 5.6 shows an example of the transition probabilities in the case $n_L = 1$.

We deliberately gave both the transition probabilities and the corresponding step probabilities at the boundary vertices to make it easy to verify that conditions 1–3 on page 92 are indeed satisfied. To verify conditions 1 and 2, one simply has to add up the relevant transition probabilities. To check condition 3, one may compute the real and imaginary parts of the first step of the random walk from each of the $n_L + 1$ boundary vertices from the step probabilities (for the results, see the following paragraph). As in section 5.2, the uniform random walk defined above will converge in the scaling limit to a reflected Brownian motion (see section 5.A for a proof). Moreover, the walk satisfies lemma 5.2. Thus, the RBM will hit any horizontal cross-section of W with the uniform distribution.

The proof of theorem 5.1 will therefore be complete if we can show that the angles of reflection of the RBM are $\vartheta_L = \alpha$ and $\vartheta_R = \beta$. As in section 5.2, the direction of reflection with respect to the left side of W is given by the expected

value of the first step from a left boundary vertex. From the step probabilities we compute

$$\mathbf{E}_z[\operatorname{Re} S_1] = \frac{1}{n_L + 1} \left[c(v - u) + b(u + v) - (a + c)(2n_L u + n_L^2(u + v)) \right], \quad (5.33)$$

$$\mathbf{E}_z[\operatorname{Im} S_1] = \frac{1}{n_L + 1} \left[-h(2c + 2(a + c)n_L) \right], \quad (5.34)$$

where z is any left boundary vertex (on row $k \geq k_0$).

Observing that $u/h = \cot \varphi$ and $v/h = \cot \psi$, this gives us the following expression for the reflection angle ϑ_L with respect to the left side of the wedge:

$$\cot(\vartheta_L + \alpha) = \frac{\cot \varphi[(a + c)(n_L^2 + 2n_L) - b + c] + \cot \psi[(a + c)n_L^2 - b - c]}{2c + 2(a + c)n_L}. \quad (5.35)$$

Substituting equations (5.5)–(5.7) yields

$$\cot(\vartheta_L + \alpha) = \frac{[(\cot \varphi + \cot \psi)n_L + \cot \varphi]^2 - 1}{2(\cot \varphi + \cot \psi)n_L + 2 \cot \varphi}. \quad (5.36)$$

According to equation (5.13), the result simplifies to

$$\cot(\vartheta_L + \alpha) = \frac{\cot^2 \alpha - 1}{2 \cot \alpha} = \cot(2\alpha). \quad (5.37)$$

Thus, the reflection angle of the Brownian motion with respect to the left side is simply $\vartheta_L = \alpha$. By symmetry, the angle of reflection with respect to the right side is β . This is consistent with the results obtained in section 5.2 and leads in the scaling limit to theorem 5.1 (see section 5.A).

5.A Scaling limits of the reflected random walks

In this section we consider the scaling limits of the reflected (uniform) random walks X introduced in sections 5.2–5.4. First we explain how we take the scaling limit exactly. We assume that the angles α and β are fixed angles in the range $(0, \pi)$ such that $\alpha + \beta < \pi$. Then the wedge $W = W_{\alpha, \beta}$, the set of vertices $G = G_{\alpha, \beta}$ and the random walk X on G are defined as before.

Given a point x in W and a natural number $N > 0$, let x_N be a vertex of G as close as possible to $N\sigma x$. Denote by μ_N the uniform measure on the collection of those vertices y on the same row as x_N such that $|y - x_N| \leq N^{1/2}$ (here the power $1/2$ is somewhat arbitrary, as any power between 0 and 1 will do). We write X^{μ_N} for the uniform random walk such that $X_0^{\mu_N}$ has law μ_N . For every

natural number $N > 0$ we define the continuous complex-valued stochastic process $Z_N = (Z_N(t) : t \geq 0)$ as the linear interpolation of the process

$$Y_N(t) = \frac{1}{N\sigma} X_{\lfloor N^2 t \rfloor}^{\mu_N} \quad (5.38)$$

making jumps at the times $\{k/N^2 : k = 1, 2, \dots\}$. Here, $\sigma^2 = 2(a + c)h^2$ is the variance of the real and imaginary parts of the steps $S_n = X_n - X_{n-1}$ of the random walk in the interior of the wedge, as before. Our goal is to identify the only possible weak limit of Z_N as $N \rightarrow \infty$ as an $\text{RBM}_{\alpha, \beta}$ in the wedge W started from x . We shall follow the argument presented by Dubédat in [31].

Theorem 5.4. *The weak limit of Z_N as $N \rightarrow \infty$ is an $\text{RBM}_{\alpha, \beta}$ in W started from x .*

Proof. We use the submartingale characterisation of reflected Brownian motion in W (see [90, theorem 2.1]), which states the following. Let $C_b^2(W)$ be the set of bounded continuous real-valued functions on W that are twice continuously differentiable with bounded derivatives. Assume that the two reflection angles ϑ_L and ϑ_R on the sides of W are given. Then the $\text{RBM}_{\vartheta_L, \vartheta_R}$ in W started from $x \in W$ is the unique continuous strong Markov process Z^x in W started from x such that for any $f \in C_b^2(W)$ with nonnegative derivatives on the boundary in the directions of reflection, the process

$$f(Z^x(t)) - \frac{1}{2} \int_0^t \Delta f(Z^x(s)) ds, \quad (5.39)$$

where Δ is the Laplace operator, is a submartingale.

From the definition of Z_N it is obvious that in the limit $N \rightarrow \infty$ the starting point of the process converges to x . To prove convergence of our random walk to an RBM it is therefore sufficient to show that there are two angles ϑ_L and ϑ_R such that if f is a function as described above, then for all $0 \leq s < t$

$$\liminf_{N \rightarrow \infty} \mathbf{E}_N \left[f(Z(t)) - f(Z(s)) - \frac{1}{2} \int_s^t \Delta f(Z(u)) du \right] \geq 0. \quad (5.40)$$

Here, \mathbf{E}_N denotes the expectation operator for the N th approximate process started near x , and we have dropped the N subscript on Z to simplify the notation. Note that the conditioning in the submartingale property is taken care of because the starting point x is arbitrary. In fact, it is sufficient to verify (5.40) up to the stopping time $\tau := \inf\{t \geq 0 : \text{Im } Z(t) \leq -R\}$ for some large number R . We will make use of this to have uniform bounds on the error terms in our discrete approximation.

We now show (5.40). Let f be a function in $C_b^2(W)$, and write $u_k = k/N^2$ for the jump times of Z . Then by Taylor's theorem, there exist (random) times T_k

between u_k and u_{k+1} such that

$$f(Z(u_{k+1})) - f(Z(u_k)) = \frac{1}{N\sigma} \left(\frac{\partial f(Z(u_k))}{\partial x} U_{k+1} + \frac{\partial f(Z(u_k))}{\partial y} V_{k+1} \right) + \frac{1}{2N^2\sigma^2} \left(\frac{\partial^2 f(Z(T_k))}{\partial x^2} U_{k+1}^2 + \frac{\partial^2 f(Z(T_k))}{\partial y^2} V_{k+1}^2 + 2 \frac{\partial^2 f(Z(T_k))}{\partial x \partial y} U_{k+1} V_{k+1} \right), \quad (5.41)$$

where U_k and V_k are the real and imaginary parts of the k th step of the underlying random walk, as before.

When we now apply the expectation operator, we distinguish between the behaviour on the boundary and in the interior. We may ignore what happens on a finite number of rows near the apex because of the negligible time spent there, see below. This takes care of the deviating definition of the transition probabilities on the first k_0 rows of the lattice described in section 5.4. If B denotes the set of boundary vertices of G (minus those on the first k_0 rows), then we may write

$$\mathbf{E}_N [f(Z(u_{k+1})) - f(Z(u_k))] = \mathbf{E}_N \left[\frac{1}{2N^2} \Delta f(Z(T_k)) + \left(\frac{1}{N\sigma} \frac{\partial f(Z(u_k))}{\partial x} U_{k+1} + \frac{1}{N\sigma} \frac{\partial f(Z(u_k))}{\partial y} V_{k+1} + O(N^{-2}) \right) 1_{\{N\sigma Z(u_k) \in B\}} \right], \quad (5.42)$$

where the $O(N^{-2})$ error term is uniform in $\{z \in W : \text{Im } z > -R\}$.

Summing over k from $\lfloor N^2(s \wedge \tau) \rfloor$ to $\lfloor N^2(t \wedge \tau) \rfloor$ yields

$$\mathbf{E}_N [f(Z(t \wedge \tau)) - f(Z(s \wedge \tau))] = \mathbf{E}_N \left[\int_{s \wedge \tau}^{t \wedge \tau} \frac{1}{2} \Delta f(Z(u)) du \right] + o(1) + \sum_{z \in B} \mathbf{E}_N [L_z] \left\{ \frac{1}{N\sigma} \frac{\partial f(z/N\sigma)}{\partial x} \mathbf{E}_z [U_1] + \frac{1}{N\sigma} \frac{\partial f(z/N\sigma)}{\partial y} \mathbf{E}_z [V_1] + O(N^{-2}) \right\}. \quad (5.43)$$

In the last line, L_z is the local time at z (the number of jumps of the random walk to z) between times $s \wedge \tau$ and $t \wedge \tau$, and \mathbf{E}_z is expectation with respect to the underlying random walk started from z . Note that the number of boundary vertices that the stopped random walk can reach is $O(N)$ and that the measure μ_N is concentrated on a set of size $O(N^{1/2})$. The following lemma, which will be proved in section 5.B.1, therefore shows that the expected local time spent on the boundary vertices up to time τ is of order $O(N^{3/2})$, allowing us to ignore the $O(N^{-2})$ term in equation (5.43) in the limit:

Lemma 5.5. *Let $M > k > 0$ be fixed natural numbers and suppose that F is a given subset of the set of vertices of G on row k . Consider the walk X^μ started with the uniform distribution μ on F and killed when it reaches row M . Then for any fixed*

vertex x of G , the expected number of visits of X^μ to x before it is killed is less than $(a+c)^{-1}N(k)/|F|$, where $|F|$ is the number of vertices in F .

Observe that the remaining term in braces in (5.43) is just the derivative of f at the boundary point $z/N\sigma$ along the direction of $\mathbf{E}_z[S_1]$. Thus, if the function f has nonnegative derivatives along this direction on the boundary of W , then the term in braces in equation (5.43) is nonnegative and the desired result (5.40) is obtained. This proves that the scaling limit of the reflected random walk is a reflected Brownian motion, and that the angles of reflection with respect to the left and right sides are given by

$$\vartheta_L + \alpha = \text{Arg}\left(-\mathbf{E}_z[S_1]\right) \quad \text{and} \quad \vartheta_R + \beta = -\text{Arg}\left(\mathbf{E}_y[S_1]\right), \quad (5.44)$$

where z is any left boundary vertex and y any right boundary vertex. Equations (5.12) and (5.37) show that $\vartheta_L = \alpha$ and $\vartheta_R = \beta$. The theorem follows. ■

Proof of theorem 5.1. Theorem 5.4 shows that the scaling limits of the random walks defined in sections 5.2 and 5.4 are $\text{RBM}_{\alpha,\beta}$ in the wedges $W_{\alpha,\beta}$. These random walks satisfy lemma 5.2. It follows that the scaling limits must hit any horizontal crosscut of the wedge at a uniformly distributed point. A simple translation by $w_{\alpha,\beta}$ then yields theorem 5.1. ■

5.B Intertwining relations and time-reversal

In this section we review some interesting properties of the uniform random walks defined in sections 5.2 and 5.4, and prove lemma 5.5 on the local time spent by these random walks at a given vertex. We shall see that the imaginary parts of the uniform random walks converge in the scaling limit to one-dimensional Brownian motions conditioned not to return to the origin. This allows us to study also the $\text{RBM}_{\alpha,\beta}$ in the domain $T_{\alpha,\beta}$ when $\alpha + \beta \geq \pi$.

For convenience, this section is divided into three subsections. Section 5.B.1 describes the intertwining relation between the uniform random walk and a random walk on the positive integers. From this relation we obtain lemma 5.5. In section 5.B.2 we study this intertwining relation in the scaling limit. This is used in section 5.B.3 to consider the behaviour of the $\text{RBM}_{\alpha,\beta}$ when $\alpha + \beta \geq \pi$.

5.B.1 Intertwining relation for the uniform walk

From the definitions of the uniform walks in sections 5.2 and 5.4 the following interesting picture arises. Started with the uniform distribution from the vertices in a given row of the lattice, the walk can be seen as a walk from row to row on

the lattice that remains uniformly distributed on the rows all the time. This can be stated more precisely in the form of an intertwining relation, as was noted for the case of symmetric wedges by Dubédat [31]. Here we shall describe the generalisation of Dubédat’s results to generic wedges.

B.3 ◀ First let us explain what is meant by an intertwining relation. Let $(P_t : t \geq 0)$ and $(P'_t : t \geq 0)$ be two Markovian semigroups with discrete or continuous time parameter and corresponding state spaces (S, \mathcal{S}) and (S', \mathcal{S}') . Suppose that K is a Markov transition kernel from S' to S . That is, K is a function $K : S' \times \mathcal{S} \rightarrow [0, 1]$ such that (1) for each fixed $x' \in S'$, $K(x', \cdot)$ is a probability measure on \mathcal{S} , and (2) for each fixed $A \in \mathcal{S}$, $K(\cdot, A)$ is \mathcal{S}' -measurable. The two semigroups (P_t) and (P'_t) are said to be *intertwined by K* if for all $t \geq 0$ and every pair $(a', A) \in S' \times \mathcal{S}$,

$$\int K(a', dx)P_t(x, A) = \int P'_t(a', dx')K(x', A). \tag{5.45}$$

In a more compact notation, the semigroups are said to be intertwined by K if for all $t \geq 0$ the identity $KP_t = P'_tK$ between Markov transition kernels from S' to S holds. Examples of such intertwining relations have been studied for instance in [26, 76].

In our case we are interested in the uniform random walk X on the graph $G = G_{\alpha, \beta}$ covering the wedge $W = W_{\alpha, \beta}$, as defined in section 5.4 or in section 5.2. Let (P_n) be its semigroup and let (P'_n) be the semigroup of the random walk on the set \mathbb{N} of natural numbers with transition probabilities

$$\begin{cases} p'(k, k) = 2b; \\ p'(k, k \pm 1) = (a + c) \frac{N(k \pm 1)}{N(k)}; \end{cases} \tag{5.46}$$

for $k > 0$ and $p'(0, 1) = 1$. Observe that $p'(k, l)$ is just equal to the conditional probability that X_{n+1} will be on row l of G , given that X_n is uniformly distributed on the vertices of row k (this follows from the fact that the transition probabilities satisfy conditions 1–3 on page 92).

Now consider the Markov transition kernel K from \mathbb{N} to G such that for each $k \in \mathbb{N}$, $K(k, \cdot)$ is the uniform measure on the vertices of row k of G . Recall that for the walk X , if X_0 is uniformly distributed on row k , then the walk will stay uniform on the rows of G afterwards (this statement is clear from the proof of lemma 5.2). It follows that for each $k \in \mathbb{N}$, $A \subset G$ and $n \geq 0$,

$$\sum_{x \in G} K(k, x)P_n(x, A) = \sum_{l \in \mathbb{N}} P'_n(k, l)K(l, A). \tag{5.47}$$

Hence we have the intertwining relation $KP_n = P'_nK$.

This discrete intertwining relation may be used to compute the Green function for the uniform walk X^0 (started from the origin), killed when it

reaches the row $M > 0$. This computation gives us a bound on the expected local time spent by the walk on a given boundary vertex of G which can be used to prove lemma 5.5:

Proof of lemma 5.5. Consider the Green function $G'_M = (I - P'_M)^{-1} = \sum_{n=0}^{\infty} (P'_M)^n$ for the random walk on \mathbb{N} with transition matrix P'_M defined by the transition probabilities of equation (5.46), except that now the walk is killed as soon as it reaches level M . It is not difficult to verify that the first row of this Green function is given by

$$G'_M[0, k] = \begin{cases} \frac{1}{(N(1)-1)(a+c)} N(k) \left(1 - \frac{N(k)}{N(M)}\right) & \text{for } k > 0; \\ 1 + \frac{a+c}{N(1)} G'_M[0, 1] & \text{for } k = 0. \end{cases} \quad (5.48)$$

Now consider the Green function G_M for the uniform walk X^0 on the graph G in W , killed when it reaches $\{z : \text{Im } z = -Mh\}$. Let us denote the j th vertex on row k of G by (j, k) . Then, by the intertwining relation (5.47), the Green function G_M is related to G'_M by

$$G_M[(0, 0), (j, k)] = \frac{1}{N(k)} G'_M[0, k] \quad \text{for } j = 0, 1, \dots, N(k) - 1, \quad (5.49)$$

since the expected local time spent at vertex (j, k) by the walk X^0 before it is killed at row M is the same for all $j = 0, 1, \dots, N(k) - 1$. It follows that the expected local time spent at any vertex (j, k) by the walk before it is killed at row M is smaller than $(a + c)^{-1}$.

Now let $T(k)$ be the first time when X^0 is on row k , and let F , x and μ be as in lemma 5.5. Then by lemma 5.2, $\mathbf{P}[X^0_{T(k)} \in F] = |F|/N(k)$. Observe that the expected number of visits of X^μ to x is equal to the expected number of visits of X^0 to x after time $T(k)$ given the event $\{X^0_{T(k)} \in F\}$. This number is bounded by the total number of visits of X^0 to x given $\{X^0_{T(k)} \in F\}$. Since

$$\mathbf{P}[X^0 \text{ visits } x \text{ } n \text{ times} \mid X^0_{T(k)} \in F] \leq \frac{\mathbf{P}[X^0 \text{ visits } x \text{ } n \text{ times}]}{\mathbf{P}[X^0_{T(k)} \in F]}, \quad (5.50)$$

we conclude that the expected number of visits of X^μ to x is bounded by the expected number of visits of X^0 to x divided by $\mathbf{P}[X^0_{T(k)} \in F]$. Together with the conclusion from the previous paragraph this proves the lemma. \blacksquare

5.B.2 Intertwining relation and time-reversal of the RBMs

In the previous subsection we considered the intertwining relation between the uniform walk on G and a random walk on the integers. Here we will turn our

attention to the scaling limit. Let Z be the $\text{RBM}_{\alpha,\beta}$ in $W = W_{\alpha,\beta}$, and let (P_t) be its semigroup. Consider the Markov transition kernel K from the positive reals \mathbb{R}_+ to W which for each fixed $y \in \mathbb{R}_+$ assigns the uniform measure to the horizontal crosscut $[-y \cot \alpha - iy, y \cot \beta - iy]$. It is clear from the intertwining relation (5.47) between the random walks that (P_t) and the semigroup of the scaling limit of the random walk on \mathbb{N} will be intertwined by K .

It remains to identify the scaling limit. We claim that this is a 3-dimensional Bessel process, or in other words, it is a Brownian motion on \mathbb{R}_+ conditioned not to hit the origin. This generalises proposition 1 in Dubédat [31] to the following statement:

Theorem 5.6. *Let Z , (P_t) and K be as above and let (P'_t) be the semigroup of the 3-dimensional Bessel process taking values in \mathbb{R}_+ . Then (P_t) and (P'_t) are intertwined by K . In particular, for all $y \geq 0$ the process $-\text{Im } Z$ where $Z(0)$ has law $K(y, \cdot)$ is a 3-dimensional Bessel process started from y .*

B.6 **◀ Proof.** As we remarked above, it is sufficient to identify the scaling limit of the random walk X' on \mathbb{N} . Since the rows of the lattice have spacing h , the proper scaling limit is obtained by considering the linear interpolations of the processes $hX'_{\lfloor n^2 t \rfloor} / n\sigma$ where $\sigma^2 = 2(a+c)h^2$ is as before, and then taking $n \rightarrow \infty$. We may derive the infinitesimal generator for the limit by computing, for a sufficiently differentiable function f on \mathbb{R}_+ ,

$$\begin{aligned} \frac{a+c}{N(\frac{n\sigma}{h}x)} \left(f\left(x + \frac{h}{n\sigma}\right) N\left(\frac{n\sigma}{h}x + 1\right) - f\left(x - \frac{h}{n\sigma}\right) N\left(\frac{n\sigma}{h}x - 1\right) \right) \\ + 2bf(x) - f(x) = \frac{1}{n^2} \left(\frac{1}{x} f'(x) + \frac{1}{2} f''(x) \right) + o(n^{-2}). \end{aligned} \tag{5.51}$$

Here $1/n^2$ is the time scaling, and we recognise in equation (5.51) the generator of the 3-dimensional Bessel process (see theorem B.16 and consult Revuz and Yor [75] chapter VI, §3 and chapter III, exercise (1.15) for more background on the 3-dimensional Bessel process and its semigroup). ■

We now turn our attention to the time-reversal of the RBMs. Precisely, let Z be an $\text{RBM}_{\alpha,\beta}$ in the triangle $T = T_{\alpha,\beta}$ started from the top and stopped when it hits $[0, 1]$. We are interested in the time-reversal \tilde{Z} of this process. From the time-reversal properties of the 3-dimensional Bessel process [75, proposition VII(4.8)] we know that until \tilde{Z} first hits the boundary of T , it is a complex Brownian motion started with the uniform distribution from $[0, 1]$ and conditioned not to return to $[0, 1]$. In fact, we can describe the full process \tilde{Z} in terms of a conditioned reflected Brownian motion. This is again a generalisation of an earlier result of Dubédat [31, proposition 2]:

Theorem 5.7. *The time-reversal of an $\text{RBM}_{\alpha,\beta}$ in the triangle $T = T_{\alpha,\beta}$, started from the top and stopped when it hits $[0, 1]$, is an $\text{RBM}_{\pi-\alpha,\pi-\beta}$ in T started with the uniform*

distribution from $[0, 1]$, conditioned not to return to $[0, 1]$ and killed when it hits the top of the triangle.

Proof. Recall the Green function of the uniform walk X^0 , equation (5.49). By Nagasawa's formula (see Rogers and Williams [77, III.42]) the time-reversal of this random walk is a Markov process with transition probabilities

$$q_M[(j, k), (l, m)] = \frac{G_M[(0, 0), (l, m)] p[(l, m), (j, k)]}{G_M[(0, 0), (j, k)]}. \quad (5.52)$$

Here, the $p[(l, m), (j, k)]$ are the transition probabilities for the walk X^0 killed at row M , as specified in section 5.4. We are interested in the transition probabilities for the reversed process in the limit $M \rightarrow \infty$. From the expression for the Green function it is clear that in the limit one gets for $k, m > 0$

$$q[(j, k), (l, m)] = p[(l, m), (j, k)]. \quad (5.53)$$

Observe in particular that in the interior of the wedge we recover the transition probabilities of the original walk. Hence, the reversed walk converges to a Brownian motion in the interior.

Moreover, by condition 1 on page 92 it is clear that at every vertex on any row $k > 0$ of the lattice, the probability that the reversed walk will step to the row $k + 1$ is equal to the probability that it will step to the row $k - 1$. Note especially that this is not only true at the interior vertices but also at the boundary vertices. Therefore, the expected step of the random walk from any vertex on the rows $k > 0$ is real. In particular, the walk is reflected on the sides of W in the real direction. It follows that the time-reversal of the reflected Brownian motion in the wedge is a reflected Brownian motion with reflection angles $\pi - \alpha$ and $\pi - \beta$. ■

5.B.3 Reflected Brownian motions for $\alpha + \beta \geq \pi$

The fact that the $\text{RBM}_{\alpha, \beta}$ is intertwined with a three-dimensional Bessel process sheds some light on the behaviour of the reflected Brownian motions with reflection angles satisfying $\alpha + \beta \geq \pi$. It is the purpose of this subsection to look at these RBMs more closely. For the duration of this subsection we will fix $\alpha, \beta \in (0, \pi)$ such that $\alpha + \beta \geq \pi$. Then an $\text{RBM}_{\alpha, \beta}$ in the domain $T = T_{\alpha, \beta}$ may be described by considering an $\text{RBM}_{\pi-\alpha, \pi-\beta}$ in the wedge $W_{\pi-\alpha, \pi-\beta}$ and putting it upside-down, as we shall explain below.

We set $x := \cos \alpha \sin \beta / \sin(\alpha + \beta)$ and $z := -\sin \alpha \sin \beta / \sin(\alpha + \beta)$. Let Z denote an $\text{RBM}_{\pi-\alpha, \pi-\beta}$ in the wedge $W_{\pi-\alpha, \pi-\beta}$, and consider in particular the process Z started with the law $K(y + z, \cdot)$ where $y \in \mathbb{R}_+$. Here, K is the Markov transition kernel from \mathbb{R}_+ to $W_{\pi-\alpha, \pi-\beta}$ introduced in section 5.B.2. Let f be the

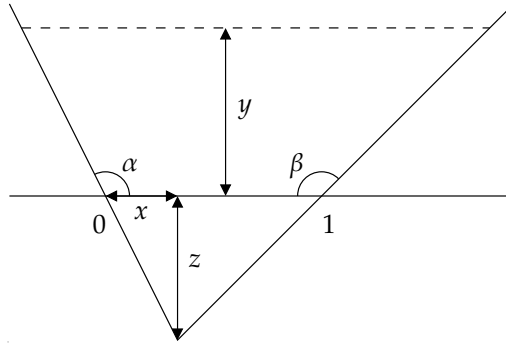


Figure 5.7. By putting a wedge upside-down we can shed some light on the $\text{RBM}_{\alpha,\beta}$ when $\alpha + \beta \geq \pi$.

transformation $f : w \mapsto \bar{w} + x - iz$ which puts the wedge upside-down as illustrated in figure 5.7, and set $Y^y(t) := f(Z(t))$. Then the process Y^y , stopped when it hits the interval $[0, 1]$, is an $\text{RBM}_{\alpha,\beta}$ in $T_{\alpha,\beta}$ started with the uniform distribution from the horizontal crosscut of $T_{\alpha,\beta}$ at altitude y .

From the intertwining relation of theorem 5.6 we conclude that the imaginary part of Y^y is a Brownian motion conditioned not to hit $-z$. It follows (see [75, corollary VI(3.4)]) that Y^y has positive probability to never reach $[0, 1]$. In fact, the probability that Y^y *does* reach $[0, 1]$ is $z/(z + y)$. It is furthermore clear from the random-walk construction and lemma 5.2 that given the event that Y^y does reach $[0, 1]$, it will arrive there with the uniform distribution.

Now let \mathbf{P}_y denote probability with respect to the process Y^y . Then by what we said above, $(y/z + 1) \mathbf{P}_y$ is a probability measure on reflected Brownian paths in $T_{\alpha,\beta}$ started from the horizontal line segment at altitude y that end on $[0, 1]$. Taking the limit $y \rightarrow \infty$ we obtain a conformally invariant probability measure on paths of $\text{RBM}_{\alpha,\beta}$ in $T_{\alpha,\beta}$ that start “with the uniform distribution from infinity” and arrive on $[0, 1]$ with the uniform distribution. Henceforth, when we speak about $\text{RBM}_{\alpha,\beta}$ with $\alpha + \beta \geq \pi$ we shall always assume that we restrict ourselves to this collection of Brownian paths and the corresponding probability measure (or conformal images of these) introduced above.

6 Hulls of local processes

Summary

We derive distribution functions associated to the hulls generated by the reflected Brownian motions introduced in chapter 5. Then we describe simulations of a special case of the Brauer loop model. We aim to test whether the self-avoiding trails defined in this model generate the same hull as one of the RBMs in the scaling limit. Comparing the distribution functions from the simulations with those of the RBMs, the results are consistent with the hypothesis that the trails generate the same hull as an $\text{RBM}_{\pi/2, \pi/2}$ in the scaling limit.

6.1 Characterising hulls of local processes

Suppose that T is the equilateral triangle in the upper half of the complex plane with corners at 0 , 1 and $a := \exp(i\pi/3)$. Let W be a stochastic process in the triangle T which starts from a . Assume that this process is local and conformally invariant. Set $\tau := \inf\{t \geq 0 : W(t) \in [0, 1]\}$ and denote by K the set of points in \bar{T} that are either on $W[0, \tau]$ or are disconnected from $\{0, 1\}$ by $W[0, \tau]$. Note that $W(\tau)$ is a random variable taking values in $[0, 1]$. We shall refer to its distribution as the *exit distribution* of the process W . As we proved in section 1.4, the distribution of the set K is completely determined by this exit distribution.

This shows that to characterise the possible laws of hulls K generated by local processes, it is sufficient to determine all the possible exit distributions for local processes in T . The two-parameter family of reflected Brownian motions studied in chapter 5 characterises a subclass of possible exit distributions for local processes. It is currently unknown which other (continuous) exit distributions are possible. Here we will therefore focus on the hulls generated by RBMs. First we give a brief summary of our main conclusions from chapter 5.

As before, we will write $T_{\alpha, \beta}$ for the triangle in the upper half-plane with corners at 0 and 1 , and interior angles α at 0 and β at 1 . The third corner will be denoted by $w_{\alpha, \beta} \in \mathbb{H}$. In case $\alpha + \beta \geq \pi$, $T_{\alpha, \beta}$ is unbounded and the third corner $w_{\alpha, \beta}$ is identified with ∞ . We have seen in chapter 5 that an $\text{RBM}_{\alpha, \beta}$ started from $w_{\alpha, \beta}$ in the domain $T_{\alpha, \beta}$ arrives on the interval $[0, 1]$ with the uniform distribution. Let us now denote by g the conformal transformation of $T_{\alpha, \beta}$ onto the equilateral triangle T which maps 0 to 0 , 1 to 1 and $w_{\alpha, \beta}$ to a . Then we conclude that the exit distribution for an $\text{RBM}_{\alpha, \beta}$ in T will be given by the image of the uniform distribution on $[0, 1]$ under the transformation g .

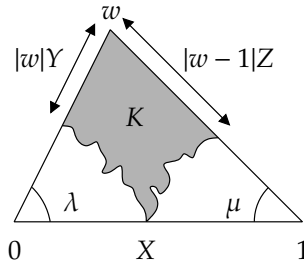


Figure 6.1. Definition of the hull K of a local process in the triangle T , and of the random variables X , Y and Z .

In particular, an $\text{RBM}_{\pi/3, \pi/3}$ has the uniform exit distribution in an equilateral triangle. Since the same is true for an SLE_6 process and for the scaling limit of the exploration process of critical percolation, these three processes all generate hulls K which have the same law. We can therefore make use of SLE computations to derive certain properties of this hull. Theorem 4.12 for dipolar SLE_6 , for instance, shows that the probability that a point $z \in T$ is in the hull K is proportional to the imaginary part of z . This implies that the expected area of the set K is $1/3$ of the area of the triangle (this is corollary 4.13).

These formulas are certainly appealing, and we would like to generalise such computations to hulls generated by other local processes, in particular those of other reflected Brownian motions. One might expect that a description of the hull generated by any RBM should be possible in terms of an SLE-like process, but such a description is not available at the moment. Here we shall therefore proceed in a different direction.

We have seen that taking the scaling limit of the exploration process of critical percolation leads to a local process which generates the same hull as an $\text{RBM}_{\pi/3, \pi/3}$. Suppose now that we consider another model which defines a path satisfying locality, and is believed to be conformally invariant in the scaling limit. Then we may ask what is the distribution of the hull generated by this random path in the limit. In this chapter we will study for instance the hull generated by a stochastic process in a model which is a special case of the Brauer model. This model will be introduced in section 6.3. Sections 6.3–6.4 discuss simulations of the model, the results of which are consistent with the hypothesis that the hull has the same distribution as the hull of an $\text{RBM}_{\pi/2, \pi/2}$.

To test this hypothesis it would in principle be sufficient to compare the limit of the exit distribution from the simulations with the exit distributions of the RBMs. But ideally, we would like to have more characteristics of the hull distribution to compare. Let us therefore introduce two new random variables associated with the hull. We consider a local process W in the triangle $T = T_{\lambda, \mu}$,

where $\lambda, \mu \in (0, \pi)$ such that $\lambda + \mu \leq \pi$. Let W be started from $w = w_{\lambda, \mu}$ and set $\tau := \inf\{t \geq 0 : W(t) \in [0, 1]\}$. Then we set $X := W(\tau)$, the *exit point* of the process W . As before, we define the *hull* K as the set of points in \bar{T} that are either on $W[0, \tau]$ or are disconnected from $\{0, 1\}$ by $W[0, \tau]$. Observe that $X = K \cap [0, 1]$.

We now introduce two new random variables Y and Z as follows. We shall denote by $|w|Y$ the distance of the lowest point of the hull on the left side to the top $w = w_{\lambda, \mu}$, and by $|w - 1|Z$ the distance of the lowest point of the hull on the right side to the top w . Thus, all three random variables X , Y and Z take on values in the range $[0, 1]$. See figure 6.1 for an illustration of the definitions. In section 6.2 we shall compute the (joint) distributions of X , Y and Z in case W is an $\text{RBM}_{\alpha, \beta}$. These distributions can then be compared with the corresponding distributions in other models, for instance using simulations as described in sections 6.3–6.4.

6.2 Distribution functions for reflected Brownian motion

In this section we derive the (joint) distribution functions of the variables X , Y and Z defined in section 6.1 for the family of reflected Brownian motions studied in chapter 5. To be precise, we fix the angles $\alpha, \beta \in (0, \pi)$ and $\lambda, \mu \in (0, \pi)$ such that $\lambda + \mu < \pi$. Throughout this section we assume that the local process we are considering is an $\text{RBM}_{\alpha, \beta}$ in the triangle $T = T_{\lambda, \mu}$ started from $w = w_{\lambda, \mu}$ (in case $\alpha + \beta \geq \pi$ we assume that we work with the probability measure introduced in section 5.B.3). Note that for more generality, we choose to derive the distribution functions in a general triangle $T = T_{\lambda, \mu}$ rather than in the domain $T_{\alpha, \beta}$.

A.6 ◀ It turns out that the marginal and joint distributions of the random variables X , Y and Z can all be expressed in terms of conformal transformations of the upper half-plane onto triangles $T_{\gamma, \delta}$. The unique conformal transformation of \mathbb{H} onto $T_{\gamma, \delta}$ that fixes 0 and 1 and maps ∞ to $w_{\gamma, \delta}$ is given by

$$F_{\gamma, \delta}(z) = \frac{\int_0^z t^{\gamma/\pi-1} (1-t)^{\delta/\pi-1} dt}{\int_0^1 t^{\gamma/\pi-1} (1-t)^{\delta/\pi-1} dt}. \quad (6.1)$$

Symmetry considerations show that the transformations satisfy

$$F_{\gamma, \delta}(u) = 1 - F_{\delta, \gamma}(1-u) \quad \text{and} \quad F_{\gamma, \delta}^{-1}(x) = 1 - F_{\delta, \gamma}^{-1}(1-x). \quad (6.2)$$

We shall now explain how we can express the distribution functions for X , Y and Z in terms of these conformal transformations.

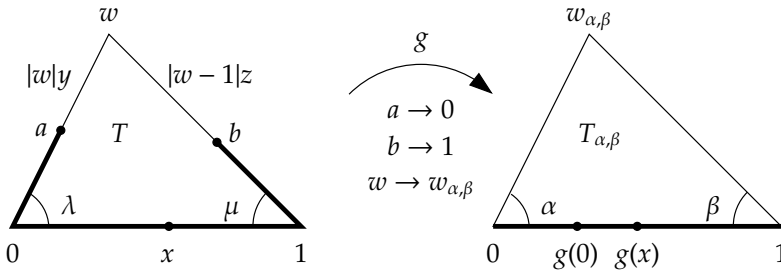


Figure 6.2. This figure illustrates how the joint distribution function of the random variables X, Y and Z can be computed. As explained in the text, the joint probability $\mathbf{P}[X \leq x, Y \leq y, Z \leq z]$ is just $g(x) - g(0)$.

The idea of the computation of $\mathbf{P}[X \leq x, Y \leq y, Z \leq z]$ is illustrated in figure 6.2. Consider an $\text{RBM}_{\alpha,\beta}$ in the triangle T started from the top w . Let $a = a(y)$ and $b = b(z)$ be the points on the left and right sides of T at distances $|w|y$ and $|w - 1|z$ from w , respectively. Stop the RBM as soon as it hits the counter-clockwise arc from a to b on the boundary (the thick line in figure 6.2). Then the probability $\mathbf{P}[X \leq x, Y \leq y, Z \leq z]$ is just the probability that this process is stopped in the interval $(0, x)$.

We now use conformal invariance and locality. Let $g = g_{a(y),b(z)}$ be the conformal map of T onto $T_{\alpha,\beta}$ that sends a to 0 , b to 1 and w to $w_{\alpha,\beta}$, as illustrated in figure 6.2. Then the probability that we are trying to compute is exactly the probability that an $\text{RBM}_{\alpha,\beta}$ in $T_{\alpha,\beta}$ started from $w_{\alpha,\beta}$ and stopped when it hits $[0, 1]$, is stopped in the interval $(g(0), g(x))$. But since the exit distribution of the RBM is uniform in $T_{\alpha,\beta}$, this probability is simply $g(x) - g(0)$. Thus,

$$\mathbf{P}[X \leq x, Y \leq y, Z \leq z] = g(x) - g(0). \tag{6.3}$$

Our next task is to find an explicit expression for this joint probability by deriving the explicit form of the map $g = g_{a(y),b(z)}$. At this point it is useful to denote by ν the third angle of the triangle $T_{\lambda,\mu}$, that is, $\nu := \pi - \lambda - \mu$. The explicit form of g is obtained by suitably combining conformal self-maps of the upper half-plane with triangle mappings. How this is done exactly is described in figure 6.3.

By studying this figure we obtain the formula for the joint distribution, given in theorem 6.1 below. As special cases this formula includes of course the joint distributions for two of the three random variables and the marginal distributions. Explicit expressions for these distributions can be obtained by sending one or two of the variables x, y and z to 1 and using the symmetry property (6.2) of the triangle mappings. For the joint distribution of X, Y and Z and for the marginal distributions we find:

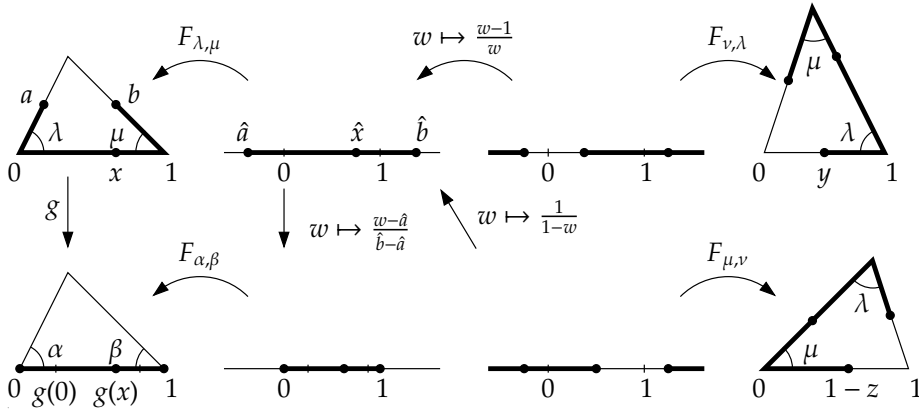


Figure 6.3. This illustration shows schematically how one obtains an explicit form for the map g in terms of the variables y and z . The notations \hat{a} , \hat{b} and \hat{x} in the figure are short for $F_{\lambda,\mu}^{-1}(a)$, $F_{\lambda,\mu}^{-1}(b)$ and $F_{\lambda,\mu}^{-1}(x)$.

Theorem 6.1. *With $a = a(y)$ and $b = b(z)$ as above we have*

$$\mathbf{P}[X \leq x, Y \leq y, Z \leq z] = F_{\alpha,\beta} \left(\frac{F_{\lambda,\mu}^{-1}(x) - F_{\lambda,\mu}^{-1}(a)}{F_{\lambda,\mu}^{-1}(b) - F_{\lambda,\mu}^{-1}(a)} \right) - F_{\alpha,\beta} \left(\frac{-F_{\lambda,\mu}^{-1}(a)}{F_{\lambda,\mu}^{-1}(b) - F_{\lambda,\mu}^{-1}(a)} \right) \quad (6.4)$$

where the images of a and b under $F_{\lambda,\mu}^{-1}$ can be expressed in terms of y and z as

$$F_{\lambda,\mu}^{-1}(a) = 1 - \frac{1}{F_{\nu,\lambda}^{-1}(y)}; \quad F_{\lambda,\mu}^{-1}(b) = \frac{1}{1 - F_{\mu,\nu}^{-1}(1-z)} = \frac{1}{F_{\nu,\mu}^{-1}(z)}. \quad (6.5)$$

Corollary 6.2. *The marginal distributions of X , Y and Z are given by*

$$\mathbf{P}[X \leq x] = F_{\alpha,\beta} \left(F_{\lambda,\mu}^{-1}(x) \right); \quad (6.6)$$

$$\mathbf{P}[Y \leq y] = F_{\beta,\alpha} \left(F_{\nu,\lambda}^{-1}(y) \right); \quad (6.7)$$

$$\mathbf{P}[Z \leq z] = F_{\alpha,\beta} \left(F_{\nu,\mu}^{-1}(z) \right). \quad (6.8)$$

Observe that the marginal distributions of the variables X , Y and Z take on particularly simple forms. These marginal distribution functions have a nice geometric interpretation. For instance, $\mathbf{P}[Y \leq y]$ is just the image of y under the transformation that maps the triangle $T_{\nu,\lambda}$ onto $T_{\beta,\alpha}$, fixes 0 and 1 and takes $w_{\nu,\lambda}$ onto $w_{\beta,\alpha}$. Similar observations hold for $\mathbf{P}[X \leq x]$ and $\mathbf{P}[Z \leq z]$.

These observations lead to some intriguing conclusions. First of all, we conclude that for an $\text{RBM}_{\pi/3,\pi/3}$ in an equilateral triangle (so that $\alpha = \beta = \lambda =$

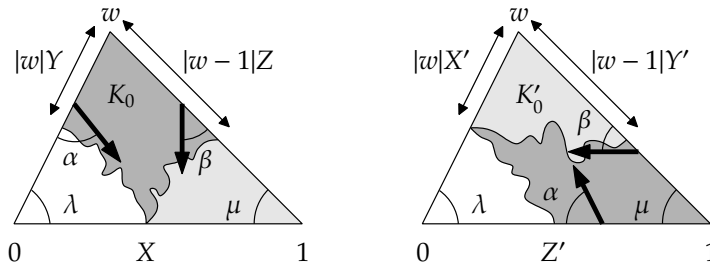


Figure 6.4. The unions K_0 and K'_0 of the shaded sets on the left and right are generated by different RBMs, but have the same law.

$\mu = \nu = \pi/3$) all three variables X , Y and Z are uniform. This is not so surprising when we realise that the hull in this case is the same as that of the exploration process of critical percolation. Indeed, in the case of percolation X and Y can be interpreted as the endpoints of the highest crossing from $w \cap 1$ of a given colour between the sides $0 \cap w$ and $0 \cup 1$ of the triangle. Thus by symmetry, if X is uniform, then so are Y and Z .

In other triangles, similar but more intricate connections exist. For example, let W be an $\text{RBM}_{\alpha,\beta}$ in $T = T_{\lambda,\mu}$ started from $w = w_{\lambda,\mu}$ and stopped when it hits $[0, 1]$, as before. Compare this process with an $\text{RBM } W'$ in T started from 1, stopped on $0 \cap w$ and reflected on $0 \cup 1$ at an angle α and on $w \cap 1$ at an angle β with respect to the boundary. Here we follow our earlier convention that small angles denote reflection away from the starting point. With this second RBM we can associate normalised random variables X' , Y' and Z' , measuring the distances of the exit point on $0 \cap w$ to w and of the “lowest points” of the hull on $w \cap 1$ and $0 \cup 1$ to w and 0, respectively. See figure 6.4. It follows from corollary 6.2 that X and Z' have the same distribution (and so do Y and X').

B.1 ◀ This result has an interesting interpretation in terms of the hulls generated by the two processes, as we shall now describe. We write Ω for the collection of closed, connected subsets K of \bar{T} such that the right side of T is in K and $T \setminus K$ is connected. We further define \mathcal{Q} as the collection of compact $A \subset \bar{T}$ such that $A = \overline{A \cap T}$, and $\bar{T} \setminus A$ is simply connected and contains the right side of T . We then endow Ω with the σ -field generated by the events $\{K \in \Omega : K \cap A = \emptyset\}$ for all $A \in \mathcal{Q}$. A similar setup was used in section 1.4. In particular, a probability measure \mathbf{P} on Ω is characterised by the values of $\mathbf{P}[K \cap A = \emptyset]$ for $A \in \mathcal{Q}$ (as in [59, lemma 3.2]), see figure 6.5.

Theorem 6.3. *Consider the processes W and W' stopped on $0 \cup 1$ and $0 \cap w$ as described above. Let K_0 and K'_0 denote the sets of points in \bar{T} that are disconnected from 0 by the paths of W and W' , respectively. Then the laws of K_0 and K'_0 on the space Ω are the same.*

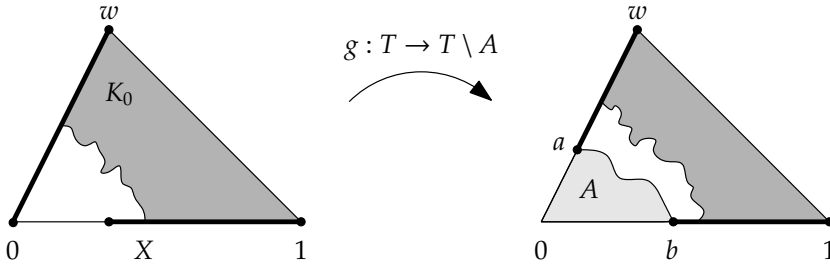


Figure 6.5. The law of the set K_0 is determined by the probabilities that K_0 avoids sets A such as shown on the right.

Proof. Let \mathbf{P} be the law of K_0 , and let $A \in \mathcal{Q}$. Denote by a and b the points of $A \cap \partial T$ closest to w and 1 along the counter-clockwise arc $w \cup 1$ of ∂T from w to 1 , respectively. Let $g : T \rightarrow T \setminus A$ be the conformal transformation that fixes 1 and w and maps 0 onto a if $\text{Im } a > 0$, and onto 0 otherwise (see figure 6.5). Then, by conformal invariance of the $\text{RBM}_{\alpha, \beta}$ in T , $\mathbf{P}[K_0 \cap A = \emptyset] = \mathbf{P}[X \in (g^{-1}(b), 1)]$ (compare this with our discussion of the locality property in section 1.4). Likewise, the law \mathbf{P}' of K'_0 satisfies $\mathbf{P}'[K'_0 \cap A = \emptyset] = \mathbf{P}'[Z' \in (g^{-1}(b), 1)]$. Since X and Z' have the same distribution (corollary 6.2), the theorem follows. ■

6.3 Simulations of self-avoiding trails

In this section we will describe simulations of a random path in a model which is a special case of the Brauer model. This model has been studied in many different forms, but has remained nameless until recently. Before we turn to the particular case we are interested in, we first give an overview of some of the forms in which the model appears in the literature.

Originally, the model was studied as a q -state solvable vertex model [86] and later as an $O(q)$ symmetric, solvable lattice model [74, 91]. More recently it was observed that the model could be seen as a model of paths on the lattice in which each closed path has a weight equal to q , where q can take non-integer values. In this language of paths each vertex can carry one of the following configurations of path segments, with the corresponding weights:

$$\begin{array}{ccc}
 \begin{array}{c} \text{┌} \\ \text{└} \\ u \end{array} &
 \begin{array}{c} \text{┐} \\ \text{┌} \\ 1 - u \end{array} &
 \begin{array}{c} \text{+} \\ (1 - q/2)u(1 - u) \end{array}
 \end{array}$$

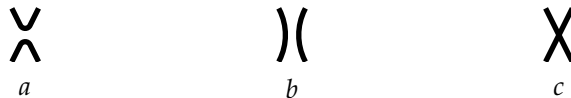
Here the weights are chosen to be solutions of the Yang-Baxter (or star-triangle) equation [13, 14]. Although the integrability condition in the Yang-Baxter

equation does not restrict q , the actual solution by means of the Bethe Ansatz was only extended to all integers [67].

The name Brauer model was given to emphasise that the transfer matrix of the model is an element of the Brauer algebra [41]. The model attracted particular attention in the limit $q \rightarrow 1$ when it describes the probability distribution of lattice paths taken by a particle that is scattered by randomly placed, static scatterers [43, 50, 79, 97]. As such it can be viewed as a Lorentz lattice gas. In these applications the vertex weights are usually not chosen as above, but instead the weights of the two configurations in which the particle is scattered are chosen to be equal and fixed in the range $(0, 1/2)$.

Another paradigm is coming from the analogy to the self-avoiding walk, as in the Brauer model a walk is not permitted to traverse a lattice edge more than once. A walk subject to this condition and with no further restrictions on the vertices is called a self-avoiding trail (SAT) [64]. We will therefore refer to the paths in the Brauer model as *trails*. In this chapter we study the model at $q = 1$ on a bounded domain, and concentrate on the hull generated by a trail of the model starting from a chosen point on the boundary.

To describe our simulations of the model more precisely we introduce some notation. For a given angle $\varphi \in (0, \pi/2)$ and integer system size $N > 0$, define the set of vertices $V = V(\varphi)$ as the set $\{2j \cos \varphi + k \exp(i\varphi) : j, k \in \mathbb{N}, j + k \leq N\}$. These vertices (after rescaling) provide a nice covering of the triangle $T_\varphi := T_{\varphi, \varphi}$ with base angle φ , see figure 6.6. Each vertex of V can carry either of the three following configurations of trail segments:



Here, the third vertex state should be interpreted as a crossing. The state of each vertex is chosen among the possibilities a , b and c independently from the states of the other vertices. The probabilities for the vertex states a , b and c are

$$p(a) = \lambda \pi 2\varphi, \quad p(b) = \lambda \pi (\pi - 2\varphi), \quad p(c) = \lambda \varphi (\pi - 2\varphi), \quad (6.9)$$

where $\lambda := [\pi^2 + \varphi(\pi - 2\varphi)]^{-1}$ provides the normalisation.

Each configuration of vertex states defines a collection of self-avoiding trails on the vertex set V . We will be interested only in those configurations in which one of these trails crosses the triangular domain from a given corner to the opposite side. To make the trail stay inside the triangle we have to impose suitable boundary conditions. We choose the boundary conditions as shown in figure 6.6. Here it is assumed that the system size N is an even number, so that the number of vertices on a side of the triangle is odd. From figure 6.6 it is clear

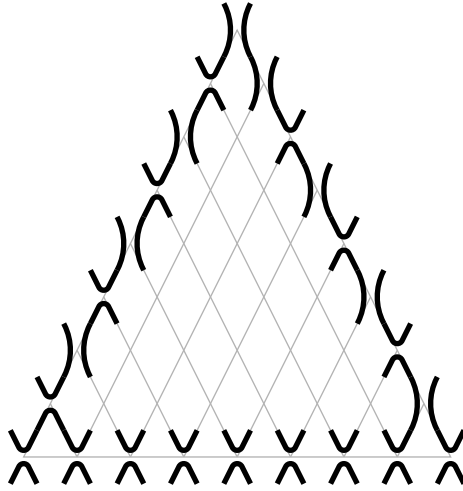


Figure 6.6. Boundary conditions for the self-avoiding trail in a triangle.

that with the chosen boundary conditions, the trails we generate can enter the triangle either from the top or from the lower-left corner. The trail then stays inside the triangle until it exits from the other of the two mentioned corners.

For our simulations we note that the self-avoiding trails can be generated dynamically as follows. Initially, only the vertex states on the boundary are fixed according to the boundary conditions. The vertex states in the interior are still undecided. The trail starts from either the top or the lower-left corner of the triangle. The steps of the trail follow the trail segments of the vertex states. Each time the trail meets a vertex whose state is still undetermined, we choose its state according to the probabilities $p(a)$, $p(b)$ and $p(c)$ given above and continue the random walk. The state of this vertex is then fixed forever onwards. The simulation stops when the trail hits a vertex on the side of the triangle opposite the starting point.

Let us point out that the trail model described above is closely related to bond percolation. Namely, take $p(c) = 0$ and let the weights of the vertex states a and b be proportional to $\sin(2\varphi/3)$ and $\sin((\pi - 2\varphi)/3)$, respectively (see [49, section 5]). Given a configuration of the model, at every vertex draw either the horizontal or the vertical edge connecting the centres of the two adjacent rhombi (see figure 6.6), such that the drawn edge does not intersect a trail segment. Then the drawn edges form a configuration of bond percolation on a rectangular lattice and its dual. On the boundary we have a percolation cluster along the base and right side of the triangle and a dual cluster along the left side. These are precisely the boundary conditions for chordal SLE_6 from the lower-left corner to the top of the triangle or vice versa.

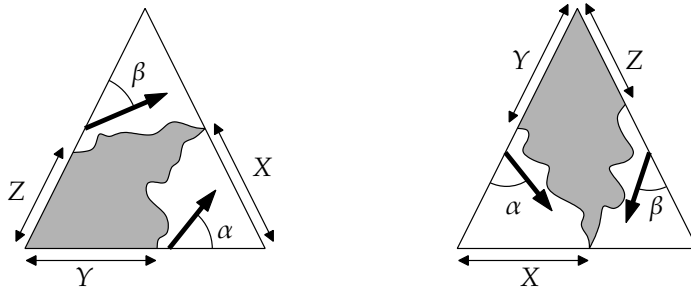


Figure 6.7. How the random variables X , Y and Z and reflection angles α and β are associated to the trails starting from different corners. For simplicity we have omitted the normalisation of X , Y and Z .

We may thus interpret the Brauer loop model as a variant of a percolation loop model with the added possibility that the loops may cross. Note that these crossings happen only with small probability, since $p(c)$ is the smallest of the three weights. One can therefore expect a self-avoiding trail to explore space much like the exploration process of critical percolation, except that occasionally the trail may cross and possibly re-enter a part of space it has already explored. This might lead one to the naive guess that in the scaling limit the trail will generate the same hull as the exploration process of critical percolation or an $\text{RBM}_{\pi/3, \pi/3}$. Our simulations show this guess to be wrong. Instead we find (see section 6.4) that our data is consistent with the hypothesis that the hull of the self-avoiding trail in the scaling limit is the same as that of an $\text{RBM}_{\pi/2, \pi/2}$.

To make the comparison with the hulls of reflected Brownian motion we measure the (joint) distributions of the random variables X , Y and Z (introduced in section 6.1) in our simulations of the Brauer loop model. The data are collected for 10^6 independent trails starting from the top and 10^6 independent trails starting from the lower-left corner on the set of vertices V for 12 different system sizes and 8 different base angles, specified in section 6.4. Below we shall describe more precisely how the data for the (joint) distributions of X , Y and Z are collected in the simulations.

We distribute the vertices of V on the three sides of the triangle over a total of 100 bins, each containing $N/100$ vertices (the number N is taken to be a multiple of 100). Since there are actually $N + 1$ vertices on each side, this means that one vertex on each side is omitted. This is the vertex in the corner of the side where the associated random variable X , Y or Z is 0. In the simulations we record the number of trails X_i that land in the i th bin for each $i = 1, 2, \dots, 100$. We also record the numbers of walks Y_i , respectively Z_i , such that the i th bin on the right, respectively left, side of the triangle (as seen from the starting point) is the bin furthest from the starting point which was visited by the trail.

Figure 6.7 illustrates how the variables X , Y and Z are associated with the hulls of trails starting from different corners. The joint distributions of these variables are recorded similarly, but instead of using 100 bins on the sides we use 50 bins to reduce memory requirements.

In this way the simulations build up histograms of the marginal and joint distributions of X , Y and Z for the self-avoiding trail that can be compared to the corresponding distributions for the reflected Brownian motions. To improve the statistics, we first merge together bins of collected data in order to distribute the numbers of trails in different bins more evenly. We shall explain below how this merging procedure works for the joint distribution of X , Y and Z . The same procedure is applied (in dimensions 2 and 1) for the joint distributions of two of the three random variables and for the marginal distributions.

For the joint distribution of X , Y and Z , from our simulations we have a total of $50 \times 50 \times 50$ cubical bins that span the unit cube with the variables X , Y and Z along the axes. We consider merging together either $10 \times 10 \times 10$, or $5 \times 5 \times 5$, or $2 \times 2 \times 2$ of these cubical bins into larger cubical bins, that together with the unmerged bins form a partition of the unit cube. Our aim is that each bin in the final partition of the unit cube represents at least 100 generated trails, 0.01% of the total. Moreover, we want each bin that represents at least 1% (10^4) of the total number of generated trails to be present in the final partition.

The merging procedure therefore works as follows. First, we consider for each of the $10 \times 10 \times 10$ cubes whether it should form a large bin, or be built up from smaller bins. So we do the following test: if we would built it up from $2 \times 2 \times 2$ bins, then would each constituting bin contain at least 100 trails, or would one of these bins contain at least 10^4 trails? If so, the $10 \times 10 \times 10$ cube is split into $2 \times 2 \times 2$ cubes. Then we test whether each of these $2 \times 2 \times 2$ cubes should form a bin, or be built up from $1 \times 1 \times 1$ bins, by the same criterion as above. Otherwise, we test whether the $10 \times 10 \times 10$ cube can be built up from $5 \times 5 \times 5$ (rather than $2 \times 2 \times 2$) cubes. If so, we test whether each of these $5 \times 5 \times 5$ cubes should form a bin, or be built up from $1 \times 1 \times 1$ bins, as before. In the end, we achieve a more even distribution of trails over a smaller number of bins, as desired.

6.4 Distribution of the hull of a self-avoiding trail

In section 6.3 we described our self-avoiding trail simulations in isosceles triangles. We carried out these simulations for 8 different triangles with base angles of 10° up to 80° with 10° intervals, and for 12 different system sizes (namely $N = 100, 200, 300, 400, 600, 800, 1200, 1600, 2000, 2400, 3200, 4000$)

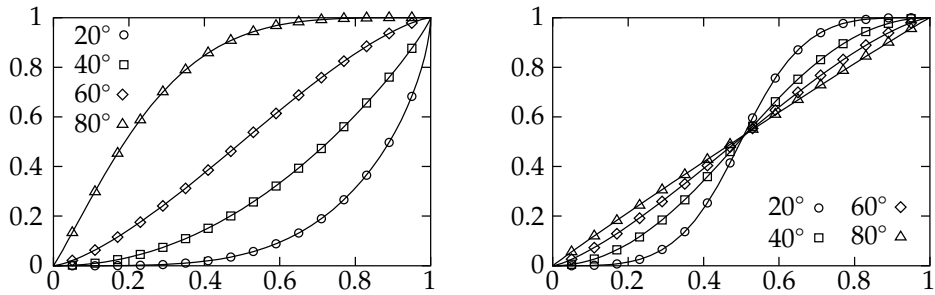


Figure 6.8. The distribution functions $\mathbf{P}[X \leq x]$ (left) and $\mathbf{P}[Y \leq y]$ (right) for the self-avoiding trail on different triangles with system size $N = 4000$, started from the lower-left corner. The solid lines are the corresponding distributions for a reflected Brownian motion for which we obtain an optimal least-squares fit. See table 6.1 for the corresponding values of α and β .

for each of these triangles. In this section we will discuss our analysis of the data collected in the simulations. As we explained, we want to compare the distribution of the hull generated by the trails with the hull distribution of reflected Brownian motion, in particular in the limit when the system size becomes large.

Our working hypothesis is therefore that the binned data collected in the simulations is predicted by the joint distribution function (6.4) for the RBM with parameters α, β for some α and β as $N \rightarrow \infty$. To test this hypothesis, we make a least-squares fit of the parameters α and β for each system size N . For every triangle T_φ on which we have simulated the model and for each of the two possible starting points, this gives us a list of the best-fit values for α and β for 12 different system sizes. We want to investigate whether these values of α and β converge to a common limit as the system size becomes larger and larger.

The least-squares fits show that the marginal distributions of X, Y and Z for the self-avoiding trail are well described by those of an RBM (see figure 6.8). More precisely, as the system size N gets larger, the value of χ^2 (the difference between the actual and the predicted number of walks in each bin squared, divided by the predicted variance in this number, summed over all the bins) goes down to a value close to the number of bins, see for instance table 6.2. However, the fitted values we obtain for α and β are not constant with the system size. More work is therefore needed to test convergence of α and β to a limit as $N \rightarrow \infty$.

We also observe from the simulations that the fitted values of α and β for the three distributions of X, Y and Z do not fully agree. It seems that the

	20°		40°		60°		80°	
	α/π	β/π	α/π	β/π	α/π	β/π	α/π	β/π
X	0.456(1)	0.484(2)	0.461(2)	0.474(2)	0.464(2)	0.464(2)	0.464(2)	0.453(2)
Y	0.456(1)	0.446(1)	0.462(2)	0.445(1)	0.464(1)	0.438(2)	0.461(2)	0.431(2)
Z	0.447(2)	0.483(2)	0.445(1)	0.475(2)	0.439(2)	0.464(2)	0.431(1)	0.452(1)

Table 6.1. Fitted values for α and β on different triangles compared for the different marginal distributions of X , Y and Z (system size $N = 4000$, trails start from the lower-left corner).

fitted values of α do agree for the distributions of X and Y , whereas the fitted values of β do agree for the distributions of X and Z . The fitted value of α for the distribution of Z agrees with the fitted value of β for the distribution of Y . See table 6.1. This observation holds both for trails starting from the top of the triangle and for trails starting from the lower-left corner at different system sizes. This is another indication that more work is required to test convergence of α and β as $N \rightarrow \infty$.

Interestingly, for trails that start in the lower-left corner of an *equilateral* triangle the fitted values of α and β do agree for the exit distribution at different system sizes (see table 6.2). In other words, the exit distribution of the trails is symmetric in an equilateral triangle. Note that this result is not trivial because our boundary conditions are not symmetric between the left side and the base of the triangle, as can be seen in figure 6.6. This tells us that our choice of boundary conditions does not destroy the isotropy of the model, and hence does not interfere with conformal invariance in the scaling limit.

Before we consider the convergence to a limit in more detail, let us also consider the joint distributions of X , Y and Z . Since the fits of the marginal distributions give different values of α and β at finite system sizes, it is to be expected that the joint distributions measured in the simulations will not be well described by those of an RBM. This is indeed what we see when we try to fit the data for the joint distributions to the distribution function for the RBMs, see for instance table 6.2. We note that the value of χ^2 for the fits of the joint distributions is several times the number of bins at small system sizes. However, χ^2 does go down as the system size increases, which is a sign that the fits become better for larger systems.

If the hull of the self-avoiding trail converges to that of a reflected Brownian motion in the scaling limit, then the fitted values of α and β should converge to a limit value as $N \rightarrow \infty$. From the change in the fitted values of α and β with system size observed in the simulations we can see that if there is convergence, then it is very slow. We make the educated guess that α and β converge with

N	Marginal distribution of X				Joint distribution of X, Y and Z			
	α/π	β/π	χ^2	#bins	α/π	β/π	χ^2	#bins
100	0.421(5)	0.439(5)	7754	99	0.428(4)	0.434(3)	8401	1193
200	0.440(2)	0.449(2)	556	100	0.436(4)	0.441(3)	8577	1317
300	0.445(3)	0.450(3)	708	100	0.440(4)	0.443(4)	8375	1207
400	0.448(2)	0.452(2)	311	100	0.442(4)	0.444(5)	8386	1193
600	0.453(2)	0.455(2)	238	100	0.445(4)	0.447(4)	8181	1200
800	0.454(2)	0.457(2)	201	100	0.448(4)	0.450(3)	8280	1310
1200	0.457(2)	0.458(2)	148	100	0.451(4)	0.452(4)	7661	1427
1600	0.460(2)	0.461(2)	160	100	0.453(4)	0.454(4)	7938	1441
2000	0.460(1)	0.461(2)	123	100	0.453(4)	0.454(4)	7392	1200
2400	0.461(2)	0.462(1)	110	100	0.455(4)	0.455(4)	7102	1083
3200	0.462(2)	0.462(2)	152	100	0.455(4)	0.456(3)	7228	1317
4000	0.464(2)	0.464(2)	126	100	0.457(3)	0.457(3)	7118	1434

Table 6.2. Fitted values for α and β together with the value of χ^2 and the number of bins for two different distributions of a trail on an equilateral triangle, started from the lower-left corner.

the system size N as $1/\log_{10} N$ (corrections that behave as a power of $\log_{10} N$ rather than as a power of N itself are consistent with earlier findings [67] and with the presence of a zero conformal weight).

To test convergence, we therefore try to make a linear fit of the fitted values of α and β for the different distributions on different triangles against $1/\log_{10} N$. We accept the linear fit if it passes each of the following three tests:

1. We look at the value of χ^2 for the fit. If this value exceeds the 10% probability threshold for the χ^2 distribution, we reject the fit.
2. We compare the value of the intercept at $N = \infty$ from the linear fit with the value we obtain if we fit the data to a parabola in $1/\log_{10} N$. If the values do not agree within 1.96 standard deviation (the Gaussian 5% level) of the linear fit, the fit is rejected.
3. We do a run test. If the data is well described by a line, then each data point should be independently above or below this line with equal probabilities. Thus we can predict how many consecutive runs of points above the line and below the line we should expect. If the probability for the number of such runs in our linear fit is less than 12%, the fit is rejected.

For more background on these (and other) kinds of tests for data fitting, the reader can consult for instance Barlow [4].

It turns out that in some cases the fitted values of α or β are acceptably linear with $1/\log_{10} N$ if we leave out the smallest system sizes. We therefore accept a linear fit if the data points for at least the 9 largest system sizes fit on a

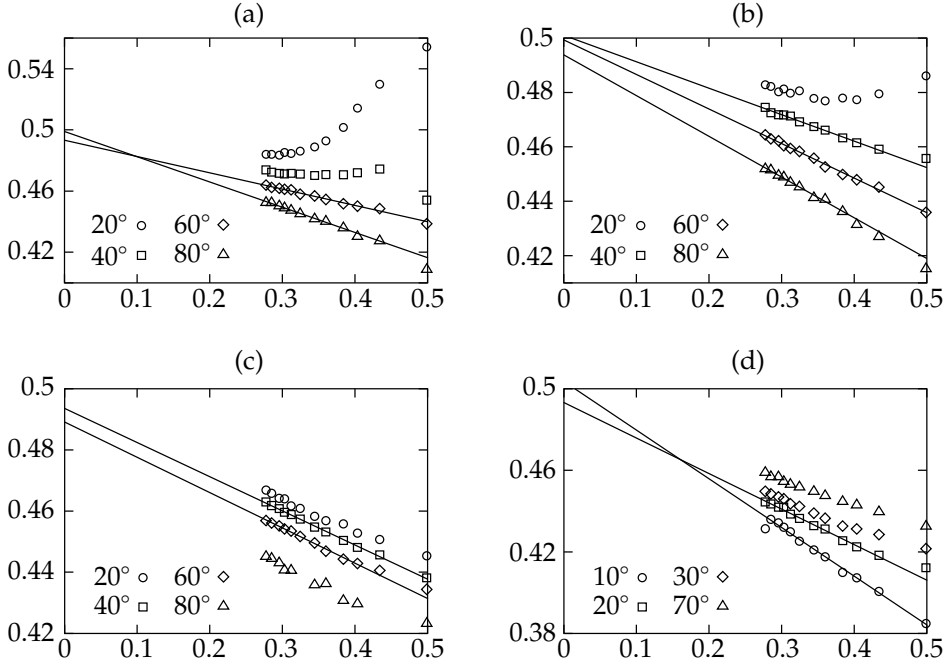


Figure 6.9. Graphs (a), (b) and (c) show the fitted values of β/π against $1/\log_{10} N$ for the marginal distributions of X and Z and the joint distribution of X, Y and Z , respectively, for trails started from the left corner. Graph (d) shows the fitted values of α/π against $1/\log_{10} N$ for the joint distribution of X, Y and Z for trails started from the top. In those cases where a linear fit is accepted, the fitted line is shown.

straight line by the three criteria stated above. We then have a total of 224 sets of data points for which we attempt a linear fit (3 marginal distribution plus 4 joint distributions for the variables X, Y and Z , times 8 different base angles, times 2 because the trails can start either from the top or the lower-left corner, times 2 variables α and β). Of these, 107 turn out to give an acceptable linear fit (see for instance figure 6.9). The other sets of data may still converge to a limit, but this cannot be seen from our simulations without further knowledge of the nature of the convergence. Clearly, for a more convincing test of convergence we need simulations on much larger systems, or a credible analytic conjecture for the nature of the convergence.

From our data we can say the following. There are 57 sets of data for which we have an accepted linear fit of α against $1/\log_{10} N$. These linear fits give us 57 values for the intercept with the α -axis as $N \rightarrow \infty$. The average and standard deviation of these values suggest that $\alpha/\pi \rightarrow 0.4948(61)$ as $N \rightarrow \infty$. Likewise, from the 50 accepted linear fits of β against $1/\log_{10} N$ we get $\beta/\pi \rightarrow 0.492(11)$

as $N \rightarrow \infty$. These results are consistent with the hypothesis that the hull of the self-avoiding trail in the scaling limit is the same as that of an $\text{RBM}_{\pi/2, \pi/2}$, that is, a reflected Brownian motion with perpendicular reflection on the boundary.

6.A Critical percolation and the last-visit distribution

We now return once again to critical percolation. In section 6.3 we explained that the self-avoiding trail model studied in this chapter becomes a model for critical bond percolation if we take the probabilities of the vertex states a and b on page 111 proportional to $\sin(2\varphi/3)$ and $\sin((\pi - 2\varphi)/3)$, respectively, and $p(c) = 0$. The paths defined by the model then correspond to the boundaries of the percolation clusters, or equivalently, to a percolation exploration path. The hull generated by a path of the model should therefore have the same law as the hull of an $\text{RBM}_{\pi/3, \pi/3}$ in the scaling limit.

Similar simulations as for the self-avoiding trails allow us to test this hypothesis. We have measured in the same way as before the joint distribution of the variables X , Y and Z on different triangles with fixed system size $N = 2000$. Our hypothesis is that this joint distribution is predicted by equation (6.4) for reflected Brownian motion with reflection angles α and β , where α and β should be equal to $\pi/3$. Table 6.3 shows the results of a least-squares fit for the reflection angles α and β , which agree with the hypothesis that the hull is the same as that of an $\text{RBM}_{\pi/3, \pi/3}$.

It was shown by Dubédat that there exists a rather surprising further connection between reflected Brownian motion and the exploration process of critical percolation. To explain this connection, suppose that W is a local process in the triangle $T = T_{\lambda, \mu}$ started from $w = w_{\lambda, \mu}$, where λ, μ are fixed angles such that $\lambda + \mu < \pi$. Let $\tau := \inf\{t \geq 0 : W(t) \in [0, 1]\}$, and let σ be the last time before τ when W visits the boundary of T . Let E denote the event that $W(\sigma)$ is on the right side of the triangle. Then we can consider the probability of the event E conditioned on $\{W(\tau) = x\}$. We call this conditional probability, which is a function of x , the *last-visit distribution* of W in T . For reflected Brownian motion this last-visit distribution is given by the following theorem, which we shall prove at the end of this section:

Theorem 6.4 (Last-visit distribution). *Suppose that W is an $\text{RBM}_{\alpha, \beta}$ in the triangle $T = T_{\lambda, \mu}$ started from $w = w_{\lambda, \mu}$. Let τ , σ and E be as above. Then*

$$\mathbf{P}[E \mid W(\tau) = x] = F_{\pi - \alpha, \pi - \beta} \left(F_{\lambda, \mu}^{-1}(x) \right). \quad (6.10)$$

where $F_{\gamma, \delta}$, given by equation (6.1), is the unique conformal transformation of \mathbb{H} onto $T_{\gamma, \delta}$ which fixes 0 and 1 and sends ∞ to $w_{\gamma, \delta}$.

	angle	from the top		from the left corner	
		α/π	β/π	α/π	β/π
joint distribution	20°	0.331(4)	0.350(4)	0.334(2)	0.334(2)
	40°	0.334(4)	0.339(3)	0.333(1)	0.334(2)
	60°	0.334(2)	0.333(1)	0.333(2)	0.335(2)
	80°	0.333(1)	0.331(1)	0.331(2)	0.335(2)
last-visit distribution	20°	0.336(2)	0.335(2)	0.332(2)	0.329(3)
	40°	0.329(4)	0.331(3)	0.332(3)	0.332(2)
	60°	0.332(3)	0.334(3)	0.332(3)	0.332(3)
	80°	0.328(4)	0.339(3)	0.327(3)	0.333(3)

Table 6.3. Fitted values for α and β on different triangles for the joint and last-visit distributions of the exploration process of critical bond percolation at system size $N = 2000$.

The last-visit distribution can also be computed rigorously for chordal SLE_6 , as was shown by Dubédat [33]. The obtained formula is exactly the formula (6.10) for an $\text{RBM}_{\pi/3, \pi/3}$. This fact is rather surprising if one considers the very different ways in which the two processes explore space: whereas an SLE_6 process never crosses itself, an $\text{RBM}_{\pi/3, \pi/3}$ crosses itself many times. Observe in particular that on the event E , the last point visited on the right side of the triangle T by an SLE_6 process must be also the lowest point of the hull on the right side. For an $\text{RBM}_{\pi/3, \pi/3}$, however, the last point visited on the right side is a.s. not the lowest point of the hull.

Let us now return to our simulations of the exploration path of critical percolation. It is quite easy to count in these simulations the number of paths that land in a given bin and visited the side to the left (and not to the right) of the starting point last before reaching the opposite side. Divided by the total number of paths that land in a given bin, this binned data can be compared to the last-visit distribution of equation (6.10). Note, however, that this binned data represents the conditional probability of E given that the path lands in an interval rather than at a given point x . To make the comparison we therefore have to integrate (6.10) with respect to the exit distribution of the exploration path.

We take the exit distribution for the paths in the simulations to be well described by the least-squares fit for the marginal distribution of X . Then we can integrate (6.10) (with α and β as parameters) with respect to this fixed exit distribution, and obtain from this the probability of E conditioned on the event that the path lands in a given bin. This can be used to make a least-squares fit for the parameters α and β of the last-visit distribution. Table 6.3 shows that our simulations for critical percolation are in agreement with the hypothesis that the last-visit distribution is given by that of an $\text{RBM}_{\pi/3, \pi/3}$.

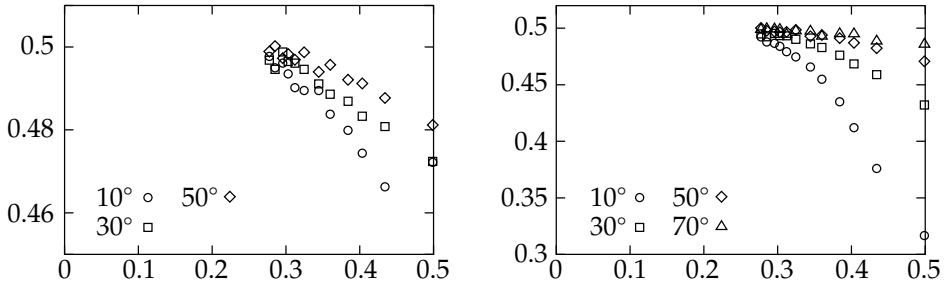


Figure 6.10. Fitted values of α/π (left) and β/π (right) plotted against $1/\log_{10} N$ for the last-visit distribution of trails starting from the lower-left corner of different triangles.

A similar analysis can be carried out for the self-avoiding trails. As before, here we face the problem that the model converges only slowly. We therefore make least-squares fits of α and β for different system sizes, and plot the results against $1/\log_{10} N$, see figure 6.10. It is clear that without further knowledge of the nature of the convergence, we cannot state with much authority what the scaling limit will be. However, our results do not exclude the possibility that the last-visit distribution for the self-avoiding trails in the scaling limit is the same as that of an $\text{RBM}_{\pi/2, \pi/2}$, just like the distribution of the hull. If this could be shown to be true, this would be an intriguing result.

We conclude this section with the proof of theorem 6.4. The proof uses the fact, discussed in section 5.B.2, that the imaginary part of an $\text{RBM}_{\alpha, \beta}$ in $T_{\alpha, \beta}$ stopped when it hits $[0, 1]$ is a 3-dimensional Bessel process, and so is the imaginary part of its time-reversal. In particular, the time-reversed process, considered up to the first time when it hits the left or right side of the triangle, is a complex Brownian motion started with the uniform distribution from $[0, 1]$ and conditioned not to return to the real line. This allows us to derive the last-visit distribution by the following computation, which generalises the computation of Dubédat [31] for the case $\alpha = \beta = \lambda = \mu = \pi/3$:

B.5 ◀ **Proof of theorem 6.4.** We want to use the fact that the time-reversal of the **B.6** $\text{RBM}_{\alpha, \beta}$ in the triangle $T_{\alpha, \beta}$ starts out as a conditioned Brownian motion. So we first map $T_{\lambda, \mu}$ onto $T_{\alpha, \beta}$ by the transformation $F_{\alpha, \beta} \circ F_{\lambda, \mu}^{-1}$. This maps the point x onto $y := F_{\alpha, \beta} \circ F_{\lambda, \mu}^{-1}(x)$. Next, let V be a Brownian motion in the upper half-plane conditioned not to hit \mathbb{R} and let S be the first time when V visits either the left or right side of $T_{\alpha, \beta}$. Then

$$\mathbf{P}[E \mid W(\tau) = x] = \lim_{\varepsilon \rightarrow 0} \int_1^{w_{\alpha, \beta}} \mathbf{P}_{y+i\varepsilon}[V(S) \in dz], \tag{6.11}$$

where the integral is over the right side of the triangle $T_{\alpha, \beta}$ and \mathbf{P}_z denotes

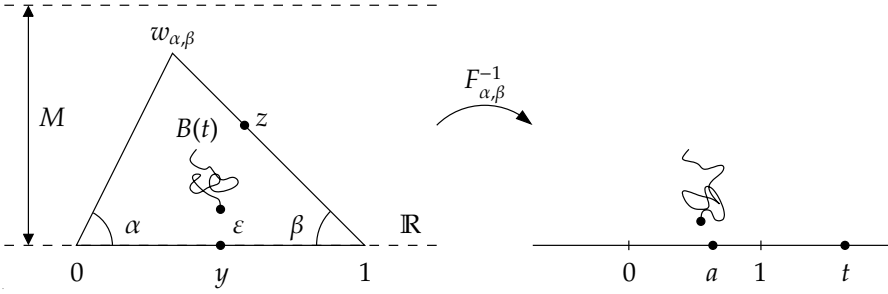


Figure 6.11. A complex Brownian motion B started from $y + i\varepsilon$ in the triangle $T_{\alpha, \beta}$ conditioned to exit the strip $\{z \in \mathbb{C} : 0 < \text{Im } z < M\}$ through the top boundary and stopped when it hits the boundary of the triangle $T_{\alpha, \beta}$ corresponds in the limit $M \rightarrow \infty, \varepsilon \rightarrow 0$ to the time-reversal of the RBM $_{\alpha, \beta}$ in the triangle started from y .

probability with respect to the conditioned Brownian motion started from z .

Now let B be a complex Brownian motion, let U be the first time when B visits either the left or right side of $T_{\alpha, \beta}$, and let U_M be the first time when B exits the strip $\{z : 0 < \text{Im } z < M\}$. Suppose that \mathbf{P}'_z denotes probability with respect to this Brownian motion started from z . Then, using the strong Markov property of Brownian motion (see figure 6.11 for a sketch), we have

$$\begin{aligned} \mathbf{P}'_{y+i\varepsilon}[V(S) \in dz] &= \lim_{M \rightarrow \infty} \mathbf{P}'_{y+i\varepsilon}[B(U) \in dz \mid \text{Im } B(U_M) = M] \\ &= \mathbf{P}'_{y+i\varepsilon}[B(U) \in dz] \lim_{M \rightarrow \infty} \frac{\mathbf{P}'_z[\text{Im } B(U_M) = M]}{\mathbf{P}'_{y+i\varepsilon}[\text{Im } B(U_M) = M]} \\ &= \mathbf{P}'_{y+i\varepsilon}[B(U) \in dz] \frac{\text{Im } z}{\varepsilon}, \end{aligned} \tag{6.12}$$

where in the last step we have used [75, proposition II(3.8)]. Combining equations (6.11) and (6.12), we see that we have to compute the limit of $\mathbf{P}'_{y+i\varepsilon}[B(U) \in dz] \text{Im } z / \varepsilon$ as $\varepsilon \rightarrow 0$. This computation can be done by using the conformal invariance of Brownian motion.

By corollary B.15, the probability that a complex Brownian motion started from $a + ib$ leaves the upper half-plane through $(-\infty, x)$ is given by

$$\int_{-\infty}^x \frac{b}{\pi b^2 + (t - a)^2} dt = \frac{1}{2} + \frac{1}{\pi} \arctan \frac{x - a}{b}. \tag{6.13}$$

Thus, mapping the triangle $T_{\alpha, \beta}$ conformally to the upper half-plane by the transformation $F_{\alpha, \beta}^{-1}$ as in figure 6.11, we can write

$$\lim_{\varepsilon \rightarrow 0} \mathbf{P}'_{y+i\varepsilon}[B(U) \in dz] \frac{\text{Im } z}{\varepsilon} = \frac{\text{Im } F_{\alpha, \beta}(t)}{\pi F'_{\alpha, \beta}(a)} \frac{dt}{(t - a)^2}, \tag{6.14}$$

where $t = F_{\alpha,\beta}^{-1}(z)$, $a = F_{\alpha,\beta}^{-1}(y) = F_{\lambda,\mu}^{-1}(x)$ and we have used

$$F_{\alpha,\beta}^{-1}(y + i\varepsilon) = a + \frac{i\varepsilon}{F'_{\alpha,\beta}(a)} + O(\varepsilon^2). \quad (6.15)$$

Therefore, using the expression (6.1) for the triangle mappings,

$$\begin{aligned} \mathbf{P}[E \mid W(\tau) = x] & \quad (6.16) \\ &= \frac{1}{\pi F'_{\alpha,\beta}(a)} \int_1^\infty \frac{dt}{(t-a)^2} \operatorname{Im} F_{\alpha,\beta}(t) \\ &= \frac{a^{1-\alpha/\pi}(1-a)^{1-\beta/\pi}}{\pi} \int_1^\infty \frac{dt}{(t-a)^2} \operatorname{Im} \int_1^t u^{\alpha/\pi-1}(1-u)^{\beta/\pi-1} du \\ &= \frac{\sin \beta}{\pi} a^{1-\alpha/\pi}(1-a)^{1-\beta/\pi} \int_1^\infty u^{\alpha/\pi-1}(u-1)^{\beta/\pi-1} \int_u^\infty \frac{dt}{(t-a)^2} du \\ &= \frac{\sin \beta}{\pi} a^{1-\alpha/\pi}(1-a)^{1-\beta/\pi} \int_1^\infty u^{\alpha/\pi-1}(u-1)^{\beta/\pi-1}(u-a)^{-1} du \\ &= \frac{\sin \beta}{\pi} a^{1-\alpha/\pi}(1-a)^{1-\beta/\pi} \int_0^1 t^{1-\alpha/\pi-\beta/\pi}(1-t)^{\beta/\pi-1}(1-at)^{-1} dt, \end{aligned}$$

where in the last step we have made the substitution $t = 1/u$.

With the help of equations 15.3.1, 15.2.5 and 15.1.20 in [71] and equations 6.1.15 and 6.1.17 in [27], the conditional expectation can be rewritten as

$$\begin{aligned} \mathbf{P}[E \mid W(\tau) = x] & \quad (6.17) \\ &= \frac{\sin \beta}{\pi} \frac{\Gamma(2-(\alpha+\beta)/\pi)\Gamma(\beta/\pi)}{\Gamma(2-\alpha/\pi)} a^{1-\alpha/\pi}(1-a)^{1-\beta/\pi} {}_2F_1(1, 2-(\alpha+\beta)/\pi; 2-\alpha/\pi; a) \\ &= \frac{\Gamma(2-(\alpha+\beta)/\pi)}{\Gamma(1-\alpha/\pi)\Gamma(1-\beta/\pi)} \int_0^a t^{-\alpha/\pi}(1-t)^{-\beta/\pi} dt \\ &= F_{\pi-\alpha,\pi-\beta}(a) = F_{\pi-\alpha,\pi-\beta}(F_{\lambda,\mu}^{-1}(x)). \end{aligned}$$

This is the desired result. ■

Appendix

A Conformal mapping theory

Summary

This appendix provides background on conformal mapping theory and complex analysis which is used throughout the thesis. We emphasise those results that are needed in SLE. All the basic results on conformal maps can be found in [1, 39]. For details on the boundary behaviour of conformal maps we refer to [73], and for details on extremal length the reader should consult [2]. Other sources for background on conformal mapping theory for SLE are [52, 53].

A.1 The Riemann mapping theorem

We start this appendix by fixing some terminology. A *curve* or *path* γ in \mathbb{C} is given by a continuous parametric representation, which we will denote by $\gamma(t)$. Thus, a curve is a mapping $\gamma : [a, b] \rightarrow \mathbb{C}$, such that $\gamma(t)$ is continuous on $[a, b]$. The curve is called *closed* if $\gamma(a) = \gamma(b)$. By an *arc* we shall always mean a curve which is not closed. If the mapping $\gamma : [a, b] \rightarrow \mathbb{C}$ is injective (one-to-one), γ is called a *Jordan arc*. A closed curve given by an injective (one-to-one) mapping $\gamma : [a, b] \rightarrow \mathbb{C}$ such that $\lim_{t \rightarrow b} \gamma(t) = \gamma(a)$ is called a *Jordan curve*.

We will call a subset A of \mathbb{C} *connected* if any two points in A can be connected by a curve lying entirely within A . A *domain* is an open connected subset of the complex plane. We call a domain *simply connected* if every closed curve in D can be deformed continuously within D to a point of D . Loosely speaking, a simply connected domain contains no holes or punctures. A domain D which is not simply connected is called *doubly connected* if its complement has a connected component A such that $D \cup A$ is simply connected. A domain bounded by a Jordan curve is called a *Jordan domain*. For any given domain D , an open Jordan arc $\gamma : (a, b) \rightarrow D$ such that $\bar{\gamma} = \gamma \cup \{\alpha, \beta\}$ with $\alpha, \beta \in \partial D$ is called a *crosscut* of D .

The *length* $L(\gamma)$ of a curve $\gamma(t)$, $a \leq t \leq b$, is defined by

$$L(\gamma) = \sup \sum_{k=1}^n |\gamma(t_k) - \gamma(t_{k-1})|, \quad (\text{A.1})$$

where the supremum is taken over all partitions $a = t_0 < t_1 < \dots < t_n = b$ and all $n \in \mathbb{N}$. The curve is called *rectifiable* if this supremum is finite. Rectifiable arcs can be used to measure distances between sets, for instance using the notion of extremal length introduced in section A.2.

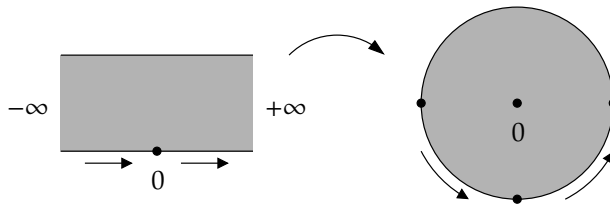


Figure A.1. An infinite horizontal strip has two distinct boundary points at $+\infty$ and $-\infty$ that map onto distinct boundary points of the unit disk.

A *conformal map* f of a simply connected domain $D \neq \mathbb{C}$ onto another simply connected domain $D' \neq \mathbb{C}$ is a one-to-one diffeomorphic map which preserves angles. That is, if γ_1 and γ_2 are two differentiable curves in D which intersect at a certain angle, then their images $f \circ \gamma_1$ and $f \circ \gamma_2$ must intersect at the same angle. Equivalently, a conformal map $f : D \rightarrow D'$ is a bijective and analytic function on D , which has nonzero derivative everywhere on D . It has an inverse f^{-1} which is also conformal. The Riemann mapping theorem states that any simply connected domain $D \neq \mathbb{C}$ can be mapped conformally onto the open unit disk \mathbb{D} :

Theorem A.1 (Riemann mapping theorem). *Let $D \neq \mathbb{C}$ be a simply connected domain in \mathbb{C} . Then there exists a conformal map f of D onto the open unit disk \mathbb{D} .*

Note that theorem A.1 says nothing about the behaviour of the map f on the boundary ∂D of \mathbb{D} . We need to make a few remarks on this. For a start we observe that the domain D need not be bounded. This means that domains can have well-defined boundary points at infinity. For example, the upper half-plane has a single boundary point at ∞ , and the infinite strip $\{z : 0 < \text{Im } z < 1\}$ has two distinct boundary points at $-\infty$ and at $+\infty$. By mapping these domains conformally onto \mathbb{D} it can be made explicit that these boundary points are well-defined, see figure A.1.

It is useful to understand when a conformal transformation of the unit disk onto a bounded domain D can be extended to the boundary. This question is answered by the following two theorems (see Pommerenke [73, chapter 2] for details and other equivalent statements):

Theorem A.2 (Continuity theorem). *Let f map \mathbb{D} conformally onto the bounded domain D . Then f has a continuous extension to $\overline{\mathbb{D}}$ if and only if ∂D is a closed curve.*

Theorem A.3 (Carathéodory). *Let f map \mathbb{D} conformally onto the bounded domain D . Then f has a continuous and injective extension to $\overline{\mathbb{D}}$ if and only if ∂D is a Jordan curve.*

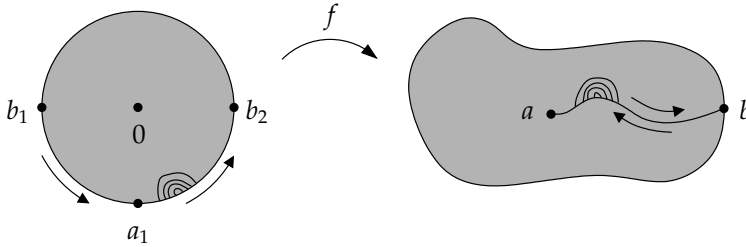


Figure A.2. Conformal transformation of the unit disk onto a slit domain. Points with the same letters correspond to each other. The crosscuts illustrate the notion of prime ends.

In this thesis we are mainly concerned with conformal maps between domains that have a continuous boundary, so that either theorem A.2 or theorem A.3 applies. The difference between theorems A.2 and A.3 is that the boundary of D in theorem A.2 can be a curve with repeated points. This implies that more than one point of $\partial\mathbb{D}$ may be mapped onto the same point of ∂D . Consider for instance the slit domain in figure A.2. Here, every point along the slit (except for the tip of slit) has two pre-images on $\partial\mathbb{D}$, and we should therefore treat a point z on the slit as a “double boundary point” of D . In the same way there can be triple boundary points and so on (of these there can be only countably many).

To deal with these and more complicated situations, the notion of *prime ends* was introduced by Carathéodory. Basically, the prime ends of a domain are equivalence classes of families (γ_n) of disjoint crosscuts of the domain with $L(\gamma_n) \rightarrow 0$ as $n \rightarrow \infty$, such that each γ_n separates γ_{n+1} from γ_0 . For instance, two distinct prime ends correspond to each point along the slit in figure A.2. One can prove that for every conformal transformation $f : \mathbb{D} \rightarrow D$, the points $z \in \partial\mathbb{D}$ correspond one-to-one with the prime ends of D . We refer to the books of Ahlfors [2, section 4.6] and Pommerenke [73, section 2.4] for details and more precise statements concerning prime ends.

In working with conformal transformations it is useful to have notions of distances and lengths available that are invariant under such transformations. A very powerful conformally invariant notion of length is *extremal length*, which will be explained in section A.2. Another conformally invariant measure related to boundary arcs of a domain D is *harmonic measure*, which we define below for a (not necessarily simply) connected domain. Proving that harmonic measure is invariant under conformal maps is simple, e.g. by applying the Cauchy-Riemann equations and using harmonicity of conformal maps.

Definition A.4 (Harmonic measure). Let D be a connected domain whose boundary

consists of a finite number of disjoint Jordan curves, and suppose that the boundary is divided into two parts A and A' , each consisting of a finite number of arcs and closed curves. Then there exists a unique bounded harmonic function $\omega(z)$ in D such that $\omega(z) \rightarrow 1$ when z tends to an interior point of A and $\omega(z) \rightarrow 0$ when z tends to an interior point of A' . The number $\omega(z)$ (which satisfies $0 \leq \omega(z) \leq 1$) is called the harmonic measure of A at the point z with respect to D .

The harmonic measure $\omega(z)$ in D of the set $A \subset \partial D$ is also equal to the probability that a complex Brownian motion in D which starts from z will hit the set A before it hits $A' = \partial D \setminus A$. For more details, see theorem B.14 in section B.6 of appendix B.

A.2 Extremal length and extremal distance

In this section we will be concerned with collections Γ of rectifiable arcs in a given domain D . Under a conformal mapping $f : D \rightarrow D^*$ this collection Γ is transformed into a collection Γ^* of rectifiable arcs in D^* . The *extremal length* of Γ , which we will define below, is a number $\lambda_D(\Gamma)$ which is invariant under conformal transformations, so that $\lambda_D(\Gamma) = \lambda_{D^*}(\Gamma^*)$. All the details for this section can be found in Ahlfors [2, chapter 4].

We consider the family of Riemannian metrics $ds = \rho(z)|dz|$ such that ρ is Borel-measurable (see section B.1) in D . Then for every ρ , any rectifiable arc γ in D has a well-defined ρ -length and the domain D has a ρ -area, defined by

$$L(\gamma, \rho) = \int_{\gamma} \rho(z) |dz|, \quad A(D, \rho) = \iint_D \rho(x + iy)^2 dx dy. \quad (\text{A.2})$$

Observe that the family of metrics considered here transforms in a conformally invariant way. That is to say, under the mapping $f : D \rightarrow D^*$ the metric $\rho(z)|dz|$ in D transforms into a metric $\rho^*(z^*)|dz^*|$ in D^* , where ρ^* and ρ are related by $\rho^*(f(z)) = \rho(z)/|f'(z)|$. In particular, if we apply the mapping f and replace ρ by ρ^* at the same time, then it is clear that $L(\gamma, \rho) = L(f \circ \gamma, \rho^*)$ and $A(D, \rho) = A(D^*, \rho^*)$.

Let us now define the ρ -length of a collection Γ of rectifiable arcs in D by

$$L(\Gamma, \rho) = \inf_{\gamma \in \Gamma} L(\gamma, \rho). \quad (\text{A.3})$$

Then by what we said above, $L(\Gamma, \rho) = L(\Gamma^*, \rho^*)$. It follows that the set of ratios $L(\Gamma, \rho)^2/A(D, \rho)$ is conformally invariant, and so is their supremum over ρ . Note also that these ratios are invariant under multiplication of ρ by a constant. We are led to the following definition:

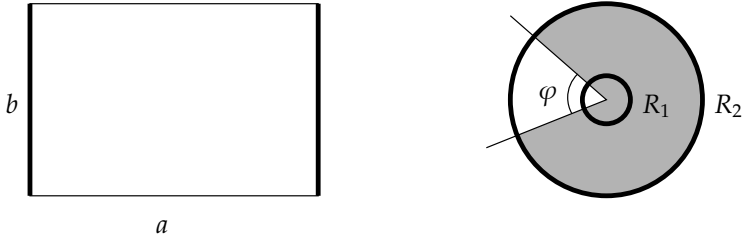


Figure A.3. The extremal distance between two opposite sides of a rectangle is equal to the aspect ratio a/b , and in a sector of the annulus $R_1 < |z| < R_2$ with opening angle φ , the extremal distance between the two components of the complement of the annulus is $(1/\varphi) \log(R_2/R_1)$.

Definition A.5 (Extremal length). *The extremal length of Γ in D is defined as*

$$\lambda_D(\Gamma) = \sup_{\rho} \frac{L(\Gamma, \rho)^2}{A(D, \rho)}, \tag{A.4}$$

where ρ is subject to the condition $0 < A(D, \rho) < \infty$.

Since the ratio $L(\Gamma, \rho)^2/A(D, \rho)$ is invariant under multiplication of ρ by a constant, several alternative definitions are possible by specifying different normalisations of the metrics ρ . It is also quite easy to see that the extremal length of Γ does not depend on D in the sense that for every open set Ω that contains the arcs $\gamma \in \Gamma$ the number $\lambda_{\Omega}(\Gamma)$ is the same. To reflect this, the notation of extremal length will henceforth be simplified to $\lambda(\Gamma)$.

We now introduce the more special notion of *extremal distance* which is of special importance to us. To define this notion, suppose that D is a domain and A, B are two set in \bar{D} . Consider the collection Γ of rectifiable arcs γ in D that connect A and B , that is, such that γ has one endpoint in A and one endpoint in B . Then the extremal length $\lambda(\Gamma)$ is called the *extremal distance* between A and B in D . We will denote this extremal distance by $d_D(A, B)$. Some special cases, which are illustrated in figure A.3, will be studied below.

Consider the rectangle $R = (0, a) \times (0, b)$ and let $A = \{iy : 0 \leq y \leq b\}$, $B = \{a + iy : 0 \leq y \leq b\}$ (the vertical sides of R). If Γ is the collection of rectifiable crosscuts of R connecting A and B , then it is not difficult to verify that $L(\Gamma, \rho)^2/A(R, \rho)$ is maximal for $\rho = 1$. Hence, $d_R(A, B) = a/b$.

In general, if we consider a collection Γ of arcs in a domain D , a metric ρ_0 such that $L(\Gamma, \rho_0)^2/A(D, \rho_0)$ is equal to $\lambda(\Gamma)$ is called an *extremal metric* for Γ in D . For another example, consider the annulus $A := \{z \in \mathbb{C} : R_1 < |z| < R_2\}$, and let C_1 and C_2 denote the inner and outer components of the boundary,

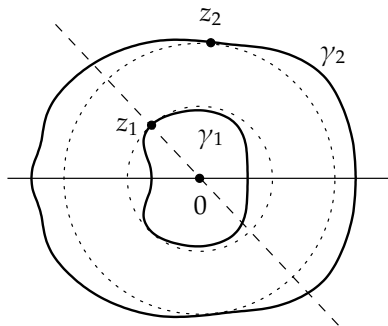


Figure A.4. Teichmüller's theorem gives a bound on the extremal distance between two crosscuts γ_1 and γ_2 of the upper half-plane in terms of the ratio $|z_2|/|z_1|$.

respectively. Then one can show that $d_A(C_1, C_2) = (1/2\pi) \log(R_2/R_1)$ because the metric $\rho(z) = 1/|z|$ is extremal in this case. If we restrict the domain A to a sector S with opening angle φ , then $d_S(C_1, C_2) = (1/\varphi) \log(R_2/R_1)$ (see figure A.3).

The notion of extremal length is quite powerful not only because it is conformally invariant, but also because it is not too difficult to derive upper and lower bounds. For instance, any choice of ρ will immediately give a lower bound for $\lambda(\Gamma)$. Another simple way of comparing extremal lengths is given by the following principle:

Theorem A.6. *If every $\gamma \in \Gamma$ contains a $\gamma^* \in \Gamma^*$, then $\lambda(\Gamma) \geq \lambda(\Gamma^*)$.*

In practice, this principle is again used mainly to find a lower bound for extremal length. Below we shall consider a useful theorem for obtaining upper bounds. First we need to introduce some terminology. Suppose that D is a doubly connected domain. Then we can consider the extremal distance in D between the two components of the complement of D . This extremal distance is called the *modulus* of D . For instance, the complement of the segments $[-1, 0]$ and $[R, +\infty]$ in \mathbb{C} is a doubly connected domain which is called the *Teichmüller annulus*. Its modulus is denoted by $\Lambda(R)$. The Teichmüller annulus is of special interest because of the following theorem:

Theorem A.7 (Teichmüller). *Of all doubly connected regions that separate the pair $\{0, -1\}$ from a pair $\{w, \infty\}$ with $|w| = R$ the one with the greatest modulus is the complement of the segments $[-1, 0]$ and $[R, +\infty]$ (i.e. the Teichmüller annulus).*

Although we formulated Teichmüller's theorem as a theorem for doubly connected regions, symmetry in the real axis can be exploited in applications

to simply connected domains. For instance, it is clear from the symmetry of the Teichmüller domain that the extremal distance between the intervals $[-1, 0]$ and $[R, +\infty]$ in the upper half of the complex plane is $2\Lambda(R)$. The upper half-plane can be mapped onto a rectangle such that the intervals $[-1, 0]$ and $[R, +\infty]$ map onto opposite sides (see section A.6.1). By studying these conformal transformations one can prove the following lemma:

Lemma A.8. *The modulus $\Lambda(R)$ of the Teichmüller annulus satisfies $\Lambda(1) = 1/2$ and $\log(16R) \leq 2\pi\Lambda(R) \leq \log(16(R+1))$.*

For another application, suppose that γ_1 and γ_2 are two crosscuts of the half-plane such that γ_1 separates the origin from γ_2 , and γ_2 separates γ_1 from ∞ . Let z_1 be a point of γ_1 with maximal modulus, and let z_2 be a point of γ_2 with minimal modulus. We are interested in $d_{\mathbb{H}}(\gamma_1, \gamma_2)$. Let γ_1^* be the union of γ_1 and its reflection in the real axis, and likewise for γ_2^* . Then it is clear from symmetry that $d_{\mathbb{H}}(\gamma_1, \gamma_2) = 2d_{\mathbb{C}}(\gamma_1^*, \gamma_2^*)$ (see figure A.4).

Now observe that the region between γ_1^* and γ_2^* is a doubly connected region which separates the pair $\{0, z_1\}$ from $\{z_2, \infty\}$. Thus Teichmüller's theorem tells us that $d_{\mathbb{C}}(\gamma_1^*, \gamma_2^*) \leq \Lambda(|z_2|/|z_1|)$. Since $d_{\mathbb{H}}(\gamma_1, \gamma_2) = 2d_{\mathbb{C}}(\gamma_1^*, \gamma_2^*)$, this gives us an upper bound for $d_{\mathbb{H}}(\gamma_1, \gamma_2)$. Note how the symmetry is exploited to create a doubly connected domain from a simply connected domain, a technique that is fruitful in many circumstances.

A.3 Conformal maps of the unit disk

In section A.1 we have seen that the Riemann mapping theorem A.1 states that every simply connected domain $D \neq \mathbb{C}$ can be mapped conformally onto the unit disk. The conformal map of a domain D onto \mathbb{D} is unique up to composition with a conformal self-map of the unit disk. The following theorem characterises these self-maps:

Theorem A.9. *The conformal self-maps of the unit disk \mathbb{D} are precisely the transformations of the form*

$$f(z) = e^{i\varphi} \frac{z - a}{1 - \bar{a}z}; \quad |z| < 1, \quad (\text{A.5})$$

where a is complex, $|a| < 1$, and $0 \leq \varphi < 2\pi$.

Theorem A.9 shows that three real parameters are needed to determine a self-map of \mathbb{D} uniquely. It follows that any conformal transformation $f : D \rightarrow \mathbb{D}$ is determined uniquely if we specify three real parameters. For example, one

commonly specifies $f(z) = 0$ and $f'(z) > 0$ (that is, $f'(z)$ is real and positive) at some specific point $z \in D$, to make the map unique.

To see that this indeed determines f uniquely, observe first that f exists by theorems A.1 and A.9. Suppose that $g : D \rightarrow \mathbb{D}$ is another conformal map such that $g(z) = 0$ and $g'(z) > 0$. Then $f \circ g^{-1}$ is a conformal self-map of \mathbb{D} which fixes the origin and has positive real derivative in 0. But then $f \circ g^{-1}$ must be the identity by theorem A.9, which shows that $f = g$. Note that as a consequence, the number $1/f'(z)$ is determined uniquely. This number is called the *conformal radius* and is a measure for the inner radius of the domain D at z , as we shall see at the end of this section.

Using the Riemann mapping theorem, we can also study conformal maps between two simply connected domains $D, D' \neq \mathbb{C}$ in the complex plane. A conformal map of D onto D' is easily defined by composing the conformal map of D onto \mathbb{D} with the inverse of the map of D' onto \mathbb{D} . Again, the map is determined uniquely if we specify three real parameters. For example, if we fix two points $z \in D$, $w \in D'$, then there is a unique conformal map f of D onto D' with $f(z) = w$ and $f'(z) > 0$.

A class of conformal maps of special interest are the transformations of the unit disk into itself (the conformal maps g_t^{-1} of radial SLE for instance belong to this class). A useful lemma on these transformations is the Schwarz lemma:

Lemma A.10 (Schwarz lemma). *Suppose that $f(z)$ is analytic on \mathbb{D} , that $f(0) = 0$ and that $|f(z)| \leq 1$ for $|z| < 1$. Then for each $z \in \mathbb{D}$, $|f(z)| \leq |z|$ and hence, $|f'(0)| \leq 1$. Moreover, if additionally $|f(z_0)| = |z_0|$ for some $z_0 \neq 0$, then there is a real constant α such that $f(z) = e^{i\alpha}z$ and hence $|f'(0)| = 1$. Conversely, if $f(0) = 0$, $|f(z)| \leq 1$ for $|z| < 1$ and $|f'(0)| = 1$, then $f(z) = e^{i\alpha}z$ for some real constant α .*

We will now study two classes of conformal maps that are defined by standard normalisations. The first class is the class of one-to-one conformal maps f of \mathbb{D} (onto some other domain) that are normalised by $f(0) = 0$ and $f'(0) = 1$. The class of these maps is usually denoted by S , and each $f \in S$ has an expansion around $z = 0$ of the form

$$f(z) = z + a_2z^2 + a_3z^3 + \cdots + a_nz^n + \cdots \quad (\text{A.6})$$

The second class of conformal maps, denoted by Σ , is the collection of one-to-one maps F defined on $\{z : |z| > 1\}$ that have an expansion of the form

$$F(z) = z + \frac{b_1}{z} + \frac{b_2}{z^2} + \cdots + \frac{b_n}{z^n} + \cdots, \quad z \rightarrow \infty. \quad (\text{A.7})$$

We will give some inequalities for the expansion coefficients (a_n) and (b_n) , and study several useful consequences. For derivations the reader is referred to Ahlfors [2, chapter 5].

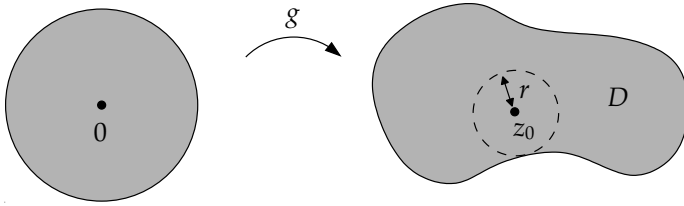


Figure A.5. The in-radius r of a domain D at z_0 , and the map g such that $g'(0)$ is the conformal radius at z_0 .

Theorem A.11 (Area theorem). *The coefficients in the expansion (A.7) of any function $F \in \Sigma$ satisfy $\sum_{n=1}^{\infty} n|b_n|^2 \leq 1$.*

For the class S , there is a famous conjecture of Bieberbach from 1916 on the expansion coefficients [19], which was finally proved by de Branges in 1985 [21] after many partial results. Most notably in the context of this thesis is that Löwner introduced his differential equation, which lies at the basis of SLE, to prove that $|a_3| \leq 3$ in 1923 [63]. His method was also a key to the final proof of the Bieberbach conjecture by de Branges.

Theorem A.12 (Bieberbach-de Branges theorem). *The coefficients in the expansion (A.6) of any function $f \in S$ satisfy $|a_n| \leq n$ for all $n \geq 2$.*

The following two theorems are consequences of the fact that $|a_2| \leq 2$. The first of these theorems provides estimates for $|f(z)|$ and $|f'(z)|$, and is known as the Koebe distortion theorem. The second theorem is the Koebe one-quarter theorem, which can be obtained directly from the distortion theorem. Indeed, if we take the limit $|z| \rightarrow 1$ in the left-most inequality of equation (A.8) below, we get the desired result. The one-quarter theorem is often used in conjunction with the Schwarz lemma to provide upper and lower bounds on a given quantity.

Theorem A.13 (Koebe distortion theorem). *The functions $f \in S$ satisfy*

$$\frac{|z|}{(1+|z|)^2} \leq |f(z)| \leq \frac{|z|}{(1-|z|)^2}; \quad \frac{1-|z|}{(1+|z|)^3} \leq |f'(z)| \leq \frac{1+|z|}{(1-|z|)^3}. \quad (\text{A.8})$$

Theorem A.14 (Koebe one-quarter theorem). *The image of the unit disk under a mapping $f \in S$ contains the disk with centre 0 and radius $1/4$.*

As an application, let us discuss the notion of conformal radius. Suppose that D is a simply connected domain and let $z_0 \in D$. Then the in-radius r of D at z_0 is defined by $r := \inf\{|z-z_0| : z \notin D\}$. It is the radius of the largest open disk with centre z_0 that fits inside D , see figure A.5. Now let g be the conformal map

of \mathbb{D} onto D such that $g(0) = z_0$ and $g'(0) > 0$. Then the unique number $g'(0)$ is called the *conformal radius* of D at z_0 . We will prove that this conformal radius is related to the in-radius by $r \leq g'(0) \leq 4r$, that is, the in-radius and conformal radius differ by at most a factor of 4.

To see this, observe that $g^{-1}(rz + z_0)$ is a map that satisfies the conditions of the Schwarz lemma A.10. It follows that $r(g^{-1})'(z_0) \leq 1$, hence $g'(0) \geq r$. On the other hand, the map $f(z) = (g(z) - z_0)/g'(0)$ is in S , and the Koebe one-quarter theorem says that $\inf\{|z| : z \notin f(\mathbb{D})\} \geq \frac{1}{4}$. From this it follows that $g'(0) \leq 4r$, and we are done. This example shows how properties such as expressed by the Schwarz lemma or the Koebe theorems can be applied to a given map g by a suitable renormalisation. Such techniques are beneficial in many circumstances to derive properties of a given conformal map g . Another example will be given in section A.4.

A.4 Conformal maps of the upper half-plane

In this section we study conformal maps of a domain D onto the complex upper half-plane \mathbb{H} . For a start, the transformation $f(w) = i(1 + w)/(1 - w)$ is a standard conformal map of the unit disk \mathbb{D} onto \mathbb{H} , which has the inverse $f^{-1}(z) = (z - i)/(z + i)$. It follows from the Riemann mapping theorem A.1 that any simply connected domain $D \neq \mathbb{C}$ can be mapped conformally onto \mathbb{H} . In complex analysis, one often does not distinguish between the half-plane and the unit disk, since one always has the freedom to map conformally from one of these spaces onto the other.

Conformal maps of simply connected domains onto the upper half-plane are unique up to composition with the conformal self-maps of the upper half-plane. The form of these maps is given by the following theorem:

Theorem A.15. *The conformal self-maps of the upper half-plane \mathbb{H} are precisely the Möbius transformations*

$$f(z) = \frac{az + b}{cz + d}; \quad \text{Im } z > 0, \quad (\text{A.9})$$

where a, b, c and d are real numbers satisfying $ad - bc > 0$.

These maps are especially effective for rearranging points on the boundary of a domain. In particular, theorem A.15 shows that the conformal self-map of \mathbb{H} which takes the points $x_1 < x_2 < x_3$ on the real line to $0, 1$ and ∞ , respectively, is unique. Furthermore, the only self-map which fixes the points $0, 1$ and ∞ is the identity. From this one can easily deduce that any conformal

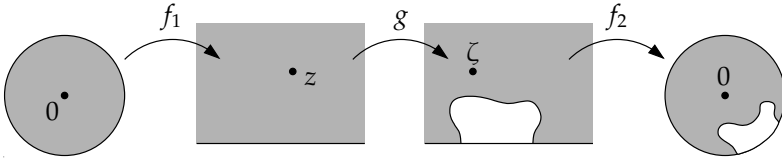


Figure A.6. Illustration of how compositions can be used to derive properties of a conformal map g .

map is determined uniquely if one specifies the images of three distinct points on the boundary (assuming that the map extends continuously to the boundary, see section A.1, theorems A.2 and A.3).

Most conformal transformations encountered in this thesis are of the form $f : D^+ \rightarrow \mathbb{H}$, where $D^+ = D \cap \mathbb{H}$ is the upper half of a domain D which is symmetric with respect to the real axis (see section A.5). To these transformations we can apply the following principle, which states that the map f extends to a conformal transformation on the domain D :

Theorem A.16 (Schwarz reflection principle). *Let D be a domain which is symmetric with respect to the real axis, and let $D^+ = D \cap \mathbb{H}$. Let $f(z)$ be an analytic function on D^+ such that $\text{Im}[f(z)] \rightarrow 0$ as $z \in D^+$ tends to \mathbb{R} . Then $f(z)$ extends to be analytic on D , and the extension satisfies $f(\bar{z}) = \overline{f(z)}$ for all $z \in D$.*

Another useful property of these conformal transformations can be obtained from the Schwarz lemma. To derive it, we will use our knowledge of how to map back and forth between the half-plane and the unit disk, and of the conformal self-maps of both spaces. This knowledge is extremely useful in deriving properties of a general conformal transformation. A standard procedure is to map these domains onto \mathbb{H} or \mathbb{D} , and then use a conformal self-map to rearrange the points in \mathbb{H} or \mathbb{D} appropriately, as we now illustrate.

Corollary A.17 (Schwarz lemma in \mathbb{H}). *Let g map \mathbb{H} into \mathbb{H} conformally. Then for all points $z = x + iy \in \mathbb{H}$,*

$$y |g'(z)| \leq \text{Im } g(z). \tag{A.10}$$

If g is not a conformal self-map of \mathbb{H} , then we have strict inequality.

Proof. The result follows by constructing a map of \mathbb{D} into \mathbb{D} satisfying the conditions of the Schwarz lemma A.10. First we map \mathbb{D} onto \mathbb{H} in such a way that 0 maps onto z , see figure A.6. To find this map, we compose the standard map of \mathbb{D} onto \mathbb{H} with an appropriate self-map of \mathbb{H} , which leads to

$$f_1(w) = x + i \frac{1+w}{1-w} y; \quad |w| < 1. \tag{A.11}$$

The map g then takes z to the image $\zeta := g(z) \in \mathbb{H}$. Next we apply a map of \mathbb{H} onto \mathbb{D} which takes ζ back to 0. To find such a map, we simply do a translation followed by a rescaling in the half-plane to move the point ζ to i , and then compose with the standard map of \mathbb{H} onto \mathbb{D} that takes i to 0. This gives the map

$$f_2(w) = \frac{w - \zeta}{w - \bar{\zeta}}; \quad w \in \mathbb{H}. \quad (\text{A.12})$$

Figure A.6 illustrates the construction.

Now we note that the composite map $f := f_2 \circ g \circ f_1$ is a map that satisfies the conditions of the Schwarz lemma. Indeed, f is analytic on the unit disk, it maps 0 to 0, and it maps the unit disk into the unit disk since g maps the half-plane into the half-plane. Hence by the Schwarz lemma,

$$|f'(0)| = |f_2'(\zeta)| |g'(z)| |f_1'(0)| \leq 1. \quad (\text{A.13})$$

Because $f_1'(0) = 2iy$ and $f_2'(\zeta) = 1/(\zeta - \bar{\zeta})$ we get

$$|f'(0)| = \frac{y}{\text{Im } \zeta} |g'(z)| \leq 1, \quad (\text{A.14})$$

which is what we wanted to prove.

Equality can only hold for a subclass of conformal self-maps of \mathbb{H} , namely for those maps that correspond to rotations of the unit disk, as should be clear from the Schwarz lemma A.10. Hence, if g is not a conformal self-map of \mathbb{H} , then we must certainly have strict inequality. ■

A.5 Hulls and capacity in the half-plane

Now let us introduce some notations that are used in SLE. We define a *hull* in the half-plane as a compact set $K \subset \overline{\mathbb{H}}$ such that $\mathbb{H} \setminus K$ is simply connected and $K = \overline{K} \cap \overline{\mathbb{H}}$ (this latter condition ensures that $K \cap \mathbb{R}$ does not stick out to the left or the right of $K \cap \mathbb{R}$). Simple examples of hulls in the upper half-plane are the straight line segment $[0, iR]$ and the closed half-disk $\{z \in \overline{\mathbb{H}} : |z| \leq R\}$.

Given a hull K , according to the Riemann mapping theorem there exists a conformal map $g_K : \mathbb{H} \setminus K \rightarrow \mathbb{H}$. To specify this map uniquely, we have to fix three real parameters. A convenient choice is to let g_K satisfy the so-called *hydrodynamic normalisation*

$$\lim_{z \rightarrow \infty} (g_K(z) - z) = 0. \quad (\text{A.15})$$

Then it is clear that the map g_K has an expansion for $z \rightarrow \infty$ of the form

$$g_K(z) = z + \frac{a_1}{z} + \frac{a_2}{z^2} + \dots \tag{A.16}$$

Since the map g_K maps $\mathbb{R} \setminus K$ into \mathbb{R} , the Schwarz reflection principle (theorem A.16) applies and the map extends to the complement in \mathbb{C} of

$$K^* = \{z : z \in K \text{ or } \bar{z} \in K\}. \tag{A.17}$$

On $\mathbb{C} \setminus K^*$, the map must satisfy $\overline{g_K(z)} = g_K(\bar{z})$, which shows that all coefficients in the expansion of g_K have to be real.

Note that the map g_K sends ∞ to ∞ and that its leading expansion coefficients for $z \rightarrow \infty$ are 1 and 0. This shows that we have indeed specified three real parameters. Two simple examples of maps g_K can be given for the hulls $[0, iR]$ and $\{z \in \mathbb{H} : |z| \leq R\}$. For the first hull the corresponding transformation is $\sqrt{z^2 + R^2}$, which has the expansion $z + R^2/2z + \dots$ for $z \rightarrow \infty$. For the second hull the normalised transformation is $z + R^2/z$. Observe that in both cases the expansion coefficient a_1 is proportional to the squared radius of the hull.

It turns out that in general, the coefficient a_1 is always bounded by the squared radius of the hull. To see this, let $R := \sup\{|z| : z \in K\}$ denote the radius of K measured from the origin. Then the map $g_K(Rz)/R$ is in the class Σ of section A.3. As a direct consequence of the Area theorem A.11, the coefficients $b_n = a_n/R^{n+1}$ in the expansion of this map for $z \rightarrow \infty$ satisfy $n|b_n|^2 \leq 1$ for all $n \geq 1$. Hence $|a_n| \leq R^{n+1}/\sqrt{n}$. A corollary of this result is that for $|z| \geq 2R$, $|g_K(z) - z| \leq R \sum_{n=1}^{\infty} 2^{-n} = R$. Thus we have:

Theorem A.18. *Let K be a hull and let $R := \sup\{|z| : z \in K\}$. Then the coefficients in the expansion (A.16) of g_K satisfy $|a_n| \leq R^{n+1}/\sqrt{n}$.*

Corollary A.19. *Let K be a hull and let $R := \sup\{|z| : z \in K\}$. Then for all $z \in \mathbb{H} \setminus K$ such that $|z| \geq 2R$, $|g_K(z) - z| \leq R$.*

The coefficient $a_1 = a_1(K)$ in the expansion (A.16) of g_K for $z \rightarrow \infty$, which depends only on K , is called the *half-plane capacity* of the hull K . We will denote this half-plane capacity henceforth by $\text{cap}_{\mathbb{H}}(K)$. The capacity $\text{cap}_{\mathbb{H}}(K)$ is clearly invariant under horizontal translations of the hull. Thus, if R is the radius of a half-disk centred on the real line that contains K , then $\text{cap}_{\mathbb{H}}(K) \leq R^2$ by theorem A.18. In the following paragraphs, three other important properties of half-plane capacity will be derived.

Positivity. The capacity of a nonempty hull K is a positive number, which we can prove as follows. Observe that the map $g = g_K^{-1}$ is a map of the half-plane \mathbb{H} into itself. Substituting $z = g_K(iy)$ (where y is assumed to be large) into

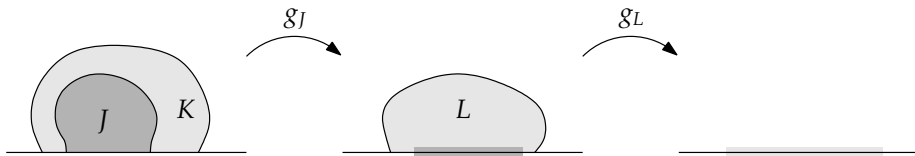


Figure A.7. Given two hulls $J \subset K$, $\text{cap}_{\mathbb{H}}(K)$ is the sum of $\text{cap}_{\mathbb{H}}(J)$ and $\text{cap}_{\mathbb{H}}(L)$, where L is the closure of the image of $K \setminus J$ under the map g_J .

corollary A.17 gives

$$\text{Im}[g_K(iy)] \left| \left(g_K^{-1} \right)'(g_K(iy)) \right| < y \quad \text{or} \quad y^2 - y \frac{\text{Im}[g_K(iy)]}{|g_K'(iy)|} > 0. \tag{A.18}$$

If one now uses the expansion of g_K for $z \rightarrow \infty$ and takes $y \rightarrow \infty$, the result $\text{cap}_{\mathbb{H}}(K) > 0$ follows immediately.

Scaling rule. Consider the hull rK where $r > 0$, and the conformal map g_{rK} that corresponds to this hull. It is obvious that another conformal map of $\mathbb{H} \setminus (rK)$ onto \mathbb{H} is given by $rg_K(z/r)$. Both maps satisfy the hydrodynamic normalisation, and since this determines the map uniquely, $g_{rK}(z) = rg_K(z/r)$. From the expansion for $z \rightarrow \infty$ we obtain the scaling relation

$$\text{cap}_{\mathbb{H}}(rK) = r^2 \text{cap}_{\mathbb{H}}(K). \tag{A.19}$$

Summation rule. The summation rule for half-plane capacities follows by considering two hulls J and K in the upper half-plane such that $J \subset K$. The corresponding conformal maps are g_J and g_K . We can define a third hull L by $L := g_J(K \setminus J)$, which has associated with it a conformal map g_L . The conformal maps are related by $g_K = g_L \circ g_J$ (see figure A.7) because both g_K and $g_L \circ g_J$ map $\mathbb{H} \setminus K$ onto \mathbb{H} and satisfy the hydrodynamic normalisation. Inserting the expansions for $z \rightarrow \infty$, we easily obtain

$$\text{cap}_{\mathbb{H}}(K) = \text{cap}_{\mathbb{H}}(J) + \text{cap}_{\mathbb{H}}(L). \tag{A.20}$$

Thus, if we have two hulls $J \subset K$, the half-plane capacity of K is the sum of the half-plane capacities of J and $L := g_J(K \setminus J)$.

To conclude this section we derive the Poisson integral representation of the map g_K for a given hull K . We assume that ∂K is a curve, so that the map g_K^{-1} extends continuously to $\overline{\mathbb{H}}$ by theorem A.2. We should note that in text-books the Poisson formula is often only discussed for the unit disk, while the half-plane case is left as an exercise (see for instance Ahlfors [1, sections 4.6.3 and 4.6.4] and Gamelin [39, section X.1]).

Theorem A.20 (Poisson formula). *Let K be a hull in the half-plane such that ∂K is a curve. Then*

$$z - g_K^{-1}(z) = \frac{1}{\pi} \int_{-\infty}^{\infty} \frac{\operatorname{Im} g_K^{-1}(x)}{z - x} dx; \quad z \in \mathbb{H}. \quad (\text{A.21})$$

Proof. Let $v(z) := \operatorname{Im}[g_K^{-1}(z) - z]$ for $z \in \overline{\mathbb{H}}$. Consider the *Poisson kernel* for the upper half-plane, defined by

$$C_t(s) := \frac{1}{\pi} \frac{t}{s^2 + t^2}; \quad s + it \in \mathbb{H}. \quad (\text{A.22})$$

It is easily verified that this kernel satisfies (i) $\int_{-\infty}^{\infty} C_t(s) ds = 1$ and (ii) for all $\delta > 0$, $\int_{|s| > \delta} C_t(s) ds \rightarrow 0$ as $t \rightarrow 0$. Now define the function \tilde{v} for $s + it \in \mathbb{H}$ by

$$\tilde{v}(s + it) := \int_{-\infty}^{\infty} C_t(s - x)v(x) dx = -\operatorname{Im} \frac{1}{\pi} \int_{-\infty}^{\infty} \frac{v(x)}{s + it - x} dx. \quad (\text{A.23})$$

From the boundedness of v (which follows from corollary A.19) and property (i) of the Poisson kernel it follows that \tilde{v} is a bounded harmonic function on \mathbb{H} . We will now show that $v = \tilde{v}$ on $\overline{\mathbb{H}}$.

To see this, note that by continuity of v on \mathbb{R} and properties (i) and (ii) of the Poisson kernel, $\tilde{v}(s + it) \rightarrow v(s)$ as $t \rightarrow 0$. Hence $\tilde{v} = v$ on \mathbb{R} . Now fix $\varepsilon > 0$. Since $g_K^{-1}(z) - z$ is bounded and tends to 0 as $z \rightarrow \infty$, there exists an $R > 0$ such that $|v(z)| < \varepsilon/2$ and $|\tilde{v}(z)| < \varepsilon/2$ for $|z| > R$. Hence $|\tilde{v}(z) - v(z)| < \varepsilon$ on $\{z : |z| > R\} \cup \mathbb{R}$. Since a bounded harmonic function attains its maximum on the boundary of a bounded domain (the Maximum Principle) and ε was arbitrary, it follows that $\tilde{v} = v$ on $\overline{\mathbb{H}}$. Thus,

$$\operatorname{Im}[z - g_K^{-1}(z)] = \operatorname{Im} \frac{1}{\pi} \int_{-\infty}^{\infty} \frac{\operatorname{Im} g_K^{-1}(x)}{z - x} dx; \quad z \in \mathbb{H}. \quad (\text{A.24})$$

The Cauchy-Riemann equations then imply that

$$\operatorname{Re}[z - g_K^{-1}(z)] = \operatorname{Re} \frac{1}{\pi} \int_{-\infty}^{\infty} \frac{\operatorname{Im} g_K^{-1}(x)}{z - x} dx + \text{constant}; \quad z \in \mathbb{H}. \quad (\text{A.25})$$

But since $g_K^{-1}(z) - z \rightarrow 0$ for $z \rightarrow \infty$, the constant must vanish. ■

This result has several important implications. For instance, upon replacing z by $g_K(z)$ in (A.21) we get

$$g_K(z) - z = \frac{1}{\pi} \int_{-\infty}^{\infty} \frac{\operatorname{Im} g_K^{-1}(x)}{g_K(z) - x} dx; \quad z \in \mathbb{H} \setminus K. \quad (\text{A.26})$$

When we now multiply both sides of (A.26) by z and send z to infinity we obtain the following expression for the half-plane capacity of K :

$$\text{cap}_{\mathbb{H}}(K) = \frac{1}{\pi} \int_{-\infty}^{\infty} \text{Im } g_K^{-1}(x) \, dx. \quad (\text{A.27})$$

Moreover, taking the derivative of equation (A.26) with respect to z tells us that

$$g'_K(z) = \left(1 + \frac{1}{\pi} \int_{-\infty}^{\infty} \frac{\text{Im } g_K^{-1}(x)}{(g_K(z) - x)^2} \, dx \right)^{-1}; \quad z \in \mathbb{H} \setminus K. \quad (\text{A.28})$$

In particular, for $x \in \mathbb{R} \setminus K$ (where g_K is well-defined by the Schwarz reflection principle, theorem A.16) we find that $0 \leq g'_K(x) \leq 1$.

A.6 The Schwarz-Christoffel formula

For any polygonal domain D bounded by finitely many straight line segments there exists a conformal map g of the upper half-plane onto D . The Schwarz-Christoffel formula is a differential equation for this map g . In fact, both equations (A.30) and (A.31) in theorem A.21 below are referred to as the Schwarz-Christoffel formula in the literature. As applications we will study mappings onto rectangles and triangles.

Theorem A.21 (Schwarz-Christoffel formula). *Suppose that D is a (bounded) polygon and g is a conformal map of the upper half-plane onto D . Let $a_1 < \dots < a_m$ be the points of \mathbb{R} that are mapped to vertices of D (it may be that additionally, ∞ is also mapped to a vertex of D). Let the interior angle of D at the vertex $w_j = g(a_j)$ be $\alpha_j\pi$, $1 \leq j \leq m$. Then*

$$\frac{g''(z)}{g'(z)} = \frac{\alpha_1 - 1}{z - a_1} + \dots + \frac{\alpha_m - 1}{z - a_m}, \quad (\text{A.29})$$

and there are constants A and B such that

$$g'(z) = A(z - a_1)^{\alpha_1 - 1} \dots (z - a_m)^{\alpha_m - 1}, \quad (\text{A.30})$$

$$g(z) = A \int_0^z (t - a_1)^{\alpha_1 - 1} \dots (t - a_m)^{\alpha_m - 1} \, dt + B. \quad (\text{A.31})$$

A.6.1 Conformal transformations onto rectangles

As a first application of the Schwarz-Christoffel formula we study maps onto rectangles. We know that for every given rectangle D there exists a unique conformal map of \mathbb{H} onto D which maps $[0, 1]$ and $[1, \infty)$ onto two given sides

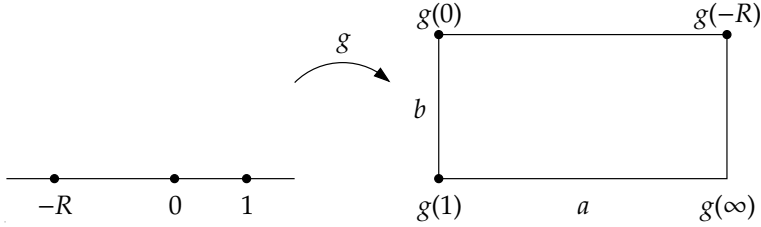


Figure A.8. Conformal transformation of the upper half-plane onto a rectangle.

of D . The other two sides of the rectangle will correspond to the intervals $(-\infty, -R]$ and $[-R, 0]$ of the real line, where $R > 0$ is a uniquely determined number. According to theorem A.21, the conformal transformation may be obtained by scaling, translation and rotation from the map

$$g(z) = \int_0^z \frac{dt}{\sqrt{t} \sqrt{t+R} \sqrt{t-1}}. \tag{A.32}$$

We now want to consider the map defined by this integral in more detail.

The image of \mathbb{H} under g can be found by studying the behaviour of the integral for real values of z . Observe that the argument of the integrand is $-\pi/2$ for $0 < t < 1$, 0 for $1 < t < \infty$, $-3\pi/2$ for $-\infty < t < -R$ and $-\pi$ for $-R < t < 0$. Hence, if we define $a = a(R)$ and $b = b(R)$ by

$$a = \int_1^\infty \frac{dt}{\sqrt{t} \sqrt{t+R} \sqrt{t-1}}; \quad b = \int_0^1 \frac{dt}{\sqrt{t} \sqrt{t+R} \sqrt{1-t}}. \tag{A.33}$$

then we see that the four corners of the rectangle $g(\mathbb{H})$ are $g(0) = 0$, $g(1) = -ib$, $g(\infty) = a - ib$ and $g(-R) = a$, see figure A.8.

It is clear from the above that there is a one-to-one correspondence between the aspect ratio a/b of the rectangle $g(\mathbb{H})$ and the number R . It will be useful to understand how the aspect ratio behaves as a function of R . For this, recall from section A.2 that a/b is equal to the extremal distance between the two vertical sides of $g(\mathbb{H})$ or, equivalently, to the extremal distance in \mathbb{H} between the intervals $[0, 1]$ and $(-\infty, -R]$. Also recall that this extremal distance is twice the modulus $\Lambda(R)$ of the Teichmüller annulus. The behaviour of the aspect ratio as a function of R is therefore estimated by the following equivalent formulation of lemma A.8:

Lemma A.22. *Let f be the conformal map of the rectangle $(0, a) \times (0, b)$ onto \mathbb{H} such that $f(ib) = 0$, $f(0) = 1$ and $f(a) = \infty$ and let $R := -f(a + ib)$. Then $R = 1$ if $a/b = 1$ and otherwise $\log(16R) \leq \pi a/b \leq \log(16(R + 1))$.*

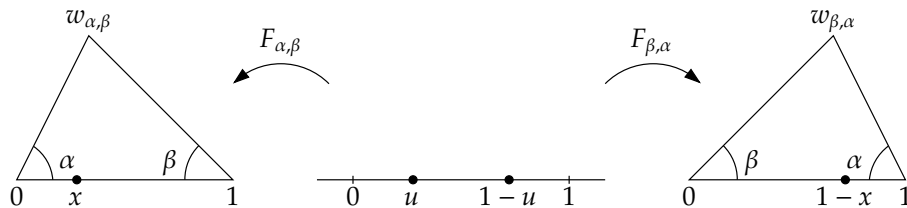


Figure A.9. Conformal transformations of the upper half-plane onto triangles.

A.6.2 Conformal transformations onto triangles

When we want to map the upper half-plane onto a triangle, the transformation can be uniquely determined by specifying the pre-images of the three corners. One convenient choice is to take the pre-images at 0, 1 and ∞ , and to normalise the triangle such that the conformal map fixes 0 and 1 and sends ∞ to the third corner of the triangle in the upper half-plane. To be precise, given two angles $\alpha, \beta \in (0, \pi)$ such that $\alpha + \beta < \pi$, we will denote by $T_{\alpha,\beta}$ the triangle which has a vertex at 0 with interior angle α , a vertex at 1 with interior angle β , and the third vertex, denoted by $w_{\alpha,\beta}$, in the upper half-plane.

Then there is a unique transformation $F_{\alpha,\beta}$ of the upper half-plane onto $T_{\alpha,\beta}$ such that $F_{\alpha,\beta}(0) = 0$, $F_{\alpha,\beta}(1) = 1$ and $F_{\alpha,\beta}(\infty) = w_{\alpha,\beta}$. According to the Schwarz-Christoffel formula, this transformation is given by the integral

$$F_{\alpha,\beta}(z) = \frac{\int_0^z t^{\alpha/\pi-1}(1-t)^{\beta/\pi-1} dt}{\int_0^1 t^{\alpha/\pi-1}(1-t)^{\beta/\pi-1} dt}. \tag{A.34}$$

This function is also known as the incomplete normalised beta-function with parameters α/π and β/π (see [27]), that is,

$$F_{\alpha,\beta}(z) = \frac{B_z(\alpha/\pi, \beta/\pi)}{B(\alpha/\pi, \beta/\pi)}. \tag{A.35}$$

From symmetry considerations it is easily seen that for real values of the argument these transformations satisfy

$$F_{\alpha,\beta}(u) = 1 - F_{\beta,\alpha}(1-u) \quad \text{and} \quad F_{\alpha,\beta}^{-1}(x) = 1 - F_{\beta,\alpha}^{-1}(1-x). \tag{A.36}$$

This is illustrated in figure A.9.

A different mapping onto the triangle $T_{\alpha,\beta}$ is obtained by choosing the pre-images of the three corners at $-1, 0$ and $+1$. As before, we may normalise the map to fix the points 0 and 1. The corresponding transformation according

to the Schwarz-Christoffel formula is then given by

$$G_{\alpha,\beta}(z) = \frac{\int_0^z t^{\alpha/\pi-1}(1-t)^{\beta/\pi-1}(1+t)^{-(\alpha+\beta)/\pi} dt}{\int_0^1 t^{\alpha/\pi-1}(1-t)^{\beta/\pi-1}(1+t)^{-(\alpha+\beta)/\pi} dt}. \quad (\text{A.37})$$

Observe that in this case the image of ∞ lies on the arc $1 \cup w_{\alpha,\beta}$ of $T_{\alpha,\beta}$. The mapping $G_{\alpha,\beta}$ does not introduce a corner here.

It can be useful for applications to extend the notation introduced above to the case where the angles $\alpha, \beta \in (0, \pi)$ satisfy $\alpha + \beta \geq \pi$. In that case we define $T_{\alpha,\beta}$ as the unbounded polygon in \mathbb{H} with a vertex at 0 with interior angle α , a vertex at 1 with interior angle β and a vertex $w_{\alpha,\beta} = \infty$. Then the transformation $F_{\alpha,\beta}$ defined by equation (A.34) is again the unique conformal transformation of \mathbb{H} onto $T_{\alpha,\beta}$ that fixes 0 and 1 and sends ∞ to $w_{\alpha,\beta}$. This transformation satisfies the symmetry property (A.36). Likewise, the transformation $G_{\alpha,\beta}$ defined by equation (A.37) is the unique conformal transformation of \mathbb{H} onto $T_{\alpha,\beta}$ that fixes 0 and 1 and sends -1 to $w_{\alpha,\beta}$.

For isosceles triangles, that is, if $\beta = \alpha$, we may simplify the notation by dropping the subscript β . We will then simply write $T_\alpha := T_{\alpha,\alpha}$, $w_\alpha := w_{\alpha,\alpha}$, $F_\alpha := F_{\alpha,\alpha}$ and $G_\alpha := G_{\alpha,\alpha}$ for the triangular domain, its vertex in the upper half-plane and the corresponding conformal transformations, respectively.

B Stochastic processes and Itô calculus

Summary

This appendix collects results on stochastic processes, martingales and stochastic calculus. First we review the measure-theoretic foundations of probability, following [3]. Then stochastic processes and martingales are introduced, with Brownian motion as the most important example. Finally, we define the Itô integral with respect to Brownian motion and consider Itô's change-of-variable formula. This part of the appendix is based on [46]. Excellent introductions to the covered material are for instance [40, 42]. An alternative standard reference on continuous martingales and Brownian motion is [75].

B.1 Probability spaces and random variables

Suppose that we perform a random experiment. Then all possible outcomes of this experiment together constitute a set Ω , which we call the *sample space*. In probability theory we are typically interested in the probability that the actual outcome of our experiment is in some given subset A of Ω , called an *event*. We denote the collection of all such events by \mathcal{F} . This collection \mathcal{F} should satisfy certain conditions. For instance, complements, intersections and unions of events should also be events.

To be precise, we require \mathcal{F} to be a σ -field over the sample space Ω . This means that \mathcal{F} is a collection of subsets of Ω satisfying the conditions

1. $\emptyset \in \mathcal{F}$;
2. if $A \in \mathcal{F}$ then $\Omega \setminus A \in \mathcal{F}$;
3. if $A_1, A_2, \dots \in \mathcal{F}$ then $\bigcup_{i=1}^{\infty} A_i \in \mathcal{F}$.

If $\mathcal{G} \subset \mathcal{F}$ is another σ -field over Ω , then \mathcal{G} is called a *sub- σ -field* of \mathcal{F} . The combination (Ω, \mathcal{F}) of a set Ω and a σ -field \mathcal{F} over Ω is called a *measurable space*.

So we have now associated with our random experiment a measurable space consisting of the sample space Ω and a collection of events \mathcal{F} . To enable us to talk about probabilities we introduce a *probability measure* \mathbf{P} on the space (Ω, \mathcal{F}) . This is a function assigning a number in the range $[0, 1]$ to every element of the σ -field \mathcal{F} . It has to satisfy the conditions

1. $\mathbf{P}[\emptyset] = 0, \mathbf{P}[\Omega] = 1$;
2. if $A_1, A_2, \dots \in \mathcal{F}$ are disjoint, then $\mathbf{P}[\bigcup_{i=1}^{\infty} A_i] = \sum_{i=1}^{\infty} \mathbf{P}[A_i]$.

The triple $(\Omega, \mathcal{F}, \mathbf{P})$ is called a *probability space*. An event whose probability is zero is called a *null event*, events which occur with probability one are said to occur *almost surely* (abbreviated *a.s.*).

At this point we would like to make the following technical remark. For a reader with no prior knowledge of measure theory it might not be clear why we introduced the σ -field \mathcal{F} : why do we not just define our probability measure on the collection of all subsets of Ω ? The point is that in general, not every choice of σ -field over a given space Ω admits the definition of an appropriate measure. We therefore have to restrict ourselves to a smaller collection of events to get a consistent theory.

For example, it is impossible to define a measure on the collection of all subsets of \mathbb{R} which assigns to each interval (a, b) the length $b - a$ (exercise 6 in section 1.4 of [3]). However, such a measure (called *Lebesgue measure*) can be defined on the smallest σ -field over \mathbb{R} containing all open intervals $(a, b) \subset \mathbb{R}$. This collection of sets is called the *Borel σ -field* over \mathbb{R} and is denoted by $\mathcal{B} = \mathcal{B}(\mathbb{R})$. Its elements are called the *Borel sets* of Ω . More generally, for any metric space Ω one can define the Borel σ -field $\mathcal{B}(\Omega)$ over Ω as the smallest σ -field containing all open subsets of Ω .

In many practical situations the collection of Borel sets is the natural σ -field to work with. Suppose for instance that our experiment consists in drawing a random number which is uniformly distributed in the interval $[0, 1]$. Then we will typically be interested only in the probability that the random number lies in some subinterval of $[0, 1]$, or in a union of such intervals, and so on. To model the experiment we can therefore use as our probability measure the Lebesgue measure restricted to the Borel subsets of $[0, 1]$.

Now that we have captured the description of a random experiment in terms of a probability space, we can introduce random variables. A *random variable* X on a given probability space $(\Omega, \mathcal{F}, \mathbf{P})$ is defined as a mapping $X : (\Omega, \mathcal{F}) \rightarrow (\mathbb{R}, \mathcal{B})$. What we mean by this notation is that X is a function assigning a real number to every element of Ω , which has the additional property that it is *measurable* with respect to \mathcal{F} : for every Borel set B , the set $\{\omega : X(\omega) \in B\}$ must be an element of \mathcal{F} . This measurability ensures that the probability of all events involving X is determined.

Indeed, it should be clear that if X is measurable, then it induces a probability measure $\mathbf{P}_X = \mathbf{P} \circ X^{-1}$ on the space $(\mathbb{R}, \mathcal{B})$ turning it into a probability space. The measure \mathbf{P}_X is called the *law of X* . More explicitly, $\mathbf{P}_X(B) = \mathbf{P}[X \in B]$ for every $B \in \mathcal{B}$, where $\mathbf{P}[X \in B]$ is the natural shorthand notation for $\mathbf{P}[\{\omega : X(\omega) \in B\}]$ (we will continue to use such shorthand notation from now on). Concepts involving the random variable X can be defined both on the probability space $(\Omega, \mathcal{F}, \mathbf{P})$ and on $(\mathbb{R}, \mathcal{B}, \mathbf{P}_X)$. For example, the distribution

function of X is defined by

$$F_X(x) := \mathbf{P}[X \leq x] = \mathbf{P}_X \left[(-\infty, x] \right] \quad (\text{B.1})$$

and its expected value is defined by

$$\mathbf{E}[X] := \int_{\Omega} X(\omega) d\mathbf{P}(\omega) = \int_{\mathbb{R}} x d\mathbf{P}_X(x). \quad (\text{B.2})$$

The reader is reminded that these integrals are Lebesgue (not Riemann) integrals with respect to the measures \mathbf{P} and \mathbf{P}_X , respectively.

An important example of a random variable is the *indicator* (or *indicator function*) 1_A of an event $A \in \mathcal{F}$. This is the random variable defined by setting

$$1_A(\omega) := \begin{cases} 1 & \text{if } \omega \in A; \\ 0 & \text{if } \omega \notin A. \end{cases} \quad (\text{B.3})$$

The state space for this random variable is $\Omega' = \{0, 1\}$, and the σ -field \mathcal{F}' consists of all subsets of Ω' . The indicator of A indicates whether the outcome of our random experiment is in A .

The concept of a random variable can be generalised to that of a *random object* (or *abstract random variable*). A random object X on a given probability space $(\Omega, \mathcal{F}, \mathbf{P})$ is a function $X : (\Omega, \mathcal{F}) \rightarrow (\Omega', \mathcal{F}')$, where Ω' is the *state space* of the object, and \mathcal{F}' is an appropriate σ -field over Ω' . Measurability in this case ensures that $\{X \in B\} \in \mathcal{F}$ for every $B \in \mathcal{F}'$, and guarantees that X induces a probability measure $\mathbf{P}_X = \mathbf{P} \circ X^{-1}$ (the *law of X*) on \mathcal{F}' .

Now let us consider the collection of sets $\{\{X \in B\} : B \in \mathcal{F}'\}$ in more detail. It is easy to show that this collection of sets is a σ -field. We call it the σ -field *generated by* the random object X , and denote it by $\sigma(X)$. Loosely speaking, it is the smallest sub- σ -field of \mathcal{F} containing all information about X . An important property of this σ -field, that may help elucidate its meaning, is the following. Suppose that Z is a random variable on $(\Omega, \mathcal{F}, \mathbf{P})$ which is measurable with respect to $\sigma(X)$. Then Z is a *function* of X , that is, there exists some $f : (\Omega', \mathcal{F}') \rightarrow (\mathbb{R}, \mathcal{B})$ such that $Z(\omega) = f \circ X(\omega)$. Conversely, for every such function f the random variable $Z = f \circ X$ is measurable with respect to $\sigma(X)$.

Suppose now that instead of a single random object, we are given a collection $\{X_i : i \in I\}$ of random objects, where I is an arbitrary index set and $X_i : (\Omega, \mathcal{F}) \rightarrow (\Omega_i, \mathcal{F}_i)$. Then we define $\sigma(X_i : i \in I)$ as the smallest sub- σ -field of \mathcal{F} containing all events of the form $\{X_i \in B_i\}$ with $i \in I$ and $B_i \in \mathcal{F}_i$. This set is called the σ -field *generated by* the random objects $\{X_i : i \in I\}$. Again we have that every random variable which is measurable with respect to $\sigma(X_i : i \in I)$ is a function(al) of these random objects and conversely, that every function(al) of these random variables is measurable with respect to $\sigma(X_i : i \in I)$.

B.2 Conditional probability and expectation

In this section we review the general notions of conditional probability and conditional expectation on a given probability space $(\Omega, \mathcal{F}, \mathbf{P})$. For the presentation we follow Ash and Doléans-Dade [3]. To get us started, consider the conditional probability of an event B given that the random object X takes the value x . We would like this conditional probability to behave like the function $g_B(x)$ in the following (Radon-Nikodým) theorem:

Theorem B.1. *Let $X : (\Omega, \mathcal{F}) \rightarrow (\Omega', \mathcal{F}')$ be a random object and let $B \in \mathcal{F}$. Then there exists a function $g_B : (\Omega', \mathcal{F}') \rightarrow (\mathbb{R}, \mathcal{B})$ such that*

$$\mathbf{P}[\{X \in A'\} \cap B] = \int_{A'} g_B(x) d\mathbf{P}_X(x) \quad \text{for all } A' \in \mathcal{F}'. \quad (\text{B.4})$$

Furthermore, if h_B is another such function, then $g_B = h_B$ a.e.

Here the qualification a.e. stands for “almost everywhere”. This means that there is a set $N \in \mathcal{F}'$ with $\mathbf{P}_X[N] = 0$ such that $g_B = h_B$ on $\Omega' \setminus N$. We remark that in probability theory we can expect many equalities to hold only “almost everywhere”. It is therefore common practice not to mention the qualification a.e. explicitly. Here we will take care to write a.e. explicitly only for the duration of this section. Returning to theorem B.1, we see that the function g_B is uniquely defined on the non-null events. We define the conditional probability of the event B given $\{X = x\}$, written $\mathbf{P}[B | X = x]$, as $g_B(x)$.

For simple cases, The conditional probability defined in this way reduces to the definition we would give intuitively. For example, suppose that A is an event having positive probability. Then we can take $X = 1_A$ in the definition and write $\mathbf{P}[B | A] = \mathbf{P}[B | X = 1]$. The reader may verify that according to theorem B.1,

$$\mathbf{P}[B | A] = \frac{\mathbf{P}[B \cap A]}{\mathbf{P}[A]} \quad \text{a.e.} \quad (\text{B.5})$$

as we expect. But whereas the intuitive definition becomes problematic when $\mathbf{P}[A] = 0$, theorem B.1 implies that it is in fact possible to extend the definition to cover this case. Moreover, theorem B.1 shows that we can define $\mathbf{P}[B | X = x]$ for an arbitrary random object X even when $\{X = x\}$ has probability zero for some, and possibly all, x .

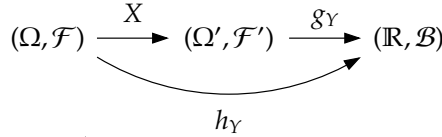
Having dealt with the conditional probability given $\{X = x\}$, we now look at conditional *expectation* given $\{X = x\}$. For a given random variable Y we define $\mathbf{E}[Y | X = x]$ as the essentially unique function $g_Y(x)$ in the (Radon-Nikodým) theorem B.2 below. It can be shown that again this definition corresponds with our intuition in simple cases. By taking $Y = 1_B$ it is also easily verified that the definition gives $\mathbf{E}[1_B | X = x] = \mathbf{P}[B | X = x]$ almost everywhere.

Theorem B.2. Let Y be a random variable and $X : (\Omega, \mathcal{F}) \rightarrow (\Omega', \mathcal{F}')$ a random object. If $\mathbf{E}[Y]$ exists, then there is a function $g_Y : (\Omega', \mathcal{F}') \rightarrow (\mathbb{R}, \mathcal{B})$ such that

$$\int_{\{X \in A'\}} Y(\omega) \, d\mathbf{P}(\omega) = \int_{A'} g_Y(x) \, d\mathbf{P}_X(x) \quad \text{for all } A' \in \mathcal{F}'. \tag{B.6}$$

Furthermore, if h_Y is another such function, then $g_Y = h_Y$ a.e.

We now make the generalisation to conditional expectation given a σ -field. As a motivation for our approach, observe that the conditional expectation given by g_Y in theorem B.2 is defined on the space (Ω', \mathcal{F}') . We may, however, turn this into a random variable h_Y on the space (Ω, \mathcal{F}) by setting $h_Y := g_Y \circ X$:



Then $h_Y(\omega)$ is the conditional expectation of Y given that X takes the value $x = X(\omega)$. In particular, one can prove that

$$\int_C Y(\omega) \, d\mathbf{P}(\omega) = \int_C h_Y(\omega) \, d\mathbf{P}(\omega) \quad \text{for all } C \in \sigma(X). \tag{B.7}$$

The random variable h_Y is a special instance of a conditional expectation given a σ -field, namely $h_Y = \mathbf{E}[Y \mid \sigma(X)]$ which we usually write as $h_Y = \mathbf{E}[Y \mid X]$. The general case is given by the following (Radon-Nikodým) theorem:

Theorem B.3. Suppose that \mathcal{G} is some general sub- σ -field of \mathcal{F} . Let Y be a random variable such that $\mathbf{E}[Y]$ exists. Then there is a function $\mathbf{E}[Y \mid \mathcal{G}] : (\Omega, \mathcal{G}) \rightarrow (\mathbb{R}, \mathcal{B})$, called the conditional expectation of Y given \mathcal{G} , such that

$$\int_C Y(\omega) \, d\mathbf{P}(\omega) = \int_C \mathbf{E}[Y \mid \mathcal{G}](\omega) \, d\mathbf{P}(\omega) \quad \text{for all } C \in \mathcal{G}. \tag{B.8}$$

Moreover, any two such functions must coincide almost everywhere.

We emphasise that we cannot just take $\mathbf{E}[Y \mid \mathcal{G}] = Y$ in theorem B.3, because $\mathbf{E}[Y \mid \mathcal{G}]$ is required to be measurable with respect to \mathcal{G} , while Y is only required to be measurable with respect to the larger σ -field \mathcal{F} . In particular, if \mathcal{G} is the σ -field generated by a collection of random variables, then $\mathbf{E}[Y \mid \mathcal{G}]$ must be a function(al) of these variables. We also emphasise that $\mathbf{E}[Y \mid \mathcal{G}]$ is itself a random variable. By taking $Y = 1_B$ in $\mathbf{E}[Y \mid \mathcal{G}]$ we obtain the conditional probability of the event B given \mathcal{G} , that is, $\mathbf{P}[B \mid \mathcal{G}] = \mathbf{E}[1_B \mid \mathcal{G}]$.

Some useful properties of conditional expectation given a σ -field are stated in theorem B.4 below. To appreciate the results, it may help the reader to think of the σ -fields \mathcal{G} and \mathcal{H} as the σ -fields generated by collections $\{X_i : i \in I\}$ and $\{X_i : i \in J\}$ of random variables, respectively, where $I \subseteq J$, and of the random variable Z as a function(al) of the variables $\{X_i : i \in I\}$.

Theorem B.4. Let X, Y and Z be random variables such that $\mathbf{E}[X], \mathbf{E}[Y], \mathbf{E}[Z]$ and $\mathbf{E}[YZ]$ exist. Let \mathcal{G} and \mathcal{H} be sub- σ -fields of \mathcal{F} such that $\mathcal{G} \subseteq \mathcal{H}$, and assume that Z is measurable with respect to \mathcal{G} . Then

1. $\mathbf{E}[X | \mathcal{G}] \geq 0$ if $X \geq 0$;
2. $\mathbf{E}[aX + bY | \mathcal{G}] = a \mathbf{E}[X | \mathcal{G}] + b \mathbf{E}[Y | \mathcal{G}]$;
3. $\mathbf{E}[\mathbf{E}[Y | \mathcal{G}]] = \mathbf{E}[Y]$;
4. $\mathbf{E}[\mathbf{E}[Y | \mathcal{H}] | \mathcal{G}] = \mathbf{E}[\mathbf{E}[Y | \mathcal{G}] | \mathcal{H}] = \mathbf{E}[Y | \mathcal{G}]$;
5. $\mathbf{E}[ZY | \mathcal{G}] = Z \mathbf{E}[Y | \mathcal{G}]$.

B.3 Stochastic processes and stopping times

A *stochastic process* is a collection $X = \{X(t) : 0 \leq t < \infty\}$ of random objects $X(t) : (\Omega, \mathcal{F}) \rightarrow (S, \mathcal{S})$ on an underlying probability space $(\Omega, \mathcal{F}, \mathbf{P})$. Note that the role of Ω is hidden in this notation; we will write $X(t, \omega)$ for the value of $X(t)$ in the realisation ω when we want to emphasise the role of Ω . Each of the random objects $X(t)$ has the same state space (S, \mathcal{S}) , that we refer to as the state space of the process. Here we will be interested only in real-valued or complex-valued stochastic processes, so that we can take $S = \mathbb{R}$ or $S = \mathbb{C}$ equipped with the Borel σ -field. The index t of the process X has a convenient interpretation as *time*. For fixed $\omega \in \Omega$, the collection $\{X(t, \omega) : t \geq 0\}$ is a *sample path* describing one of the possible trajectories of the process through time.

We say that a stochastic process is *continuous* if its sample paths are continuous in time. A real-valued continuous stochastic process X can be regarded as a random object on $(\Omega, \mathcal{F}, \mathbf{P})$ taking values in the collection $C[0, \infty)$ of continuous real-valued functions on $[0, \infty)$. With a suitable metric on these functions, for example (as in [46, section 2.4]) the metric

$$\rho(\omega_1, \omega_2) := \sum_{n=1}^{\infty} \frac{1}{2^n} \max_{0 \leq t \leq n} (|\omega_1(t) - \omega_2(t)| \wedge 1), \quad (\text{B.9})$$

we can associate with $C[0, \infty)$ the collection of Borel sets $\mathcal{B}(C[0, \infty))$, and we have $X : (\Omega, \mathcal{F}) \rightarrow (C[0, \infty), \mathcal{B}(C[0, \infty)))$. The random object X then induces a probability measure $\mathbf{P}_X = \mathbf{P} \circ X^{-1}$ on the space of continuous functions, called the *law of the process* X . The law of a complex continuous process is defined analogously.

If we have a stochastic process X , then each of the random variables $X(t)$ has to be measurable with respect to the σ -field of the underlying sample space. But in many practical situations, we really want the variable $X(t)$ to depend only on the information we have about the process up to time t and not on the future. For this reason we introduce the notion of a *filtration*. A

filtration $\{\mathcal{F}_t\}$ is a family $\{\mathcal{F}_t : t \geq 0\}$ of σ -fields such that $\mathcal{F}_s \subseteq \mathcal{F}_t \subseteq \mathcal{F}$ for every $s < t$. We set $\mathcal{F}_\infty = \sigma(\cup_{t \geq 0} \mathcal{F}_t)$, the smallest σ -field containing all the \mathcal{F}_t . We say that the process X is *adapted* to the filtration $\{\mathcal{F}_t\}$ if $X(t)$ is measurable with respect to \mathcal{F}_t for every $t \geq 0$. We may then think of \mathcal{F}_t as representing all the information available about the process X up to time t .

For every process X there is a natural filtration to which the process is adapted, namely the filtration $\{\mathcal{F}_t^X\}$ where $\mathcal{F}_t^X := \sigma(X(s) : 0 \leq s \leq t)$. We call $\{\mathcal{F}_t^X\}$ the filtration *generated* by the process X . Its composite σ -fields are the smallest σ -fields with respect to which each of the variables $X(s)$ up to a certain time t are measurable. In practice one often works instead with a filtration whose σ -fields are larger. In particular, one commonly assumes that the filtration $\{\mathcal{F}_t\}$ satisfies the following *usual conditions*:

1. Each \mathcal{F}_t contains all null events;
2. $\{\mathcal{F}_t\}$ is *right-continuous*: $\mathcal{F}_t = \mathcal{F}_{t+}$ where $\mathcal{F}_{t+} := \cap_{\varepsilon > 0} \mathcal{F}_{t+\varepsilon}$.

The first condition says that we can know beforehand all the things that are *not* going to happen to our process. The second condition says that at time t we cannot learn anything new about the process by peaking infinitesimally far into the future.

Often we will be interested in the value of a stochastic process at a random time T which is determined by the sample path of the process X up to the present, but does not depend on the future. To this aim we introduce the notion of *stopping time*. We assume that our probability space is equipped with a filtration $\{\mathcal{F}_t\}$. Then a stopping time is a random variable T taking values in $[0, \infty]$ such that the event $\{T \leq t\}$ is an element of \mathcal{F}_t for every $t \geq 0$. In words, T is a stopping time if we can decide on the basis of the information about our process up to time t whether the stopping time occurs before or at time t . We write $X(T)$ for the state of our random process X at the stopping time, that is, $X(T, \omega) := X(T(\omega), \omega)$.

An important example of a random time is the first time when the process X hits some subset $A \in \mathcal{S}$ of the state space. More precisely, if we define $T_A := \inf\{t \geq 0 : X(t) \in A\}$, then T_A is called the *hitting time* of the set A . We will mainly be interested in continuous real-valued or complex-valued processes, for which one can show that $\{T_A \leq t\}$ is in \mathcal{F}_t for all $t \geq 0$ if A is closed. The hitting time T_A is then also a stopping time for the filtration $\{\mathcal{F}_t\}$.

We now turn to the class of *Markov processes*. A Markov process X is a stochastic process satisfying the *Markov property*:

$$\mathbf{P}[X(t) \in B \mid X(t_1) = x_1, \dots, X(t_n) = x_n] = \mathbf{P}[X(t) \in B \mid X(t_n) = x_n] \quad (\text{B.10})$$

for all $B \in \mathcal{S}$, all possible states x_1, \dots, x_n and any given sequence of times $0 \leq t_1 < \dots < t_n < t$. More formally, if the process X is adapted to the

filtration $\{\mathcal{F}_t\}$, then the Markov condition is equivalent to the statement that for all $0 \leq s < t$,

$$\mathbf{P}[X(t) \in B \mid \mathcal{F}_s] = \mathbf{P}[X(t) \in B \mid X(s)]. \quad (\text{B.11})$$

In words, the Markov property states that conditioned on the present value of the process, the future is independent of the past.

If in addition $\mathbf{P}[X(t) \in B \mid X(s)]$ depends on time only through the increment $t - s$ and not through the particular value of s , the Markov process is called *time-homogeneous*. For a time-homogeneous process, let us write P_{t-s} for the transition function such that

$$\mathbf{P}[X(t) \in B \mid \mathcal{F}_s] = P_{t-s}(X(s), B). \quad (\text{B.12})$$

Then for each $t > 0$, P_t is a *Markov kernel*, that is, a function $P_t : S \times S \rightarrow [0, 1]$ such that (1) for each fixed $x \in S$, $P_t(x, \cdot)$ is a probability measure on S , and (2) for each fixed $B \in \mathcal{S}$, $P_t(\cdot, B)$ is \mathcal{S} -measurable (see [75, chapter 3]). Furthermore, for any $s, t > 0$ we have by the Markov property

$$P_{s+t}(x, B) = \int P_s(x, dy) P_t(y, B). \quad (\text{B.13})$$

This is the *Chapman-Kolmogorov equation*, which may be written more compactly as $P_{s+t} = P_s P_t$. Thus the collection of Markov kernels forms a semigroup, commonly referred to as *the semigroup of X*.

Suppose now that X is a time-homogeneous Markov process and that T is a stopping time for this process. Then X is said to have the *strong Markov property* if, conditioned on $X(T)$, the process after time T is again a Markov process which is independent from the events prior to T , and if this post- T process has the same transition probabilities as X . That is, X is a strong Markov process if

$$\mathbf{P}[X(T+t) \in B \mid \mathcal{F}_T] = P_t(X(T), B) \quad (\text{B.14})$$

for all stopping times T and all $t \geq 0$, $B \in \mathcal{S}$. Here, \mathcal{F}_T is the σ -field of all events that are *prior* to T . These are the events $A \in \mathcal{F}$ such that $A \cap \{T \leq t\} \in \mathcal{F}_t$ for all $t \geq 0$ (the reader may check that for $T = t$ fixed, \mathcal{F}_T is just \mathcal{F}_t).

B.4 Martingales and optional sampling

An important class of real or complex stochastic processes is the class of martingales. These are “fair” or “unbiased” processes in the sense that, conditioned

on all information about the process up to the present time, the expected value of the process at any time in the future is equal to its present value. Another way of expressing this is to say that martingales are processes without “drift”. We will return to this point of view in section B.6. In this section we collect some important results on martingales. We start by giving a precise definition.

Definition B.5 (Martingale). Let $X = \{X(t) : t \geq 0\}$ be a real or complex stochastic process adapted to a filtration $\{\mathcal{F}_t\}$ and such that $\mathbf{E}|X(t)| < \infty$ for every $t \geq 0$. Then X is said to be a martingale if $\mathbf{E}[X(t) | \mathcal{F}_s] = X(s)$ a.s. for every $0 \leq s < t < \infty$.

The definition shows that a martingale is indeed a fair process: if $X(t)$ represents the fortune at time t of a gambler playing a fair game, then his expected fortune at a fixed time in the future is the same as his current fortune. But what if the gambler is allowed to stop playing at a *random* time? In particular, assuming that the gambler cannot look into the future, can he expect to increase his fortune by choosing a favourable stopping time? It is the purport of Doob’s *optional sampling theorem* B.7 to state precisely under what conditions the answer to this question is negative. This involves the notion of a *last element* of a martingale X , which we introduce first.

Let X be a martingale with respect to the filtration $\{\mathcal{F}_t\}$. Suppose that there exists an integrable, \mathcal{F}_∞ -measurable random variable $X(\infty)$ such that $\mathbf{E}[X(\infty) | \mathcal{F}_t] = X(t)$ for all $0 \leq t < \infty$ (here we recall that $\mathcal{F}_\infty = \sigma(\cup_{t \geq 0} \mathcal{F}_t)$). Then we say that the process $\{X(t) : 0 \leq t \leq \infty\}$ is a martingale with last element $X(\infty)$. We can now state a condition for a martingale to have a last element, and then we formulate Doob’s optional sampling theorem.

Theorem B.6 (Martingale convergence theorem). Let X be a right-continuous martingale adapted to the filtration $\{\mathcal{F}_t\}$. Assume that $C := \sup_{t \geq 0} \mathbf{E}|X(t)| < \infty$. Then $X(\infty, \omega) := \lim_{t \rightarrow \infty} X(t, \omega)$ exists for almost every $\omega \in \Omega$ and $\mathbf{E}|X(\infty)| < \infty$. Moreover, if $\sup_{t \geq 0} \mathbf{E}|X(t)|^p < \infty$ for some $p > 1$, then $\{X(t) : 0 \leq t \leq \infty\}$ is a martingale with last element $X(\infty)$.

Theorem B.7 (Optional sampling theorem). Let X be a martingale with right-continuous sample paths and last element $X(\infty)$ adapted to the filtration $\{\mathcal{F}_t\}$. Let $S \leq T$ be two stopping times of $\{\mathcal{F}_t\}$. Then

$$\mathbf{E}[X(T) | \mathcal{F}_S] = X(S) \quad \text{a.s.} \tag{B.15}$$

In particular, $\mathbf{E}[X(T)] = \mathbf{E}[X(0)]$.

We have seen that a martingale is a process whose expected value does not change in time. For more generality, we may also consider processes whose current value is smaller or larger than the expected value in the future. Such processes are called *submartingales* and *supermartingales*, respectively. To be precise, a submartingale is a real process X adapted to a filtration $\{\mathcal{F}_t\}$ such that

$\mathbf{E}[X(t)] < \infty$ for every $t \geq 0$ and $\mathbf{E}[X(t) \mid \mathcal{F}_s] \geq X(s)$ for every $0 \leq s < t < \infty$. If $\mathbf{E}[X(t) \mid \mathcal{F}_s] \leq X(s)$ instead, then the process is called a supermartingale.

It turns out that every continuous, nonnegative submartingale can actually be written as the sum of a martingale and an increasing process. Here, by an *increasing process* we mean a process A adapted to $\{\mathcal{F}_t\}$ such that for almost every $\omega \in \Omega$, $A(0, \omega) = 0$ and $t \mapsto A(t, \omega)$ is a nondecreasing, right-continuous function. Moreover, we require that $\mathbf{E}[A(t)] < \infty$ for every $t \geq 0$.

Theorem B.8 (Doob-Meyer decomposition). *Suppose that X is a continuous, nonnegative submartingale with respect to a filtration $\{\mathcal{F}_t\}$ satisfying the usual conditions. Then X admits the unique decomposition $X(t) = M(t) + A(t)$ as the sum of a continuous martingale M and a continuous increasing process A .*

Let us now consider a real, continuous martingale X . We assume that this martingale is *square-integrable*, that is, $\mathbf{E}[X(t)^2] < \infty$ for every $t \geq 0$. One can show that then the process $X^2 = \{X(t)^2 : t \geq 0\}$ is a nonnegative submartingale. Hence this process has a unique Doob-Meyer decomposition. The natural increasing process in this decomposition is called the *quadratic variation* of the process X . It is denoted by $\langle X \rangle$. In other words, $\langle X \rangle$ is the unique increasing process such that $X^2 - \langle X \rangle$ is a martingale.

Likewise, if X and Y are two continuous square-integrable martingales, then both processes $(X + Y)^2 - \langle X + Y \rangle$ and $(X - Y)^2 - \langle X - Y \rangle$ are martingales. Hence the difference $4XY - [\langle X + Y \rangle - \langle X - Y \rangle]$ is also a martingale. We define the *cross-variation process* $\langle X, Y \rangle$ of X and Y by

$$\langle X, Y \rangle(t) := \frac{1}{4}[\langle X + Y \rangle(t) - \langle X - Y \rangle(t)], \quad t \geq 0. \quad (\text{B.16})$$

Then $\langle X, Y \rangle$ is the unique process of the form $A = A^+ - A^-$, where A^+ and A^- are continuous and increasing, such that $XY - A$ is a martingale. In particular, $\langle X, X \rangle = \langle X \rangle$. These definitions of quadratic variation and cross-variation can be extended to martingales that are not square-integrable.

B.5 Brownian motion

The most important example of a continuous martingale which is also a strong Markov process is Brownian motion. In this section we collect properties of Brownian motion, but we start with its definition. *Standard Brownian motion* is defined as a real-valued continuous process B adapted to a filtration $\{\mathcal{F}_t\}$ on some probability space $(\Omega, \mathcal{F}, \mathbf{P})$, such that $B(0) = 0$ a.s. and for $0 \leq s < t$, the increment $B(t) - B(s)$ is independent of the events in \mathcal{F}_s and is normally distributed with mean zero and variance $t - s$.

It is not obvious that a process satisfying the conditions of the definition exists. There are however several ways of constructing such a process (see for instance [46, chapter 2]). As we discussed in section B.3, we may regard a Brownian motion B as a random object taking values in $C[0, \infty)$. The law \mathbf{P}_B of the process is then a measure on the space $(C[0, \infty), \mathcal{B}(C[0, \infty)))$, and is called the *Wiener measure*. The space $(C[0, \infty), \mathcal{B}(C[0, \infty)), \mathbf{P}_B)$ is regarded as the canonical probability space for one-dimensional Brownian motion.

The extension of Brownian motion to more dimensions is straightforward. In d dimensions, we consider d independent standard one-dimensional Brownian motions B_1, \dots, B_d . We then define d -dimensional standard Brownian motion as the process B given by $B(t) = (B_1(t), \dots, B_d(t))$. Likewise, Brownian motion in the complex plane can be defined as the process given by $B(t) = B_1(t) + iB_2(t)$. It is of course equivalent to Brownian motion in \mathbb{R}^2 .

Let us now explore some properties of Brownian motion. First we note that from the definition of one-dimensional standard Brownian motion it is easily seen that this process is a Markov process with semigroup

$$P_t(x, A) = \mathbf{P}[B(s + t) \in A \mid B(s) = x] = \int_A \frac{1}{\sqrt{2\pi t}} e^{-(y-x)^2/2t} dy, \tag{B.17}$$

where $x \in \mathbb{R}$ and A is a Borel set. The integrand in this expression is known as the *Gauss kernel* or *heat kernel*. Note that at every time s it is as if the Brownian motion starts afresh from the position $B(s)$ (this the time-shift transformation in lemma B.9 below). In fact, this holds even if s is a stopping time for the Brownian filtration. More precisely, if T is a stopping time, then $B(T + t) - B(T)$ is a standard Brownian motion which is independent of the events $A \in \mathcal{F}_T$ prior to T . In other words, Brownian motion has the strong Markov property. Other equivalence transformations for Brownian motion are given by the following lemma:

Lemma B.9. *Let $B = \{B(t) : t \geq 0\}$ be standard Brownian motion adapted to $\{\mathcal{F}_t\}$. Then so are the processes obtained from each of the following transformations:*

1. *Symmetry:* $-B(t)$ with filtration $\{\mathcal{F}_t\}$.
2. *Scaling:* $X(t) = B(ct) / \sqrt{c}$ with filtration $\{\mathcal{F}_{ct}\}$ defined for $c > 0$.
3. *Time-inversion:* $Y(t) = 1_{\{t>0\}}tB(1/t)$ with filtration $\{\mathcal{F}_t^Y\}$.
4. *Time-shift:* $Z(t) = B(s + t) - B(s)$ with filtration $\{\mathcal{F}_{s+t}\}$ defined for $s > 0$.

A standard Brownian motion B is a process which has *stationary, independent increments*. By this we mean that if $0 \leq t_0 < t_1 < \dots < t_n < \infty$, then the increments $\{B(t_j) - B(t_{j-1}) : j = 1, \dots, n\}$ are independent and their distributions depend on t_j, t_{j-1} only through the difference $t_j - t_{j-1}$. Conversely one can show that any continuous real-valued process X which has stationary, independent increments can be decomposed as $X(t) = B(ct) + bt$, where B is

standard Brownian motion, $c > 0$ is the *diffusion constant* and b the *drift* of the process X . An elementary proof can be found for instance in [44, sections 1.4 and 1.10].

That one-dimensional Brownian motion is also a continuous martingale is clear from the fact that the increments $B(t) - B(s)$ have mean zero and are independent from \mathcal{F}_s . It is not hard to verify that the process $B(t)^2 - t$ is also a martingale. In view of the Doob-Meyer decomposition theorem B.8, this implies that the quadratic variation of B is given by $\langle B \rangle(t) = t$. It turns out that this result characterises Brownian motion among the class of continuous martingales, as the following theorem shows. On the other hand, every continuous martingale is a time-change of Brownian motion:

Theorem B.10 (Lévy’s martingale characterisation of Brownian motion).

Let X be a continuous process in \mathbb{R}^d adapted to $\{\mathcal{F}_t\}$ such that for every $1 \leq k \leq d$, $M_k(t) := X_k(t) - X_k(0)$ is a continuous martingale relative to $\{\mathcal{F}_t\}$, and the cross-variations are given by $\langle M_j, M_k \rangle(t) = \delta_{jk}t$. Then X is d -dimensional Brownian motion.

Theorem B.11 (Time-change of Brownian motion). *Let M be a continuous martingale adapted to the filtration $\{\mathcal{F}_t\}$ (which satisfies the usual conditions) such that $\lim_{t \rightarrow \infty} \langle M \rangle(t) = \infty$ a.s. Define for each $0 \leq s < \infty$ the stopping time $T(s) := \inf\{t \geq 0 : \langle M \rangle(t) > s\}$. Then the time-changed process*

$$B(s) := M(T(s)), \quad \mathcal{G}_s := \mathcal{F}_{T(s)}; \quad 0 \leq s < \infty \tag{B.18}$$

is a standard Brownian motion adapted to $\{\mathcal{G}_s\}$. In particular, the filtration $\{\mathcal{G}_s\}$ satisfies the usual conditions and we have a.s.

$$M(t) = B(\langle M \rangle(t)); \quad 0 \leq t < \infty. \tag{B.19}$$

B.6 Stochastic integration and stochastic calculus

In this section we consider Itô’s definition of stochastic integration with respect to Brownian motion. Then we introduce the Itô calculus, leading to a change-of-variable formula which is the stochastic analogue of the chain rule. We stress the fact that Itô integrals are martingales and discuss the significance of this result for applications of stochastic calculus.

We start with the definition of the Itô integral with respect to Brownian motion. Suppose that B is a standard Brownian motion adapted to the filtration $\{\mathcal{F}_t\}$ which we assume to satisfy the usual conditions (section B.3). We want to define an integral of the form

$$I_X(t) = \int_0^t X(s) dB(s) \tag{B.20}$$

for a suitable integrand X . This integral can be defined for all measurable processes X adapted to $\{\mathcal{F}_t\}$ such that $\mathbf{E}[\int_0^t X(s)^2 ds] < \infty$ for all $t > 0$. Below we shall define this integral in the case where X is *continuous* in addition.

First we approximate the process X by a simple process which takes on only finitely many values in any interval $[0, t)$:

$$X^{(n)}(t) = \begin{cases} n \int_{(k-1)/n}^{k/n} X(s) ds & \text{for } \frac{k}{n} < t \leq \frac{k+1}{n}, 1 \leq k \leq n^2 - 1; \\ 0 & \text{for } t \leq 1/n \text{ or } t > n, \end{cases} \quad (\text{B.21})$$

where k and n are positive integers. Observe that the interval of integration in (B.21) does not match with the interval for t . This is done deliberately to make $X^{(n)}(t)$ depend only on the history of the process, that is, to make $X^{(n)}(t)$ measurable with respect to \mathcal{F}_t . It can be shown that $X^{(n)}(t)$ approaches $X(t)$ in mean-square (that is, $\mathbf{E}|X^{(n)}(t) - X(t)|^2 \rightarrow 0$) if we send n to infinity. This allows us to define the stochastic integral (B.20) as the mean-square limit of a simple integral.

The simple integral of $X^{(n)}$ with respect to Brownian motion is defined by the sum

$$\int_0^t X^{(n)}(s) dB(s) := \sum_{i=1}^{\infty} X^{(n)}(t_i^{(n)} \wedge t) [B(t_i^{(n)} \wedge t) - B(t_{i-1}^{(n)} \wedge t)], \quad (\text{B.22})$$

where $t_i^{(n)} = i/n$ and $s \wedge t := \min(s, t)$. The stochastic integral (B.20) is defined as the limit of this expression as $n \rightarrow \infty$. It can be shown that also discontinuous adapted processes X can be approximated by simple processes, which allows us to define the integral in a similar way for discontinuous integrands.

We now list some properties of the Itô integral (B.20). The most important result is that the integral is a continuous square-integrable martingale starting from 0, so that $\mathbf{E}[I_X(t) | \mathcal{F}_s] = I_X(s)$ for $0 \leq s < t < \infty$. The quadratic variation of this process is given by $\langle I_X \rangle(t) = \int_0^t X(s)^2 ds$. Quite remarkably, it is in fact true that any continuous square-integrable martingale M can be written as

$$M(t) = M(0) + \int_0^t X(s) dB(s), \quad t \geq 0 \quad (\text{B.23})$$

for a suitable adapted process X satisfying $\mathbf{E}[\int_0^t X(s)^2 ds] < \infty$ for all $t > 0$. This direct connection between martingales and Itô integrals is very valuable in the theory of stochastic processes.

The stochastic integral (B.20) is often written in its differential form

$$dI_X(t) = X(t) dB(t). \quad (\text{B.24})$$

The stochastic process I_X defined through this equation may be regarded as a Brownian motion that at time t has an instantaneous variance $X(t)^2$. One can also consider a stochastic process which looks like a Brownian motion with instantaneous variance $X(t)^2$ and drift $Y(t)$ at time t , where both X and Y must be adapted to the filtration $\{\mathcal{F}_t\}$. Then this process satisfies the stochastic differential equation

$$dZ(t) = Y(t) dt + X(t) dB(t). \quad (\text{B.25})$$

The corresponding stochastic integral is

$$Z(t) = Z(0) + \int_0^t Y(s) ds + \int_0^t X(s) dB(s), \quad (\text{B.26})$$

where the first integral is an ordinary integral and the second an Itô integral. Such a process is called a *semimartingale*. It is to be noted that this process is a martingale with respect to $\{\mathcal{F}_t\}$ if and only if the drift term $Y(t)$ vanishes for all $t \geq 0$.

Suppose now that Z is a semimartingale given by equation (B.26). Then what is the differential equation for the process $f \circ Z$, which is a function of Z ? The answer is given by Itô's change-of-variable formula. Associated with this formula is the Itô stochastic calculus, which is based on the same principle as ordinary differential calculus: one considers the infinitesimal increment of $f \circ Z(t)$ over the time increment dt , keeping terms up to first order in dt . However, in stochastic calculus we must treat the stochastic increment $dB(t) = B(t + dt) - B(t)$ as an increment of order $(dt)^{1/2}$ so that in particular $dB(t)^2 = dt$ (see for instance Gardiner [40] for a nice discussion). With these rules of calculus one can derive Itô's formula:

Theorem B.12 (Itô's formula). *Let $f : \mathbb{R} \rightarrow \mathbb{R}$ be a function which is twice continuously differentiable. Suppose that Z satisfies the stochastic differential equation*

$$dZ(t) = Y(t) dt + X(t) dB(t) \quad (\text{B.27})$$

as discussed above, where B is standard Brownian motion. Then the stochastic process $f \circ Z$ satisfies

$$df(Z(t)) = \left[Y(t)f'(Z(t)) + \frac{1}{2}X(t)^2 f''(Z(t)) \right] dt + X(t)f'(Z(t)) dB(t). \quad (\text{B.28})$$

This formula expresses the process $f \circ Z$ as the sum of an ordinary integral and an Itô integral. The fact that any Itô integral defines a martingale now leads to the important conclusion that the process $f \circ Z$ of the theorem is a martingale with respect to the filtration of the Brownian motion if and only if the drift term in Itô's formula (B.28) vanishes. This relates the martingale

property of $f \circ Z$ to a differential equation for f , thus providing the key to the computation of many results in this thesis.

We can extend Itô's formula to more dimensions using the same principles of stochastic calculus. That is, one again considers infinitesimal increments up to first order in dt . The increments of the different components B_i of the Brownian motion are to be treated again as increments of order $(dt)^{1/2}$. In more dimensions, however, we have the extra constraint that products like $dB_i(t)dB_j(t)$ for $i \neq j$ vanish because the two components of the Brownian motion are independent. With these rules of calculus one can derive the following version of Itô's formula:

Theorem B.13 (Multi-dimensional Itô formula). *Let $f(t, x) : [0, \infty) \times \mathbb{R}^d \rightarrow \mathbb{R}$ be a function which is continuously differentiable in t and twice continuously differentiable in each of the coordinates x_i , $1 \leq i \leq d$. Suppose that the process $Z = (Z_1, \dots, Z_d)$ satisfies*

$$dZ_i(t) = Y_i(t) dt + \sum_{j=1}^d X_{ij}(t) dB_j(t), \tag{B.29}$$

where $B = (B_1, \dots, B_d)$ is standard d -dimensional Brownian motion adapted to the filtration $\{\mathcal{F}_t\}$ satisfying the usual conditions. Then

$$df(t, Z(t)) = \left[\sum_{i=1}^d Y_i(t) \frac{\partial f(t, Z(t))}{\partial x_i} + \frac{1}{2} \sum_{i,j,k=1}^d X_{ik}(t) X_{jk}(t) \frac{\partial^2 f(t, Z(t))}{\partial x_i \partial x_j} \right] dt + \frac{\partial f(t, Z(t))}{\partial t} dt + \sum_{i,j=1}^d X_{ij}(t) \frac{\partial f(t, Z(t))}{\partial x_i} dB_j(t). \tag{B.30}$$

As an application of Itô's formula, let us now prove the following theorem for complex Brownian motion:

Theorem B.14. *Suppose that $D \subset \mathbb{C}$ is a connected domain whose boundary consists of a finite number of disjoint Jordan curves, such that ∂D is the union of two disjoint sets A and A' , each consisting of a finite number of arcs and closed curves. Let B be complex Brownian motion starting from $z \in D$, and set $T := \inf\{t \geq 0 : B(t) \in \partial D\}$. Then $\mathbf{P}[B(T) \in A] = \omega(z)$, where $\omega(z)$ is the harmonic measure at z of the set A with respect to D (see definition A.4 in section A.1).*

Proof. It is clear from the definition of harmonic measure that $\omega(B(T)) = 1_{\{B(T) \in A\}}$ a.s. By applying the two-dimensional Itô formula to $\omega \circ B$ one can see that the stopped process $\omega(B(t \wedge T))$ is a bounded martingale, because ω is a harmonic function. Hence $\mathbf{P}[B(T) \in A] = \mathbf{E}[\omega(B(T))] = \mathbf{E}[\omega(B(0))] = \omega(z)$ by Doob's optional sampling theorem B.7. ■

Corollary B.15. *Let B be complex Brownian motion started from $z = x + iy \in \mathbb{H}$ and set $T := \inf\{t \geq 0 : B(t) \in \mathbb{R}\}$. Then the probability that $B(T) \in (-\infty, 0)$ is given by*

$$\omega(z) = \int_{-\infty}^0 \frac{y}{\pi} \frac{dt}{y^2 + (t-x)^2} = \frac{1}{2} - \frac{1}{\pi} \arctan(x/y). \tag{B.31}$$

Proof. The function $\omega(z)$ is harmonic, tends to 0 as z tends to $(0, \infty)$ and tends to 1 as z tends to $(-\infty, 0)$. The result follows from theorem B.14. ■

For another application, let $B = (B_1, \dots, B_d)$ be a d -dimensional Brownian motion. Let R be the process such that $R(t)$ is the distance of $B(t)$ to the origin, that is

$$R(t) := \sqrt{B_1(t)^2 + \dots + B_d(t)^2}, \quad t \geq 0. \tag{B.32}$$

Then R is called a *Bessel process* with dimension d . Itô's formula (B.30) applied to the function $f(x) := (x_1^2 + \dots + x_d^2)^{1/2}$ can be used to derive heuristically a stochastic differential equation for the process R . Although the function f is not differentiable at the origin, it is possible to work around this problem to show that the following result is still correct:

Theorem B.16. *Let $d \geq 2$ be an integer. The Bessel process R with dimension d satisfies the differential equation*

$$dR(t) = \frac{d-1}{2R(t)} dt + dW(t), \tag{B.33}$$

where W is the standard, one-dimensional Brownian motion

$$W := \sum_{j=1}^d W_j \quad \text{with} \quad W_j(t) := \int_0^t \frac{B_j(s)}{R(s)} dB_j(s); \quad 1 \leq j \leq d. \tag{B.34}$$

Here, to show that W is standard one-dimensional Brownian motion one can use Itô's formula to find the differential equation for W^2 . This shows that the natural increasing process in the Doob-Meyer decomposition (theorem B.8) of W^2 is t and hence, $\langle W \rangle(t) = t$. The result then follows from Lévy's martingale characterisation theorem B.10.

Bibliography

- [1] Ahlfors, L. V. (1966, 2nd edition). *Complex analysis: an introduction to the theory of analytic functions of one complex variable*. New York: McGraw-Hill.
- [2] Ahlfors, L. V. (1973). *Conformal invariants: topics in geometric function theory*. New York: McGraw-Hill.
- [3] Ash, R. B. & Doléans-Dade, C. A. (2000, 2nd edition). *Probability & measure theory*. Burlington, MA: Harcourt/Academic Press.
- [4] Barlow, R. J. (1989). *Statistics. A guide to the use of statistical methods in the physical sciences*. Chichester: John Wiley & Sons.
- [5] Bauer, M. & Bernard, D. (2002). SLE $_{\kappa}$ growth processes and conformal field theories. *Phys. Lett. B* 543, pp. 135–138. [[math-ph/0206028](#)].
- [6] Bauer, M. & Bernard, D. (2003). Conformal field theories of stochastic Loewner evolutions. *Comm. Math. Phys.* 239, pp. 493–521. [[hep-th/0210015](#)].
- [7] Bauer, M. & Bernard, D. (2003). SLE martingales and the Virasoro algebra. *Phys. Lett. B* 557, pp. 309–316. [[hep-th/0301064](#)].
- [8] Bauer, M. & Bernard, D. (2004). CFTs of SLEs: the radial case. *Phys. Lett. B* 583, pp. 324–330. [[math-ph/0310032](#)].
- [9] Bauer, M. & Bernard, D. (2004). Conformal transformations and the SLE partition function martingale. *Ann. Henri Poincaré* 5, pp. 289–326. [[math-ph/0305061](#)].
- [10] Bauer, M. & Bernard, D. (preprint). Loewner chains. [[cond-mat/0412372](#)].
- [11] Bauer, M. & Bernard, D. (preprint). SLE, CFT and zig-zag probabilities. [[math-ph/0401019](#)].
- [12] Bauer, M., Bernard, D. & Houdayer, J. (2005). Dipolar stochastic Loewner evolutions. *J. Stat. Mech. Theory Exp.* P03001, 18 pp. [[math-ph/0411038](#)].
- [13] Baxter, R. J. (1978). Solvable eight-vertex model on an arbitrary planar lattice. *Philos. Trans. Roy. Soc. London Ser. A* 289, pp. 315–346.

- [14] Baxter, R. J. (1982). *Exactly solved models in statistical mechanics*. London: Academic Press.
- [15] Baxter, R. J. (1986). q colourings of the triangular lattice. *J. Phys. A* 19, pp. 2821–2839.
- [16] Baxter, R. J., Kelland, S. B. & Wu, F. Y. (1976). Equivalence of the Potts model or Whitney polynomial with an ice-type model. *J. Phys. A* 9, pp. 397–406.
- [17] Beffara, V. (2004). Hausdorff dimensions for SLE_6 . *Ann. Probab.* 32, pp. 2606–2629. [[math.PR/0204208](#)].
- [18] Beffara, V. (preprint). The dimension of the SLE curves. [[math.PR/0211322](#)].
- [19] Bieberbach, L. (1916). Über die Koeffizienten derjenigen Potenzreihen, welche eine schlichte Abbildung des Einheitskreises vermitteln. *S.-B. Preuss. Akad. Wiss.* 38, pp. 940–955.
- [20] Blöte, H. W. J. & Deng, Y. (2003). Conformal invariance and simulations in curved geometries. *Phys. A* 321, pp. 59–70.
- [21] Branges, L. de (1985). A proof of the Bieberbach conjecture. *Acta Math.* 154, pp. 137–152.
- [22] Camia, F. & Newman, C. M. (preprint). The full scaling limit of two-dimensional critical percolation. [[math.PR/0504036](#)].
- [23] Cardy, J. (1987). Conformal invariance. In C. Domb & J. L. Lebowitz (Eds.), *Phase transitions and critical phenomena*, vol. 11, pp. 55–126. London: Academic Press.
- [24] Cardy, J. (1992). Critical percolation in finite geometries. *J. Phys. A* 25, pp. L201–L206.
- [25] Cardy, J. (2005). SLE for theoretical physicists. *Ann. Physics* 318, pp. 81–118. [[cond-mat/0503313](#)].
- [26] Carmona, P., Petit, F. & Yor, M. (1998). Beta-gamma random variables and intertwining relations between certain Markov processes. *Rev. Mat. Iberoamericana* 14, pp. 311–367.
- [27] Davis, P. J. (1972, 10th edition). Gamma function and related functions. In M. Abramowitz & I. Stegun (Eds.), *Handbook of mathematical functions with formulas, graphs, and mathematical tables*, chap. 6, pp. 253–293. New York: John Wiley.
- [28] Deng, Y. & Blöte, H. W. J. (2002). Conformal invariance of the Ising model in three dimensions. *Phys. Rev. Lett.* 88, 190602, 4 pp.
- [29] Deng, Y. & Blöte, H. W. J. (2003). Bulk and surface critical behavior of the three-dimensional Ising model and conformal invariance. *Phys. Rev. E* 67, 066116, 8 pp.
- [30] Dubédat, J. (2003). SLE and triangles. *Electron. Comm. Probab.* 8, pp. 28–42. [[math.PR/0212008](#)].
- [31] Dubédat, J. (2004). Reflected planar Brownian motions, intertwining relations and crossing probabilities. *Ann. Inst. H. Poincaré Probab. Statist.* 40, pp. 539–552. [[math.PR/0302250](#)].

- [32] Dubédat, J. (2005). SLE(κ, ρ) martingales and duality. *Ann. Probab.* 33, pp. 223–243. [math.PR/0303128].
- [33] Dubédat, J. (preprint). Excursion decompositions for SLE and Watts' crossing formula. [math.PR/0405074].
- [34] Duplantier, B. (1999). Harmonic measure exponents for two-dimensional percolation. *Phys. Rev. Lett.* 82, pp. 3940–3943.
- [35] Duplantier, B. (2000). Conformally invariant fractals and potential theory. *Phys. Rev. Lett.* 84, pp. 1363–1367.
- [36] Fortuin, C. M. & Kasteleyn, P. W. (1972). On the random cluster model 1: Introduction and relation to other models. *Physica* 57, pp. 536–564.
- [37] Friedrich, R. & Werner, W. (2002). Conformal fields, restriction properties, degenerate representations and SLE. *C. R. Math. Acad. Sci. Paris* 335, pp. 947–952. [math.PR/0209382].
- [38] Friedrich, R. & Werner, W. (2003). Conformal restriction, highest-weight representations and SLE. *Comm. Math. Phys.* 243, pp. 105–122. [math-ph/0301018].
- [39] Gamelin, T. W. (2001). *Complex analysis*. Undergraduate Texts in Mathematics. New York: Springer-Verlag.
- [40] Gardiner, C. W. (1983). *Handbook of stochastic methods for physics, chemistry and the natural sciences*, vol. 13 of *Springer Series in Synergetics*. Berlin: Springer.
- [41] Gier, J. de & Nienhuis, B. (2005). Brauer loops and the commuting variety. *J. Stat. Mech. Theory Exp.* 006, 10 pp.
- [42] Grimmett, G. & Stirzaker, D. (2001, 3rd edition). *Probability and random processes*. New York: Oxford University Press.
- [43] Gunn, J. M. F. & Ortuño, M. (1985). Percolation and motion in a simple random environment. *J. Phys. A* 18, pp. L1095–L1101.
- [44] Itô, K. (1969). *Stochastic processes*. Lecture Notes Series, No. 16. Aarhus: Matematisk Institut, Aarhus Universitet.
- [45] Kadanoff, L. P. (1966). Scaling laws for Ising models near T_c . *Physics* 2, pp. 263–271.
- [46] Karatzas, I. & Shreve, S. E. (1991, 2nd edition). *Brownian motion and stochastic calculus*, vol. 113 of *Graduate Texts in Mathematics*. New York: Springer-Verlag.
- [47] Kennedy, T. (2002). Monte Carlo tests of stochastic Loewner evolution predictions for the 2D self-avoiding walk. *Phys. Rev. Lett.* 88, 130601, 4 pp. [math.PR/0112246].
- [48] Kennedy, T. (2004). Conformal invariance and stochastic Loewner evolution predictions for the 2D self-avoiding walk – Monte Carlo tests. *J. Statist. Phys.* 114, pp. 51–78. [math.PR/0207231].
- [49] Kenyon, R. (preprint). An introduction to the dimer model. [math.CO/0310326].
- [50] Kong, X. P. & Cohen, E. G. D. (1989). Anomalous diffusion in a lattice-gas wind-tree model. *Phys. Rev. B* 40, pp. 4838–4845.

- [51] Kufarev, P. P. (1947). A remark on integrals of Loewner's equation. *Doklady Akad. Nauk SSSR* 57, pp. 655–656. In Russian.
- [52] Lawler, G. F. (2004). An introduction to the stochastic Loewner evolution. In V. A. Kaimanovich, K. Schmidt & W. Woess (Eds.), *Random walks and geometry*, pp. 261–293. Berlin: Walter de Gruyter. <http://www.math.duke.edu/~jose/papers.html>.
- [53] Lawler, G. F. (2005). *Conformally invariant processes in the plane*, vol. 114 of *Mathematical Surveys and Monographs*. Providence, RI: Amer. Math. Soc.
- [54] Lawler, G. F., Schramm, O. & Werner, W. (2001). One-arm exponent for critical 2D percolation. *Electron. J. Probab.* 7, 13 pp. [math.PR/0108211].
- [55] Lawler, G. F., Schramm, O. & Werner, W. (2001). Values of Brownian intersection exponents I: Half-plane exponents. *Acta Math.* 187, pp. 237–273. [math.PR/9911084].
- [56] Lawler, G. F., Schramm, O. & Werner, W. (2001). Values of Brownian intersection exponents II: Plane exponents. *Acta Math.* 187, pp. 275–308. [math.PR/0003156].
- [57] Lawler, G. F., Schramm, O. & Werner, W. (2002). Analyticity of intersection exponents for planar Brownian motion. *Acta Math.* 189, pp. 179–201. [math.PR/0005295].
- [58] Lawler, G. F., Schramm, O. & Werner, W. (2002). Values of Brownian intersection exponents III: Two-sided exponents. *Ann. Inst. H. Poincaré Statist.* 38, pp. 109–123. [math.PR/0005294].
- [59] Lawler, G. F., Schramm, O. & Werner, W. (2003). Conformal restriction: the chordal case. *J. Amer. Math. Soc.* 16, pp. 917–955. [math.PR/0209343].
- [60] Lawler, G. F., Schramm, O. & Werner, W. (2004). Conformal invariance of planar loop-erased random walks and uniform spanning trees. *Ann. Probab.* 32, pp. 939–995. [math.PR/0112234].
- [61] Lawler, G. F., Schramm, O. & Werner, W. (2004). On the scaling limit of planar self-avoiding walk. In *Fractal geometry and applications: a jubilee of Benoît Mandelbrot, Part 2*, vol. 72 of *Proc. Sympos. Pure Math.*, pp. 339–364. Providence, RI: Am. Math. Soc. [math.PR/0204277].
- [62] Lind, J. R. (2005). A sharp condition for the Loewner equation to generate slits. *Ann. Acad. Sci. Fenn. Math.* 30, pp. 143–158. [math.CV/0311234].
- [63] Löwner, K. (1923). Untersuchungen über schlichte konforme Abbildungen des Einheitskreises. I. *Math. Ann.* 89, pp. 103–121.
- [64] Lyklema, J. W. (1985). The growing self-avoiding trail. *J. Phys. A* pp. L617–L624.
- [65] Ma, S.-K. (1976). *Modern Theory of Critical Phenomena*, vol. 46 of *Frontiers in Physics*. Reading, MA: Benjamin.
- [66] Marshall, D. E. & Rohde, S. (2005). The Loewner differential equation and slit mappings. *J. Amer. Math. Soc.* 18, pp. 763–778.
- [67] Martins, M. J., Nienhuis, B. & Rietman, R. (1998). Intersecting loop model as a solvable super spin chain. *Phys. Rev. Lett.* 81, pp. 504–507.

- [68] Nienhuis, B. (1982). Exact critical point and critical exponents of $O(n)$ models in two dimensions. *Phys. Rev. Lett.* 49, pp. 1062–1065.
- [69] Nienhuis, B. (1984). Critical behavior of two-dimensional spin models and charge asymmetry in the Coulomb Gas. *J. Statist. Phys.* 34, pp. 731–761.
- [70] Nienhuis, B. (1987). Coulomb Gas formulation of two-dimensional phase transitions. In C. Domb & J. L. Lebowitz (Eds.), *Phase transitions and critical phenomena*, vol. 11, pp. 1–53. London: Academic Press.
- [71] Oberhettinger, F. (1972, 10th edition). Hypergeometric functions. In M. Abramowitz & I. Stegun (Eds.), *Handbook of mathematical functions with formulas, graphs, and mathematical tables*, chap. 15, pp. 555–566. New York: John Wiley.
- [72] Pfeuty, P. & Toulouse, G. (1977). *Introduction to the renormalization group and to critical phenomena*. London: John Wiley.
- [73] Pommerenke, C. (1992). *Boundary behaviour of conformal maps*, vol. 299 of *Grundlehren der Mathematischen Wissenschaften*. Berlin: Springer-Verlag.
- [74] Reshetikhin, N. Y. (1983). The functional equation method in the theory of exactly soluble quantum systems. *Sovjet Phys. JETP* 57, pp. 691–696.
- [75] Revuz, D. & Yor, M. (1991). *Continuous martingales and Brownian Motion*, vol. 293 of *Grundlehren der Mathematischen Wissenschaften*. Berlin: Springer-Verlag.
- [76] Rogers, L. C. G. & Pitman, J. W. (1981). Markov functions. *Ann. Probab.* 9, pp. 573–582.
- [77] Rogers, L. C. G. & Williams, D. (1994, 2nd edition). *Diffusions, Markov processes, and martingales. Volume 1: Foundations*. Wiley Series in Probability and Mathematical Statistics. Chichester: John Wiley.
- [78] Rohde, S. & Schramm, O. (2005). Basic properties of SLE. *Ann. of Math.* (2) 161, pp. 883–924. [math.PR/0106036].
- [79] Ruijgrok, T. W. & Cohen, E. G. D. (1988). Deterministic lattice gas models. *Phys. Lett. A* 133, pp. 415–418.
- [80] Saleur, H. & Duplantier, B. (1987). Exact determination of the percolation hull exponent in two dimensions. *Phys. Rev. Lett.* 58, pp. 2325–2328.
- [81] Schäfer, L. (1976). Conformal covariance in the framework of Wilson’s renormalization group approach. *J. Phys. A* 9, pp. 377–395.
- [82] Schramm, O. (2000). Scaling limits of loop-erased random walks and uniform spanning trees. *Israel J. Math.* 118, pp. 221–288. [math.PR/9904022].
- [83] Schramm, O. (2001). A percolation formula. *Electron. Comm. Probab.* 6, pp. 115–120. [math.PR/0107096].
- [84] Schramm, O. & Sheffield, S. (preprint). The harmonic explorer and its convergence to SLE(4). [math.PR/0310210].
- [85] Schramm, O. & Wilson, D. B. (preprint). SLE coordinate changes. [math.PR/0505368].
- [86] Schultz, C. L. (1981). Solvable q -state models in lattice statistics and Quantum Field Theory. *Phys. Rev. Lett.* 46, pp. 629–632.

- [87] Smirnov, S. (2001). Critical percolation in the plane: conformal invariance, Cardy's formula, scaling limits. *C. R. Acad. Sci. Paris Sér. I Math.* 333, pp. 239–244.
- [88] Smirnov, S. (unpublished). Critical percolation in the plane. I. Conformal invariance and Cardy's formula. II. Continuum scaling limit. <http://www.math.kth.se/~stas/papers/>.
- [89] Smirnov, S. & Werner, W. (2001). Critical exponents for two-dimensional percolation. *Math. Res. Lett.* 8, pp. 729–744. [math.PR/0109120].
- [90] Varadhan, S. R. S. & Williams, R. J. (1985). Brownian motion in a wedge with oblique reflection. *Comm. Pure App. Math.* 38, pp. 405–443.
- [91] Vega, H. J. de & Karowski, M. (1987). Exact Bethe Ansatz solution of $O(2n)$ symmetric theories. *Nucl. Phys. B* 280, pp. 225–254.
- [92] Werner, W. (2004). Girsanov's transformation for $SLE(\kappa, \rho)$ processes, intersection exponents and hiding exponents. *Ann. Fac. Sci. Toulouse Math.* (6) 13, pp. 121–147. [math.PR/0302115].
- [93] Werner, W. (2004). Random planar curves and Schramm-Loewner evolutions. In *Lectures on probability theory and statistics*, vol. 1840 of *Lecture notes in Math.*, pp. 107–195. Berlin: Springer. [math.PR/0303354].
- [94] Werner, W. (2005). Conformal restriction and related questions. *Probab. Surv.* 2, pp. 145–190. [math.PR/0307353].
- [95] Wilson, D. B. (1996). Generating random spanning trees more quickly than the cover time. In *Proceedings of the Twenty-eighth Annual ACM Symposium on the Theory of Computing (Philadelphia, PA, 1996)*, pp. 296–303. New York: ACM.
- [96] Wilson, K. G. & Kogut, J. (1974). The renormalization group and the ϵ expansion. *Physics Reports* 12, pp. 75–199.
- [97] Ziff, R. M., Kong, X. P. & Cohen, E. G. D. (1991). Lorentz lattice-gas and kinetic-walk model. *Phys. Rev. A* 44, pp. 2410–2428.

Samenvatting

Conform invariante paden in de tweedimensionale statistische fysica

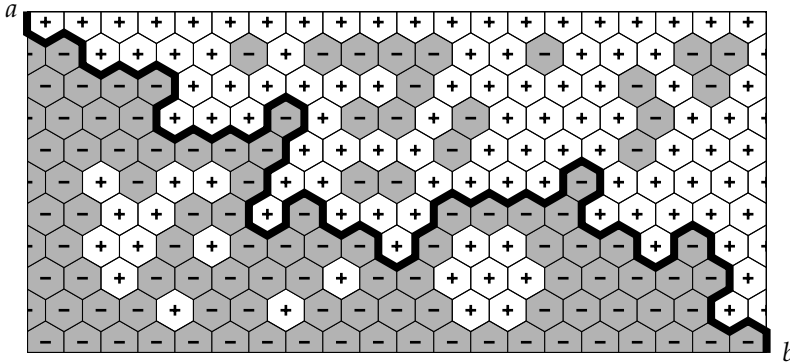
Met een handleiding over Schramm-Löwner Evolutie

Dit proefschrift handelt over geometrische aspecten van door het toeval bepaalde paden, hieronder kortweg *toevalspaden* genoemd. Met name worden paden bekeken die men krijgt door van statistische modellen op een rooster de schaallimiet te nemen, d.w.z. de limiet waarin de roosterafstand naar nul gaat. Enkele jaren geleden werd door Schramm een nieuwe methode geïntroduceerd waarmee zulke paden wiskundig beschreven kunnen worden, die bekend is onder de naam Schramm-Löwner Evolutie (SLE). Deze methode heeft nieuwe inzichten opgeleverd in de schaallimieten van kritische modellen, en biedt een nieuwe manier om berekeningen te doen aan deze modellen.

De hoofdstukken 1–4 van dit proefschrift kunnen worden beschouwd als een handleiding over SLE. In deze hoofdstukken wordt uitgelegd wat SLE precies is en hoe het verband wordt gelegd met tweedimensionale statistische modellen. Ook worden enkele voorbeelden gegeven van SLE-berekeningen aan eigenschappen van kritische modellen. De hoofdstukken 5 en 6 breiden de reikwijdte van dit proefschrift uit naar andere toevalspaden in twee dimensies, die nauw verwant zijn aan de SLE-paden. Hieronder volgt een samenvatting waarin per hoofdstuk een en ander nader wordt toegelicht.

1 Toevalspaden in statistische modellen

Om uit te leggen welk aspect van een kritisch model wordt beschreven door SLE richten we ons op twee voorbeelden. Bekijk bijvoorbeeld het Isingmodel op een rechthoek, bedekt met een zeshoekig rooster. De spinvariabelen s_j leven op de zeshoeken en kunnen de waarden $+1$ of -1 aannemen, zoals is aangegeven in figuur 1. De kans op een bepaalde configuratie van de spins is evenredig met het Boltzmann-gewicht $\exp(\beta \sum_{\langle j,k \rangle} s_j s_k)$, waarin β de inverse



Figuur 1. Een toevalspad van het Isingmodel in een rechthoek.

temperatuur is en de som genomen wordt over alle paren van naburige spins. Als randcondities leggen we op dat alle spins met de klok mee van een hoek a naar de tegenoverliggende hoek b positief zijn, en alle spins tegen de klok in van a naar b negatief. Dan is er in elke toegestane configuratie een toevalspad over de zijden van de zeshoeken van a naar b waarlangs aan de linkerkzijde alleen positieve spins liggen, en aan de rechterzijde alleen negatieve. Zie figuur 1. Het is dit pad dat vermoedelijk op het kritische punt van het Isingmodel in de schaallimiet wordt beschreven door SLE.

We kunnen de statistische verdeling van de configuraties van plussen en minnen in figuur 1 ook op een andere manier dan in het Isingmodel vastleggen. We kunnen bijvoorbeeld voor elke zeshoek in het interieur van de rechthoek onafhankelijk een zuivere munt opwerpen. Bij kop krijgt de zeshoek een $+$, bij munt een $-$. Dit definieert een model dat equivalent is met kritische percolatie op het driehoekige rooster. Opnieuw is er een toevalspad van a naar b met aan de linkerkzijde alleen plussen en aan de rechterzijde alleen minnen. Van dit pad is bewezen dat het in de schaallimiet wordt beschreven door SLE.

2 Schramm-Löwner Evolutie (SLE)

Beschouw een pad $\gamma(t)$ in de bovenste helft van het (complexe) vlak dat begint in de oorsprong en groeit naar oneindig als functie van t . Neem aan dat als dit pad zichzelf of de reële as raakt op tijdstip t , het pad zijn weg vervolgt in de onbegrensde component van het complement van $\gamma[0, t]$ in het halfvlak. Zo'n pad kan worden beschreven met een differentiaalvergelijking voor de conforme transformaties die de onbegrensde component van het complement van $\gamma[0, t]$ afbeelden naar het halfvlak. De differentiaalvergelijking wordt aangedreven

door een continue reële functie ξ die het pad γ volledig beschrijft. Deze methode om een pad γ te beschrijven werd geïntroduceerd door Löwner, en wordt ook wel Löwner Evolutie genoemd.

De hierboven gedefinieerde toevalspaden van het Isingmodel en van percolatie kunnen door conforme transformatie worden afgebeeld op paden in het bovenste halfvlak van de oorsprong naar oneindig. Passen we vervolgens de methode van Löwner toe op deze paden, dan kan men aantonen dat de functie ξ voor deze paden de kansverdeling moet hebben van een Brownse beweging met een zekere diffusieconstante $\kappa > 0$. Dit werd voor het eerst (en voor een ander model) geconstateerd door Schramm, die daarop de oplossingen van Löwner's vergelijking waarbij ξ een Brownse beweging is "Stochastische Löwner Evolutie" (SLE) doopte. Tegenwoordig spreken we liever van Schramm-Löwner Evolutie.

Het blijkt dat Löwner's vergelijking voor verschillende waardes van κ paden genereert met verschillende karakteristieken. Er zijn drie fases te onderscheiden. Voor $\kappa \leq 4$ hebben de paden geen raakpunten met zichzelf of de reële as. Voor $4 < \kappa < 8$ hebben de paden wel zulke raakpunten, maar de paden liggen niet dicht in het halfvlak. Voor $\kappa \geq 8$ bezoeken de paden elk punt in het halfvlak. Voor $\kappa \leq 8$ is de Hausdorff-dimensie van de SLE-paden $1 + \kappa/8$. Verschillende waardes van κ coderen voor verschillende (kritische) modellen.

3 Verbanden tussen SLE en statistische modellen

Als voorbeelden van kritische modellen die in de schaallimiet beschreven kunnen worden door SLE hebben we tot nu toe alleen het Isingmodel en percolatie bekeken. Voor het Isingmodel vermoedt men dat het toevalspad beschreven wordt door SLE met $\kappa = 3$. Voor percolatie is bewezen dat het toevalspad wordt beschreven door SLE met $\kappa = 6$. Een model dat speciaal is ontworpen zodat de schaallimiet SLE met $\kappa = 4$ moet zijn, is de zogenaamde "harmonische verkenners" (*harmonic explorer*). Dit model lijkt erg op percolatie, behalve dat nu de kans op een + of een - wordt bepaald door de waarde van een harmonische functie. Ook van de gewone toevalswandeling waarvan de lussen in chronologische volgorde worden gewist (*loop-erased random walk*) en van de uniforme overspannende boom (*uniform spanning tree*) zijn de schaallimieten bekend: SLE met $\kappa = 2$ en $\kappa = 8$, respectievelijk.

Er zijn ook nog andere voorbeelden van modellen waarvoor het verband met SLE niet is bewezen maar wel wordt vermoed. Zo vermoedt men dat de schaallimiet van de zelf-vermijdende wandeling (*self-avoiding walk*) SLE is met $\kappa = 8/3$. Verder denkt men dat de schaallimiet van het Fortuin-Kasteleyn

clustermodel voor $q \in [0, 4]$ beschreven wordt door SLE waarbij het verband tussen q en κ wordt gegeven door $q = 2 + 2 \cos(8\pi/\kappa)$. Ook het $O(n)$ model heeft vermoedelijk SLE als schaallimiet, met $n = -2 \cos(4\pi/\kappa)$.

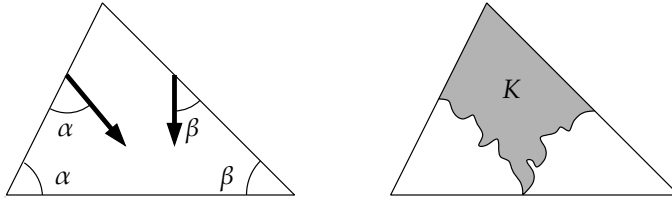
4 SLE-berekeningen voor kritische modellen

Een interessant aspect van SLE is dat het ons in staat stelt berekeningen te doen aan eigenschappen van de kritische modellen die erdoor worden beschreven. Bekijk bijvoorbeeld weer een toevalspad in een rechthoek van hoek a naar hoek b , zoals getekend in figuur 1. Voor SLE met $4 < \kappa < 8$ kunnen we de kans berekenen dat het gegenereerde toevalspad de rechterzijde van de rechthoek bereikt alvorens de bodem te raken. Voor kritische percolatie ($\kappa = 6$) kan men uit dergelijke berekeningen de exponenten afleiden waarmee de kans dat het toevalspad de rechthoek k keer oversteekt naar 0 gaat als de rechthoek steeds langer wordt. Dankzij SLE is er nu een volledig rigoureuze afleiding van deze kritische exponenten mogelijk.

Van een geheel andere soort is het volgende resultaat. Beschouw een toevalspad van SLE in het bovenste halfvlak van de oorsprong naar oneindig. Dan kan de kans worden berekend dat een gegeven punt z in het halfvlak aan de rechterzijde van het pad ligt. Dit is een voorbeeld van een resultaat dat niet eerder met fysische argumenten is gevonden. Vergelijkbare berekeningen zijn mogelijk voor een andere versie van SLE, dipolar SLE genaamd. In dipolar SLE begint het toevalspad in een gegeven punt a op de rand van het domein en eindigt in een door het toeval bepaald punt op de rand tussen twee gegeven punten b en c in. In het Isingmodel verkrijgt men zo'n pad bijvoorbeeld door positieve randcondities te nemen tussen a en b , negatieve tussen a en c en vrije tussen b en c .

5 Gereflecteerde Brownse beweging

We richten nu onze aandacht op een heel ander model. Neem een driehoek waarvan de basis op de reële as ligt, de basishoeken links en rechts respectievelijk α en β zijn, en de derde hoek zich in het bovenste halfvlak bevindt. Met een gereflecteerde Brownse beweging in de driehoek bedoelen we een toevalsproces dat twee-dimensionale Brownse beweging is in het interieur van de driehoek en gereflecteerd wordt onder een vaste hoek met een zijde van de driehoek als het proces de zijde raakt. Hierbij mogen de reflectiehoeken op de linkerzijde en op de rechterzijde van de driehoek verschillend zijn.



Figuur 2. Links de reflectiehoeken waarbij een gereflecteerde Brownse beweging gestart vanuit de top van de driehoek met de uniforme verdeling op de basis aankomt, en rechts het omhulsel K .

Het blijkt dat zo'n gereflecteerde Brownse beweging een speciale eigenschap heeft als de reflectiehoek op de linkerzijde gelijk is aan α en op de rechterzijde gelijk aan β (zie figuur 2). In dat geval is het punt waar het proces voor het eerst de basis van de driehoek raakt namelijk uniform verdeeld als de Brownse beweging wordt gestart in de top van de driehoek. Dit kan men aantonen door op de driehoek een goed gekozen discrete toevalswandeling te beschouwen en daarvan de schaallimiet te nemen.

6 Omhulsels van lokale processen

Definieer nu het omhulsel K (*hull*) van de hierboven beschreven gereflecteerde Brownse beweging als volgt. We beschouwen het door de Brownse beweging afgelegde pad tot het moment dat de basis van de driehoek voor het eerst wordt geraakt. Het omhulsel K bestaat uit al die punten van de driehoek die ofwel op dit pad liggen, ofwel door dit pad worden afgesneden van de twee basishoeken van de driehoek, zie figuur 2. Men kan aantonen dat de kansverdeling van K volledig wordt vastgelegd door de kansverdeling van het punt waar de Brownse beweging de basis voor het eerst raakt.

Op grond hiervan weten we dat het omhulsel K van een gereflecteerde Brownse beweging met reflectiehoeken van 60° dezelfde kansverdeling heeft als het omhulsel van het pad van SLE met $\kappa = 6$, dat op zijn beurt de schaallimiet is van het toevalspad van kritische percolatie. Het toevalspad van kritische percolatie is nauw verwant aan een ander toevalspad, dat wel een zelf-vermijdend spoor (*self-avoiding trail*) wordt genoemd. Uit computersimulaties blijkt echter dat het omhulsel van een zelf-vermijdend spoor niet dezelfde verdeling heeft als het omhulsel van SLE met $\kappa = 6$. De resultaten van de simulaties zijn wel consistent met de hypothese dat het omhulsel van een zelf-vermijdend spoor overeenkomt met het omhulsel van een gereflecteerde Brownse beweging met reflectiehoeken van 90° .

Dankwoord

bedankt

Dit woord is gericht aan allen die op wat voor manier dan ook hebben bijgedragen aan de totstandkoming van dit proefschrift. In de eerste plaats wil ik mijn promotor, Bernard Nienhuis, bedanken voor de kans die hij mij bood om het hier beschreven onderzoek te doen. Ik dank al mijn collega's van het Instituut voor Theoretische Fysica voor de goede jaren die ik er heb doorgebracht. Paula, Lotty en Yocklang, jullie ondersteuning was onontbeerlijk. Mijn collega-promovendi Jasper, Bastian, Leo, Rob en Srdjan bedank ik voor alle plezierige contacten.

Er werd door mij buiten het instituut bijna dagelijks ontspanning en afleiding gezocht achter de piano. Voor alle voortgang die ik daarbij heb geboekt dank ik in de eerste plaats Gert. Behalve gertzelf wil ik ook graag zijn mede-werkers bedanken, voor de soms plotseling mooie momenten.

Tenslotte wil ik mijn vrienden en familie bedanken voor alle steun in de afgelopen jaren. Maarten en Jasper, jullie betrouwbare vriendschap is en blijft van grote waarde. Ik ben er trots op dat jullie mij bij de promotie als paranimfen terzijde willen staan. Deb, you are one of the best friends anyone could ever wish for. Too bad we will never make the 147. Mijn ouders Piet en Tineke, en mijn broer Joost dank ik voor alle steun en interesse, hoe moeilijk het soms ook was om te begrijpen wat mij bezig hield. De laatste woorden zijn voor Willemien. Dank, voor alle liefde, geduld en geloof in mij.